CELLULAR AND SUBCELLULAR MECHANISMS OF VENTRICULAR MECHANO-ARRHYTHMOGENICITY

by

Breanne A. Cameron

Submitted in partial fulfilment of the requirements
for the degree of Doctor of Philosophy

at

Dalhousie University
Halifax, Nova Scotia
July 2021

Dalhousie University is located in Mi'kma'ki,
the ancestral and unceded territory of the Mi'kmaq.
We are all Treaty people.

DEDICATION PAGE

For my dad, for giving me the love of the heart. Your brilliance and kindness will always be my biggest inspiration in all things.

&

For my mom, for giving me her resilience and humour (even though she would swear I'm adopted and/or she took the wrong kid home). I finally got you something to put on the fridge.

&

For my Neno (Neens, Neen Bean, etc.), for keeping my feet grounded, but always helping my mind soar. I love you.

TABLE OF CONTENTS

LIST OF FIGURES

ABSTRACT

The heart is an electro-mechanical pump with feedback mechanisms for responding to acute changes in its mechanical environment. This requires cellular and subcellular elements of cardiac mechano-sensitivity, including mechano-electric effectors (*e.g.*, mechano-sensitive channels), mechano-electric transducers (*e.g.*, the microtubule network, MTN), and mechano-electric mediators (*e.g.*, ROS and Ca^{2+}), which allow the heart to respond to mechanical stimuli through electrophysiological changes. While critical for tuning normal electro-mechanical function, disease-related alterations in cardiac mechano-sensitivity can contribute to arrhythmogenesis. The overall goal of my thesis was to investigate cellular and subcellular mechanisms of mechano-arrhythmogenicity in models of two specific pathologic states: acute ischaemia and hypertension.

Arrhythmogenesis in acute ischaemia involves the combination of stretch at the ischaemic border zone, and alterations in voltage-Ca^{2+} dynamics that create a 'vulnerable period' (VP) for mechano-arrhythmogenicity during which Ca^{2+} remains high in repolarising cells. The goal of this project was to: (i) determine if ischaemia enhances mechano-sensitive mechano-electric mediator production; (ii) isolate the role of the VP in mechano-arrhythmogenicity; and (iii) identify mechanisms underlying mechano-arrhythmogenicity during acute ischaemia. We showed that during ischaemia, mechano-arrhythmogenicity is enhanced specifically in the VP, and involves ROS, intracellular Ca^{2+}, and the mechano-sensitive, Ca^{2+} permeable TRPA1 channel. Further, we showed that stretch-induced increases in ROS and Ca^{2+} spark production is enhanced in ischaemia, suggesting increased mechano-sensitivity, which may contribute to an arrhythmogenic substrate and/or modulate the activity of TRPA1 channels.

In hypertension, acute hemodynamic fluctuations in the presence of structural remodelling contribute to the high arrhythmic burden. Increased MTN density or stability (*via* detyrosination or acetylation) may increase mechano-sensitivity by enhancing mechano-transduction or mechano-effector activity (*e.g.*, TRPA1 channels), consequentially reducing the stretch-threshold for arrhythmias. The goal of this project was to assess the role of acute changes in MTN density and stability in mechano-arrhythmogenicity. We demonstrated that increasing MTN detyrosination, rather than stiffness or acetylation, enhances mechano-arrhythmogenicity, which can be mitigated by blocking TRPA1.

Overall, the results of my thesis have given us further insight into mechanisms underlying mechanically-induced arrhythmias in acute ischaemia and hypertension, and in particular, have demonstrated the exciting potential for TRPA1 as a source of ventricular mechano-arrhythmogenicity.

LIST OF ABBREVIATIONS USED

ADP	Adenosine diphosphate
AITC	Allyl isothiocyanate
APD	Action potential duration
ATP	Adenosine triphosphate
Ca^{2+}	Calcium
$[Ca^{2+}]_i$	Free intracellular calcium concentration
CaMKII	Ca^{2+}-calmodulin-dependent protein kinase II
CaTD	Calcium transient duration
COL	Colchicine
DCF	2',7'-dichlorofluorescein diacetate
DMSO	Dimethyl-sulfoxide
DNT	Dantrolene
DPI	Diphenyleneiodonium
ECC	Excitation contraction coupling time
EDFLR	End-diastolic force-length relationship
ESFLR	End-systolic force-length relationship
GLIB	Glibenclamide
K^+	Potassium
K_{ATP}	ATP-sensitive potassium channel
LV	Left ventricular
MAP4	Microtubule associated protein 4
MEC	Mechano-electric coupling

MSC	Mechano-sensitive channel
MSC_{NS}	Cation non-specific mechano-sensitive channel
MSC_K	Potassium-specific mechano-sensitive channel
MTN	Microtubule network
Na^+	Sodium
NAC	N-acetyl-L-cysteine
NaCN	Sodium cyanide
NCX	Sodium/Ca^{2+}-exchanger
NOX2	NADPH oxidase 2
NPR	Normal paced rhythm
NT	Normal Tyrode
PIN	Pinacidil
PTL	Parthenolide
PVC	Premature ventricular contraction
PZT	Piezo-electric translators
RyR	Ryanodine receptors
ROS	Reactive oxygen species
SEM	Standard error of the mean
SI	Simulated ischaemia
STP	Streptomycin
TAX	Paclitaxel
TnC	Troponin C
TRP	Transient receptor potential channels

TRPA1	Transient receptor potential ankyrin-1
TRPV4	Transient receptor potential vanilloid-4
TUB	Tubacin
VP	Vulnerable period
X-ROS	NOX2-dependent stretch-induced ROS production

ACKNOWLEDGEMENTS

There are not enough words to express how grateful I am to everyone who helped me get to this point, especially during the *many* times I believed I couldn't.

I would like to begin by expressing my gratitude to my external examiner, Andrew McCulloch. I have been excited to have you on board since we met at the MEC meeting. Thank you so much for agreeing to take on the task, I only wish it could have been in person. To all of the wonderful members of my committee, Drs. Susan Howlett, Stefan Krueger, and Yassine El Hiani, I am so thankful for all of your support in our meetings and throughout the course of my degree. Stefan, without your help with the fluorescence imaging early on, this would have been a *much* shorter thesis (!). Yassine, your excitement over presentation details always brings me so much joy. Susan, I consider myself so lucky to have had the opportunity to work with and learn from you. Without your encouragement, I never would have believed myself capable of giving a talk, let alone pursuing a PhD! Thank you for always lending an ear, offering words of wisdom, and giving me a little push when I needed it. I hope to be able to help someone else one day the way you helped me.

Next, I would like to thank all of the members of the Department of Physiology and Biophysics. To all of the PI's, admin, facilities management personnel, staff, and students, it has been an honour to work and learn alongside all of you.

Thank you to Gentaro, Keiko, and Kai for making my experience in Japan one of the best times of my life. I feel so fortunate to have learned from your expertise, and to have experienced a part of your culture. Thank you to Peter Kohl for your mentorship and guidance (even though you thought I was Brian). I am constantly learning from you, and I can't wait to continue that in Germany. You have single-handedly changed the way I

envisioned conferences would feel like, and I am so grateful to have experienced one of your events.

To the members of the Quinn lab, thank you for being there to celebrate the successes and laugh through the failures with me. Sara and Eilidh, I still swear it was just cell water in my eye when I found out about Japan. I am so fortunate to have been lab mates with two powerhouse STEMINISTS. I will miss our accidental cider adventures most of all – Jimmy Neutron forever. To the chonks (PH, PY), not even Frodo can break this Fellowship. Thank you for the daily BBQ's, constant laughter, semi-decent memes, and huge amounts of support. To Matt, aside from the copious amounts of technical help, I am most grateful for your (best) friendship. To all the newer members of the TAQ lab, I wish I had the chance to know you better (COVID), but I know you are all in the best hands. I look forward to seeing you all at meetings!

To my friends, thank you for your understanding (especially with my terrible skills at answering messages) and support in everything I do. I am so beyond grateful to have you all in my life. A special thanks to Kaitlynne – if you could only have one person cheering you on at an event, she would be the one to choose.

To my family (Pro-clan, Blackwell-clan, and Cameron-clan), thank you for all of your love, I hit the jackpot with this family. To Radmila, Dale (Benedict), and Slavko, thank you for your interest in everything I do, and most of all, thank you for Neno! To my parents: Dad, once I realised becoming the Queen of England was not a realistic job aspiration, I looked to you and your love of the heart for inspiration. It started as a way to join in on your dinner conversations about work, but you made it become more than that. It is because of you and your passion that I was drawn to the heart. Thank you for that, it

is the greatest gift I could ask for – this one's for you. Mom, I am so grateful for all of your help along the way. For always being there to listen to me when I need it, to make sure I actually do the normal functions required for life (though, I still believe coffee counts toward my water intake), and to cheer me on. You are so much more like Grandma than you realise, and I am so grateful I have a little part of her here with me to see this through.

To Neno, I couldn't have done this without you. Thank you for your patience and understanding, for listening to me panic about the most minute details of my PowerPoints, for playing concerts for me when I'm missing live music, for letting me get 100 pets, for laughing at my jokes when I'm sleep deprived, and for loving me unconditionally.

Finally, thank you to Alex Quinn and his family. Alex, you asked me once if I knew who my favourite childhood teacher was and why. I told you it was my Grade 6 teacher, because he was the first one to ask me my name, and that not letting that teacher know the impact he had by doing that one simple act was one of my deepest regrets. So, in getting wiser, I want you to know how profoundly you have changed my life. You asked me what I needed in a supervisor, and you gave it to me. You challenged and inspired me. You thought the reason I decided to pursue a PhD was because the project took off, but I hope you know that it was because I wanted to work *with you*. Thank you for being the only person who is more obsessive than me about details. Thank you for being the most excited person in the room at literally any moment. Thank you for giving me opportunities to travel the world, and for giving me the strongest foundation I could have ever imagined. To Renae, Freida, and Eiler, thank you for giving up family time so TAQ can help us all out. I know how precious that time is, and so I hope you know how grateful we all are.

CHAPTER 1: INTRODUCTION

The contents of this introduction are being prepared as an invited Chapter for *Cardiac and Vascular Biology* (**Cameron BA**, Kohl P, Quinn TA. Cellular and subcellular mechanisms of ventricular mechano-arrhythmogenicity. In: Hecker M, Duncker DJ, eds. *Cardiac Mechanobiology in Physiology and Disease*. Berlin, Springer; In Preparation. [Invited - Deadline June 30, 2021]). I am writing the manuscript in consultation with Dr. Alex Quinn and Prof. Dr. Peter Kohl.

1.1. Cardiac Mechano-Electric Regulatory Loop

The ultimate goal of the heart is to meet the systemic demand for blood flow, which is achieved through an elegant coordination of its electrical excitation and mechanical pumping action.[232] Even under physiological conditions, the haemodynamic demand of the body is constantly in flux, whether due to postural or circadian oscillations, exercise, or autonomic responses. To facilitate matching supply to these changes in demand, an intricately connected system has evolved that tethers the electrical and mechanical function of the heart through a feed-forward ('excitation-contraction coupling'),[18] and feed-back ('mechano-electric coupling,' MEC) system.[145,146,227,232,236,276] Together, these processes dynamically regulate cardiac function and form the "mechano-electric regulatory loop" (Fig. 1.1).[232] This intricate system of auto-regulation allows the heart to acutely sense and respond to changes in its electrical[18] or mechanical environment.[232] With pathophysiological mechanical perturbations or disease-related alterations in this system, however, mechano-electric coupling can instead destabilise cardiac rhythm and drive atrial or ventricular arrhythmogenesis.[8,9,10,13,53,263,264,272,276,]

This chapter will explore the mechanisms and contribution of mechano-electric coupling to ventricular arrhythmias by describing what is known about the relevant cellular and subcellular components of ventricular myocyte mechano-sensitivity to stretch (*i.e.,* mechano-electric effectors, transducers, and mediators) and how pathophysiologic changes in mechano-sensitivity, myocardial mechanics, or the mechanical environment, may contribute to stretch-induced alterations in cardiac electrophysiology that lead to arrhythmogenesis (hereafter referred to as 'mechano-arrhythmogenicity'), with a focus on two disease states: acute regional ischaemia and chronic hypertension.

1.1.1. Mechano-Electric Coupling in Ventricular Myocytes

Perhaps the most apparent evidence for mechano-electric coupling in the ventricles is premature electrical excitation secondary to an acute mechanical stimulus.[22,69,80,96,237,267,310,325] An extreme example of this occurs in *Commotio cordis* or with precordial thump, by which a sudden blow to the precordium can immediately initiate or terminate disturbances in ventricular rhythm, including fibrillation.[86,144,165,171,172,173,232] In ventricular myocytes, the tendency for stretch to cause premature electrical excitation depends on both stretch magnitude and its timing during the action potential.[232] In the case of the former, this indicates that there is a stretch magnitude-dependent threshold for initiating electrical excitation. In the case of the latter, this highlights the importance of the underlying electrophysiological state. During electrical diastole, stretch will tend to depolarise the membrane potential, and if supra-threshold, result in electrical excitation. In electrical systole, a stretch will instead alter repolarisation. This effect will either shorten the action potential, or lead to action potential lengthening and possibly early-afterdepolarisation-like activity, depending on stretch magnitude, duration, and the specific phase of the action potential in which it occurs.[22,32,40,69] As a result, pathophysiologic alterations in ventricular mechano-sensitivity (which may allow a smaller mechanical stimulus to drive supra-threshold electrical changes) or action potential morphology (which may alter the phase of repolarisation during which a mechanical stimulus occurs) may affect the magnitude- and/or temporal-dependence of ventricular mechano-arrhythmogenicity.[232]

In addition to driving mechano-arrhythmogenicity, at the level of the whole heart, MEC can heterogeneously alter action potential duration (APD), refractoriness,[32,40] and conduction velocity[326] (due to varied expression of mechano-sensitive channels[186,279] and

background electrical activity),[232] which may create an arrhythmogenic substrate and facilitate re-entrant electrical activity.

1.2. Ventricular Myocyte Mechano-Sensitivity

The effects of MEC in ventricular myocytes reflect the combined contribution of the various elements underlying cellular mechano-sensitivity, including those that drive the electrical response to a mechanical stimulus ('mechano-electric effectors'),[216] those that transduce the stimulus ('mechano-electric transducers'),[36,132,244] and those that mediate the response ('mechano-electric mediators').[41,116,121,221,224] One should note, however, that while for the purpose of considering their contributions to mechano-arrhythmogenicity, it is useful to categorise mechano-sensitive elements in such a way, in reality, cardiac mechano-sensitivity is driven by an highly integrated, inter-dependent network of components that influence each other's function, and thus the components may cross these artificial boundaries.

1.2.1. Mechano-Electric Effectors

Mechano-electric effectors cause an electrophysiological change in response to a mechanical stimulus.[216] The primary mechano-electric effectors in ventricular myocytes are mechano-sensitive ion channels (MSC), whose current is gated or augmented by stretch, leading to depolarisation (and if suprathreshold, excitation) or altered repolarisation (affecting APD) of cellular membrane potential (Fig. 1.2).[142,216] While the exact molecular identity of the MSC driving MEC in the heart remains a topic of debate, they can be divided into two groups based on their principal ion permeability: cation non-specific MSC (MSC_{NS}, which will cause depolarisation or altered repolarisation) and

potassium (K^+)-selective MSC (MSC_K, which will only lead to repolarisation).[216,232] The relative balance of MSC_{NS} and MSC_K currents elicited by a stretch will determine whether it has a depolarising or repolarising effect.[142]

1.2.1.1. MSC_{NS}

Most acute effects of myocardial stretch on cardiac electrophysiology can be explained by an MSC_{NS} with a reversal potential of ~0 mV (which is positive to the resting membrane potential of a ventricular myocyte, ~-90 mV, but negative to its membrane potential during the action potential plateau, ~20 mV).[216] As a result, the timing of stretch during the action potential[142] determines whether MSC_{NS} passes an inward current, depolarising the cell[60] (and if supra-threshold causing excitation),[242] or an outward current leading to repolarisation.[325] Despite experimental and computational evidence of stretch-induced excitation[79,80,96,107,140,142] and its pharmacological prevention,[16,64,69,85,107,199,310] there have been no single channel recordings of MSC_{NS} in ventricular myocytes (possibly due to them being embedded in the cellular microarchitecture, preventing their measurement by patch clamp).[216] While this difficulty in obtaining single-channel measurements has resulted in the molecular identity of the MSC_{NS} involved remaining elusive, there are currently two groups of ion channels thought to make important contributions: Piezo and Transient Receptor Potential (TRP) channels.[216,232]

The discovery of Piezo channels garnered a great deal of excitement as a potential key MSC_{NS} in cardiac myocytes.[56] Piezo channel kinetics make it a perfect contender,[216,292] yet while it appears that Piezo channels are expressed in atrial fibroblasts,[122] only small amounts of Piezo mRNA have been found in cardiac myocytes (from mice)[56] and no

functional Piezo channels have been shown in ventricular myocytes from any species. Therefore, there is currently no evidence for a role of Piezo in ventricular mechano-arrhythmogenicity.

TRP channels are a ubiquitously expressed group of channels comprised of six subfamilies, many of which are expressed in the heart.[105] TRP channels have garnered recent interest regarding their role in the pathological progression of hypertrophy, heart failure, and ischaemia, as well as in arrhythmogenesis.[73,111,305] As TRP channels can pass inward or outward currents, and some have been shown to be inherently mechano-sensitive[112] (although that is a controversial subject),[202] their potential role in ventricular mechano-arrhythmogenicity warrants further investigation.

1.2.1.2. MSC_K

The identity of MSC_K channels in the heart is well established. TREK-1 and 2 are outwardly rectifying K^+ channels with a reversal potential similar to the resting potential of ventricular myocytes (~-90 mV).[216] As a result, they pass a repolarising current during stretch, regardless of stretch timing. Accordingly, they are not involved in stretch-induced excitation, and their relative contribution to mechano-electric coupling is generally believed to be low compared to MSC_{NS}.[232] However, in disease states that activate additional mechano-sensitive K^+ currents, such as during ischaemia (in which ATP-sensitive K^+, K_{ATP}, channels are activated and their mechano-sensitivity is increased; discussed below), the contribution of MSC_K may become more relevant.[166,232,293,294]

1.2.2. Mechano-Electric Transducers

Mechano-electric transducers sense a mechanical stimulus and transmit it to the mechano-electric effectors and mediators, which then elicit and modulate the electrophysiological response.[36,244] In ventricular myocytes, microtubules are particularly important for mechano-electric transduction[36,116,123,132,218,221,244] (although other cytoskeletal elements such as titin, focal adhesion proteins, and integrins, along with mechano-sensitive enzymes, may also be involved).[102,120]

1.2.2.1. Microtubules

Through interactions with membrane-associated proteins and intermediate proteins (*e.g.,* desmin), microtubules form physical links between the extracellular matrix and intracellular myofibrils.[36] These links create a rigid scaffold conferring structural integrity to the ventricular myocyte, while at the same time allowing microtubules to transduce mechanical signals to other mechano-sensitive cellular components.[36,132,243,244]

Mechano-transduction is enabled by the load bearing ability of microtubules, a characteristic demonstrated by their buckling behaviour during cell contraction[243] and that is enhanced by their lateral reinforcement.[24] This ability has been shown to be a result of the specific interaction between the intermediate protein desmin[243] and detyrosinated microtubules.[243,247] Detyrosination is a post-translational modification that confers stability to microtubules by simultaneously preventing degradation of existing microtubules and forming tight junctions with desmin, resulting in a shift from low-energy sliding to energy-costly buckling of microtubules during cell contraction.[243] Other, less explored post-translational modifications may also increase the load-bearing capabilities of

microtubules,[15,123] such as acetylation, which confers resistance to microtubule breakage during repetitive mechanical stimulation, resulting in more long-lasting ('aged') microtubules.[218,321] Thus, a denser, more detyrosinated (and physically anchored) and/or acetylated microtubule network (MTN) would be expected to have enhanced mechano-transduction potential. Indeed, it has been shown that increased MTN density, detyrosination, and acetylation enhances microtubule-dependent mechano-electric mediator production (*i.e.,* stretch-induced increases in intracellular Ca^{2+} and NADPH oxidase 2 (NOX2)-dependent ROS production, X-ROS),[46,132] warranting particular consideration of their potential role in mechano-arrhythmogenicity.

1.2.3. Mechano-Electric Mediators

Ventricular mechano-electric mediators are direct products of intracellular mechano-transduction that modulate the electrophysiological response to a mechanical stimulus.[41,121,224] The principal factors known to be important in ventricular myocytes are the stretch-induced release of intracellular Ca^{2+}[115,116,254] and X-ROS[221,224] (although other important factors may exist),[121] which have been shown to modulate the activity of potential mechano-electric effectors (such as Transient Receptor Potential Ankyrin-1, TRPA1, channels)[5,332] and to increase other trans-sarcolemmal depolarising currents (for instance, *via* the sodium (Na^+)/Ca^{2+} exchanger, NCX).[137,155] At the same time, they may also influence mechano-transduction by increasing the post-translational modification of microtubules (*e.g.,* acetylation),[87] which will further enhance mechano-transduction,[46] resulting in a positive feedback system that will further increase myocyte mechano-sensitivity.

1.2.3.1. Mechano-Sensitive Ca^{2+} Handling

In ventricular myocytes, multiple aspects of intracellular Ca^{2+} handling are mechano-sensitive and influence cytosolic Ca^{2+} levels. Free cytosolic Ca^{2+} during systole is affected by the length-dependent modulation of the Ca^{2+}affinity of troponin C (TnC), which is increased by stretch, resulting in more Ca^{2+} being bound to the myofilaments during stretch.[2] Upon release of stretch, the rapid dissociation of Ca^{2+} from TnC causes a surge of cytosolic Ca^{2+}.[295] At the same time, stretch causes an acute increase in individual Ca^{2+} release events from the sarcoplasmic reticulum (Ca^{2+} sparks) *via* ryanodine receptors (RyR).[115,116] These two mechano-sensitive Ca^{2+} handling processes interact and perhaps balance each other under normal conditions, but pathologic alterations in RyR open probability (for instance due to oxidation, nitrosylation, or membrane potential depolarisation)[14,220,221,222,249] or in myofilament Ca^{2+} binding affinity[108] can disrupt this balance, resulting in Ca^{2+}-mediated arrhythmogenesis. This is particularly true in diseases associated with altered mechanics[138] or mechano-sensitive Ca^{2+} handling processes, such as ischaemia,[33] in which subcellular Ca^{2+} fluxes can lead to potentially arrhythmogenic Ca^{2+} waves.[137]

1.2.3.2. X-ROS

The stretch-induced increase in Ca^{2+} spark rate is itself affected by another mechano-electric mediator: X-ROS.[221] Importantly, in the context of ventricular mechano-sensitivity, X-ROS (and thus, mechano-sensitive Ca^{2+} release) is dependent on the integrity of the MTN,[116,221] and increasing MTN stability enhances X-ROS production.[132] The importance of X-ROS for ventricular mechano-sensitivity is supported by the observation

that it is graded by stretch magnitude and cyclic (more than static) stretch (as is experienced during regular cardiac activity),[223] and has been suggested to balance the length-dependent buffering of cytosolic Ca^{2+} by TnC,[169] thereby potentially contributing to the tuning of Ca^{2+} signalling to hemodynamic load.[169,223] Importantly, in pathologic settings, an increase in X-ROS could contribute to mechano-arrhythmogenicity by sensitising mechano-electric effectors,[332] promoting RyR Ca^{2+} leak,[221] and stabilising microtubules (through an increase in acetylation),[87] thereby increasing mechano-sensitivity and its contribution to arrhythmogenic triggers and substrate.

1.3. Ventricular Mechano-Arrhythmogenicity

Ventricular mechano-arrhythmogenicity, whereby a mechanical stimulus elicits an arrhythmogenic change in electrophysiology, is a consequence of ventricular myocyte mechano-sensitivity. It requires a sufficiently large and specifically timed mechanical stimulus to be sensed by the mechano-electric effectors, either directly or *via* mechano-electric transducers, with modulation by mechano-electric mediators. This effect can be augmented by changes in ventricular mechano-sensitivity that occur with disease, which may alter the likelihood that a given stimulus will overcome the magnitude- and temporally-dependent threshold for triggering an arrhythmia.[232] Existing clinical evidence of ventricular mechano-arrhythmogenicity has been corroborated in experimental studies that have helped elucidate potential underlying mechanisms.

1.3.1. Clinical Evidence

One of the most dramatic clinical examples of ventricular mechano-arrhythmogenicity is in the setting of *Commotio cordis*, during which a non-contusional impact to the precordium can result in transient rhythm disturbances or, in rare cases, ventricular fibrillation.[144] In fact, ventricular fibrillation in this setting remains one of the leading causes of sudden cardiac death among young athletes, and is one of the primary reasons automated external defibrillators are located in sporting facilities where this event is most likely to occur.[177,178] Ventricular mechano-arrhythmogenicity is more commonly observed during clinical procedures in which contact of medical instruments (*e.g.,* central vascular or intracardiac catheters, electrodes) with the myocardium causing local tissue deformation can lead to ectopic excitation and ventricular tachy-arrhythmias[23,61,71,77,110,152,157,158,170,187,266,270] (although, as with precordial stimulation, this can also revert established arrhythmias to normal sinus rhythm).[95,213] Ventricular mechano-arrhythmogenicity can additionally be seen during acute increases in ventricular loading leading to premature excitation, such as with balloon valvuloplasty.[162]

The risk of an abnormal mechanical stimulus triggering an arrhythmia is enhanced by cardiovascular disease. In patients with established structural heart disease, acute fluctuations in ventricular volume or pressure are more likely to result in premature excitation and sustained tachyarrhythmias.[263,272,276] Indeed, arrhythmia incidence in these patients is affected by pharmacological modulation,[259] circadian oscillation,[195] or daily variation of blood pressure,[240] such that acute increases in ventricular load are associated with higher rates of arrhythmias. There is also evidence that local changes in myocardial mechanics play a role in mechano-arrhythmogenicity, as wall motion abnormalities in

patients with ischaemic heart disease are correlated with an increased prevalence of premature excitation during acute fluctuations in load.[264] Interestingly, this effect also works in reverse: in patients suffering from chronic ventricular volume overload and tachyarrhythmias, acute ventricular unloading can result in temporary termination of ventricular tachyarrhythmias (for as long as the reduction in load is maintained).[4,109,159,214,308,311]

1.3.2. Experimental Studies

Experimental models have been an effective tool for better understanding these clinical observations of ventricular mechano-arrhythmogenicity. For instance, in the case of *Commotio cordis*, an experimental pig model of an impact to the chest has demonstrated the critical factors necessary for the induction of ventricular fibrillation: the impact needs to occur specifically (i) in space (directly over the heart)[171] and (ii) in time (~15-30 ms before the peak T wave of ventricular repolarisation),[173] and (iii) be of a certain magnitude.[172] Isolated heart experiments[231] and computational modelling[86,165] have further shown that ventricular excitation induced by impact[3] depends on the degree of myocardial deformation, and must overlap the trailing wave of the previous sinus excitation to initiate ventricular fibrillation, thus highlighting the critical spatio-temporal nature of a mechanical stimulus for mechano-arrhythmogenicity.

Experimental studies have also demonstrated the ability of acute changes in ventricular load to lead to premature excitation and tachyarrhythmias. If sufficiently large, transient increases in intraventricular volume during diastole cause cellular depolarisation, and if supra-threshold, can trigger excitation.[22,64,66,69,79,80,96,97,98,107,140,200,211,212,237,

[257,267,310,325] Ectopic excitation has also been observed in experiments involving rapid increases in aortic blood pressure, [260,261,262] which may be a consequence of post-systolic myocardial deformation.[93] When applied during systole, acute ventricular loading tends to instead heterogeneously alter repolarisation and refractoriness, furnishing an arrhythmogenic substrate.[16,17,22,27,31,32,40,57,58,59,62,63,69,89,94,106,153,160,237,238,239,271,296,298,313,325,326] In fact, in the isolated heart, an acute increase in intraventricular pressure has been shown to be as arrhythmogenic as the substrate created by the acidified catecholamine-rich milieu or electrical remodeling associated with heart failure.[233] It is important to note that, while changes in intraventricular volume or pressure presumably affect the entire ventricle, whether applied in diastole or systole the response is generally spatially heterogeneous. Myocardial stiffness varies across the ventricle, so stretch, and the resulting depolarisation, will be non-uniform,[40,257] with excitation originating from areas of the largest stretch (typically in the left ventricular free wall or the right ventricular outflow tract).[40,80,257]

There are two cardiac disease states that particularly highlight the above considerations and in which ventricular mechano-arrhythmogenicity may be a principal contributor to the associated arrhythmic burden – acute regional ischaemia and chronic hypertension – which are described in the following sections.

1.4. Evidence for Ventricular Mechano-Arrhythmogenicity in Cardiac Disease

1.4.1. Acute Regional Ischaemia

Acute regional ischaemia is a mismatch between the supply and demand of blood to a localised area of the heart due to occlusion of a coronary artery.[38] It is characterised by three hallmark pathophysiological changes to the cellular substrate: hypoxia (reduced

oxygen levels), hyperkalemia (increased extracellular K^+ concentration), and acidosis (decreased intracellular pH), which drive pro-arrhythmic electrophysiological changes and arrhythmias that occur in a temporally bi-modal fashion during periods termed phase 1a (up to ~10 min following artery occlusion) and 1b (~15-60 min after occlusion). The arrhythmias occurring in phase 1a appear to relate primarily to cellular hyper-excitability, however, due to the progressive nature of ischaemia, excitability in phase 1b is reduced below normal levels, despite a higher incidence of deadly ventricular arrhythmias.[38,124] It has been suggested that arrhythmogenesis in phase 1b instead involves the combination of (i) myocardial stretch in the ischaemic border zone,[84,161,219,246,283] and (ii) alterations in voltage-Ca^{2+} dynamics that create a 'vulnerable period' (VP) for mechano-arrhythmogenicity in late repolarisation, during which Ca^{2+} remains high in repolarising (and therefore, progressively re-excitable) cells.[13,280]

1.4.1.1. Arrhythmogenic Effects

1.4.1.1.1. Hypoxia

Reduced blood flow due to coronary artery occlusion results in a decrease in the interstitial oxygen content (*i.e.,* hypoxia) that elicits a metabolic shift in ventricular cells from aerobic to anaerobic glycolysis. This change in energy metabolism results in a progressive decrease of adenosine triphosphate (ATP) and a simultaneous increase of adenosine diphosphate (ADP), such that the ATP:ADP ratio is decreased, leading to activation of K_{ATP} channels.[38] Their activation increases the overall outward repolarising K^+ current and shortens the APD to a greater extent than the Ca^{2+}-transient duration,[124] generating the potentially VP described above[13,280] (a similar VP may facilitate arrhythmogenesis during β-adrenergic

stimulation in failing human hearts).[156] Of note, results from computational modelling suggest that the VP in ischaemia may be spatially heterogenous, as variation in K_{ATP} expression across the heart results in non-homogeneous APD shortening.[186] This heterogeneity may be further increased by regionally altered ventricular mechanics (discussed below) due to K_{ATP} channel mechano-sensitivity,[294] which is in fact enhanced in ischaemia.[166,293]

1.4.1.1.2. Hyperkalemia

The combination of K_{ATP} activation and reduced blood flow results in the extracellular accumulation of K^+, known as hyperkalemia.[38] An increase in extracellular K^+ causes a shift in the Nernst potential for K^+, which results in depolarisation of the resting membrane potential of ventricular cells. Hyperkalemia occurs in a temporally bimodal fashion due to the initial preservation of Na^+/K^+-ATPase function, which partially counteracts the increase in K_{ATP}-mediated K^+ efflux and its extracellular accumulation. Initially, this accounts for the hyper-excitable state in phase 1a, as the resting membrane potential approaches the threshold for fast Na^+ channels and action potential generation. However, once ATP reserves are depleted, the loss of Na^+/K^+-ATPase activity results in a greater, secondary rise in extracellular K^+. This leads to a further increase in the resting membrane potential, which begins to inactivate fast Na^+ channels, reducing cell excitability and prolonging the effective refractory period ('post-repolarisation refractoriness').[12,124] In the regionally ischaemic whole heart, the level of hyperkalemia is graded across the border zone between ischaemic and healthy tissue, resulting in an injury current that flows from

the depolarised ischaemic tissue to the electrotonically coupled healthy tissue and contributes to its hyper-excitability.[52,55]

1.4.1.1.3. Acidosis

The metabolic shift to anaerobic glycolysis due to a reduced oxygen supply enhances proton production, which leads to cellular acidosis. As a result, a compensatory efflux of hydrogen through the Na^+/hydrogen-ATPase causes an increase in intracellular Na^+, which drives NCX to operate in reverse mode, ultimately leading to intracellular Ca^{2+} accumulation. Additionally, acidosis causes inhibition of fast Na^+ and L-type Ca^{2+} channels,[12,124] along with gap junctions.[91]

1.4.1.1.4. Electrophysiological Changes

At the cellular level, the effects of hypoxia, hyperkalemia, and acidosis manifest as (i) morphological changes to the action potential – shortened APD, increased resting membrane potential, and reduced action potential amplitude and upstroke rate – and (ii) reduced intercellular conduction through gap junction uncoupling.[38,124] In the whole heart, heterogeneous APD reduction results in dispersion of cell excitability and repolarisation, particularly at the border zone, which along with heterogeneous effects on conduction can be highly arrhythmogenic (Fig.1.3).[52,124]

1.4.1.1.5. Alterations in Ca^{2+} Handling

Ischaemia ultimately leads to an increase in diastolic Ca^{2+} within the cytosol, due to: (i) Ca^{2+} influx driven by membrane depolarisation and reverse mode NCX activity (secondary

to the acidosis-induced increase in intracellular Na^+ *via* the Na^+-hydrogen exchanger); (ii) decreased Ca^{2+} uptake by the sarco-endoplasmic reticulum ATPase due to reduced ATP; and (iii) an increase in Ca^{2+} leak from the sarcoplasmic reticulum, driven by an increase in the open probability of ryanodine receptors (RyR) due to membrane depolarisation[249] and increased cytosolic Ca^{2+} and ROS. For a comprehensive review on Ca^{2+} handling in ischaemia, please see the review by Baumeister and Quinn, 2016.[12]

1.4.1.2. Changes in Myocardial Strain

Altered metabolic activity and intracellular Ca^{2+} handling during regional ischaemia impacts myocardial contraction, resulting in areas of heterogeneous strain. This is particularly evident at the ischaemic border zone where there is systolic stretch of weakened myocardium, especially as the fully ischaemic tissue stiffens in phase 1b.[84,161,219,246,283] These changes in myocardial strain have been suggested to be mechano-arrhythmogenic, supported by the correlation between wall motion abnormalities and the incidence of ventricular fibrillation seen in patients with coronary artery disease.[264] Experimentally, it has been shown that the magnitude of tissue stretch in ischaemia is related to the onset ventricular fibrillation[103] and that the end-diastolic length of the ischaemic region is a strong predictor of ventricular fibrillation occurrence.[8,9,10] Moreover, in isolated hearts, arrhythmia incidence during acute regional ischaemia is load-dependent[13,53,211] and tends to originate at the border zone,[53] where computational modelling suggests mechano-electric-effector-mediated depolarisation and conduction slowing can trigger mechano-arrhythmogenicity.[125] This may be further enhanced by mechano-electric mediators, as the increase in Ca^{2+} sparks and ROS that occur with stretch

are potentiated by ischaemia,[33] possibly due to a deficit in antioxidant capacity.[168] In fact, enhancement of mechano-electric mediators in regions of stretched myocardium has been shown to cause focal Ca^{2+} waves,[192] which, if occurring at the ischaemic border zone where the injury current tends to reduce the excitation threshold,[52] may additionally contribute to triggers or a substrate for mechano-arrhythmogenicity.

1.4.1.3. Potential Mechanisms of Mechano-Arrhythmogenicity in Acute Regional Ischaemia

Mechano-arrhythmogenicity in acute regional ischaemia appears to involve the coalescent effects of a decreased excitation threshold, a pro-arrhythmic electrophysiological substrate, and myocardial stretch, particularly at the ischaemic border zone. As the outcome of myocardial stretch is dependent on both its magnitude and timing in relation to background electrical activity, ischaemic effects on elements of ventricular mechano-sensitivity or electrophysiology may increase the likelihood that a mechanical stimulus will elicit an arrhythmia. The enhanced production of mechano-electric mediators in ischaemia (stretch-induced Ca^{2+} sparks and X-ROS),[33] in addition to the increased sensitivity of RyR (and ensuing Ca^{2+} release) secondary to attenuated glutathione levels,[168] suggest that there is indeed an increase in mechano-sensitivity. Heterogeneous stretch may therefore lead to localised changes that enhance both arrhythmogenic triggers and substrate, through modulation of mechano-electric effector activation or gating kinetics (discussed in detail in Chapters 3-6) and secondary to increased cytosolic Ca^{2+} and ROS levels.[5,184,332] The heterogeneous expression of mechano-sensitive[293,294] K_{ATP} channels[186] (or other SAC_K)[279]

across the heart, combined with heterogeneous mechanics, will additionally drive dispersion of repolarisation and conduction block,[54] favouring re-entrant electrical activity.

Mechano-arrhythmogenicity may be further facilitated by ischaemic changes in voltage-Ca^{2+} dynamics that generate a VP for arrhythmias in late repolarisation. At the cellular level, the VP represents a phase of the cardiac cycle in which cytosolic Ca^{2+} is still elevated in a cell that is becoming re-excitable. Abbreviation of the APD in ischaemia increases the duration of this period, while at the same time, increases the likelihood that stretch will occur when a cell is excitable.

1.4.2. Hypertension

Hypertension, defined as a systolic blood pressure (BP) ≥130mmHg or diastolic BP ≥80mmHg,[314] results in an increase in afterload, and thus the load against which the ventricles (and ventricular myocytes) must contract.[81] The persistent stress experienced by the ventricular myocardium in hypertension results in the stimulation of mechano-sensitive pathways in ventricular myocytes. This leads to compensatory structural remodelling, which can ultimately result in decompensated heart failure.[149,174] It remains unclear whether the compensatory and decompensatory phases are in fact two distinct stages, in which the former is a cardioprotective response to maintain cardiac function and the latter is a longer-term degradation of function, or whether the load response is a continuum of remodeling in which there is a shifting balance of adaptive and maladaptive effects. Regardless, myocardial remodelling in hypertension may enhance mechano-sensitivity, which can contribute to increased mechano-arrhythmogenicity. This is thought to contribute to the increased incidence of premature excitation in patients with

hypertension[272] that occur with acute fluctuations in ventricular load (such as during circadian[195] or pharmacologic[259] modulation of BP), which can interact with the arrhythmogenic substrate associated with remodelled myocardium to cause sudden cardiac death.[128,181,233,235,258,282,324] Further, mechano-arrhythmogenicity in hypertension may be enhanced by regional ischaemic episodes that occur with wall thickening and microvasculature remodelling,[68] through mechanisms described in the previous section.

1.4.2.1. Structural Remodelling

1.4.2.1.1. Hypertrophy

Remodelling in hypertension is characterised by a concentric thickening of the ventricle (*i.e.,* hypertrophy) to compensate for the increased wall stress associated with chronically elevated afterload. This phenomenon can be explained by Laplace's law: T=(P*R)/2m, as hypertension causes an increase in ventricular pressure (P), and consequently, wall stress (or tension, T). In response, the ventricular wall thickens (m) by adding sarcomeres in parallel, thereby increasing the size of existing myocytes, rather than adding new cells. The degree of ventricular thickening then scales with the increase in pressure to normalise stress.[149,174]

It has been suggested that microtubules may play a critical role in the hypertrophic remodelling seen in hypertension,[36] as it is prevented by disrupting microtubule polymerisation in animal models of pressure overload.[74,255,287] While the contribution of microtubules to hypertrophy is not fully understood, it may relate to altered gene expression *via* mechano-transduction,[36] or to disorganisation of microtubules and associated

intermediate proteins[39,92,247] that may impair accurate mRNA delivery and protein synthesis necessary for sarcomere assembly.[36,163,251,253]

1.4.2.1.2. Microtubule Network

In addition to chamber thickening, chronic hypertension results in progressive remodelling of the cytoskeleton, characterised by changes in the density (*via* polymerisation) and stability (*via* post-translational modifications, intermediate protein linkages, and microtubule associated proteins) of the MTN.[48,134]

While both clinical preparations[37,39] and experimental models[274,323] have demonstrated an increased MTN density in hypertension, whether microtubule proliferation begins during hypertrophy, or is a consequence of the transition to decompensation, is unclear (although discrepancies may relate to inconsistencies between hypertensive models, both in terms of species as well as the method of its induction).[275] However, regardless of the moment of onset, the MTN has been consistently shown to become denser and more stable in hypertension.[37,39,205,274,323,330] MTN remodelling appears to contribute to altered contractile function of ventricular myocytes, as their hyper-polymerisation in healthy cells decreases contractility, while their de-polymerisation in myocytes from failing (and thus hyper-polymerised) hearts improves contractility.[148,244,288] While this does indeed suggest a clear role for the MTN in contractile dysfunction seen in hypertension, the *relative* contribution of the observed increase in the rate of microtubule polymerisation (which would present as an increase in tubulin content) *versus* enhanced stability of existing microtubules (which would manifest as more post-translationally

modified and aged microtubules) to altered contractile function warrants consideration.[15,36,39,244]

It has been shown that during contraction, microtubules buckle at wavelengths corresponding to the distance between sarcomere units.[243] This process was demonstrated to be dependent on the level of detyrosination, a post-translational modification of α-tubulin that involves the removal of the C-terminal tyrosine to expose a glutamate at the newly formed C-terminus.[123,250] This suggests that the load-bearing capability of microtubules, and by extension, their mechano-sensitivity and contribution to mechano-electrical transduction, depends on their stability (through detyrosination), rather than their density alone. Therefore, modulation of microtubule detyrosination in hypertension may have profound effects on ventricular mechano-sensitivity and the resultant mechano-arrhythmogenicity.

1.4.2.1.2.1 Microtubule Post-Translational Modifications

Microtubule detyrosination confers stability to the MTN by preventing catastrophe of existing microtubules (resulting in more aged microtubules) and facilitating cross-linking with intermediate proteins[36,150,167] (*e.g.*, desmin).[243,247] This results in a shift from low resistance sliding of microtubules during contraction, to high-energy buckling.[39,243,244] In fact, in human[39] and murine cardiomyocytes,[132] inhibition of detyrosination results in a reduction in both the frequency and organisation of buckling behaviour, with an associated increase in contractility, suggesting an attenuation of their resistance to compression and load bearing capability. Conversely, enhancing detyrosination (without a change in MTN density) increases both cell stiffness and viscosity, with an associated decrease in

contractility.[132,243] This suggests that enhanced detyrosination alone could account for increased ventricular stiffness and impaired contractility in cardiomyocytes subjected to pressure overload. In fact, in addition to the observed overall increase in MTN detyrosination in hypertension, in failing human cardiomyocytes there is an upregulation of both a gene encoding a pre-detyrosinated tubulin,[39] as well as the detyrosination promoting microtubule associated protein 4 (MAP4).[42] As a consequence, suppression of detyrosination in cardiomyocytes from pressure overload patients improves contractile function, the degree of which scales with initial cardiomyocyte stiffness.[39,243] These observations may have important clinical relevance, as cardiomyocytes from patients presenting with heart failure with preserved ejection fraction (HFpEF, a condition for which known mechanisms and effective therapy are lacking) showed the most impediment to contractility before treatment, and thus the greatest improvement with inhibition of detyrosination.[39]

1.4.2.1.2.2. Desmin and Microtubule Associated Proteins

In human pressure overload, there is an upregulation of desmin,[39] an intermediate filament protein known to bind specifically to detyrosinated tubulin and cause its load-bearing, bucking behaviour.[243,247] However, this upregulation is partially comprised of an isoform prone to misfolding and aggregation,[39] which may explain observations of misalignment of microtubules and desmin, [36,39,92] and potentially contribute to decompensated heart failure due to improper trafficking of sarcomere precursors.[36,163,251,253] Microtubule associated protein 4 (MAP4) has also been shown to be increased in hypertension, both during hypertrophy and in the transition to heart failure.[42] As MAP4 functions to both

stabilise microtubules (by preventing their disassembly) and to promote detyrosination,[39,42,277] the early upregulation of MAP4 during hypertrophy may increase detyrosination-mediated microtubule stabilisation, which in turn sensitises mechano-transduction and, by extension, mechano-sensitivity.

1.4.2.2. Potential Mechanisms of Mechano-Arrhythmogenicity in Hypertension

Hypertensive remodelling of the ventricular cytoskeleton results in a dense, stable MTN that is laterally reinforced within the cell (*via* junctional interactions between detyrosinated tubulin, desmin, and MAP4).[36] Increased lateral reinforcement facilitates the load-bearing capability of the MTN, and consequently, its ability to transduce mechanical stimuli.[24] The proliferated and reinforced cytoskeleton in hypertension thus contributes to increased cellular stiffness and mechano-sensitivity. In this mechano-hyper-sensitive setting, the magnitude of a mechanical stimulus needed to elicit an electrical response should be reduced, such that a smaller fluctuation in ventricular load may trigger an arrhythmia. A role for increased MTN mechano-sensitivity in mechano-arrhythmogenicity has been corroborated in several experimental models, including one in which an acute pharmacologically-induced increase in microtubule proliferation and detyrosination in the whole heart (with paclitaxel) was associated with an increased prevalence of acute volume pulse-induced mechano-arrhythmogenicity.[212]

Enhanced mechano-transduction associated with elevated levels of microtubule detyrosination in hypertension will increase the production of mechano-electric mediators. Indeed, X-ROS production and Ca^{2+} spark frequency have been shown scale with acute alterations in detyrosination levels.[132] Further, NOX2 is upregulated in hypertension, which

will additionally enhance the effect of the MTN on X-ROS production.[151] In addition to ROS-mediated sensitisation of RyR promoting Ca^{2+} leak,[221,222] ROS leads to an increase in the auto-phosphorylated form of Ca^{2+}/calmodulin-dependent kinase II (CaMKII).[72] Increased CaMKII activity may further contribute to aberrant Ca^{2+}-handling through diastolic RyR leak,[1] thus promoting an arrhythmogenic substrate (*i.e.*, elevated cytosolic Ca^{2+} levels) for mechano-arrhythmogenicity. Mechano-electric mediators may additionally modulate the activity of mechano-electric effectors (*i.e.*, MSC),[5,332] whose intracellular trafficking and mechanical stimulation with stretch may be affected by alterations of the MTN in hypertension.[216] As such, pathologic remodelling of mechano-transducers and the resultant effect on ventricular mechano-sensitivity may contribute to both triggers and substrate for mechano-arrhythmogenicity in hypertension.

1.5. Goals and Hypotheses

It is clear that the heart responds to acute changes in its mechanical environment through an intricate mechano-sensory system that manifests in responses at the cellular and subcellular level.[146] Pathologic changes in myocardial mechanics and haemodynamics result in altered mechano-sensitivity, such that acute fluctuations in load become emergent triggers for arrhythmic activity *via* mechanically-induced changes in electrophysiology or intracellular Ca^{2+} ('mechano-arrhythmogenicity').[232] Despite the prevalence of cardiac disease states characterised by altered myocardial mechanics, contractile dyskinesis, and increased external load, molecular mechanisms driving mechano-arrhythmogenicity remain poorly defined.[10,216] **Ultimately, the goal of my dissertation is to identify specific**

cellular and subcellular mechanisms of ventricular mechano-arrhythmogenicity by investigating models of two pathologic states: acute ischaemia and chronic hypertension. This was broken up into four discrete projects, described below.

1.5.1. Project 1

Changes in mechano-electric mediators of mechano-arrhythmogenicity during acute ischaemia. During acute ischaemia, there is an increased incidence of mechano-arrhythmogenicity that appears to relate to aberrations in subcellular Ca^{2+} handling, as buffering intracellular Ca^{2+} in this setting reduces arrhythmia incidence.[13] Under physiological conditions, Ca^{2+} spark rate is acutely increased by stretch,[116] due to mechano-sensitive X-ROS production.[221] In acute regional ischaemia, there is an increase in the baseline level of Ca^{2+} sparks and ROS,[179,234] as well as localised stretch of ischaemic tissue,[53] each of which has been implicated in arrhythmogenesis. **Thus, the goal of my first study was to investigate the effect of ischaemia on the mechanically-induced increase in Ca^{2+} sparks and ROS in ventricular myocytes. I hypothesised that ischaemia potentiates the stretch-induced increase in Ca^{2+} spark rate and ROS production, and consequently contributes to aberrant Ca^{2+} handling.**

1.5.2. Project 2

The role of changes in voltage-Ca^{2+} dynamics in ventricular mechano-arrhythmogenicity during acute ischaemia. Previous work in the whole heart has demonstrated that ischaemia results in the temporal uncoupling of voltage -Ca^{2+} recovery dynamics, facilitated by hypoxia-induced activation of K_{ATP} channels.[13] This results in a

potentially VP in late repolarisation during which intracellular Ca^{2+} levels remain high in repolarising (and thus, progressively re-excitable) tissue.[13,34,280] To determine if a stretch during this VP can act as a mechanical trigger for premature excitation, and to isolate the specific mechanistic role of this VP in mechano-arrhythmogenicity (without the additional electrophysiological changes that accompany ischaemia), cellular investigations in which the cell's environment can be controlled and in which stretch can be timed precisely around the VP are required. **Thus, the goal of my second study was to define mechanisms of mechano-arrhythmogenicity during acute alterations in voltage-Ca^{2+} dynamics induced by K_{ATP} activation in ventricular myocytes. I hypothesised that K_{ATP} activation (with pinacidil) would result in a cellular VP, and that stretch-induced arrhythmia incidence would be enhanced specifically in that period.**

1.5.3. Project 3

Cellular mechanisms of mechano-arrhythmogenicity during acute ischaemia. The motivation for my third project was driven by results found in **Projects 1 and 2**. **Project 1** demonstrated that ischaemia enhances mechano-sensitive Ca^{2+} spark rate and X-ROS production,[33] while **Project 2** showed that a specific mechano-sensitive[25] and Ca^{2+}-permeable channel (TRPA1)[193] can act as a source for mechano-arrhythmogenicity through a Ca^{2+}-mediated mechanism.[34] **Thus, the goal of my third project was to investigate the importance of TRPA1 and alterations in Ca^{2+} and ROS for mechano-arrhythmogenicity in ventricular myocytes during acute ischaemia, and to define the specific role of the VP. As TRPA1 has been recently shown to be activated in**

ischaemia,[47] presumably through an increase in intracellular Ca^{2+} or ROS levels,[5,332] I hypothesised that TRPA1 may indeed play an important role in mechano-arrhythmogenicity during acute ischaemia. Further, while my results described above found that pinacidil increases mechano-arrhythmogenicity in a temporally-independent manner,[34] I hypothesised that, in full ischaemia, the generation of an ischaemic VP, concomitant with aberrations in Ca^{2+} handling and ROS production, may result in a pro-arrhythmic substrate that is prone to mechanically-induced triggering of arrhythmic events specifically in the VP.

1.5.4. Project 4

The importance of mechano-transducers for mechano-arrhythmogenicity in chronic hypertension. The integrity of the MTN, which is dependent on the density (*via* polymerisation) and stability (*via* post-translational modifications) of the microtubules,[36] has been previously implicated in mechano-transduction and the generation of mechano-electric mediators (*e.g.*, X-ROS, Ca^{2+} sparks).[132] Detyrosination is a post-translational modification of microtubules that confers stability and facilitates junctional interactions with intermediate proteins (*e.g.*, desmin), thereby facilitating load-bearing capabilities and mechano-transduction.[243,247] Experimental reduction of microtubule detyrosination or polymerisation has resulted in the prevention of stretch-induced increases in Ca^{2+} spark rate and X-ROS.[132] Increased expression of detyrosinated tubulin, on the other hand, as occurs in some chronic cardiac pathologies (*e.g.*, hypertrophy or Duchenne's muscular dystrophy),[15,250] has been shown to increase the magnitude of X-ROS and stretch-induced Ca^{2+} sparks.[132] Additionally, an increased incidence of mechano-arrhythmogenicity has

been demonstrated in these pathologies. This increase in mechano-arrhythmogenicity is believed to be due to alterations in the MTN resulting in an increased mechano-sensitivity, and consequential increase in mechano-chemical mediators.[46,132] Pharmacological agents allow us to acutely modify the integrity of the MTN, in order to isolate its specific contribution to mechano-arrhythmogenicity. **Thus, the goal of my fourth project was to investigate the effect of acute alterations in the density (*via* changes in polymerisation) or stability (*via* post-translational modifications) of the MTN on the incidence of mechano-arrhythmogenicity in ventricular myocytes. I hypothesised that increasing the density or stability of the MTN would result in an increased incidence of stretch-induced arrhythmias, and that this effect could be mitigated by disrupting the MTN integrity.**

1.6. Figures

Figure 1.1 | **The cardiac mechano-electric regulatory loop**. Concept map for the cardiac mechano-electric regulatory loop describing the feedforward and feedback links between mechanical and electrical activity in the heart. (From Quinn and Kohl, 2020).

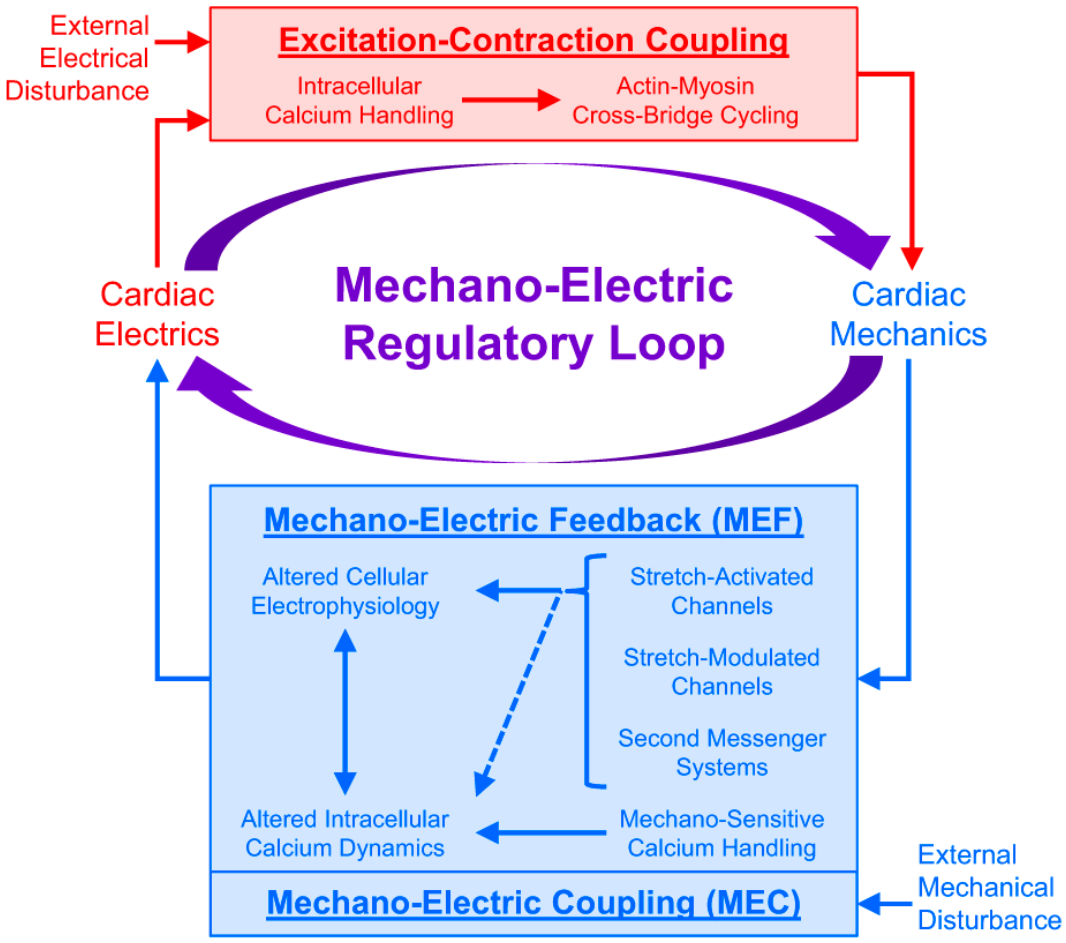

Figure 1.2 | **Mechano-gated and mechano-sensitive ion channels**. The various mechano-gated and mechano-sensitive ion channels and the organisms in which they are found. Mechano-gated channels are those whose activity is directly influenced by stretch, whereas mechano-sensitive channels are those that are primarily activated by other factors, but whose activity can be modulated by stretch. Of the channels found in mammals (white box), red indicates those with reported expression in the heart. Underlined channels have been identified as mechano-gated channels (From Peyronnet et al., 2016)

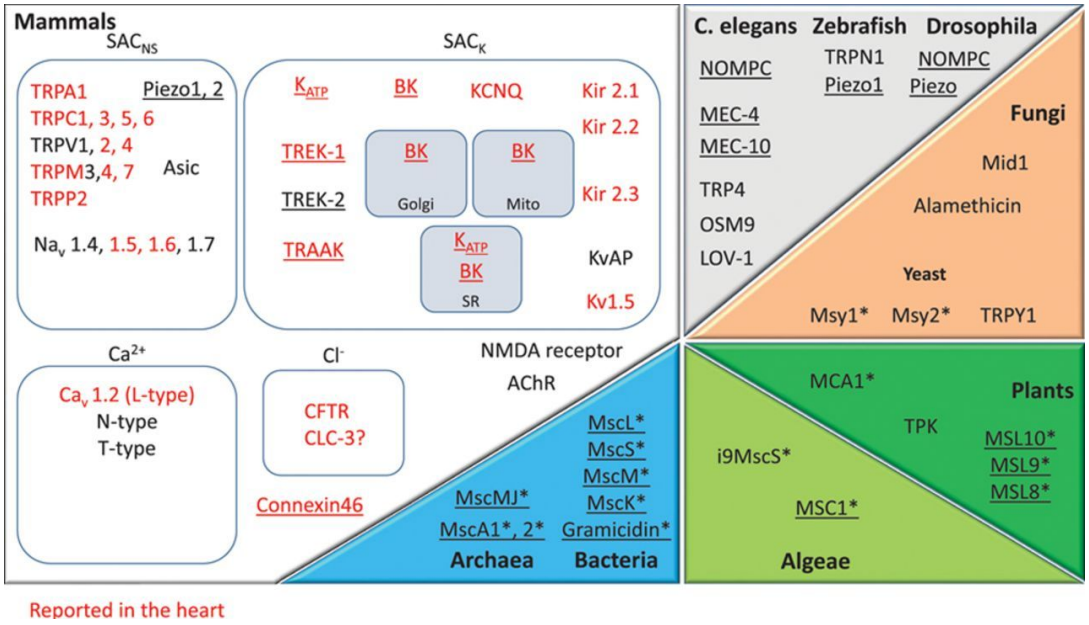

Figure 1.3 | Schematic of the electrophysiological changes during ischaemia. Schematic of substrate-level changes during ischaemia, and how they influence the morphology of the cardiac action potential and conduction.

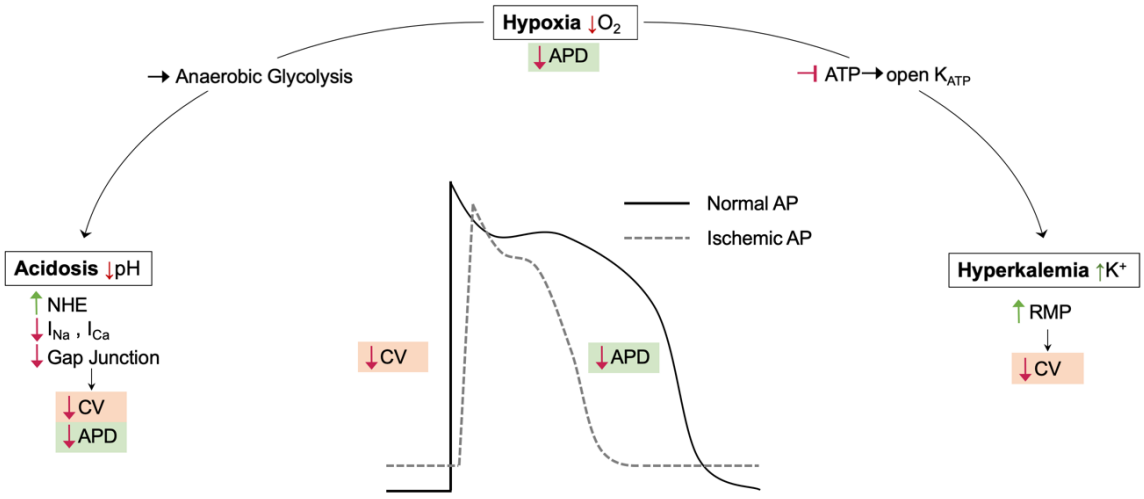

CHAPTER 2: ISCHAEMIA ENHANCES THE ACUTE STRETCH-INDUCED INCREASE IN CALCIUM SPARK RATE IN VENTRICULAR MYOCYTES

The contents of this chapter reflect work that is currently available as a published manuscript in a special issue of *Frontiers in Physiology* (Cameron BA, Kaihara K, Kai H, Iribe G, Quinn TA. Ischemia enhances the acute stretch-induced increase in calcium spark rate in ventricular myocytes. *Front Physiol*. 2020; 11:289). In consultation with Drs. Alex Quinn and Gentaro Iribe, I was directly involved in the conception and design of the study. To carry out this research, I was awarded a joint Mitacs-Japan Society for the Promotion of Science (JSPS) Globalink Fellowship to perform a collaborative study with Dr. Gentaro Iribe at his lab in Okayama, Japan. I performed all the experiments, acquired and analysed all data, wrote the initial draft of the manuscript, and revised it with the help of Drs. Quinn and Iribe.

2.1. Abstract

Rationale: In ventricular myocytes, Ca^{2+} spark rate is acutely increased by stretch, due to a stretch-induced increase of ROS production. In acute regional ischaemia, there is an increase in Ca^{2+} sparks and ROS production, and stretch of ischaemic tissue, each of which may be arrhythmogenic. Yet, whether there is an effect of ischaemia on the stretch-induced increase in Ca^{2+} spark rate and ROS has not been tested. We hypothesised that ischaemia would enhance mechano-sensitive Ca^{2+} sparks rate and ROS production. **Methods:** Murine ventricular myocytes (male, C57BL/6J) were loaded with fluorescent dye to detect Ca^{2+} sparks (4.6 μM Fluo-4) or ROS (1 μM DCF), exposed to normal Tyrode (NT) or simulated ischaemia (SI) solution (hyperkalemia [15mM potassium], acidosis [6.5 pH], and metabolic inhibition [1mM sodium cyanide, 20mM 2-deoxyglucose]), and subjected to sustained stretch using carbon fibres (~10% increase in sarcomere length, 15s). Ca^{2+} spark rate and ROS production were measured by confocal microscopy. **Results:** Baseline Ca^{2+} spark rate was greater in SI than NT (2.54±0.11 *vs* 0.29±0.05 sparks·s^{-1}·100 μm^{-2}; $p<0.0001$). Stretch resulted in an acute increase in Ca^{2+} spark rate in both SI and NT (SI: 3.03±0.13; NT: 0.49±0.07 sparks·s^{-1}·100 μm^{-2}; $p<0.0001$), with a greater increase in SI than NT (+0.49±0.04 *vs* +0.20±0.04 sparks·s^{-1}·100 μm^{-2}; $p<0.001$). Similarly, baseline rate of ROS production was greater in SI than NT (1.01±0.01 *vs* 0.98±0.01 normalized slope; $p<0.05$), as was the increase with stretch (+12.5±2.6 *vs* +2.1±2.7%; $p<0.05$). **Conclusion:** Ischaemia enhances the stretch-induced increase of Ca^{2+} spark rate and ROS production in ventricular myocytes. This effect may be important for premature excitation and/or in the development of an arrhythmogenic substrate in acute regional ischaemia.

2.2. Introduction

In cardiac myocytes, Ca^{2+} sparks represent the elementary release of Ca^{2+} from the sarcoplasmic reticulum (the cell's primary Ca^{2+} store) *via* RyR, and thus play a critical role in intracellular Ca^{2+} handling. The frequency of Ca^{2+} sparks is determined by RyR open probability, which under normal conditions, is primarily influenced by the free intracellular Ca^{2+} concentration ($[Ca^{2+}]_i$) and the concentration of Ca^{2+} in the sarcoplasmic reticulum.[43] In pathological settings, an elevation in Ca^{2+} spark rate, due to increased $[Ca^{2+}]_i$ or altered RyR function (secondary to metabolic, adrenergic, or genetic changes, or to channel phosphorylation, oxidation, or nitrosylation),[220] has been implicated in the induction of aberrant Ca^{2+} waves and deadly cardiac arrhythmias.[137]

Recently, it has been shown that stretch of single ventricular myocytes can also acutely increase Ca^{2+} spark rate,[116] which has been suggested to perhaps "tune" excitation-contraction coupling in the whole heart,[220,222,224] thus contributing to the Frank Starling mechanism[230] and acting to maintain contractile homogeneity across the ventricles by normalizing inter-cellular contractile force.[35,228] Follow up studies have shown that the acute stretch-induced increase in Ca^{2+} sparks results from a microtubule-dependent increase in ROS production by NOX2 with stretch, termed X-ROS.[221] Further, Ca^{2+} spark rate and X-ROS production have been found to be enhanced by cyclic stretch (as occurs during filling with each heartbeat) and graded by stretch amplitude and frequency, which may additionally tune the mechanical activity and redox state of cardiac myocytes to changes in physiological demand.[223]

An acute stretch-induced increase in Ca^{2+} sparks may be particularly relevant in disease states associated with heterogeneous changes in the heart's mechanical activity.[226]

In patients suffering from acute regional ischaemia, there is stretch of ischaemic tissue, with the magnitude of stretch relating to the prevalence of ventricular fibrillation.[7,8,9,11,103] Moreover, there is a correlation between wall motion abnormalities and arrhythmia incidence in ischaemia,[30,264] with ectopic excitation often originating from regions where systolic segment lengthening occurs.[53,154] In experimental models of non-uniform contraction, on the other hand, there is an increase in ROS production localised to stretched regions, which results in the activation of Ca^{2+} waves.[192] Thus, in ischaemia, a stretch-induced increase in Ca^{2+} sparks may act as a trigger, or contribute to the substrate, for the associated arrhythmias.[124]

Myocardial ischaemia is also associated with an increase in $[Ca^{2+}]_i$,[12] leading to a rise in CaMKII activity,[180] which increases phosphorylation of RyR and the frequency of Ca^{2+} sparks.[176] Computational modelling has suggested that an elevation in $[Ca^{2+}]_i$ associated with hyperkalemia-induced membrane depolarisation, along with a consequential reduction in NCX-mediated Ca^{2+} efflux and an increase in sarcoplasmic reticulum Ca^{2+} content, may also contribute to an increase in Ca^{2+} spark rate during ischaemia.[249] Ca^{2+} spark rate is further increased in ischaemia by an increase in ROS,[234] including a contribution of enhanced NOX2 activity,[67] which increases the open probability of RyR by *S*-glutathionylation,[248] and sensitizes RyR to cytoplasmic Ca^{2+}.[14,327] In fact, an increased Ca^{2+} spark rate has been shown to be a contributor to the elevation in $[Ca^{2+}]_i$ in ischaemia.[179] At the same time, ischaemia is associated with a reduction of the key anti-oxidant glutathione,[75,217]which computational modelling has suggested may increase the effects of stretch-induced ROS on Ca^{2+} sparks, by limiting cellular reducing capacity through a decrease in glutathione, resulting in a consequential increase in the open

probability of RyR during stretch.[168] Combined, these effects on RyR activity and its modulators suggests that ischaemia may modulate the response of Ca^{2+} sparks to stretch, yet the effect of ischaemia on the stretch-induced increase in Ca^{2+} spark rate has not been investigated.

We hypothesized that in simulated ischaemic conditions, there would be an enhancement of the stretch-induced increase in Ca^{2+} sparks, with an associated potentiation of the stretch-induced increase in ROS production. Ventricular myocytes isolated from mice were subjected to a single controlled stretch using carbon fibres in physiologic or simulated ischaemic conditions.[116] Fluorescent confocal microscopy was used to monitor $[Ca^{2+}]_i$ or ROS to assess the effect of stretch on Ca^{2+} spark rate and ROS production in these conditions. Our results demonstrate that ischaemia enhances the stretch-induced increase of Ca^{2+} spark rate in isolated ventricular myocytes, with an associated enhancement of stretch-induced ROS production. The enhanced mechano-sensitive production of these mechano-electric mediators (*i.e.,* intracellular Ca^{2+} and ROS) may contribute to the lethal arrhythmias that occur in the setting of acute ischaemia.

2.3. Methods

2.3.1. Ethics Statement

Experiments were performed in accordance with the Guidance Principles for the Care and Use of Animals established by the Council of the Physiological Society of Japan. The experimental protocol was reviewed and accepted by the Animal Subjects Committee of Okayama University Graduate School of Medicine, Dentistry, and Pharmaceutical

Sciences. Details of experimental protocols have been reported following the Minimum Information about a Cardiac Electrophysiology Experiment (MICEE) reporting standard.[225]

2.3.2. Ventricular Myocyte Isolation

Ventricular myocytes were isolated from mice as previously described.[117,118] Mice (male C57BL/6J, 8-12 weeks old) were administered an intraperitoneal injection of heparin sodium (100 I.U.; Wockhardt, Mumbai, India). After 30 min, surgical anesthesia was induced by inhalation of isoflurane (IsoFlu; Abbott Laboratories, Abbott Park, USA) followed by rapid cardiac excision, aortic cannulation, and Langendorff perfusion for enzymatic cell isolation. Hearts were perfused at a rate of 4 mL/min for 3 min with Ca^{2+}-free solution (composition in mM: 128 NaCl, 2.6 KCl, 1.18 $MgSO_4$, 1.18 KH_2PO_4, 10 HEPES, 20 Taurine, 11 Glucose; pH 7.47 adjusted with NaOH), followed by 5-6 min of perfusion with 30 mL of Ca^{2+}-free solution that included 6 mg of the enzyme blend Liberase TM Research Grade (Roche, Basel, Switzerland). The ventricles were harvested by cutting along the atrioventricular border, and then cut into 1-2 mm^3 cubes and gently agitated in oxygenated Ca^{2+}-free solution. The supernatant containing ventricular cells was collected, the remaining tissue was resuspended in fresh Ca^{2+}-free solution, and the above procedure was repeated in triplicate. The collected supernatant was passed through a nylon mesh and centrifuged at 15 × g for 3 min, followed by resuspension of the resulting cell pellet in normal Tyrode's solution (NT, composition in mM: 140 NaCl, 5.4 KCl, 1.8 $CaCl_2$, 1 $MgCl_2$, 5 HEPES, 11 Glucose; pH 7.4 adjusted with NaOH). Cells were kept at room temperature (~22°C) until ready to be used.

2.3.3. Single-Cell Stretch

Two groups of quiescent ventricular myocytes were considered: a control group (exposed to NT) and a simulated ischaemia group (exposed to an ischaemic solution containing [in mM]: 140 NaCl, 15 KCl, 1.8 $CaCl_2$, 1 $MgCl_2$, 10 HEPES, 1 NaCN, 20 2-deoxyglucose, and with pH adjusted to 6.5 using NaOH,[139,196] which mimicked the ~30 min time point of ischaemia (phase 1b)[78,197,210,289,312,317] through hyperkalemia [15 mM extracellular potassium], extracellular acidosis [pH 6.5], and metabolic inhibition [block of oxidative phosphorylation with 1 mM NaCN and inhibition of anaerobic glycolysis with 20 mM 2-deoxyglucose]). Within a 30 min window from the beginning of exposure to the simulated ischaemia solution, healthy cells (rod-shaped with clear striations, an intact membrane with no signs of blebbing, and no spontaneous intracellular Ca^{2+} waves before stretch) were subjected to a controlled, axial stretch at a single time point using the carbon fibre technique, as has been previously described for axial stretch of single ventricular myocytes.[114,116] Cells were placed on coverslips coated with poly-2-hydroxyethyl methacrylate (poly-HEMA; Sigma-Aldrich, Tokyo, Japan) to prevent cellular adhesion. Carbon fibres (10 μm in diameter) mounted in glass capillaries that adhere to isolated cells through biophysical interactions[215] were attached to either end of an individual cell. For experiments examining the effect of stretch on Ca^{2+} sparks, one 'compliant' (1.2 mm) and one 'stiff' (0.6 mm) carbon fibre were used, while for the ROS experiments two compliant (1.2 mm) carbon fibres were used (Tsukuba Material Information Laboratory, Tsukuba, Japan). Tri-axial positioning of the carbon fibres was performed by custom-made three-axis hydraulic manipulators (Narishige, Tokyo, Japan), with the compliant fibres mounted on piezo-electric translators (P-621.1 CL; Physik Instrumente, Karlsruhe, Germany) and

the stiff fibre held stationary. While the unidirectional stretch using one stiff stationary and one compliant translating carbon fibre was sufficient for the Ca^{2+} spark experiments, this produced too much cellular motion under the detector during stretch for ROS production to be measured. The bi-directional stretch using two compliant translating carbon fibres reduced the level of cell motion, so allowed for more accurate measurements of ROS. Whole-cell axial stretch was applied by a 20 μm increase in the separation of the piezo-electric translators and held for 15 s, controlled by custom-written LabView software and a fast analogue-to-digital converter (NI USB-6259; National Instruments, Austin, USA), which has been shown previously to result in a ~10% increase in sarcomere length.[119]

2.3.4. Measurement of Ca^{2+} Spark Rate

Detection of Ca^{2+} sparks in ventricular myocytes was performed similar to a previously described technique.[116] Cells were incubated with Fluo-4-AM (4.6 μM, 10 min; Invitrogen, Carlsbad, California). Confocal images (XY, 30 fps, CSU-X1; Yokogawa, Tokyo, Japan) were obtained by excitation with a 488 nm laser and fluorescence emission collected above 505 nm. Ca^{2+} sparks were detected in the cellular region between the carbon fibres using custom LabVIEW software. Ca^{2+} spark rate was calculated by counting the number of sparks detected over 5 s, excluding duplicate counts by subtracting single-coordinate spark fluorescence that exceeded one contiguous frame, and was normalised by area (to control for variability in cell size) and reported as sparks$\cdot s^{-1} \cdot 100\ \mu m^{-2}$. The rate of image acquisition limited additional measurements of spark dynamics. Ca^{2+} spark rate was measured over three 5 s intervals: immediately before stretch, during stretch (immediately after its application), and immediately following complete release of stretch. Any cell in

which an intracellular Ca^{2+} wave or synchronised sarcoplasmic reticulum Ca^{2+} release occurred during the analysis window was excluded (8% of cells in both conditions).

2.3.5. Measurement of ROS Production

The rate of intracellular ROS production was measured using 2',7'-dichlorofluorescein diacetate (DCF) as previously described.[119] Cells were loaded with DCF (1 μm, 20 min; Life Technologies Japan, Tokyo, Japan) and confocal images (FV1000; Olympus Corporation, Tokyo, Japan) were captured (XY, 1.27 fps) by excitation with a 488 nm laser and fluorescence emission collected above 500 nm. As DCF fluorescence is known to be artificially amplified by continuous light exposure,[221,223] a low laser intensity was used. ROS production rate was measured in the cellular region between the carbon fibres with custom LabView software as the slope of the increase in fluorescence over three 15 s intervals: immediately before, during, and immediately following release of stretch.

2.3.6. Statistics

Data are presented as mean ± standard error of the mean (SEM). For the Ca^{2+} spark rate measurements, as the data was not normally distributed, Kruskal-Wallis test with *pot-hoc* Dunn's multiple comparisons test was used to assess Ca^{2+} spark rate over time, and Wilcoxon paired, or Mann-Whitney unpaired tests were used for comparison of group means. For the ROS measurements, two-tailed paired or unpaired Student's t-tests were used for comparison of group means. $p < 0.05$ was considered statistically significant.

2.4. Results

2.4.1. Effect of Stretch on Ca^{2+} Spark Rate During Simulated Ischaemia

Figure 2.1 shows surface plots of Fluo-4 fluorescence derived from a line of pixels across the confocal images of a cell, demonstrating the effect of stretch on the occurrence of Ca^{2+} sparks in single mouse ventricular myocytes exposed to either NT (Fig. 2.1a) or simulated ischaemia (Fig. 2.1b). Ca^{2+} sparks occur more frequently in simulated ischaemia than NT, and acutely increase in both groups during stretch, with a return to normal levels after stretch release.

Figure 2.2 shows the Ca^{2+} spark rate before, during, and after stretch, and the change with stretch, in cells of the NT or simulated ischaemia group over the 30 min measurement window. Cells were subjected to stretch at a single time point and values from all cells stretched within 5 min intervals were averaged. There was no effect of time on Ca^{2+} spark rate (Fig. 2.2a) or its change with stretch (Fig. 2.2b) in the NT group, as values before, during, and after stretch and the change with stretch did not vary over the 30 min. There was variation of Ca^{2+} spark rate over 30 min in the simulated ischaemia group (Fig. 2.2c; $p<0.05$ by Kruskal-Wallis test), however, values only differed between the 6-10 min and 26-30 min time points ($p<0.01$, by *post hoc* Dunn's multiple comparisons test), and there was no effect of time on the change in Ca^{2+} spark rate with stretch (Fig. 2.2d). Thus, as the change in Ca^{2+} spark rate with stretch did not vary over the 30 min experimental window in either group, all cells in each group were averaged for further analysis.

Figure 2.3 shows the effect of stretch on Ca^{2+} spark rate averaged across all cells in the NT (n=33 cells, N=9 mice) or simulated ischaemia (n=103 cells, N=10 mice) group. The average Ca^{2+} spark rate was higher in simulated ischaemia than NT (Fig. 2.3a), both

at baseline (2.54 ± 0.11 *vs* 0.29 ± 0.05 sparks·s^{-1}·100 μm^{-2}, p<0.0001 by Mann-Whitney unpaired test) and during stretch (3.03 ± 0.13 *vs* 0.49 ± 0.07 sparks·s^{-1}·100 μm^{-2}; p<0.0001). With stretch, Ca^{2+} spark rate was acutely increased in both NT (+0.20 ± 0.04 sparks·s^{-1}·100 μm^{-2}; p<0.0001 by Wilcoxon paired test) and simulated ischaemia (+0.49 ± 0.04 sparks·s^{-1}·100 μm^{-2}; p<0.0001), with a larger increase in Ca^{2+} spark rate with stretch in simulated ischaemia compared to NT (p<0.0001; Fig. 2.3b).

2.4.2. Effect of Stretch on ROS Production During Simulated Ischaemia

To determine whether the observed enhancement of the stretch-induced increase in Ca^{2+} sparks in simulated ischaemia compared to NT is associated with a concomitant enhancement of the stretch-induced increase in ROS production that has been shown by others,[221] cells were loaded with DCF to assess the rate of ROS production before and during stretch (measured as the slope of the change in DCF fluorescence over time). Figure 2.4 shows the effect of stretch on the rate of ROS production in cells exposed to NT (n=12 cells, N=4 mice) or simulated ischaemia (n=11 cells, N=8 mice). The rate of ROS production was greater in simulated ischaemia than in NT both at baseline (1.01 ± 0.01 *vs* 0.98 ± 0.01 normalised slope; p<0.05 by two-tailed unpaired Student's t-test) and during stretch (1.14 ± 0.03 *vs* 1.00 ± 0.03; p<0.01, Fig. 2.4a). With stretch, the rate of ROS production was acutely increased in simulated ischaemia (+12.5 ± 2.6%; p<0.001 by two-tailed paired Student's t-test), but not in NT (+2.1 ± 2.7%; Fig. 2.4b).

2.5. Discussion

This study sought to determine the effect of ischaemia on the increase in Ca^{2+} spark rate and ROS production that occurs with stretch in ventricular myocytes. It was found that in simulated ischaemic conditions, the basal level of both Ca^{2+} spark rate and ROS production were greater than in control, and that the increase in spark rate with stretch was enhanced in ischaemic conditions. The enhanced response of Ca^{2+} spark rate to stretch represents a potential contributing mechanism to aberrant Ca^{2+} handling in ischaemia, and could be a source of premature excitation and the arrhythmogenic substrate in this setting.

2.5.1. Mechanisms of Ventricular Arrhythmias in Acute Regional Ischaemia

Acute regional ischaemia is a major cause of sudden cardiac death,[245,331] with lethal ventricular arrhythmias accounting for 80% of all cases without a prior history of heart disease.[198] Arrhythmias in the first hour of ischaemia (during which approximately 50% of all sudden cardiac deaths occur)[65] are both focal and re-entrant in nature, resulting from a combination of ischaemia-induced changes in electrical, mechanical, and biochemical properties of the myocardium.[38,124]

The arrhythmogenic changes in ventricular myocyte electrophysiology during acute ischaemia have been extensively studied.[38,124] The most prominent effects include: (i) a decrease in ATP, pH, and the fast N^+ and L-type Ca^{2+} currents; (ii) an increase in intracellular Ca^{2+} and Na^+ concentrations; and (iii) activation of the K_{ATP} current. At the same time, extracellular K^+ concentration and catecholamine levels are also increased. All of the above changes (other than the increase in catecholamine levels) were simulated or present in the current study. These effects have been shown to result in arrhythmogenic

alterations of the ventricular action potential, including: (i) depolarisation of the resting membrane potential; (ii) a decrease in the action potential upstroke, amplitude, and duration; and (iii) an increase in the effective refractory period.

Other, poorly understood cell-level effects are thought to contribute to ventricular arrhythmias in acute ischaemia, including cell stretch and changes in intracellular Ca^{2+} handling. The acute phase of ischaemia is associated with tissue stretch, which may result in ectopic excitation,[53,154] and whose magnitude correlates with the prevalence of ventricular fibrillation.[7,8,9,11,103] At the same time, acute ischaemia causes an increase in the frequency of Ca^{2+} sparks that contributes to an increase in $[Ca^{2+}]_i$.[179] The increase in $[Ca^{2+}]_i$ is thought to be arrhythmogenic[12] by driving excitatory after-depolarisations.[20,318,320] Thus, if links exist between cell stretch and altered Ca^{2+} handling in ischaemia, they could represent important mechanisms for arrhythmogenesis.

2.5.2. Effects of Stretch on Ca^{2+} Spark Rate

The frequency of Ca^{2+} sparks is determined by RyR open probability, which is strongly influenced by $[Ca^{2+}]_i$ and the concentration of Ca^{2+} in the sarcoplasmic reticulum.[43] Previous studies have shown that in healthy conditions, stretch acutely increases the frequency of Ca^{2+} sparks in ventricular cells,[116] which is the result of an increase X-ROS production facilitated by mechano-transduction *via* the microtubules.[221] Interestingly, Ca^{2+} spark rate and X-ROS production are further increased by cyclic stretch (compared to sustained stretch), which is more similar to what occurs in the regularly beating heart.[223] This response is also graded by the amplitude and frequency of stretch,[223] and so may help match the $[Ca^{2+}]_i$ and redox state of cardiac myocytes to changes in physiological demand.

In many diseases, there is an increase in the frequency of Ca^{2+} sparks, often due to an increase in $[Ca^{2+}]_i$ or altered RyR function (relating to cellular changes such as membrane depolarisation[249] or increased ROS),[220] which has the potential to lead to intracellular Ca^{2+} waves and cardiac arrhythmias.[137] This includes diseases in which there are changes in cardiac mechanics resulting in regions of localised tissue stretch.[226] For instance, in an experimental model of non-uniform myocardial contraction, it has been shown that there is an increase in ROS production localised to stretched regions, which can result in intracellular Ca^{2+} waves.[192] Interestingly, in a similar experimental model, it was found that Ca^{2+} waves in fact relate to the rapid shortening of muscle immediately after a period of stretch,[136] due to a surge in intracellular Ca^{2+} as it dissociates from TnC.[295] This Ca^{2+} surge is precipitated by a length-dependent increase in the affinity of TnC for Ca^{2+},[2] and can result in after-depolarisations, premature excitation,[188] and sustained arrhythmias.[189]

In the present study, we observed an acute increase in basal Ca^{2+} spark rate in ischaemia, which was further increased with stretch. This mechano-sensitive increase in Ca^{2+} spark rate was greater than that seen under normal conditions, representing an enhancement of the stretch-induced effect. Further, there was a higher baseline level of ROS production in ischaemia compared to control, as well as a greater increase in ROS production with stretch that may contribute to the higher levels of Ca^{2+} sparks (although, the difference in baseline level of ROS production between simulated ischaemia and control was small (3%), so may in fact not be physiologically significant).

While it is speculated that the enhancement of the stretch-induced increase in Ca^{2+} sparks in ischaemic conditions may represent an arrhythmogenic mechanism, we observed

few stretch-induced intracellular Ca^{2+} waves or synchronised sarcoplasmic reticulum Ca^{2+} release events, and the amount did not differ between ischaemic and control cells (1 *vs* 0% incidence of intracellular Ca^{2+} waves; 7 *vs* 5% occurrence of synchronized sarcoplasmic reticulum Ca^{2+} release events).

2.5.3. Mechanisms of Enhanced Mechano-Transduction in Ischaemic Conditions

The enhancement of the mechano-sensitive increase in mechano-electric mediators (*i.e.,* Ca^{2+} spark rate and ROS production) during ischaemia may result from effects on various factors involved in the stretch-induced response.[126,303] Ischaemia may increase the mechano-sensitivity or responsiveness of NOX2, and mechano-transduction may be increased due to changes in microtubule properties, cell stiffness, or MSC function (including TRP channels), resulting in greater X-ROS production with stretch. Alternatively (or additionally), rather than through an increase in the production of X-ROS, the effect of ROS levels on Ca^{2+} spark rate could be related to the reduction of anti-oxidants in the cell (as suggested by computational modelling),[168] as the key anti-oxidant glutathione is reduced in ischaemia.[75] At the same time, there could be a contribution of emergent, X-ROS-independent mechano-transduction pathways (*e.g.*, *via* direct effects relating to the baseline increase in $[Ca^{2+}]_i$ or ROS with ischaemia on MSC activity, CaMKII activation, RyR sensitivity to Ca^{2+}, or mitochondrial-derived Ca^{2+} and ROS production). These possibilities warrant further investigation, as they may represent novel anti-arrhythmic targets in acute ischaemia.

2.5.4. Comparison of Results to Previous Studies

In our work, under normal conditions, we observed an increase in the Ca^{2+} spark rate with axial stretch of isolated mouse ventricular myocytes, as has been previously reported by others in both rat[116,221] and mouse.[221] We did not, however, see an increase in ROS production with stretch (~2%; measured as the change in the slope of DCF fluorescence), as has been shown in other studies (~70% for rat, ~40% for mouse).[221] In ischaemic conditions, we did see a statistically significant stretch-induced increase in ROS production (~13%), along with a greater increase in Ca^{2+} spark rate than control (suggesting the increase in ROS might be involved), yet this increase was still much lower than the previously reported control values. The reason for this discrepancy is unclear. It may relate to methodological differences, or differences in data handling. Our experiments involved the stretch of ventricular myocytes using 10 μm diameter compliant carbon fibres, which stick to the cells through biophysical interactions.[215] The previous work from Prosser et al. (2011)[221] used 20 μm stiff glass rods adhered to the cells with a biological adhesive (Myotak, composed of laminin, entactin, heparin sulfate proteoglycan, gentamicin, Dulbecco's Modified Eagle Medium, collagen IV, Alexa Fluor-647 conjugated to bovine serum albumin, and an inert alumina silica aggregate with a diameter of 1 μm, dissolved in 100 μM BSA). While it was reported that none of these components are harmful to cells (as normal cell morphology and robust contractions are maintained for up to two hours following cell attachment), it could be there are unappreciated effects of Myotak on ROS production, which could account for the greater effect in the previous work. Alternatively, differences in imaging methods (for instance whole cell confocal measurements in the current study *vs* line scans in the previous report) or data analysis (such as measurement of

DCF fluorescence slope by fitting a linear relation across the entire stretch period *vs* the peak DCF slope extracted from a polynomial fit) might also be involved.

2.5.5. Potential Limitations

In the current study, ischaemia was simulated by a solution which mimicked the ~30 min time point of ischaemia (phase 1b),[78,197,210,289,312,317] including hyperkalemia, acidosis, and metabolic inhibition. Previous studies that exposed isolated ventricular myocytes to simulated ischaemic conditions have used a similar approach, but have simulated hypoxia by the use of a 90% nitrogen-10% carbon dioxide gas phase directed over the cell chamber,[50,206] or by bubbling the cell chamber with nitrogen to displace oxygen from the solution.[280] These methods, however, are not compatible with the carbon fibre technique or our fluorescence imaging, as they cause mechanical disruption and motion artefact. As such, we simulated hypoxia by targeting cellular oxygen metabolism through a combined block of oxidative phosphorylation (with sodium cyanide, NaCN) and anaerobic glycolysis (with 2-deoxyglucose), as previously reported.[139,196] One concern with this approach might be the effect of NaCN on cell viability. While we found that a majority of the cells exposed to our simulated ischaemia solution remained viable over the 30 min experimental period, to mitigate any concern that tested cells were unhealthy, we included only myocytes that appeared rod-shaped with clear striations, had an intact membrane with no signs of blebbing, and displayed no spontaneous intracellular Ca^{2+} waves. A second concern may be that the method of simulating ischaemia used in this study, as NaCN directly affects mitochondrial function, which is the main producer of ROS, this may have contributed to the attenuated levels of ROS production measured in our model.

Temperature has been previously shown to affect Ca^{2+} sparks, with a higher spark rate, amplitude, and time to peak at room temperature compared to 37°C, due to effects on sarcoplasmic reticulum Ca^{2+} stores and RyR function.[76,82] While our experiments were performed at room temperature (~22°C), this is in-line with previous studies testing the effect of stretch on Ca^{2+} sparks,[116,221] and it is not believed that that the associated difference in baseline spark rate is responsible for the fundamental effect of stretch on the frequency of Ca^{2+} sparks, nor the difference in the response of Ca^{2+} spark rate to stretch between NT and ischaemic cells (although, it may impact the magnitude of the response). Related to this concern, the increase in Ca^{2+} spark rate in ischaemia compared to control, as well as its increase with stretch, could be partially related to changes in intracellular Ca^{2+}, however this was not measured in the current study, as it would require the use of a ratiometric Ca^{2+}-imaging approach).

2.6. Conclusion

In the current study, we have demonstrated that ischaemia enhances the acute increase in Ca^{2+} spark rate that occurs with stretch of isolated ventricular myocytes, and an enhancement of stretch-induced ROS production. While the mechanisms of this enhanced mechano-electric mediator production remain unknown, they may contribute to the generation of Ca^{2+}-induced arrhythmias in acute ischaemia, and thus represent potential therapeutic targets for lethal arrhythmias.

2.7. Statements

2.7.1. Author Contributions

BAC contributed to the design of the study, performed the experimental work, analyzed the data, and wrote the manuscript. HK and KK provided technical support for the experiments. GI and TAQ contributed to the design of the study and revised the manuscript. All authors approved the final submission.

2.7.2. Funding

This work was supported through a Mitacs - Japan Society for the Promotion of Science (JSPS) Internship funded by a Mitacs Globalink Research Award and a JSPS International Research Fellowship (IT11003 to B.C.), by the JSPS (KAKENHI 17K01359 and 15K21745 to G.I.), by the Canadian Institutes of Health Research (MOP 342562 to T.A.Q.), and by the Natural Sciences and Engineering Research Council of Canada (RGPIN-2016-04879 to T.A.Q.). TAQ is a National New Investigator of the Heart and Stroke Foundation of Canada.

2.8. Figures

Figure 2.1 | Effect of sustained axial stretch on Ca^{2+} spark production in a single quiescent mouse ventricular myocyte exposed to NT or simulated ischaemia. Fluorescence surface plots are derived from a line of pixels across a cell in either NT (**a**), or a simulated ischaemic solution (**b**), showing the relative Fluo-4 fluorescence (F_{REL}) before, during, and after 15 s of stretch (dashed red lines).

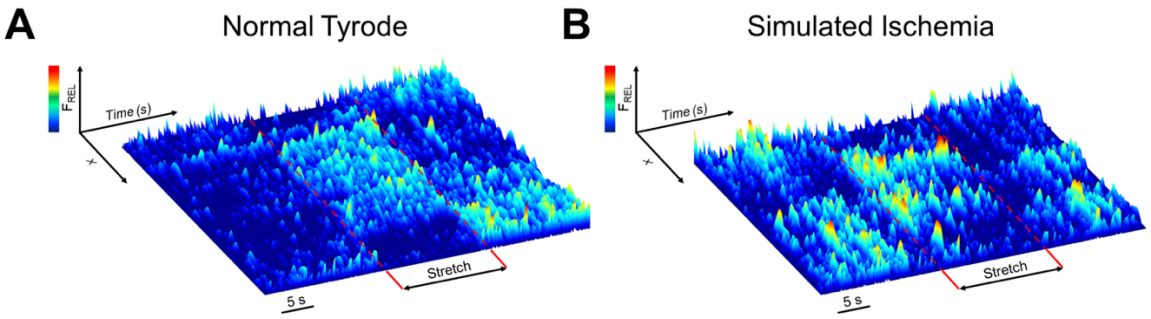

Figure 2.2 | Effect of duration of exposure to NT or simulated ischaemia on the Ca^{2+}spark rate in quiescent mouse ventricular myocytes. Average measured Ca^{2+} spark rate before (Baseline), during (Stretch), and after stretch (Release) (**a, c**), as well as the change in Ca^{2+} spark rate with stretch (Δ Ca^{2+} spark rate; **b, d**), over the 30 min measurement window in cells exposed to either NT (**a**, **b**; blue) or simulated ischaemia (**c**, **d**; red). Cells were subjected to stretch at a single time point and values from all cells stretched within 5 min intervals were averaged (presented as mean ± SEM). *N* = mice; *n* = cells. **p*<0.01 by *post hoc* Dunn's multiple comparisons test.

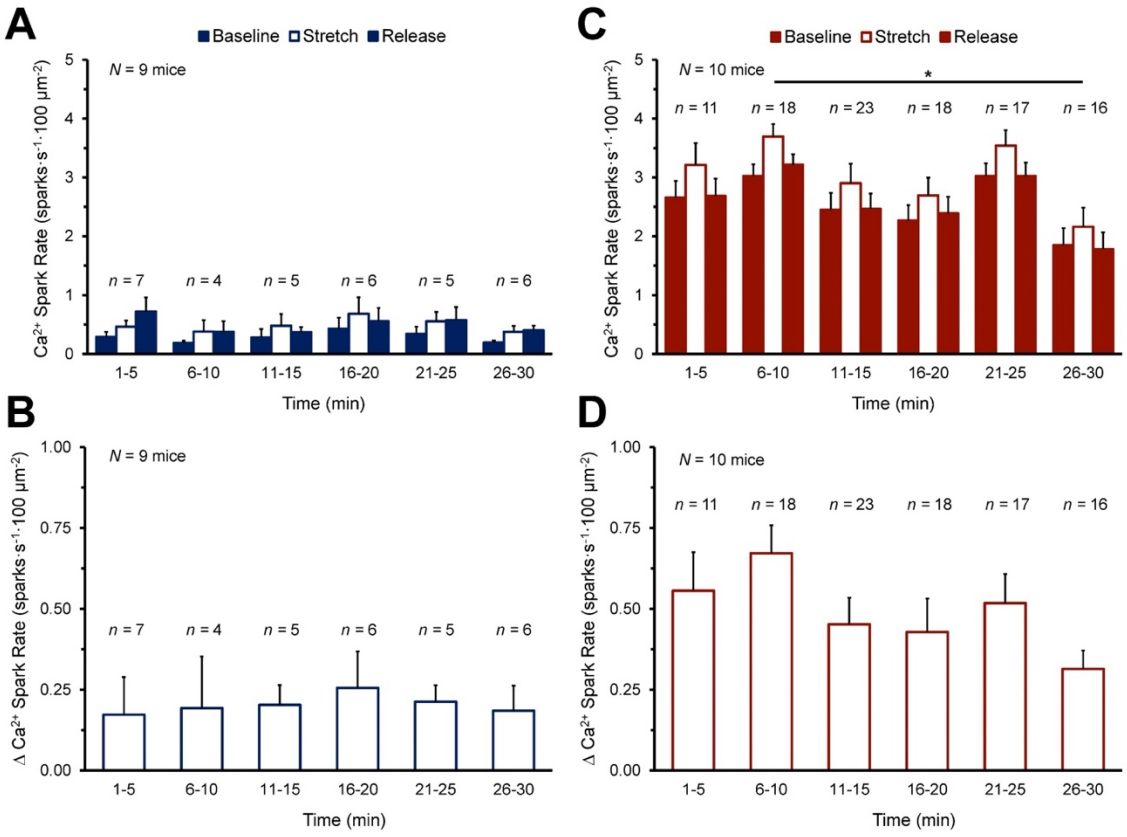

Figure 2.3 | Effect of stretch on Ca^{2+} spark rate in quiescent mouse ventricular myocytes exposed to either NT or simulated ischemia. Average measured Ca^{2+} spark rate before (Baseline) and during stretch (Stretch; **a**) and the change in Ca^{2+} spark rate with stretch (Δ Ca^{2+} spark rate; **b**) averaged across all cells exposed to either NT (blue) or a simulated ischaemia (red) solution (presented as mean ± SEM). *p<0.0001 by Wilcoxon paired test; #p<0.0001 by Mann-Whitney unpaired test. N = mice; n = cells.

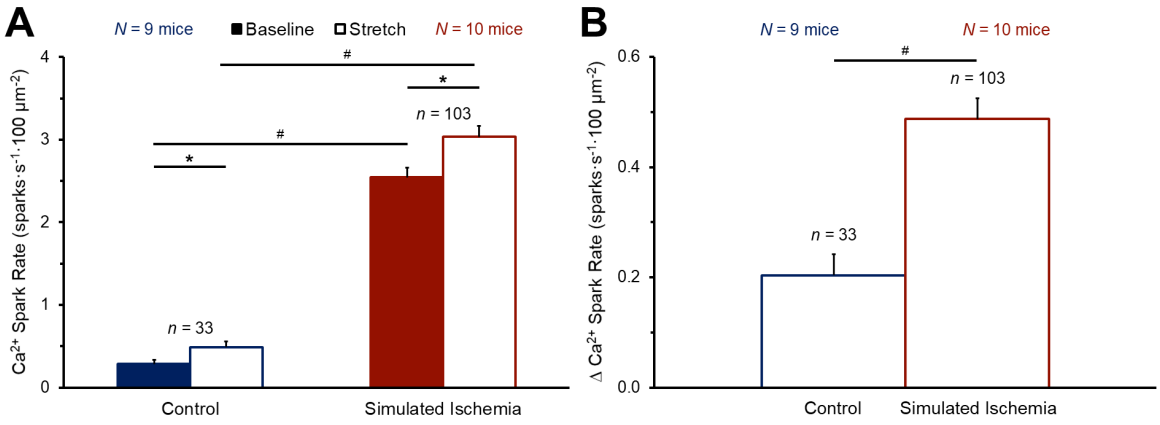

Figure 2.4. | Effect of stretch on the rate of ROS production in quiescent mouse ventricular myocytes exposed to either NT or simulated ischaemia. Average rate of ROS production (quantified as the slope of the change in 2',7'-dichlorofluorescein diacetate, DCF, fluorescence over time) before (Baseline) and during stretch (Stretch; **a**) and the change in ROS production with stretch (Δ ROS production; **b**) averaged across all cells exposed to either NT (blue) or a simulated ischaemia (red) solution (presented as mean ± SEM). **p*<0.001 by two-tailed, paired Student's t-test; #*p*<0.05 and ##*p*<0.01, by two-tailed, unpaired Student's t-test. *N* = mice; *n* = cells.

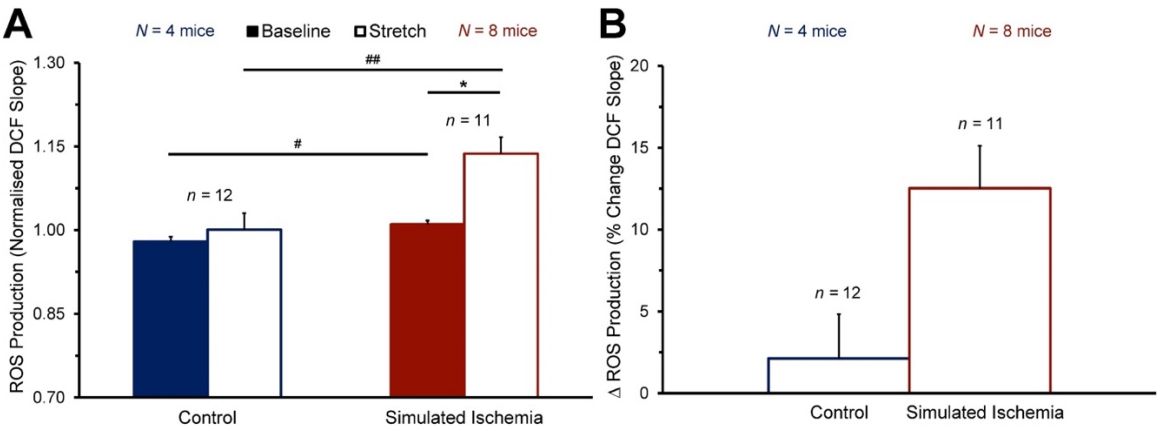

CHAPTER 3: TRPA1 CHANNELS ARE A SOURCE OF CALCIUM-DRIVEN CARDIAC MECHANO-ARRHYTHMOGENICITY

The contents of this chapter represent work that is currently available as a preprint on *bioRxiv* (Cameron BA, Stoyek MR, Bak JJ, Quinn TA. TRPA1 channels are a source of calcium-driven cardiac mechano-arrhythmogenicity. *bioRxiv*. 2020) and is formatted for submission to *Nature*. In consultation with Dr. Alex Quinn, I was directly involved in the conception and design of the study and the development and establishment of the methodology. I performed all experiments and acquired and analysed all data (with the exception of the immunochemistry, Western blot, and patch clamp experiments and data), wrote the initial draft of the manuscript, and revised it with the help of Dr. Quinn, Dr. Rémi Peyronnet, and Prof. Dr. Peter Kohl. Supplemental figures for this chapter are found in Appendix Chapter 2.

3.1. Summary Paragraph

Maintenance of normal cardiac function involves an important intrinsic regulatory loop, in which electrical excitation causes the heart to mechanically contract,[18] and the mechanical state of the heart directly affects its electrical acticvity.[232] In diseases that affect myocardial mechanical properties and function, it is thought that this feedback of mechanics to electrics may contribute to arrhythmogenesis ('mechano-arrhythmogenicity').[226] However, the molecular identity of the specific factor(s) underlying mechano-arrhythmogenicity are unknown.[216] Here we show in rabbit ventricular myocytes that mechano-sensitive[25,51,133,193,208,256,291] TRPA1 channels[183] are a source of cardiac mechano-arrhythmogenicity through a Ca^{2+}-mediated mechanism. Using a cell-level approach involving rapid, transient stretch of single ventricular myocytes, we found that activation of TRPA1 channels results in the appearance of stretch-induced arrhythmias, with arrhythmic triggers mediated by increased diastolic levels of cytosolic Ca^{2+} and sustained arrhythmic activity driven by cytosolic Ca^{2+} oscillations. This stretch-induced activity was modulated by microtubules and prevented by pharmacological TRPA1 channel block or cytosolic Ca^{2+} buffering. Our results demonstrate that TRPA1 channels can act as a trigger for stretch-induced excitation and create a substrate for sustained arrhythmias. TRPA1 may thus represent a novel anti-arrhythmic target in cardiac diseases in which TRPA1 channel activity is augmented.[47,164,194,301,302]

3.2. Main Text

Feedback is an essential element of biological function and is fundamental to the control and adaptation of physiological activity. A prime example of this process is seen in the heart, an electro-mechanical pump in which electrical excitation of cardiac myocytes causes their contraction through a feedforward mechanism involving triggered release of Ca^{2+} from intracellular stores (*i.e.,* excitation contraction coupling).[18] Feedback in this system involves the influence of the mechano-sensitivity of cardiac myocytes on their electrical activity through MEC.[232] In healthy conditions, this feedback is important for the maintenance of normal cardiac function.[228] However, in diseases involving hemodynamic overload or altered myocardial mechanical properties or function, MEC may instead contribute to cardiac arrhythmias through mechanically-induced arrhythmogenic electrophysiological effects (*i.e.,* mechano-arrhythmogenicity).[226] While the influence of MEC on cardiac electrophysiology is well established,[232] the molecular identity of the specific factor(s) involved, especially those underlying mechano-arrhythmogenicity, is still being explored.[216]

Here we utilised a cell-level approach for investigating mechanisms of mechano-arrhythmogenicity, which allows for the precise control of single cell mechanical load with a carbon fibre-based system.[114] This is combined with simultaneous fluorescence imaging of transmembrane voltage and cytosolic Ca^{2+}, video-based measurement of sarcomere dynamics, and pharmacological interrogation of the suspected mechanisms mediating arrhythmias that occur with cell stretch. Recent results from rabbit isolated heart studies suggest that ventricular mechano-arrhythmogenicity in acute regional ischemia (that occurs with occlusion of a coronary artery) is caused by a mechano-sensitive, Ca^{2+}-mediated

mechanism. This is thought to be facilitated by a dissociation of the recovery of membrane potential and cytosolic Ca^{2+} concentration during ischaemia, reflected by a relative difference in action potential and Ca^{2+}-transient shortening by K_{ATP} channel activation.[13] This creates a VP for Ca^{2+}-mediated arrhythmias during late repolarisation, as cytosolic Ca^{2+} remains elevated while myocytes become progressively re-excitable[278,280] (a similar VP has been shown to occur during β-adrenergic stimulation in failing human hearts).[156] In the present study, we utilised our single cell system to investigate the specific influence of a K_{ATP} channel activation-induced VP (without the additional components of ischaemia) on the susceptibility of left ventricular myocytes to stretch-induced premature excitation and sustained arrhythmic activity, and to identify underlying mechanisms of ventricular mechano-arrhythmogenicity.

K_{ATP} channels were activated by application of pinacidil (50 μM, continuous superfusion), an agonist of sulfonylurea receptor (SUR)2A/K_{ir}6.2 in cardiac and skeletal muscle.[83] To assess effects on the relative recovery time of voltage and Ca^{2+}, and the size of the resultant VP, we used a single-excitation/dual-emission fluorescence (di-4-ANBDQPQ and Fluo5-F) imaging approach[229] to simultaneously record action potentials and Ca^{2+} transients in electrically-paced (1 Hz) rabbit left ventricular myocytes under carbon fibre control (Fig. 3.1a). With pinacidil exposure, both APD and Ca^{2+} transient duration (CaTD) were decreased (Fig. 3.1b, c). However, the decrease of APD was significantly greater than CaTD, resulting in the formation of a cellular VP (defined as the period during which myocytes start to become re-excitable and cytosolic Ca^{2+} remains elevated, calculated as the difference between 50% of APD and 80% of CaTD; Fig. 3.1b, d). This response is in keeping with behaviour previously observed in the whole heart

during acute ischemia[13,280] (as well as with hypoxia alone).[278] After 5 min of pinacidil exposure, there were no further significant alterations in APD, CaTD, or the VP (Fig. 3.1c, d).

Having shown that K_{ATP} channel activation created a VP in our isolated cells, we sought to determine whether stretch specifically in the VP resulted in an increase in mechano-arrhythmogenicity. Rapid, transient stretch – as would occur with systolic stretch of patho-physiologically weakened tissue in the whole heart – was applied with carbon fibres adhered to either end of single cells under piezo-electric translator control (Fig. 3.2a). Stretch (which was applied such that there was a range of percent sarcomere stretch, stretched sarcomere length, and maximal applied stress within a cell; Supplemental Fig. 3.1) was timed from the pacing stimulus to occur either during the VP or in diastole (Fig. 3.2b, c) in cells exposed to physiologic or pinacidil-containing solution. Stretch resulted in a variety of changes in rhythm (revealed by tracking of sarcomere length), including premature contractions (defined as 1 or 2 stretch-induced contractions in the absence of electrical stimulation; Fig. 3.2d) and a variety of other arrhythmic behavior (*i.e.*, refractoriness resulting in a single [Fig. 3.2e] or multiple [Fig. 3.2f] missed beats, or sustained activity that either spontaneously resolved [Fig. 3.2g] or was terminated by an additional stretch [Fig. 3.2h]). It was found that the incidence of arrhythmic activity was greater in pinacidil-treated cells than in control, however, it was not different for stretch applied during the VP compared to stretch in diastole (Fig. 3.3a and Supplemental Fig. 3.3), suggesting that the pinacidil-treated cells were overall more prone to mechano-arrhythmogenicity.

As previous work in the whole heart has shown that the magnitude of tissue deformation is a key determinant of mechano-arrhythmogenicity,[231] we also assessed the effect of stretch characteristics on arrhythmia incidence. Increasing the piezo-electric translator displacement from 20 to 40 μm resulted in an increase in the percent sarcomere stretch, stretched sarcomere length, and maximal applied stress, parameters which scaled with the piezo-electric translator displacement (Supplemental Fig. 3.1). Yet, both in control and pinacidil-treated cells, there was no significant effect on mechano-arrhythmogenicity with stretch in the VP or diastole (although, there was a clear trend towards greater arrhythmia incidence with greater stretch; Supplemental Fig. 3.3), suggesting that factors beyond the stretch characteristics measured play a role in determining the occurrence of stretch-induced arrhythmias.

To rule out the possibility that arrhythmias were the result of stretch-induced cellular damage, contractile function was assessed before and after stretch at each magnitude. Both in control and pinacidil-treated cells, diastolic sarcomere length and the maximal rate and percent sarcomere shortening during contraction, before and after successive stretches with increased piezo-electric translator displacement, were not significantly different (Supplemental Fig. 3.4). These parameters were also not significantly different before stretch and after return to steady state following sustained arrhythmic activity (Supplemental Fig. 3.5), further suggesting that cellular damage was not involved.

As we found that pinacidil increased the incidence of stretch-induced arrhythmias (an effect that was not restricted to the VP), we sought to determine the source of the overall increase in mechano-arrhythmogenicity. K_{ATP} channels are mechano-sensitive, with their current being increased by stretch when active,[294] so it is tempting to think they may have

been involved. However, as K_{ATP} channels are highly selective for K^+, they have a reversal potential of ~-90 mV and conduct an outward K^+ current over the working membrane potential of ventricular myocytes. As a result, their activation in ventricular myocytes will always drive repolarisation, so they cannot account for the stretch-induced excitation seen in the present study (and, in fact, would be expected to oppose depolarisation). Alternatively, while pinacidil is often thought of as a specific activator of K_{ATP} channels, it has also been shown to increase the activity of TRPA1 channels in HEK293 cells,[175] resulting in trans-membrane Ca^{2+} influx. Importantly, TRPA1 channels: (i) are inherently mechano-sensitive[193] and contribute to mechanically-evoked action potentials[133] and currents in sensory neurons,[25,291] astrocytes,[208] and vertebrate hair cells,[51] (ii) have been shown be functionally expressed in mice and to drive changes in rhythm in response to mechanical stimulation in the *Drosophila* heart[256] (although, others have found conflicting results regarding their functional expression in mice)[104] and (iii) are important in a range of cardiovascular functions and pathologies.[302] We hypothesised, that if TRPA1 channels are indeed functionally expressed in rabbit ventricular myocytes, then they may contribute to the increased mechano-arrhythmogenicity seen in our experiments.

To assess the presence of TRPA1 in the rabbit left ventricle, we measured TRPA1 protein expression in left ventricular free wall tissue by western blotting, which revealed robust expression (Supplemental Fig. 3.6a). Functional expression of TRPA1 channels in left ventricular myocytes was evaluated by measuring ion channel activity in cell-attached patches during application of the TRPA1 channel-specific agonist, allyl isothiocyanate (AITC; 50 μM),[127] which has been shown to activate TRPA1 in human adult ventricular cardiac fibroblasts,[207] among other cell types. It was found that AITC exposure caused an

increase in total current, while there was no current change in time-matched controls (Supplemental Fig. 3.6b, c).

As the above results suggest that TRPA1 is functionally expressed in rabbit ventricular myocytes, pinacidil-induced activation of mechano-sensitive TRPA1 channels may indeed account for the increase in mechano-arrhythmogenicity seen in our pinacidil experiments We further explored their potential involvement by applying a non-specific blocker of MSC_{NS} (streptomycin;[315] 50 μM, 5 min superfusion) or a specific TRPA1 channel blocker, which has been shown to inhibit TRPA1 current and mechanically-induced excitation in sensory neurons[25,133,291] (HC-030031,[182] 10 μM, 30 min incubation), to pinacidil-treated cells. Both streptomycin and HC-030031 reduced the incidence of arrhythmias with stretch in both the VP and in diastole (Fig. 3.3a; arrhythmia incidence remained low in control cells, Supplemental Fig. 3.2). Importantly, streptomycin and HC-030031 appeared to have no other functional effects, as diastolic and contractile function was preserved with their application in control cells (Supplemental Fig. 3.7).

Next, as TRPA1 channels preferentially pass Ca^{2+} into cells (~5× that of Na^{+}),[21] we assessed whether Ca^{2+} plays a role in the observed mechano-arrhythmogenicity by buffering cytosolic Ca^{2+} with BAPTA-AM (1 μM, 20 min incubation), which has been previously shown, in ventricular myocytes, to prevent stretch-induced changes in cardiac electrophysiology related to changes in intracellular Ca^{2+}.[29] BAPTA reduced arrhythmia incidence both in the VP and during diastole in pinacidil-treated cells (Fig. 3.3a). To explore whether there may also have been a contribution to the observed mechano-arrhythmogenicity by intracellular Ca^{2+} release from the sarcoplasmic reticulum, RyR were stabilised in their closed state with dantrolene (1 μM, 5 min of superfusion, which does not

affect Ca^{2+}-induced Ca^{2+} release or contraction),[99] however, this had no effect on arrhythmia incidence. In control cells, the incidence of stretch-induced arrhythmias remained low during exposure to BAPTA or dantrolene (Supplemental Fig. 3.2), and there was no effect on the diastolic sarcomere length or the maximal rate of systolic sarcomere shortening, although there was a slight decrease in the percent sarcomere shortening, presumably due to the binding of Ca^{2+} by BAPTA or a reduction in sarcoplasmic reticulum Ca^{2+} release by dantrolene (Supplemental Fig. 3.7).

We then sought to specifically confirm that TRPA1 channels can act as a source of mechano-arrhythmogenicity. Cells were exposed to AITC (10 μM, 5 min superfusion), which has been shown to enhance the response of TRPA1 channels to mechanical stimulation,[25] followed by diastolic stretch. AITC increased arrhythmia incidence compared to both control and pinacidil-treated cells (Fig. 3.3b), which was prevented by co-application of HC-030031 (Fig. 3.3b). Finally, as with pinacidil-treated cells, BAPTA prevented the increase in stretch-induced arrhythmias seen in AITC-treated cells (Fig. 3.3b), further supporting a role of Ca^{2+} in the increase in mechano-arrhythmogenicity.

While the above findings strongly suggest a role of TRPA1 in the observed stretch-induced arrhythmias, in our patch-clamp experiments, we did not find an increase in TRPA1 current when the cell membrane was stretched by negative pipette pressure. However, as there is a large body of evidence demonstrating that interactions between TRP channels and microtubules are important for TRP channel function,[265] we hypothesised that microtubule-mediated mechano-transduction during axial cell stretch may be necessary for a mechanically-induced response (which would not have been engaged during membrane stretch by patch pipette). To test for the importance of microtubules in mechano-

arrhythmogenicity, cells were exposed to paclitaxel (10 μM, 90 min incubation) to increase the polymerisation and stabilisation of microtubules,[252] which has been shown to increase the probability of stretch-induced arrhythmias in the isolated rabbit heart.[212] Using immunofluorescence imaging, we found that paclitaxel increased microtubule density (Supplemental Fig. 3.8) and resulted in an increase in the incidence of stretch-induced arrhythmias (Fig. 3.3b). Interestingly, this increase appears to occur through an interaction with TRPA1 channels, as blocking them with HC-030031 prevented the increase in mechano-arrhythmogenicity following paclitaxel treatment (Fig. 3.3b).

Our results to this point suggested that Ca^{2+} (and perhaps a smaller amount of Na^{+}) passing through mechano-sensitive TRPA1 channels acts as a trigger for stretch-induced premature contractions, however, the source of the sustained arrhythmic activity induced by stretch remained unclear. As TRPA1 channel activity has been shown to cause an increase in diastolic Ca^{2+} concentration in ventricular myocytes,[6] which can create an arrhythmogenic substrate[155] and further activate TRPA1 channels,[332] we hypothesised that effects on cytosolic Ca^{2+} may account for the increase in sustained arrhythmic activity observed in our experiments. We measured cytosolic Ca^{2+} concentration using a ratiometric fluorescence technique (Fura Red, AM; K_d = 400 nM), which showed that both pinacidil and AITC increased Ca^{2+} in diastole (Fig. 3.3c). Interestingly, this increase was reduced by blocking TRPA1 channels with HC-030031 in AITC-, but not pinacidil-treated cells (Fig. 3.3c), suggesting that the increase in diastolic Ca^{2+} with AITC and pinacidil may be occurring through different mechanisms (we could not measure the effects of BAPTA on cytosolic Ca^{2+}, as its Ca^{2+} buffering combined with buffering by Fura Red stopped cells from contracting). While this suggests a role for increased cytosolic Ca^{2+} in mechano-

arrhythmogenicity, changes in repolarisation can also destabilise the electrical activity of ventricular myocytes. Thus, in the pinacidil-treated cells, a stretch-induced increase in K_{ATP} current may also have directly contributed to the sustained arrhythmias,[294] and may account for the temporary refractoriness caused by stretch in some cells. That said, explicit evidence for a direct role of Ca^{2+} in the sustained arrhythmic activity came from dual voltage-Ca^{2+} fluorescence imaging, which revealed an increase in cytosolic Ca^{2+}, along with Ca^{2+} oscillations, that precede oscillations in voltage, indicating that Ca^{2+} was driving the aberrant behaviour (Fig. 3.4a).

Finally, with an increase in cytosolic Ca^{2+}, there is the possibility that a change in cellular mechanics may also contribute to an increase in mechano-arrhythmogenicity by enhancing mechano-transduction or altering stretch characteristics. However, there was no effect of pinacidil on cell stiffness or elastance (measured as the slope of end-diastolic or end-systolic stress-length relationship in contracting cells; Supplemental Fig. 3.9), or the percent sarcomere stretch, stretched sarcomere length, or maximal applied stress during stretch (Supplemental Fig. 3.1), suggesting that changes in cellular mechanics were not involved (although there was a shift in the stiffness and elastance curves to the right in pinacidil-treated cells, indicating an increase in diastolic and systolic load, Supplemental Fig. 3.9). Further, in a subset of pinacidil-treated cells, for which two consecutive diastolic stretches of the same magnitude did, and did not, result in an arrhythmia, the characteristics of each stretch were similar (Supplemental Fig. 3.10), suggesting that stretch characteristics were not the primary determinant of the occurrence of stretch-induced arrhythmias.

Taken together, our results suggest that TRPA1 channels are a source of Ca^{2+}-mediated cardiac mechano-arrhythmogenicity. Figure 3.4b summarises our results and presents a working model of the role that TRPA1 channels play in triggering stretch-induced excitation and creating a substrate for sustained arrhythmic activity. As has been shown recently for transient receptor potential vanilloid-4 (TRPV4) channels in mouse hearts,[290] TRPA1 channels are mechano-sensitive and with stretch allow Ca^{2+} (and some Na^{+}; ~1/5 of Ca^{2+})[21] to enter the cell. This trans-sarcolemmal influx of cations will depolarise cell membrane potential. At the same time, the associated increase in cytosolic Ca^{2+} concentration will further depolarise membrane potential *via* electrogenic forward-mode NCX current, while also creating an arrhythmia-sustaining substrate.[155] If the combined depolarisation is sufficiently large, it will cause excitation and premature contraction of the cell. Further, TRPA1 channel activity itself is directly modulated by cytosolic Ca^{2+} in a bimodal fashion.[299] As a result, an increase in Ca^{2+} will potentiate TRPA1 channel activity, thus increasing its contribution to mechano-arrhythmogenicity, but at a certain level, will inactivate the channels, thus limiting the degree of Ca^{2+} overload and preventing lethal cell damage.[299] In our experiments, exposure to AITC caused direct activation of TRPA1, while pinacidil either directly activated TRPA1 channels, or did so indirectly *via* an increase in cytosolic Ca^{2+}. In both cases this would lead to an enhanced depolarising current during stretch (acting as a trigger for premature excitation) and would increase cytosolic Ca^{2+} levels (further driving depolarisation and acting as a substrate for sustained arrhythmias). In this way, TRPA1 channels act as the central player in a feed-forward loop that increases Ca^{2+}-dependent mechano-arrhythmogenicity. The role of TRPA1 in the stretch-induced arrhythmias observed in our model is further supported by the reduction in arrhythmia

incidence with specific block of TRPA1 channels by HC-030031, or non-specific block of MSC by streptomycin. Interestingly, the contribution of TRPA1 to mechano-arrhythmogenicity appears to depend on microtubules, as an increase in their polymerisation and stability with paclitaxel increased stretch-induced arrhythmia incidence, which was prevented by HC-030031. Additionally, the contribution of Ca^{2+} influx as an arrhythmic trigger, and Ca^{2+} overload as a sustaining substrate during TRPA1 activation, is supported by the reduction in stretch-induced arrhythmias with block of TRPA1 channels by HC-030031 and buffering of Ca^{2+} by BAPTA.

These findings have potentially important implications for anti-arrhythmic treatment in cardiac diseases in which TRPA1 channel expression or activity is augmented.[302] This is especially true for diseases in which additional factors that activate TRPA1 channels are present (*e.g.*, oxidative stress),[5] as the response of TRPA1 channels to mechanical stimulation is enhanced by an increase in its baseline activity.[25] For instance, acute myocardial ischemia is associated with TRPA1-mediated myocardial damage[47] and lethal ventricular arrhythmias that are thought to involve contributions of altered tissue mechanics, intracellular Ca^{2+} handling, and oxidative stress,[38] so targeting TRPA1 channels in that setting could help prevent multiple detrimental outcomes (and perhaps even promote post-ischemic myocardial repair).[164] This may also be true in chronic pathologies associated with changes in cardiac mechanics, intracellular Ca^{2+}, oxidative stress, and other TRPA1 modulating factors,[183] and in which lethal arrhythmias occur, such as ventricular pressure overload (TRPA1 inhibition has been shown to reduce hypertrophy and fibrosis in that setting),[301] making TRPA1 channels a novel anti-arrhythmic target with exciting therapeutic potential.[194]

3.3. Methods

3.3.1. Animal Model

Experiments involved the use of female New Zealand White rabbits (2.1 ± 0.2 kg, Charles River) - the most relevant small animal model for cardiac arrhythmia research[48] - and were conducted in accordance with the ethical guidelines of the Canadian Council on Animal Care, with protocols approved by the Dalhousie University Committee for Laboratory Animals, or by the local Institutional Animal Care and Use Committee at the University of Freiburg (Regierungspräsidium Freiburg, X-16/10R). Details have been reported following the Minimum Information about a Cardiac Electrophysiology Experiment (MICEE) reporting standard.[225]

3.3.2. Cell Isolation

Animals were euthanised by ear vein injection of pentobarbital (140 mg/kg) and heparin (1,500 units/kg, Sigma-Aldrich), followed by rapid excision of the heart, aortic cannulation, and Langendorff perfusion (20 mL/min) with 37°C normal Tyrode (NT) solution (containing, in mM: 120 NaCl, 4.7 KCl, 1 $MgCl_2$, 1.8 $CaCl_2$, 10 glucose, 10 HEPES [Sigma-Aldrich], with pH adjusted to 7.40 ± 0.05 with NaOH and an osmolality of 300 ± 5 mOsm/L) bubbled with 100% oxygen. After a rest period of 15 min, the perfusate was switched to Ca^{2+}-free solution (containing, in mM: 117 NaCl, 10 KCl, 1 $MgCl_2$, 10 creatine, 20 taurine, 5 adenosine, 2 L-carnitine, 10 glucose, 10 HEPES [Sigma-Aldrich], with pH adjusted to 7.40 ± 0.05 with NaOH and an osmolality of 300 ± 5 mOsm/L) with the addition of 0.018 mM EGTA (Sigma-Aldrich) for 5 min. The perfusate

was then switched to digestion solution, comprised of Ca^{2+}-free solution with the addition of 200 U/mL Collagenase II (Worthington Biochemical Corporation), 0.06 mg/mL Protease XIV (from *Streptomyces griseus*, Sigma Aldrich), and 100 μM $CaCl_2$ for 5 min, at which point the perfusion rate was reduced to 15 mL/min until the heart became flaccid and jelly-like (~10-12 min). The left ventricular free wall was removed and placed into 50 mL of stop solution, comprised of Ca^{2+}-free solution with the addition of 0.5 % bovine serum albumin (Sigma Aldrich) and 100 μM $CaCl_2$. The tissue was agitated, the solution filtered through a 300 μm nylon mesh, the tissue returned to fresh stop solution and re-agitated, and the solution filtered. The cell-containing solution was divided into 2 mL microcentrifuge tubes and maintained at room temperature.

3.3.3. Carbon Fibre Method

Cells were stretched by the carbon fibre method, adapted from previous work.[114] Briefly, a pair of carbon fibres (12-14 μm in diameter, gift of Prof. Peter Kohl, Institute for Experimental Cardiovascular Medicine, University Heart Centre Freiburg / Bad Krozingen) were mounted with cyanoacrylate adhesive in borosilicate glass capillaries pulled from glass tubes (1.12 mm inner / 2 mm outer diameter, World Precision Instruments) and bent at 30° 1.2 mm from the end to allow near-parallel alignment of the carbon fibres with the bottom of the experimental chamber. The left and right carbon fibre were trimmed to 1.2 mm and 0.6 mm in length from the end of the glass capillary, respectively, so that one fibre was relatively compliant and the other relatively stiff. Each carbon fibre was mounted in a microelectrode holder (MEH820, World Precision Instruments) coupled to a three-axis water hydraulic micromanipulator (MHW-103,

Narishige) and mounted on a linear piezo-electric translator (P-621.1CD, Physik Instrumente). The carbon fibre position was controlled by a piezo amplifier / servo controller (E-665.CR, Physik Instrumente) driven by a voltage signal generated from a DAQ device (USB-6361; National Instruments) dictated by custom-written routines in LabVIEW (National Instruments). Carbon fibre stiffness was calculated by pressing a fibre against a force transducer system (406A, Aurora Scientific), measuring the force for given displacements of the piezo-electric translator, and fitting the data by linear regression to the formula: stiffness = force / piezo-electric translator displacement. This allowed measurement of force applied during cell stretch by measuring carbon fibre bending through monitoring piezo-electric translator and carbon fibre tip positions (described below) and applying the formula: force = stiffness × (change in distance between carbon fibre tips - change in distance between piezo-electric translators). Force was then converted to stress by dividing by the unstretched cross-sectional area (CSA), determined by assuming that the cross section is an ellipse with CSA = π*(width/2)*(thickness/2) and thickness = width/3.

3.3.4. Single Cell Stretch

Before use, half of the supernatant from the cell-containing microcentrifuge tube was removed and replaced by room temperature NT for 10 min (so that cells were exposed to 50% normal Ca^{2+}), after which all of the supernatant was removed and replaced by NT. A small drop of solution was added to an imaging chamber (RC-27NE2, Warner Instruments) containing 1 mL of NT maintained at 35°C by a temperature controller (TC-344C, Warner Instruments) and mounted on an inverted fluorescence microscope (IX-73, Olympus) with

a 40× objective (UPLFLN40X, Olympus). The surface of the coverslip on the bottom of the chamber was coated with poly-2-hydroxyethyl methacrylate (poly-HEMA, Sigma-Aldrich) to prevent cell adhesion. Once the cells had settled, 1 Hz bipolar electrical field stimulation (SIU-102, Warner Instruments) was commenced, and normally contracting rod-shaped myocytes with clear striations and well-defined membranes and no signs of blebbing were randomly selected. Electrical stimulation was stopped, and the carbon fibres were positioned at either end of the long-axis of a cell and gently lowered onto the cell surface using the hydraulic micromanipulators. Adhesion of the cell to the carbon fibres was confirmed by raising the cell off of the coverslip. Once cell attachment was established, electrical stimulation was recommenced, and cells contracted against the fibres for ~1-2 min to improve electrostatic interactions responsible for adhesion. Cells were then superfused at 2.1 mL/min through an inline heater (SF-28, Warner Instruments) with either NT or pinacidil-containing solution (to activate K_{ATP} channels) for 5 min. Transient stretch (20 μm piezo-electric translator displacement applied and removed at a rate of 0.7 μm/ms) was then applied (Fig. 3.2a) during mid-diastole (600 ms delay after an electrical stimulus), followed by a 10 s wait, stretch during the VP (150 ms delay, chosen so that a majority of stretches [whose duration increased with greater piezo-electric translator displacement] would occur over the entire VP, based on the average VP timing measured by simultaneous voltage-Ca^{2+} imaging, described below), and after another 10 s wait, was repeated. This protocol was duplicated at increasing magnitudes of piezo-electric translator displacement (30 and 40 μm, to generate a range of stretch-induced changes in sarcomere length), with 30 s between repetitions, for a total of 12 stretches (Fig. 3.2b).

3.3.5. Assessment of Stretch Effects

Throughout the protocol, sarcomere length and piezo-electric translator and carbon fibre tip positions were monitored and recorded at 240 Hz (Myocyte Contractility Recording System, IonOptix). From this, cellular contractile function (diastolic sarcomere length, maximal rate and percent sarcomere shortening) and characteristics of cell stretch (percent sarcomere stretch, stretched sarcomere length, and maximal applied stress) were measured. Arrhythmic activity was assessed from sarcomere length measurements, which revealed stretch-induced premature contractions (defined as 1 or 2 unstimulated contractions after stretch) or other arrhythmic activity (including refractoriness, resulting in a single or multiple missed beats, or sustained activity that either spontaneously resolved or was terminated by an additional stretch). Examples of each classification of stretch-induced arrhythmias is provide in Fig. 3.2. When a sustained arrhythmia occurred, the next stretch was delayed by the appropriate amount after it resolved (either 10 or 30 s). Any stretch that resulted in slippage of the carbon fibres, or a sustained arrhythmia that did not spontaneously resolve or could not be terminated by a maximum of 2 stretches was excluded (< 1% of all cells), as cell damage could not be excluded as a cause.

3.3.6. Pharmacological Interventions

Pharmacologic agents dissolved in distilled water, dimethyl sulfoxide (DMSO), or ethanol, as appropriate, were added to the perfusate and continuously perfused for 5 min before cell stretch. Agents included: BAPTA-AM (1 μM, to buffer cytosolic Ca^{2+}, with the concentration determined in preliminary experiments by titrating to a value that caused a ~10% decrease in percent sarcomere shortening during contraction, Abcam), dantrolene (1

μM, to stabilize RyR, Abcam), streptomycin (50 μM, to non-specifically block MSC, Sigma-Aldrich), HC-030031 (10 μM, to specifically block TRPA1 channels, Abcam), allyl isothiocyanate (AITC, 10 μM, to activate TRPA1 channels, Sigma-Aldrich), and paclitaxel (10 μM, to increase the polymerisation and stabilisation of microtubules, Abcam). For BAPTA-AM, HC-030031, and paclitaxel, cells were incubated for 20, 30 min, or 90 min respectively in NT prior to superfusion.

3.3.7. Dual Parametric Voltage-Ca^{2+} Fluorescence Imaging

The Ca^{2+}-sensitive dye Fluo-5F AM (5 μM, ThermoFisher Scientific) and Pluronic F-127 (0.02 %, Biotium) dissolved in DMSO were added to the cell-containing microcentrifuge tube during cellular suspension in the 50% Ca^{2+} solution, and was subsequently incubated in the dark for 20 min. The supernatant was then replaced with fresh NT, the voltage-sensitive dye di-4-ANBDQPQ (20 μM, University of Connecticut Health Centre) dissolved in ethanol was added to the tube, and the cells were incubated in the dark for 14 min. The supernatant was again replaced with fresh NT, probenecid (1 mM, Sigma-Aldrich) was added to the tube, and the cells were maintained in the dark at room temperature. When ready for imaging, the solution containing dye-loaded cells was gently agitated with a transfer pipette, and a small drop of solution was added to 1 mL of NT in the imaging chamber. Carbon fibres were then adhered to a cell as described above (carbon fibres reduced motion artefact associated with cell movement in the vertical plane during contraction, allowing fluorescence measurements to be made without an excitation-contraction uncoupler). Fluorescence was excited by a mercury lamp (U-HGLGPS, Olympus) passed through a 466/40 nm bandpass filter (FF01-466/40, Semrock) and

reflected onto the sample by a 495 nm dichroic mirror (FF495-Di03, Semrock). For simultaneous measurement of transmembrane voltage and cytosolic Ca^{2+}, each fluorescent signal was projected onto one-half of a 128 × 128-pixel, 16-bit electron-multiplying charge-coupled device (EMCCD) camera sensor (iXon3, Andor Technology) using an emission image splitter (Optosplit II; Cairn Research), and recorded at 500 fps with 2 ms exposure time and maximum electron-multiplying gain. The two signals were split with a 685 nm dichroic mirror (FF685-Di02, Semrock) and Flou-5F emission was collected with a 525/50 nm bandpass filter (FF03-525/50, Semrock) and di-4-ANBDQPQ emission with a 700 nm long-pass filter (HQ700lp; Chroma Technology). A schematic of the imaging setup is provided in Fig. 3.1a.

Analysis of voltage-Ca^{2+} signals was performed using custom routines in Matlab (R2018a, MathWorks). Fluorescence for each signal was averaged over the entire cell, a temporal filter (50 Hz low-pass Butterworth) was applied, and bleaching was eliminated by fitting the resulting signal with a second-order polynomial and subtracting the result. From the corrected signals, time to 50% or 80% recovery of the APD (APD_{50} or APD_{80}) or CaTD ($CaTD_{50}$ or $CaTD_{80}$) were averaged over 3 consecutive cardiac cycles. The VP was calculated as the difference between $CaTD_{80}$ and APD_{50}, plus the difference between the timing of the action potential and Ca^{2+} transient upstrokes (excitation-contraction coupling time, ECC, see Fig. 3.1b): $VP = ECC + (CaTD_{80} - APD_{50})$.

3.3.8. Ratiometric Cytosolic Ca^{2+} Fluorescence Imaging

Imaging of cytosolic Ca^{2+} levels was performed using the ratiometric Ca^{2+}-sensitive dye Fura Red AM (K_d = 400 nM, AAT Bioquest). Cells were loaded with the dye by incubating

with 5 μM of the dye, 0.02 % Pluronic F-127, and 1 mM probenecid dissolved in DMSO in the dark for 20 min. Fluorescence was excited by alternating light pulses from two white light-emitting diodes (CFT-90-W; Luminus Devices), one with a 420/10 nm bandpass filter (FF01-420/10, Semrock) and the other with a 531/22 nm bandpass filter (FF02-531/22, Semrock), which were combined into the microscope excitation light path with a 455 nm dichroic mirror (AT455dc, Chroma Technology) and reflected onto the sample by a 562 nm dichroic mirror (T562lpxr, Chroma Technology). Fluorescence was measured through a 632/60 nm bandpass filter (AT635/60m, Chroma Technology) with the EMCCD camera at 500 fps with 2 ms exposure time and maximum electron-multiplying gain. Light pulses and camera frame acquisition were synchronised with a custom control box (provided by Dr. Ilija Uzelac, Georgia Institute of Technology) so that alternating frames corresponded to the signal generated by each of the two excitation wavelengths.

Analysis of cytosolic Ca^{2+} was performed using custom routines in Matlab. Fluorescence was averaged over the entire cell and a temporal filter (50 Hz low-pass Butterworth) was applied. The two Ca^{2+} signals were separated, and the ratio of the signals was calculated. Any remaining bleaching was eliminated by fitting the resulting signal with a second-order polynomial and subtracting the result. From the corrected signals, the minimum value for each cardiac cycle (representing a relative measurement of diastolic Ca^{2+} concentration) was measured and averaged over 3 consecutive cardiac cycles.

3.3.9. Cell Immunofluorescence

Coverslips (22 mm round; VWR) were coated with laminin (100 μg/mL from Engelbreth-Holm-Swarm murine sarcoma basement membrane diluted in PBS, Sigma-Aldrich) and

stored in a 12-well plate (VWR). Isolated myocytes in NT solution were added to each well and maintained at room temperature for 3 hours to seed. In half of the wells, paclitaxel (10 μM) was added after the first 90 minutes. Cells were then fixed removing the NT and submerging the cover slips in ice cold methanol and incubated for 7 min at -20°C. Methanol was removed and cover slips were rinsed 5 times with phosphate buffered saline (PBS, Sigma-Aldrich) to remove excess methanol. Cover slips were stored in PBS until staining.

For staining, coverslips were bathed in blocking solution (5% BSA in PBS, Sigma-Aldrich) at room temperature. After 1 hour, plates were transferred to 100 μL of a primary antibody storage solution (5% BSA in PBS) in a custom-built humidity chamber (glass petri dish lined with a PBS-soaked Kimwipe and sealed with Parafilm). Diluted primary antibody (100 uL of 1:200 rat anti-rabbit α-tubulin, Clone YL1/2, Invitrogen) was placed on the parafilm, and the coverslip was mounted cell-side down and incubated at 4°C for 1 hour. Coverslips were subsequently washed in quadruplicate (5 min each) with PBS and diluted secondary antibody (1:500 goat anti-rat IgG Alexa Fluor 488 conjugate, Invitrogen) was applied as above. Following secondary antibody staining, coverslips were mounted to glass slides with mounting medium (ProLong Glass Antifade Mountant with NucBlue Stain, ThermoFisher).

Imaging of the fixed and stained myocytes was performed on an inverted confocal microscope (TCS SP8, Leica) system with a 40× oil, 1.3 NA objective (HC Plan APOCHROMAT CS2, Leica) and Lightning deconvolution software to obtain near super-resolution images. Samples were illuminated with a 488 nm solid state laser at 1.2% intensity and the photomultiplier tube (PMT) detectors were set to collect between 503-577 nm. A 1.5 μM z-stack of 3 images was obtained. Maximum projections of confocal z-

sections were generated using Leica LAS X 3D viewer software. Images were then analysed in a blinded fashion using custom software in Fiji (kindly shared by Matthew Caporizzo and Benjamin Prosser, Department of Physiology, University of Pennsylvania Perelman School of Medicine, Philadelphia, USA) to determine microtubule density, calculated as the fraction of cell area.[39] Briefly, cells were manually traced and a threshold for microtubule positive pixels was determined from a background region within the cell with no visible microtubule fluorescence. This was used to generate a binary image of the cell to calculate the microtubule positive fraction of the total cell area.

3.3.10. Tissue Western Blotting

Boiled samples of left ventricular free wall (20 μg) were separated (4% stacking gel) and resolved *via* 7.5% sodium dodecyl sulfate-polyacrylamide gel electrophoresis (Mini-PROTEAN SDS-PAGE, BioRad). Samples were loaded alongside 10 μl protein ladder (Precision Plus Protein Standards Kaleidoscope ladder, BioRad). Self-cast gels (Mini-PROTEAN, BioRad) were run on ice at 90V for 30 min and 120V until the dye front migrated to the bottom edge of the gel on ice in 1X Tris/Glycine/SDS electrophoresis buffer (BioRad). Samples were wet-transferred to nitrocellulose (0.2 μm, BioRad) at 100V for 1.5 hours buried in ice. Membranes were briefly rinsed in double-distilled water, and equal protein transfer was confirmed by incubating the membranes in stain (Pierce Reversible Memcode Stain, Thermo Scientific) for 5 min. The stained blot was labeled and imaged (ChemiDoc MP Imaging System, BioRad) before removing the stain (Pierce Stain Eraser, Thermo Scientific). Membranes were then blocked in 5% skim-milk in 1X Tris-Buffered-Saline-Tween 20 (TBS-T, Sigma-Aldrich) for 60 min. Membranes were subsequently

incubated at 4ºC overnight with primary antibodies (1:2000 monoclonal anti-TRPA1 antibody produced in mouse, Sigma-Aldrich, and 1:3000 anti- myosin heavy chain (MF20), Hybridoma Bank) diluted in 1% skim-milk in TBS-T with sodium azide. Blots were then incubated with secondary antibody (1:4000 horseradish peroxidase HRP-conjugated anti-mouse, Jackson Labs) for 1 hour in 5% skim-milk at room temperature. Immunoreactivity was then measured (Clarity Western Enhanced Chemiluminescence Substrate, with a ChemiDoc MP Imaging System, BioRad). Membranes were stripped by incubation in 25 mL of 0.5 M Tris-HCl/SDS buffer supplemented with 125 μL 2-mercaptoethanol (Sigma-Aldrich) for 1 hour and re-probed.

3.3.11. Patch-Clamp Current Recordings

Cells for patch clamp experiments were isolated from acute ventricular slices. Briefly, animals were anaesthetised by intramuscular injection of esketamine hydrochloride (0.5 mL/kg) and 2% xylazine hydrochloride (0.2 mL/kg). Under sedation, an anaesthetic mixture of sodium-heparin (1,000 units/mL) and esketamine hydrochloride (25 mg/mL) were injected intravenously. Euthanasia was induced by intravenous injection of sodium-thiopental (25 mg/mL) until apnoea. The heart was then excised, cannulated, and Langendorff perfused (20 mL/min) for 2 min with 37°C modified NT solution (containing, in mM: 137 NaCl, 4 KCl, 10 $MgCl_2$, 1.8 $CaCl_2$, 10 glucose, 10 HEPES, 10 creatine, 20 taurine, 5 adenosine, 2 L-carnitine; with pH adjusted to 7.30 ± 0.05 with NaOH) bubbled with 100% oxygen, followed by 2 min with 37°C cutting solution (containing, in mM: 138 NaCl, 5.4 KCl, 0.33 NaH_2PO_4; 2.0 $MgCl_2$, 0.5 $CaCl_2$, 10 HEPES, 30 2,3-butanedione 2-monoxime (BDM); with pH adjusted to 7.30 ± 0.05 with NaOH) bubbled with 100%

oxygen. The left ventricular free wall was cut into approximately 0.8 mm x 0.8 mm chunks, embedded in 4% low melting point agarose, dissolved in cutting solution, and cut into 300 μm thick slices using a vibrating microtome (7000 smz-2, Campden Instruments Ltd) with stainless-steel blades (7550-1-SS, Campden Instruments Ltd) at 4°C, a frequency of 60 Hz, an amplitude of 1.5 mm, a velocity of 0.05 mm/s, and Z-deflection calibrated to values below 1 μm. Slices were stored at 4°C in cutting solution until digestion.

Slices were digested at 37°C in petri dishes (35 mm) placed on a heated orbital shaker (50-65 rpm). Slices were washed three times with digestion solution (containing, in mM: 100 NaCl, 15 KCl, 2.5 KH_2PO_4, 2 $MgCl_2$, 10 glucose, 10 HEPES, 20 taurine, 20 L-glutamic acid monopotassium salt, 30 BDM; with 2 mg/mL bovine serum albumin and pH adjusted to 7.30 ± 0.05 with NaOH), including a 1 min incubation for each wash. Slices were then digested for 12 min by including protease type XXIV (0.5 mg/mL; Sigma-Aldrich), followed by three more washes. Digestion was continued by adding 200 μL of Liberase™ TL Research Grade (0.25 mg/mL; Hoffmann-La Roche) per 2 mL of digestion solution, supplemented with 5 μM $CaCl_2$. When slices started to appear accordion-like (~25-50 min), they were washed three times with digestion solution containing 10 mg/mL bovine serum albumin and mechanically dissociated using forceps and gentle pipetting with Pasteur pipettes. Ca^{2+} concentration was increased in a step-wise fashion every 5 min (5 μM, 12 μM, 20 μM, 42 μM, 84 μM, 162 μM, 266 μM, 466 μM, 827 μM, and 1 mM), during which time BDM was gradually decreased to a final concentration of 13 mM. The tissue was filtered through a 1 mm nylon mesh and allowed to settle in a conical centrifuge tube for 15-20 min. The supernatant was removed by washing with modified NT. Quality of the

preparation was assessed by the percentage of rod-shaped cells, the response to electrical pacing, and the resting sarcomere length.

Sarcolemmal ion channel activity was recorded at room temperature (21 ± 2°C) using the patch-clamp technique with voltage clamped at +40 mV. Fire-polished soda-lime glass capillaries (1.15 ± 0.05 mm inner / 1.55 ± 0.05 mm outer diameter; VITREX Medical A/S) were pulled using a two-stage pipette-puller (PC-10, Narishige) to create the micropipettes required for patch-clamping. Average pipette resistance was 1.36 ± 0.10 MΩ. Recordings were obtained in cell-attached configuration using a patch-clamp amplifier (Axopatch 200B, Axon Instruments) and a digitizer interface (Axon Digidata 1440A, Axon Instruments). Currents were acquired at 20 kHz sampling rate (interval 50 µs), and low-pass filtered at 1 kHz. Currents were analysed with pCLAMP 10.6 software (Axon Instruments). The bath solution contained (in mM): 155 KCl, 3 $MgCl_2$, 5 EGTA, 10 HEPES (Sigma-Aldrich), with pH adjusted to 7.2 ± 0.05 using KOH and an osmolality of 300 ± 5 mOsm/L. The solution was stored at room temperature. Pipette solution for cell-attached recordings contained (in mM): 150 NaCl, 5 KCl, 10 HEPES, 2 $CaCl_2$ with pH adjusted to 7.4 ± 0.05 using NaOH and an osmolality of 300 ± 5 mOsm/L. The pipette solution also contained 10 mM tetraethylammonium chloride (TEA), 5 mM 4-aminopyridine, and 10 mM glibenclamide to inhibit eventual contaminating K^+ channels. These ionic conditions were used previously to describe cation non-selective channels.[53] AITC was added to the bath solution before use and perfused *via* a local perfusion system. Flow rate was adapted by adjusting the height of reservoirs for gravity-fed flow to 1 mL/min. Recordings were analysed in Clampfit 10.6. Average current was calculated over at least 10 s for each condition.

3.3.12. Statistics

Statistics were performed using GraphPad Prism 9. Differences in arrhythmia incidence were assessed using chi-square contingency tables and Fisher's exact test. Differences between group means were assessed by two-tailed, paired or unpaired Student's t-test (for normally distributed data), Wilcoxon matched-pairs (paired) or Mann-Whitney (unpaired) test (for data that was not normally distributed), one-way ANOVA with Tukey *post-hoc* tests (for normally distributed data), or Kruskal-Wallis with Dunn's multiple comparisons test (for data that was not normally distributed), where appropriate. The relevant test is indicated in the figure captions. p-<0.05 was considered significant. Figures indicate the number of replicates used in each experiment (N = rabbits, n = cells, m = stretches).

3.3.13. Code Availability

All custom computer source code used in this study is available from the corresponding author upon reasonable request.

3.3.14. Data Availability

The datasets generated during and/or analysed during the current study are available from the corresponding author upon reasonable request.

3.4. Statements

3.4.1. Acknowledgements

We thank Gentaro Iribe and Keiko Kaihara for technical assistance with cell stretch and Ilija Uzelac for technical assistance with electronic LED control. Carbon fibres are a gift from Jean-Yves LeGuennec. This work was supported by the Canadian Institutes of Health Research (MOP 342562 to T.A.Q.); by the Natural Sciences and Engineering Research Council of Canada (RGPIN-2016-04879 to T.A.Q.); by the Dalhousie Medical Research Foundation (T.A.Q.); by the Canadian Foundation for Innovation (32962 to T. A. Q.); and by the Heart and Stroke Foundation of Canada through a National New Investigator award (T.A.Q.).

3.4.2. Author Contributions

B.A.C. and T.A.Q. designed the study, interpreted the data, and wrote the manuscript; B.A.C. performed and analysed all the cell stretch and fluorescence imaging experiments and isolated cells for the immunofluorescence experiments; M.R.S. contributed to experimental design and setup; J.G. isolated cells for the patch-clamp experiments; R.P. performed the patch-clamp experiments and analysed the data; M.S.C performed and analysed the Western experiments; and J.J.B performed and analysed the immunofluorescence experiments. All authors read and approved the manuscript.

3.5. Figures

Figure 3.1 | Dissociation of the recovery of membrane potential and cytosolic Ca^{2+} in isolated left ventricular myocytes by activation of K_{ATP} channels with pinacidil. a, Schematic of the single-excitation/dual-emission fluorescence imaging approach, utilising a single camera-image splitter system. **b,** Representative trace of an action potential (AP, blue) and calcium transient (CaT, red) simultaneously recorded by fluorescence imaging in a contracting rabbit isolated left ventricular myocyte before (left) and after (right) 5 min of pinacidil exposure, and the associated vulnerable period (VP, green, defined as the period during which myocytes start to become re-excitable while cytosolic Ca^{2+} remains elevated, and is calculated as the difference between 50% of APD [APD_{50}], and 80% recovery of cytosolic Ca^{2+} [$CaTD_{80}$]). ECC is excitation-contraction coupling time. **c,** APD_{50} (blue), $CaTD_{80}$ (red), and **d**, VP (green) over 10 min of normal Tyrode (NT, solid) or pinacidil (PIN, dashed) superfusion. Differences assessed by one-way ANOVA, with Tukey *post-hoc* tests. *p<0.05 for NT compared to PIN; †p<0.05 for the change over time; $^{\#}p$<0.05 for the change over time of APD_{50} compared to CaTD. Error bars represent standard error of the mean. N = rabbits, n = cells.

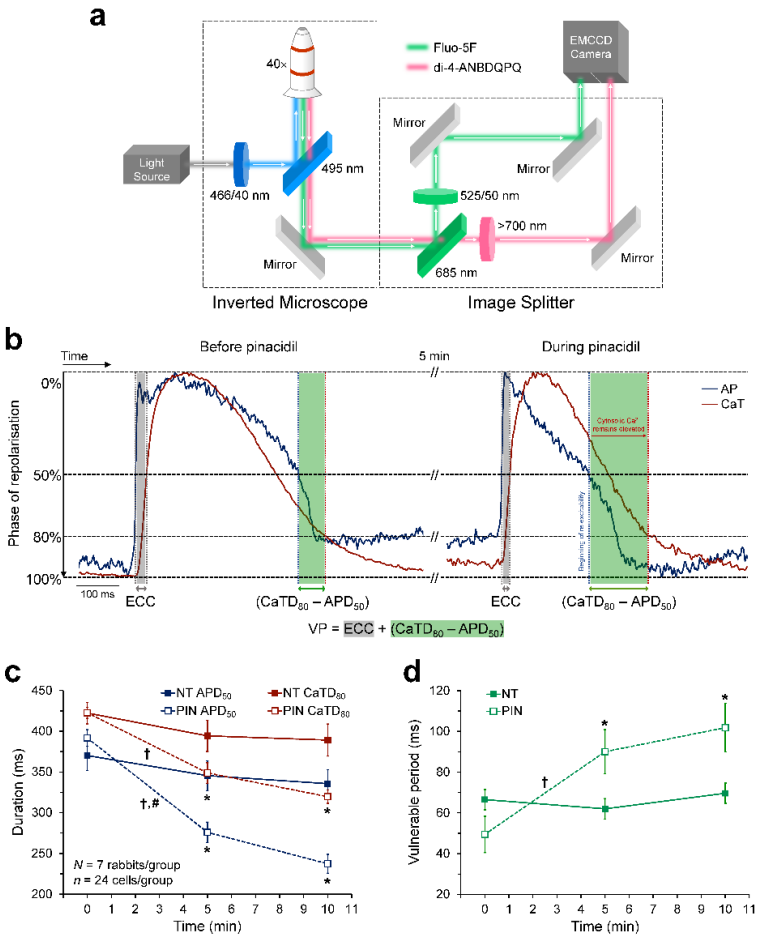

Figure 3.2 | Arrhythmias elicited by rapid, transient stretch of single left ventricular myocytes. a, Brightfield image of a rabbit isolated left ventricular myocyte before (left) and during (right) axial stretch using a carbon fibre-based system. Scale bar, 10 μm. **b**, Schematic of the stretch protocol. **c**, Representative sarcomere length trace in a cell exposed to pinacidil, paced at 1 Hz (orange dots), and stretched (green segments of trace) in diastole (stretches 1 and 3) or during the VP (stretches 2 and 4) that did not result in an arrhythmia. **d,** Stretch-induced premature contraction (blue segment). **e,** Stretch-induced refractoriness resulting in **e,** a single or **f,** multiple missed beats (red segments). **g,** Stretch-induced sustained arrhythmic activity (red segment) that spontaneously resolved, or **h,** that was terminated by an additional stretch (second green bar).

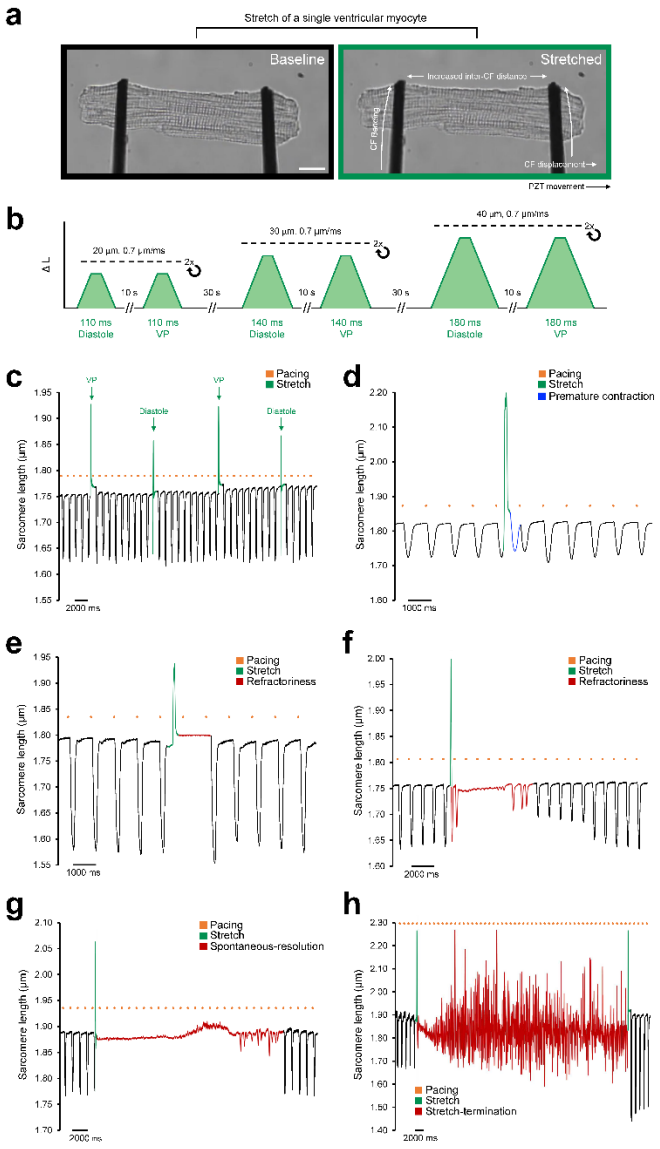

Figure 3.3 | Effects of pharmacological interventions on mechano-arrhythmogenicity. a, Incidence of premature contractions (blue) and other arrhythmic activity (shades of red) with rapid, transient stretch of rabbit isolated left ventricular myocytes during diastole or the vulnerable period (VP) in cells exposed to one of the following treatments: normal Tyrode (NT); pinacidil (PIN, K_{ATP} channel agonist); PIN + streptomycin (STP, cation non-selective mechano-sensitive channel blocker); PIN + HC-030031 (TRPA1 channel antagonist); PIN + BAPTA (cytosolic calcium, Ca^{2+}, chelator); or PIN + dantrolene (DNT, ryanodine receptor stabiliser). MSC, mechano-sensitive channel. Differences assessed using chi-square contingency tables and Fisher's exact test. **p*<0.05, ***p*<0.01, ****p*<0.001 for Diastole; #*p*<0.05, ##*p*<0.01, ###*p*<0.001 for VP. **b**, Incidence of arrhythmias with stretch during diastole in cells exposed to one of the following treatments: NT; PIN; allyl isothiocyanate (AITC, transient receptor potential kinase ankyrin 1, TRPA1, channel agonist); AITC + HC-030031; AITC + BAPTA; paclitaxel (TAX, microtubule stabiliser); or TAX + HC-030031. Differences assessed using chi-square contingency tables and Fisher's exact test. **p*<0.05, ***p*<0.01, ****p*<0.001. **c,** Percent change in diastolic cytosolic Ca^{2+} concentration from control after exposure to one of the following treatments: PIN; AITC; PIN + HC-030031; or AITC + HC-030031. Differences assessed using two-tailed, unpaired Student's t-test between groups within PIN or AITC treatment. **p*<0.05. Error bars represent standard error of the mean. *N* = rabbits, *n* = cells, *m* = stretches.

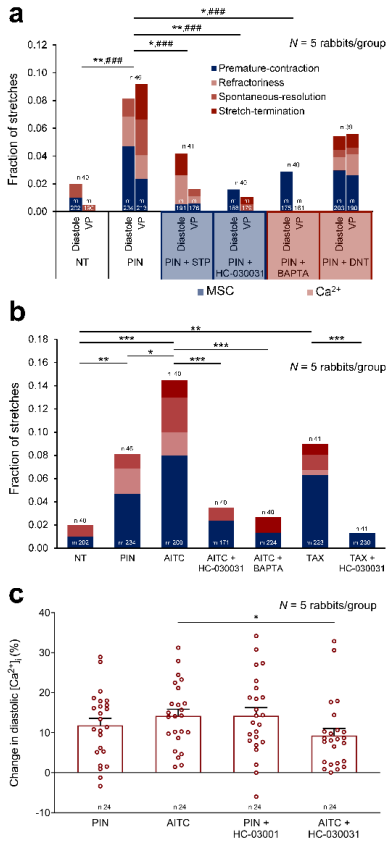

Figure 3.4 | Role of TRPA1 channels and cytosolic Ca^{2+} in ventricular mechano-arrhythmogenicity. a, Representative trace of voltage (blue) and cytosolic calcium (Ca^{2+}, red) simultaneously recorded by fluorescence imaging in a rabbit isolated left ventricular myocyte exposed to pinacidil (PIN) before and after a rapid, transient stretch (green) that resulted in sustained arrhythmic activity. **Blue inset**, Fluorescence trace (top) and phase plot (bottom) showing changes in voltage preceding Ca^{2+} before stretch. **Red inset**, cytosolic Ca^{2+} oscillations preceding changes in voltage during a sustained arrhythmia after stretch. **b,** Schematic representation of the mechanisms underlying Ca^{2+}-mediated mechano-arrhythmogenesis involving transient receptor potential kinase ankyrin 1 (TRPA1) channels. AITC, Allyl isothiocyanate; NCX, sodium-Ca^{2+} exchanger; PIN, pinacidil; STP, streptomycin.

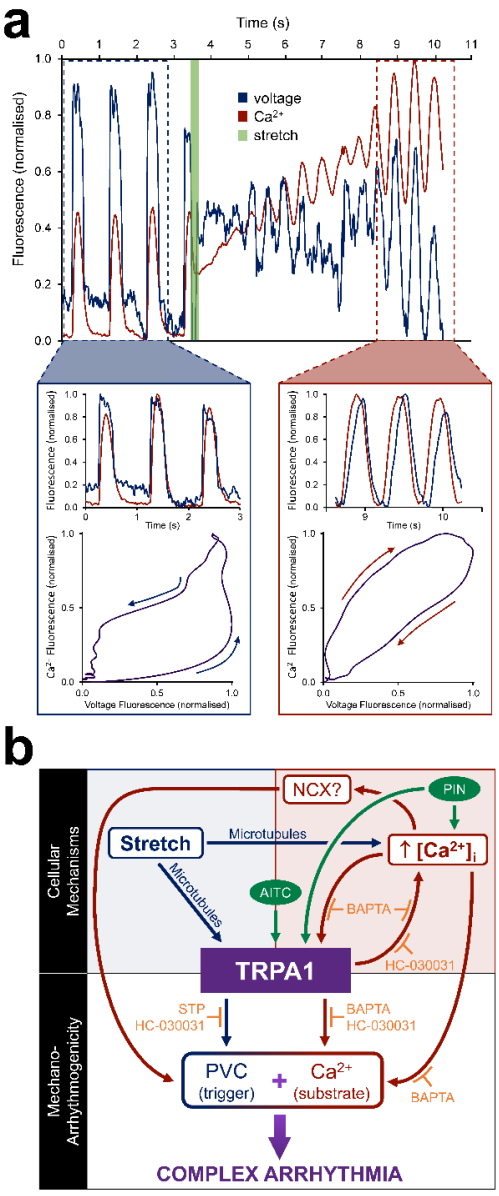

CHAPTER 4: ISCHAEMIC MECHANO-ARRHYTHMOGENICITY IS ENHANCED IN LATE REPOLARISATION AND DRIVEN BY A TRPA1-, CALCIUM-, AND ROS-DEPENDENT MECHANISM

The contents of this chapter reflect work that is formatted for submission to *Circulation Research*. This manuscript has been selected as a finalist in the 2021 Heart Rhythm Society Young Investigator Competition and is thus currently embargoed from journal submission. In consultation with Dr. Alex Quinn, I was directly involved in the conception and design of the study and the development and establishment of the applied methodology. I performed all experiments, acquired and analysed all data, wrote the initial draft of the manuscript, and revised it with the help of Dr. Quinn. Supplemental figures for this chapter are found in Appendix Chapter 3.

4.1. Abstract

Rationale: Cardiac dyskinesis in regional ischaemia results in arrhythmias through mechanically-induced changes in electrophysiology ('mechano-arrhythmogenicity') that involve ischaemic alterations in voltage-Ca^{2+} dynamics, creating a VP in late repolarisation. **Objective:** To determine cellular mechanisms of ventricular mechano-arrhythmogenicity in ischaemia and define the importance of the VP. **Methods and Results:** Voltage-Ca^{2+} dynamics were simultaneously monitored in rabbit ventricular myocytes by dual-fluorescence imaging to assess the VP in control and simulated ischaemia. The VP was longer in simulated ischaemia than in control (146±7 *vs* 54±8ms*;* $p<0.0001$) and was reduced by blocking K_{ATP} channels with glibenclamide (109±6ms; $p<0.0001$). Cells were rapidly stretched (10-18% increase in sarcomere length over 110-170ms) with carbon fibres during diastole or the VP. Mechano-arrhythmogenicity, associated with stretch and release in the VP, was greater in simulated ischaemia than control (7 *vs* 1% of stretches induced arrhythmias; $p<0.005$) but was similar in diastole. Arrhythmias during the VP were more complex than in diastole (100 *vs* 69% had sustained activity; $p<0.05$). In the VP, incidence was reduced with glibenclamide (2%; $p<0.05$), by chelating intracellular Ca^{2+} (BAPTA; 2%; $p<0.05$), blocking mechano-sensitive TRPA1 (HC-030031; 1%; $p<0.005$), or by scavenging (NAC; 1%; $p<0.005$) or blocking ROS production (DPI; 2%; $p<0.05$). Ratiometric Ca^{2+} imaging revealed that simulated ischaemia increased diastolic Ca^{2+} (+9±1%, $p<0.0001$), which was not prevented by HC-030031 or NAC. **Conclusions:** In ischaemia, mechano-arrhythmogenicity is enhanced specifically during the VP and is mediated by ROS, TRPA1, and Ca^{2+}.

4.2. Introduction

Regional ischaemia due to coronary artery occlusion is associated with ventricular arrhythmias and sudden cardiac death.[245] While arrhythmogenesis in ischaemia is multi-faceted,[38] mechanical heterogeneity, acting through mechano-electric coupling mechanisms ('mechano-arrhythmogenicity'), is thought to be a contributing factor.[232] This is supported by a strong correlation between regional ventricular wall motion abnormalities and arrhythmias in patients with coronary artery disease.[30,264] In animal models, these arrhythmias have been shown to originate at the ischaemic border, [53,154] a site of systolic stretch (or 'paradoxical segment lengthening') of weakened ischaemic myocardium.[226] Consequently, arrhythmia incidence in ischaemia is ventricular load-dependent, [53,211] with distension of the ischaemic region being a strong predictor of ventricular fibrillation.[8,9,11,103] Computational modelling has suggested that mechano-arrhythmogenicity in ischaemia is the result of stretch-activated ion channel-mediated depolarisation at the ischaemic border, which contributes to ectopic foci (if supra-threshold), or conduction slowing and block (if sub-threshold).[125,143,241] Yet, the identity of the mechano-sensitive ion channels involved remains unknown,[216] and their role as drivers of mechano-arrhythmogenicity in ischaemia has not been experimentally confirmed.[10]

Recent evidence from rabbit isolated heart studies suggests that ventricular mechano-arrhythmogenicity in regional ischaemia is Ca^{2+}-mediated,[13] and may relate to a VP in late repolarisation during which a temporal dissociation between the recovery of membrane potential and cytosolic Ca^{2+} concentration results in Ca^{2+} remaining elevated as myocytes become re-excitable[13,280] (a similar VP has been shown to occur during beta-adrenergic stimulation in failing human hearts).[156] Further work has shown that the

mechano-sensitive,[193] Ca^{2+}-permeable[21] TRPA1 channel[302] can act as a source for Ca^{2+}-mediated mechano-arrhythmogenicity in ventricular myocytes by triggering premature excitation and creating a substrate for more complex arrhythmic activity.[34] Since the response of TRPA1 to mechanical stimulation is dependent on its baseline activity,[25] which is increased in ischaemia[47] as it is agonised by multiple ischaemic factors (*e.g.*, increased cytosolic Ca^{2+} and reactive oxygen species, ROS),[5,332] TRPA1 may be involved in ischaemic mechano-arrhythmogenicity.

Other mechano-sensitive processes, such as mechano-electric mediator production (e.g., X-ROS, Ca^{2+} sparks),[116,221] may additionally contribute to mechano-arrhythmogenicity in this setting. As these mechanically-induced effects are enhanced in ischaemia (as demonstrated in Chapter 2 of this thesis),[33] regional stretch may lead to localised increases in ROS and cytosolic Ca^{2+}, resulting in arrhythmic activity.[188]

The goal of this study was to investigate cellular mechanisms of ischaemic mechano-arrhythmogenicity and the importance of the VP. Rabbit isolated ventricular myocytes exposed to simulated ischaemic conditions were stretched in diastole and during the VP using a carbon-fibre-based system, combined with dual-parametric fluorescence imaging of voltage and cytosolic Ca^{2+}, video-based measurement of sarcomere dynamics, and pharmacological interrogations. It was hypothesised that the incidence of stretch-induced arrhythmias would be greatest in the VP, and driven by a TRPA1-, Ca^{2+}-, and ROS-mediated mechanism.

4.3. Methods

4.3.1. Ethics Statement

Experiments were conducted in accordance with the ethical guidelines of the Canadian Council on Animal Care with all protocols approved by the Dalhousie University Committee for Laboratory Animals. All details have been described following the Minimum Information about a Cardiac Electrophysiology Experiment (MICEE) reporting standard.[225]

4.3.2. Ventricular Myocyte Isolation

Single ventricular myocytes were enzymatically isolated from female New Zealand White rabbits (2.1 ± 0.2 kg, Charles River) as previously described by our group (and detailed in Chapter 3).[34] Rabbits were euthanised by overdose through injection of pentobarbital (140 mg/kg) and heparin (1,500 units/kg, Sigma-Aldrich) into the marginal ear vein, followed by swift cardiac excision, aortic cannulation, and Langendorff perfusion (20 mL/min, 3-roller Watson-Marlow pump) with normal Tyrode (NT, 37 °C) solution (containing, in mM: 142 NaCl, 4.7 KCl, 1.0 $MgCl_2$, 1.8 $CaCl_2$, 10 glucose, 10 HEPES [Sigma-Aldrich], with pH adjusted to 7.40 ± 0.05 with NaOH and an osmolality of 300 ± 5 mOsm/L) bubbled with 100 % oxygen, for 10 min. The perfusate was then switched to a Ca^{2+}-free solution (containing, in mM: 117 NaCl, 10 KCl, 1 $MgCl_2$, 10 creatine, 20 taurine, 5 adenosine, 2 L-carnitine, 10 glucose, 10 HEPES [Sigma-Aldrich], with pH adjusted to 7.40 ± 0.05 with NaOH and an osmolality of 300 ± 5 mOsm/L) with the addition of 0.018 mM EGTA (Sigma-Aldrich), for 5 min. To begin enzymatic digestion, the perfusate was changed to the digestion solution (5 min at 20 mL/min, Gilson minipuls 3 pump) comprised of Ca^{2+}-

free solution with the addition of 200 U/mL Collagenase II (Worthington Biochemical Corporation), 0.06 mg/mL Protease XIV (from *Streptomyces griseus*, Sigma Aldrich), and 100 μM $CaCl_2$, followed by a reduction in the perfusion rate to 15 mL/min until the heart became flaccid (~10-12 min). The left ventricular free wall was then removed and placed into 50 mL of stop solution, comprised of Ca^{2+}-free solution with 0.5 % BSA (Sigma Aldrich) and 100 μM $CaCl_2$. The ventricle was agitated and filtered through a 300 μm nylon mesh. The filtered tissue was resuspended in fresh stop solution, re-agitated, and re-filtered. The cell solution was split into 2 mL microcentrifuge tubes (VWR) and kept at room temperature (~22 °C, minimum 10 min). For experimentation, 1 mL of the supernatant was replaced with NT and the cells were left to equilibrate (10 min). The supernatant was then replaced with 100 % NT.

4.3.3. Carbon Fibre Technique

Cells were subjected to unidirectional axial stretch using the carbon fibre method previously described for stretch of ventricular myocytes.[33,34,116] In brief, a pair of carbon fibres (12-14 μm in diameter) affixed to glass capillaries (1.12 mm inner / 2 mm outer diameter, World Precision Instruments) with cyanoacrylate adhesive were fastened in microelectrode holders (MEH820, World Precision Instruments) coupled to triaxial water hydraulic micromanipulators (MHW-103, Narishige) and mounted on linear piezo-electric translators (P-621.1CD, Physik Instrumente). The left and right fibre were trimmed to 1.2 mm (compliant, translating fibre) and 0.6 mm (stiff, stationary fibre) in length, respectively.[33,34] Carbon fibre position was controlled by a piezo amplifier/servo controller (E-665.CR, Physik Instrumente) driven by a voltage signal generated from a DAQ device

(USB-6361; National Instruments) and dictated by custom LabVIEW routines (National Instruments). Carbon fibre stiffness was calibrated with a force transducer system (406A, Aurora Scientific). Force was measured for a given piezo-electric translator displacement and fitted by linear regression to the formula: stiffness = force / piezo-electric translator displacement. Carbon fibre bending was calculated by monitoring piezo-electric translator and carbon fibre tip positions (recorded at 240 Hz, Myocyte Contractility Recording System, IonOptix) and applying the formula (carbon fibre bend = change in fibre tip distance - change in distance between piezo-electric translators). Stretch force was assessed from these values (force = carbon fibre stiffness x carbon fibre bend).

4.3.4. Cellular Stretch

The cellular stretch protocol was adapted from previous work by our group.[34] Briefly, a drop of the cell-containing solution was added to an imaging chamber (RC-27NE2, Warner Instruments) mounted on an inverted fluorescence microscope (IX-73, Olympus) with a 40× objective (UPLFLN40X, Olympus). The chamber contained 1 mL of either NT or a simulated ischaemic solution to mimic approximately 30 min of acute ischaemia[78,197,210,289,312,317] (containing, in mM: 140 NaCl, 15 KCl, 1.8 $CaCl_2$, 1 $MgCl_2$, 10 HEPES, 1 NaCN, and 20 2-deoxyglucose to block oxidative phosphorylation and anaerobic glycolysis; pH adjusted to 6.5 with NaOH), maintained at 35 °C by a temperature controller (TC-344C, Warner Instruments).[33,139,196] The coverslip on the bottom of the chamber was coated with 20 µL poly-2-hydroxyethyl methacrylate (poly-HEMA, Sigma-Aldrich) to prevent cellular adhesion. Once the cells had settled, bipolar electrical field stimulation (1 Hz, SIU-102, Warner Instruments) was commenced and contracting cardiomyocytes that

were rod-shaped and clearly striated with intact membranes were chosen at random. Following cellular selection, pacing was halted, and the carbon fibres were positioned at the lateral ends of the long axis of a cell and gently lowered onto the cell membrane using the triaxial hydraulic micromanipulators. Electrostatic adhesion of the cell to the fibres was confirmed by raising the cell off of the coverslip.[215] Once cell attachment was established, electrical stimulation was recommenced, and cells contracted against the carbon fibres for ~1-2 min to improve adhesion. After 5 min in the stop bath, unidirectional transient stretch (~112-173 ms total duration) using the compliant fibre was applied at a specific delay post-electrical stimulation, such that it occurred in two distinct time points of the electrical cycle: in mid-diastole or during the VP (as determined in initial experiments by simultaneous voltage-Ca^{2+} fluorescence-based imaging in each treatment, described below). This was repeated once for a total of four stretches, as follows: (i) mid-diastole (600 ms delay after an electrical stimulus in all treatments), followed by a 10 s pause, and (ii) during the VP (delay adjusted to 300, 150, or 210 ms in NT, simulated ischaemia alone, or simulate ischaemia with glibenclamide, respectively) in late repolarisation, followed by a 10 s pause. This protocol was repeated at increasing magnitudes of piezo-electric translator displacement (20, 30, and 40 μm, with an average 10±1, 16±1, and 18±2% change in sarcomere length, respectively), with 30 s between each increase in magnitude, for a total of 12 stretches (Fig. 4.2a, b).

4.3.5. Assessment of Mechano-Arrhythmogenicity

Contractile function (diastolic and systolic sarcomere length, rate and percent sarcomere shortening, and decay rate of sarcomere relaxation) and characteristics of stretch (percent

change in sarcomere length, stretched sarcomere length, and applied force) were assessed by monitoring sarcomere length, and piezo-electric translator and carbon fibre tip positions (as described above). Arrhythmic activity with stretch was classified from sarcomere measurements into either (i) premature contractions (PVC, 1 or 2 unstimulated contractions), or (ii) complex activity (including delayed arrhythmic activity and sustained arrhythmic activity that either spontaneously resolved or was terminated by an additional stretch; Fig. 4.2). When an arrhythmia occurred, the next stretch was delayed by the appropriate amount (either 10 or 30 s). To control for cellular damage, any stretch that resulted in carbon fibre slippage, or a sustained arrhythmia that could not be terminated by a maximum of 2 stretches was excluded.

4.3.6. Pharmacology

Pharmacologic agents were dissolved in distilled water or dimethyl sulfoxide (DMSO) as appropriate. Agents included: BAPTA-AM (to chelate cytosolic Ca^{2+}; 1 μM with 20 min pre-incubation; Abcam), dantrolene (to stabilise RyR; 1 μM with 5 min pre-incubation; Abcam), HC-030031 (to block TRPA1 channels; 10 μM with 30 min pre-incubation; Abcam), N-acetyl-L-cysteine (NAC, to scavenge intracellular ROS; 10 mM with 20 min pre-incubation; Sigma), diphenyleneiodonium (DPI, to block NADPH oxidase; 3 μM with 60 min pre-incubation; Abcam), or glibenclamide (to block K_{ATP} channel activity; 20 μM with 15 min pre-incubation; Abcam).

4.3.7. Dual Parametric Voltage-Ca^{2+} Fluorescence Imaging

The Ca^{2+}-sensitive dye Fluo-5F AM (5 μM, ThermoFisher Scientific) and Pluronic F-127 (0.02 %, dissolved in DMSO, Biotium) were added to a microcentrifuge tube containing cells in 50% NT and 50% stop solution (20 min). The supernatant was then replaced with fresh, full Ca^{2+} NT, and the voltage-sensitive dye di-4-ANBDQPQ (20 μM, University of Connecticut Health Centre) dissolved in ethanol was added to the tube (14 min). The supernatant was again replaced with fresh NT, probenecid (1 mM, Sigma-Aldrich) was added, and the cells were maintained in the dark at room temperature until use (maximum 1 hour). When ready for imaging, the solution containing dye-loaded cells was gently agitated with a transfer pipette and a small drop was added to 1 mL of the relevant solution (NT or simulated ischaemia) in the imaging chamber. Carbon fibres were adhered (as described above) to allow for proper positioning of cells, and to reduce motion with cellular contraction in the direction perpendicular to the imaging plane, allowing for imaging without the use of an excitation-contraction uncoupler. Fluorescence was excited by a mercury lamp (U-HGLGPS, Olympus) passed through a 466/40 nm bandpass filter (FF01-466/40, Semrock) and reflected onto the sample by a 495 nm dichroic mirror (FF495-Di03, Semrock). For simultaneous measurement of transmembrane voltage and intracellular Ca^{2+}, each fluorescent signal was projected onto one-half of a 128 × 128-pixel, 16-bit electron-multiplying charge-coupled device (EMCCD) camera sensor (iXon3, Andor Technology) using an emission image splitter (Optosplit II; Cairn Research) and recorded at 500 fps with 2 ms exposure and maximum electron-multiplying gain. The two signals were split with a 685 nm dichroic mirror (FF685-Di02, Semrock), Fluo-5F emission was collected with a 525/50 nm bandpass filter (FF03-525/50, Semrock), and di-4-ANBDQPQ

emission was collected with a 700 nm long-pass filter (HQ700lp; Chroma Technology). A schematic of the imaging setup is provided in Fig. 4.1a.

Analysis of voltage-Ca^{2+} signals was performed using custom Matlab routines (R2018a, MathWorks). Whole-cell fluorescence was averaged, a temporal filter (50 Hz low-pass Butterworth) was applied, and bleaching was eliminated by fitting diastolic fluorescence over time with a second-order polynomial function and subtracting the result. From these signals, time to 20, 30, 50, or 80 % recovery of the APD or CaTD were averaged over 3 consecutive cardiac cycles. The VP was calculated as the difference between $CaTD_{80}$ and APD_{50}, a period during which myocytes start to become re-excitable while cytosolic Ca^{2+} remains elevated,[34] plus the difference between the timing of the action potential and Ca^{2+} transient upstrokes (ECC): VP = ($CaTD_{80}$ - APD_{50}) + ECC (Fig. 4.1b).

For assessment of the mechanical phase (stretch and/or release) around the VP during fluorescence imaging (Fig. 4.2b, c, d), cells loaded with the voltage and Ca^{2+} indicators were stretched twice during photoexcitation (40 μm piezo-electric translator displacement) with a 10 s pause in-between: once in diastole, and once in the VP. APD, CaTD, and VP values in these cells were calculated as above, and cross-compared with the timing of stretch, release, both stretch and release, or neither within the VP.

4.3.8. Ratiometric Ca^{2+} Fluorescence Imaging

Ratiometric Ca^{2+} levels were assessed using the Ca^{2+} indicator Fura Red-AM (5 μM; AAT Bioquest). Cells loaded with the dye were incubated with Pluronic F-127 (0.02 %) and probenecid (1 mM, dissolved in DMSO) for 20 min. Excitation was induced using alternating pulses from two white light-emitting diodes (CFT-90-W; Luminus Devices)

each with a bandpass filter (420/10 nm, FF01-420/10, Semrock; or 531/22 nm, FF02-531/22, Semrock) that were combined into the microscope excitation light path with a 455 nm dichroic mirror (AT455dc, Chroma Technology) and reflected onto the sample by a 562 nm dichroic mirror (T562lpxr, Chroma Technology). Fluorescence emission was measured through a 632/60 nm bandpass filter (AT635/60m, Chroma Technology) with an EMCCD camera at a rate of 500 fps, with 2 ms exposure time and maximum electron-multiplying gain. Light pulses and camera frame acquisition were synchronised with a custom control box (supplied by Dr. Ilija Uzelac, Georgia Institute of Technology) so that alternating frames corresponded to the signal generated by the two excitation wavelengths.

Analysis of intracellular Ca^{2+} was performed using custom Matlab routines. Whole-cell fluorescence was averaged, and a temporal filter (50 Hz low-pass Butterworth) was applied. The two Ca^{2+} signals were separated, and the ratio was calculated. Any remaining baseline drift was eliminated by fitting the resulting diastolic fluorescence signal with a second-order polynomial function and subtracting the result. From the corrected signals, the minimum value for each cardiac cycle (representing the diastolic Ca^{2+} level) was averaged over 3 consecutive cardiac cycles. To assess changes in intracellular Ca^{2+} following exposure to simulated ischaemia, cells were first imaged in NT to get a baseline value, followed by a change to the simulated ischaemia solution by perfusion at 2.1 mL/min through an inline heater (SF-28, Warner Instruments) for 2 min. Perfusion was stopped, and cells were maintained in the ischaemic solution for 5 min before the second measurements were recorded.

4.3.9. Statistics

Statistics were performed using GraphPad Prism 9. Differences in arrhythmia incidence were assessed using chi-square contingency tables and Fisher's exact test. Differences between group means were assessed by two-tailed, paired or unpaired Student's t-test (for normally distributed data) or Wilcoxon matched-pairs test (for data that was not normally distributed), one-way ANOVA with Tukey *post-hoc* tests (for normally distributed data), or Kruskal-Wallis with Dunn's multiple comparisons test (for non-normally distributed data), where appropriate. $p< 0.05$ was considered significant. The relevant test and number of replicates is indicated in each figure caption (N = rabbits, n = cells, m = stretches, c = complex arrhythmias).

4.4. Results

4.4.1. Simulated Ischaemia Creates a VP That Can be Reduced by Blocking K_{ATP} Channels.

The fluorescence imaging approach for APD and CaTD (Fig. 4.1a) revealed that stop bath exposure to simulated ischaemia (5 min) decreased both APD ($APD_{50,NT}$ = 381±11 ms *vs* $APD_{50,SI}$ = 221±8 ms; $p<0.0001$) and CaTD ($CaTD_{80,NT}$ = 433±9 ms *vs* $CaTD_{80,SI}$ = 358±8 ms; $p<0.0001$) compared to control (Fig. 4.1b, c and Supplemental Fig. 4.1a, b). This increased the VP (= ($CaTD_{80}$ – APD_{50}) + ECC) in ischaemic cells (VP_{NT} = 66±12 ms *vs* VP_{SI} = 145±6 ms; $p<0.0001$; Fig. 4.1d). The simulated ischaemia-induced decrease in APD was attenuated by pre-incubation with the K_{ATP} antagonist glibenclamide ($APD_{50,GLIB}$ = 282±8 ms; $p<0.0001$; Fig. 4.1b, c, Supplemental Fig. 4.1c), with no effect on CaTD

($CaTD_{80,GLIB}$ = 384±8 ms), ultimately reducing the duration of the VP ($VP_{,GLIB}$ = 109±6 ms; p<0.05), although, it remained longer than in control (p<0.005; Fig. 4.1d).

4.4.2. Transient Stretch of Ventricular Myocytes Results in Arrhythmias

Stretch of ventricular myocytes with carbon fibres (Fig. 4.2a, b, c) resulted in premature excitation (1-2 unstimulated contractions; Fig. 4.2d) and complex activity, including delayed transient rhythm disturbances (Fig. 4.2e) and sustained arrhythmic activity that either spontaneously resolved (Fig. 4.2f), or that was terminated by an additional stretch (Fig. 4.2g). To ensure arrhythmic activity was not the result of stretch-induced cellular damage, parameters of contractile function (diastolic sarcomere length, maximal rate of shortening, and percent sarcomere shortening) were measured immediately before and after completion of a stretch-induced event, all of which showed no change, suggesting that cellular damage had not occurred (Supplemental Fig. 4.2). Stretch characteristics were measured at each increasing piezo-electric translator displacement, which corresponded with an increase in percent sarcomere stretch (10.7±1, 16±2, and 18.5±2 %; p<0.005, stretched sarcomere length (2.04±0.02, 2.15±0.02, and 2.21±0.03 μm; p<0.0001), and stretch force (0.55±0.01, 0.80±0.05, and 0.98±0.05 μN; p<0.0001). Importantly, while stretch characteristics scaled with piezo-electric translator displacement in all cells, absolute values of stretch parameters (percent sarcomere stretch, stretched sarcomere length, and stretch force) varied at baseline between cells, reflecting the physiological heterogeneity of cells in the ventricle with respect to their intrinsic stiffness and response to an ischaemic insult.[139] Notably, the diastolic sarcomere length within a given cell was maintained after stretch at each magnitude, indicating that carbon fibre slippage and

subsequent cell buckling did not occur (Supplemental Fig. 4.3). Surprisingly, however, increased piezo-electric translator displacement did not correspond with a significant increase in arrhythmic incidence in either control or ischaemic cells (although a clear trend was present, Supplemental Fig. 4.4). As there was no effect of piezo-electric translator displacement magnitude on arrhythmia incidence, stretches with all displacements were pooled for subsequent analysis.

4.4.3. Mechano-Arrhythmogenicity is Enhanced in Late Repolarisation in Ischaemic Cells

To assess whether mechano-arrhythmogenicity is dependent on stretch timing, transient stretch was applied in mid-diastole or during the VP in control and ischaemic cells (average VP timing for each group was determined in advance by fluorescence imaging, reported above, Fig. 4.1d). We showed that the incidence of stretch-induced arrhythmias was increased in ischaemic cells compared to control in the VP (6.8 *vs* 1.2% of stretches induced arrhythmias; $p<0.005$) but not in diastole (5.1 *vs* 3.1%). Additionally, in ischaemic cells, arrhythmias generated in the VP were proportionally more complex than those generated in diastole (100 vs 69% of events had complex activity; $p<0.05$; Fig. 4.3). Fluorescence-based measurement of APD and CaTD during stretch was performed in a subset of cells to assess the temporal relation of the stretch pulse (stretch and/or release) to the VP, and its effect on arrhythmia incidence. This showed that 96% of cases had either stretch, stretch release, or both occur within the cell-specific VP, with 4% of stretches missing it entirely (Supplemental Fig. 4.5a). Of those cases with some portion of the stretch pulse within the VP, 52% had both stretch and release within the VP, 41% only had release,

and 7% only had stretch (Supplemental Fig. 4.5b). Yet, 100% of cases that resulted in an arrhythmia were attributed to both stretch and release within the VP (which represented 50% of those stretches; Supplemental Fig. 4.5b, c). We then sought to assess whether mechano-arrhythmogenicity in ischaemic cells was affected by a reduced VP by blocking K_{ATP} channels (Fig.4.1b, d). Pre-incubating ischaemic cells with glibenclamide reduced arrhythmia incidence in the VP compared to ischaemia alone (2.1 *vs* 6.8% of stretches; $p<0.05$) with no effect on diastolic incidence (4.8 *vs* 5.1%; Fig. 4.3).

4.4.4. TRPA1 Channels and ROS Mediate Ischaemic Mechano-Arrhythmogenicity in the VP

We next aimed to determine mechanisms underlying the observed increase in mechano-arrhythmogenicity during the ischaemic VP. As we have previously shown that TRPA1 channels can act as a source for mechano-arrhythmogenicity,[34] and it is known that TRPA1 channel activity is increased in ischaemia,[47] we tested the effects of a specific TRPA1 blocker on arrhythmia incidence. Incubating cells with HC-030031 prior to ischaemia exposure reduced arrhythmia incidence with stretch in the VP compared to ischaemia alone (0.9 *vs* 6.8%; $p<0.005$), with no change in diastolic incidence (4.7 *vs* 5.1%), suggesting a role for TRPA1 channels in ischaemic mechano-arrhythmogenicity (Fig. 4.4a).

Interestingly, while fluorescence imaging our ischaemic cells, we observed a further increase in mechano-arrhythmogenicity during the VP (28.6 *vs* 6.8%; $p<0.005$), as well as an increase in diastole (14.3 *vs* 4.9%; $p<0.05$; Fig. 4.4b). However, this increase was only greater when the cells (loaded with Fluo-5F and di-4-ANBDQPQ) were exposed to photo-activation of the fluorescent dyes (arrhythmia incidence without light exposure:

VP = 15.8% and diastole = 10.0%; Fig. 4.4b). As fluorophore photo-activation is associated with ROS generation,[328] which is increased in ischaemia,[33] this suggested that ROS might contribute to the observed arrhythmias. To test this, we chelated intracellular ROS with NAC and found that arrhythmia incidence in the VP decreased compared to ischaemia alone (0.8 *vs* 6.8%; $p<0.0005$), with no effect in diastole (2.3 *vs* 5.1%; Fig. 4.4c). Further, as we have previously shown that X-ROS production is enhanced in ischaemia (demonstrated in Chapter 2),[33] we tested the effect of the NOX2 inhibitor DPI to block X-ROS production in ischaemic cells. DPI also reduced arrhythmia incidence in the VP (2.4 vs 6.8%; $p<0.05$) and had no effect in diastole (3.9 *vs* 5.1%; Fig. 4.4c). Combined, this data suggests that ROS, possibly through its effects on TRPA1,[5] is a mediator of ischaemic mechano-arrhythmogenicity.

4.4.5. Ischaemic Ca^{2+} Loading is Necessary, but Insufficient for Mechano-Arrhythmogenicity

As we have previously shown that increased cytosolic Ca^{2+} is necessary for TRPA1-mediated mechano-arrhythmogenicity,[34] we sought to assess whether it also has a role in the stretch-induced arrhythmias observed in the present study. We first buffered cytosolic Ca^{2+} in ischaemic cells with BAPTA-AM and found that arrhythmia incidence was decreased in the VP (2.4 *vs* 6.8%; $p<0.05$). While this supports a necessary role for Ca^{2+} in ischaemic mechano-arrhythmogenicity, surprisingly, arrhythmia incidence in these cells was simultaneously increased in diastole compared to control (8.5 *vs* 3.1%; $p<0.05$; Fig. 4.5a). Next, we assessed whether Ca^{2+} release from the sarcoplasmic reticulum *via* RyR may be involved in the observed arrhythmogenic role of cytosolic Ca^{2+} (like X-ROS,

stretch-induced Ca^{2+}-sparks are also enhanced by ischaemia).[33] To test this, RyR in ischaemic cells were stabilised in their closed state with dantrolene. However, this had no effect on arrhythmia incidence at either point in the cardiac cycle (VP = 4.4% and diastole = 6.7%; Fig. 4.5a). Finally, as diastolic Ca^{2+} loading in ischaemia itself can be arrhythmogenic,[12] we wanted to directly assess changes in cytosolic Ca^{2+} in our model. Through ratiometric Ca^{2+} imaging (using Fura Red-AM), we found that diastolic Ca^{2+} was increased with ischaemia exposure (+9.3±1.1% change $p<0.0001$). Yet, while block of TRPA1 (with HC-030031) or chelation of ROS (with NAC) decreased mechano-arrhythmogenicity in ischaemia, they did not prevent the increase in cytosolic Ca^{2+} (+10.0±1.0 or +12.3±1.4%), suggesting that neither TRPA1 nor ROS are solely responsible for the elevated Ca^{2+} levels in our ischaemic cells (Fig. 4.5b).

4.5. Discussion

In this study, we aimed to define cellular mechanisms of ischaemic mechano-arrhythmogenicity and the importance of the VP using rabbit ventricular myocytes exposed to simulated ischaemic conditions, and subjected to controlled stretch. We showed that mechano-arrhythmogenicity was enhanced only in the VP during simulated ischaemia, that arrhythmias generated in the VP were more complex than those in diastole, and that mechano-arrhythmogenesis in the VP involved TRPA1, cytosolic Ca^{2+}, and ROS.

4.5.1. Role of the VP in Ca^{2+}-Mediated Mechano-Arrhythmogenicity During Ischaemia

In the whole heart, ischaemia-induced K_{ATP} channel activation has been shown to cause a larger decrease in APD than CaTD, such that cytosolic Ca^{2+} remains high in repolarising (and thus progressively re-excitable) tissue, resulting in a VP in late repolarisation for Ca^{2+}-mediated arrhythmic activity.[12,280] Elevated cytosolic Ca^{2+} can be arrhythmogenic by driving forward-mode (electrogenic) NCX activity, approaching or exceeding the threshold for premature excitation.[137,155] Indeed, it has been shown that the generation of a VP through pharmacological K_{ATP} activation (with pinacidil)[34,280] or β-adrenergic stimulation[156] facilitates arrhythmogenesis. In ischaemia, the arrhythmogenic potential of the VP may be exacerbated by transmural heterogeneity of K_{ATP} channel expression[186] and the facilitation of cytosolic Ca^{2+} loading at faster heart rates.[156] Acute stretch may further increase cytosolic Ca^{2+} *via* Ca^{2+} influx through MSC,[28] which may also drive depolarisation and premature excitation by Na^{+} influx.[216] Furthermore, stretch has been shown to increase the affinity of myofilaments for Ca^{2+}, such that systolic stretch causes excess myofilament Ca^{2+} loading.[28] Upon stretch release, dissociation of this excess myofilament-bound Ca^{2+} can produce a surge in cytosolic Ca^{2+}, which may induce sarcoplasmic reticulum Ca^{2+} release and generate Ca^{2+} waves, or drive NCX-mediated membrane depolarisation and induce premature excitation.[135] Combined, these mechanisms may be sufficient to drive mechano-arrhythmogenicity in the VP.

In the present study, we demonstrated the emergence of a cellular VP in cells exposed to simulated ischaemia (Fig. 4.1). When transient stretch was timed to occur in the VP (Fig. 4.2), there was an increase in arrhythmia incidence that did not occur with stretch

in diastole (Fig. 4.3), thus revealing a temporal-dependence of ischaemic mechano-arrhythmogenicity. When the length of the VP was reduced by blocking K_{ATP} channels (Fig. 4.1), there was a reduction in arrhythmia incidence (Fig. 4.3), further supporting the importance of the VP for ischaemic mechano-arrhythmogenicity. The question of whether stretch, stretch release, or a combination of the two is critical to mechano-arrhythmogenicity in this setting remains an open question. Fluorescence-based measurement during stretch in the present study, however, revealed that all stretches that resulted in an arrhythmia had both stretch and release occur within the VP (Supplemental Fig. 4.5), suggesting that a combination of the two may be necessary for mechano-arrhythmogenicity. This may also partly explain why we did not see a higher incidence of stretch-induced arrhythmias in ischaemic cells, as well as why reducing (but not eliminating) the VP with glibenclamide attenuated arrhythmia incidence.

4.5.2. Role of Mechano-Sensitive TRPA1 Channels in Ischaemic Mechano-Arrhythmogenicity

A principal question underlying mechano-arrhythmogenicity is the identity of the MSCs involved.[216] We have demonstrated that TRPA1 channels can act as a source for Ca^{2+}-mediated mechano-arrhythmogenicity in ventricular myocytes.[34] The potential role for TRPA1 channels in stretch-induced arrhythmias during ischaemia is supported by their inherent mechano-sensitivity,[193] their preferential permeability to Ca^{2+},[21] and their activation by ischaemic factors, namely ROS[5] (being the TRP channel most sensitive to oxidation)[322] and Ca^{2+},[332] (which is in fact bimodal, such that increased cytosolic Ca^{2+} enhances inward current to a point, after which greater increases in Ca^{2+} begin to inactivate

channels).[299] To test for their involvement, the specific TRPA1 blocker HC-030031 was used, which reduced arrhythmia incidence only in the VP (Fig. 4.4), supporting the role of TRPA1 channels in ischaemic mechano-arrhythmogenicity.

The finding that mechano-arrhythmogenicity was exclusively increased during late repolarisation may also be related to a specific property of TRPA1 channels. While TRPA1 has been classically considered a non-voltage dependent channel, it has recently been shown that, under normal conditions, it is activated and inactivated by voltage at potentials outside the physiological range (+90 to +170 mV) so that voltage is not a relevant factor for its kinetics.[183] However, when exposed to non-electrophilic agonists[184] or elevated Ca^{2+},[332] there is a leftward shift in its voltage activation into the physiological range. Further, continual TRPA1 agonism has been shown to de-sensitise the channel to Ca^{2+}-mediated inhibition, effectively resulting in a sensitised channel with a physiological voltage dependence.[184,185] Thus, in ischaemia, increases in cytosolic Ca^{2+} and ROS may not only increase TRPA1 channel activity directly, but also indirectly through reduced Ca^{2+}-mediated inhibition and modulation of its voltage dependence.

4.5.3. Role of Intracellular ROS in Ischaemic Mechano-Arrhythmogenicity

ROS production is increased in ischaemia,[33,38] which may contribute to mechano-arrhythmogenicity by increasing baseline TRPA1 activity,[5] and thus its response to mechanical stimulation.[25] The potential mechanistic role of ROS in our ischaemic cells was first revealed in our fluorescence imaging experiments, as fluorophore photo-activation, which generates ROS,[328] resulted in an overall increase in arrhythmia incidence (Fig. 4.4b). To more directly test the contribution of ROS to the observed arrhythmias, intracellular

ROS was scavenged with NAC, or its NOX2 production was blocked with DPI, both of which decreased arrhythmia incidence in the VP (Fig. 4.4c). The importance of ROS for arrhythmogenesis may extend beyond its potential effect on TRPA1 activity. Stretch-induced ROS production has been shown to influence myofilament Ca^{2+} sensitivity and Ca^{2+} wave propagation,[190,191] and to enhance mechano-sensitive sarcoplasmic reticulum Ca^{2+} release *via* RyR,[33] so it may additionally contribute to mechano-arrhythmogenicity through effects on cytosolic Ca^{2+}.

4.5.4. Role of Cytosolic Ca^{2+} in Ischaemic Mechano-Arrhythmogenicity

Ischaemic mechano-arrhythmogenicity in the VP appears to be mediated by cytosolic Ca^{2+}, which is increased in ischaemia.[12] This was supported by the observation that chelating cytosolic Ca^{2+} with BAPTA reduced arrhythmias in the VP (although, paradoxically, it increased premature excitation in diastole, perhaps due to an increase in the driving force for Ca^{2+} influx with cytosolic Ca^{2+} buffering; Fig. 4.5a). This suggests that not only is Ca^{2+} involved in stretch-induced arrhythmias during ischaemia, but also their temporal dependence. Ischaemic potentiation of stretch-induced Ca^{2+} release *via* RyR has been suggested to be arrhythmogenic by contributing to cytosolic Ca^{2+} load and NCX-mediated membrane depolarisation.[12,33] However, dantrolene (a RyR stabiliser) had no effect on arrhythmia incidence, suggesting that mechano-sensitive RyR release was not playing a critical role in arrhythmogenesis. Another potential mechanism of increased cytosolic Ca^{2+} is its direct activation of TRPA1 channels.[332] Similar to elevated levels of ROS, this increase in baseline TRPA1 activity may increase their response to mechanical stimulation.[25] Importantly, however, as cytosolic Ca^{2+} was not reduced by the TRPA1

blocker HC-030031 or the ROS scavenger NAC (Fig. 4.5b), despite a reduction in arrhythmias (Figs. 4.44a, c), it appears that cytosolic Ca^{2+} is necessary, but not sufficient for ischaemic mechano-arrhythmogenicity.

4.6. Conclusion

Ultimately, the observed ischaemic mechano-arrhythmogenicity within the VP appears to relate to an increase in TRPA1 channel activity, driven by elevated intracellular ROS and cytosolic Ca^{2+} levels. Targeting TRPA1 channels in this setting may help prevent electrical dysfunction and myocardial damage.[47] The same may be true in other pathologies associated with changes in cardiac mechanics and TRPA1 modulating factors,[183] such as ventricular pressure overload, in which TRPA1 has been shown to be involved in pathological changes[301] and mechano-arrhythmogenicity is thought to occur,[226] making TRPA1 channels a novel anti-arrhythmic target with exciting therapeutic potential.[194]

4.7. Statements

4.7.1. Acknowledgements

Carbon fibres were a gift from Jean-Yves LeGuennec and supplied by P. Kohl. We thank G. Iribe and K. Kaihara for technical assistance with the carbon fibre method, and I. Uzelac for supplying the electronic LED control.

4.7.2. Sources of Funding

This work was supported by the Dalhousie Medical Research Foundation (Hoegg Graduate Studentship to B.A.C and Capital Equipment Grant to T.A.Q.), the Canadian Institutes of Health Research (MOP 342562 to T.A.Q.), the Natural Sciences and Engineering Research Council of Canada (RGPIN-2016-04879 to T.A.Q.), the Heart and Stroke Foundation of Canada (National New Investigator Award to T.A.Q.), and the Canadian Foundation for Innovation (32962 to T.A.Q.).

4.7.3. Author contributions

B.A.C. and T.A.Q. designed the study, interpreted the data, and wrote the manuscript; B.A.C. performed the experiments and analysed the data.

4.8. Figures

Figure 4.1 | Temporal uncoupling of voltage-Ca^{2+} dynamics in single ventricular myocytes exposed to simulated ischaemia is reduced by block of K_{ATP}- channels with glibenclamide. a, Schematic of the single-excitation/dual-emission fluorescence imaging technique, utilising voltage (di-4-ANBDQPQ, 20 μM for 14 min) and Ca^{2+} (Fluo-5F-AM, 5 μM for 20 min) fluorescent indicators and a single camera-image splitter system. **b,** Representative trace of an action potential (AP, blue) and Ca^{2+} transient (CaT, red) simultaneously recorded by fluorescence imaging in a contracting, paced (1 Hz) ventricular myocyte after 5 min exposure to either control (left), or to simulated ischaemia solution alone (middle) or following pre-incubation with glibenclamide (20 μM for 15 min, right). The calculated vulnerable period (VP = [$CaTD_{80}$ - APD_{50}] + ECC) is shown in green. APD_{50}, action potential duration at 50% repolarisation; $CaTD_{80}$, calcium transient duration at 80% recovery; ECC, excitation-contraction coupling. **c,** Average APD_{50} (blue) and $CaTD_{80}$ (red) after 5 min in either normal Tyrode (NT), or in simulated ischaemia (SI) alone or with glibenclamide (SI + GLIB). **d,** Average calculated VP in NT, SI, or SI + GLIB. Differences assessed by one-way ANOVA, with Tukey *post-hoc* tests. **p*<0.05 between groups. Error bars represent standard error of the mean. *N* = rabbits, *n* = cells.

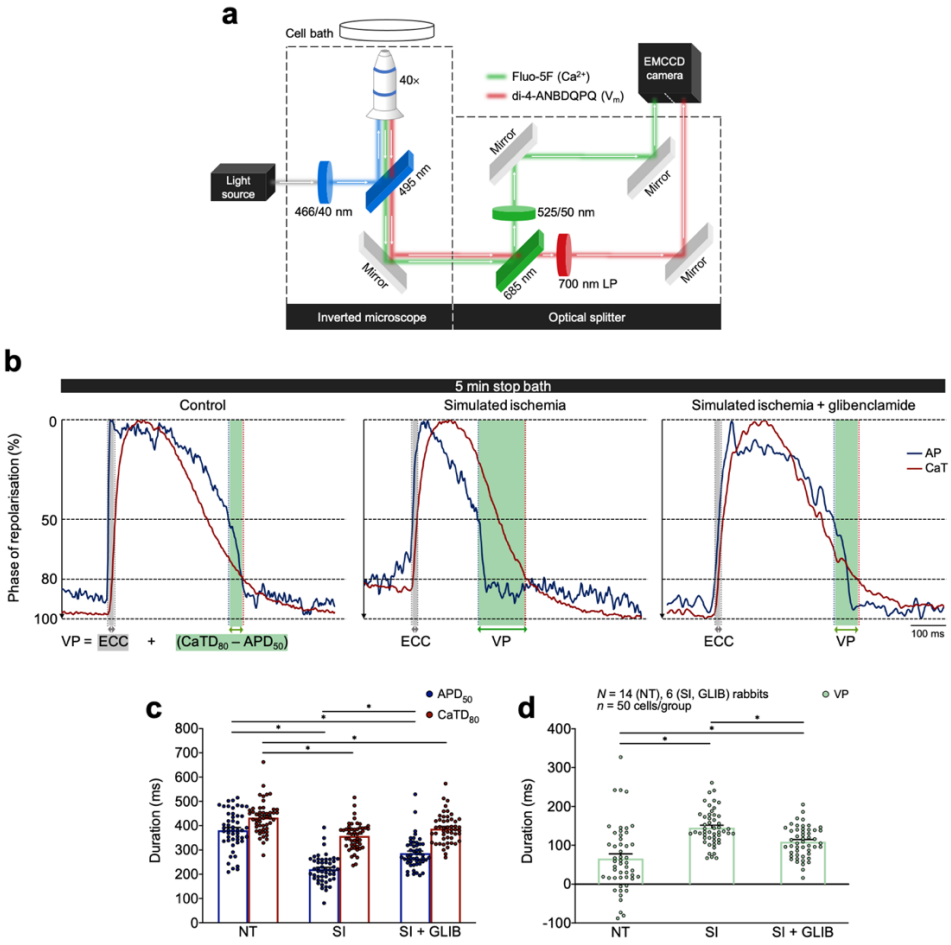

Figure 4.2 | Protocol for the timed transient stretch of single ventricular myocytes and classification of associated arrhythmias. a, Brightfield image of a rabbit single ventricular myocyte before (top) and (bottom) during unidirectional axial stretch using a carbon-fibre based system at increasing magnitudes of piezo displacement (left to right: 20, 30, and 40 µm). **b**, Schematic of the protocol for stretch of a single myocyte timed in mid-diastole and the vulnerable period (VP) in control, or in simulated ischaemia (SI) alone or following pre-incubation with glibenclamide (20 µM for 15 min, GLIB). **c**, Representative measurement of sarcomere length in a cell exposed to simulated ischaemia during 1 Hz pacing (orange dots) and stretched in diastole and the VP (green) that maintained normal paced rhythm (NPR). **d,** Stretch-induced premature ventricular contraction (PVC, blue segment). **e,** Stretch-induced delayed complex arrhythmia (red segment). **f,** Stretch-induced sustained arrhythmic activity that spontaneously resolved. **g,** Stretch-induced sustained arrhythmic activity that was terminated by rescue stretches (second and third green bars), and a later PVC with stretch.

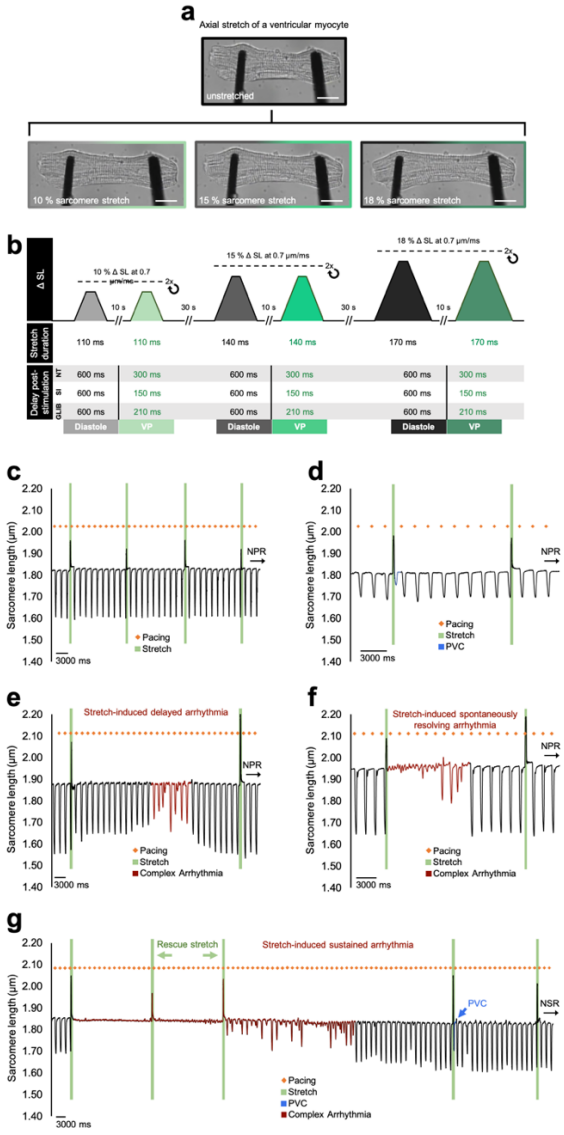

Figure 4.3 | Role of the VP in ischaemic mechano-arrhythmogenicity. a, Incidence of premature excitation (PVC, blue) and complex arrhythmias (red) with transient stretch of rabbit ventricular myocytes during diastole or the vulnerable period (VP) in cells exposed to 5 min of normal Tyrode (NT), or to either simulated ischaemia alone (SI) or following pre-incubation with glibenclamide (20 μM for 15 min, SI + GLIB) to reduce the VP (green). Differences in arrhythmic incidence assessed using chi-square contingency tables and Fisher's exact test. *p<0.05 between groups, **p<0.05 between diastolic and VP complexity within a treatment. N = rabbits, n = cells, m = stretches.

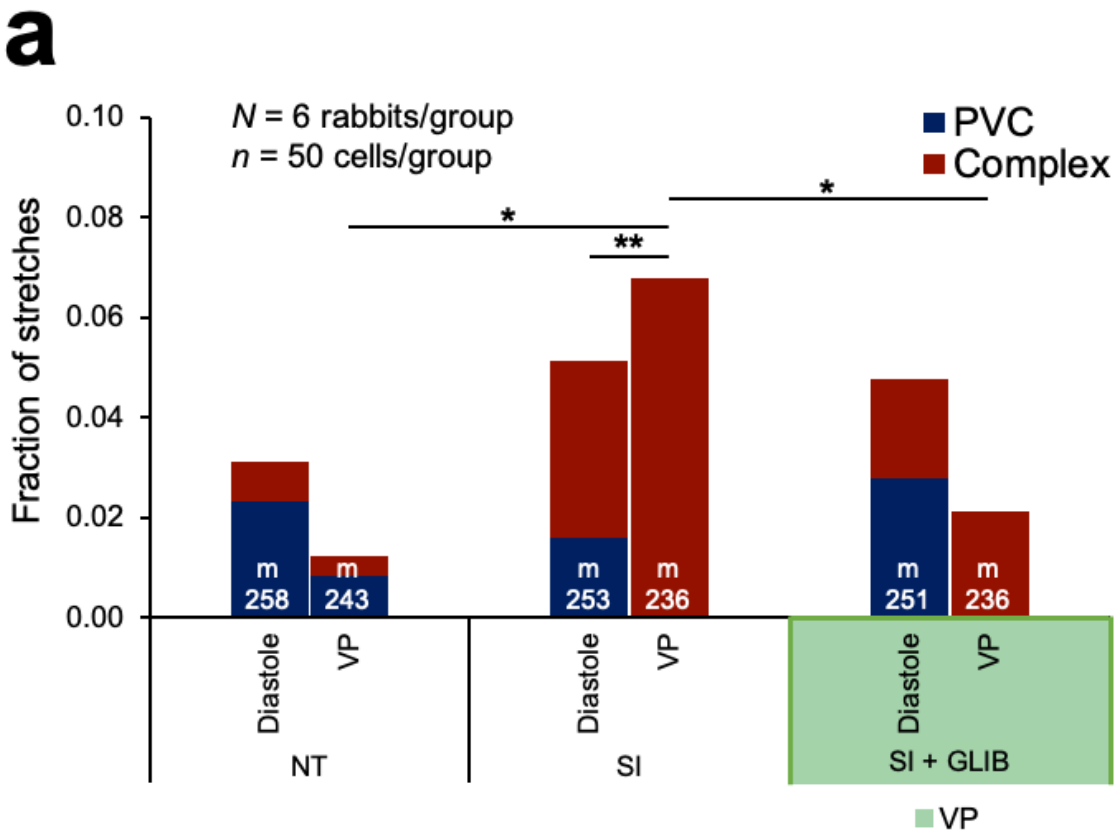

Figure 4.4 | Role of ROS and TRPA1 channels in ischaemic mechano-arrhythmogenicity. a, Incidence of premature excitation (PVC, blue) and complex arrhythmias (red) with transient stretch of rabbit ventricular myocytes during diastole or the vulnerable period (VP) in cells exposed to 5 min of simulated ischaemia (SI) pre-incubated with the TRPA1 inhibitor, HC-030031 (10 μM for 30 min). **b**, Incidence of arrhythmias with stretch during diastole or the VP in ischaemic cells incubated with the voltage (di-4-ANBDQPQ, 20 μM for 14 min) and Ca^{2+} (Fluo-5F-AM, 5 μM for 20 min) fluorescent indicators, without (middle) or with (right) photo-activation. **c**, Incidence of arrhythmias with stretch during diastole or the VP in cells exposed to 5 min of SI pre-incubated with either the ROS scavenger, N-acetyl-L-cysteine (NAC, 10 mM for 20 min), or the NADPH-oxidase inhibitor, diphenyleneiodonium (DPI, 3 μM for 60 min), to block ROS production. Differences in arrhythmic incidence assessed using chi-square contingency tables and Fisher's exact test. *p<0.05 between groups. N = rabbits, n = cells, m = stretches.

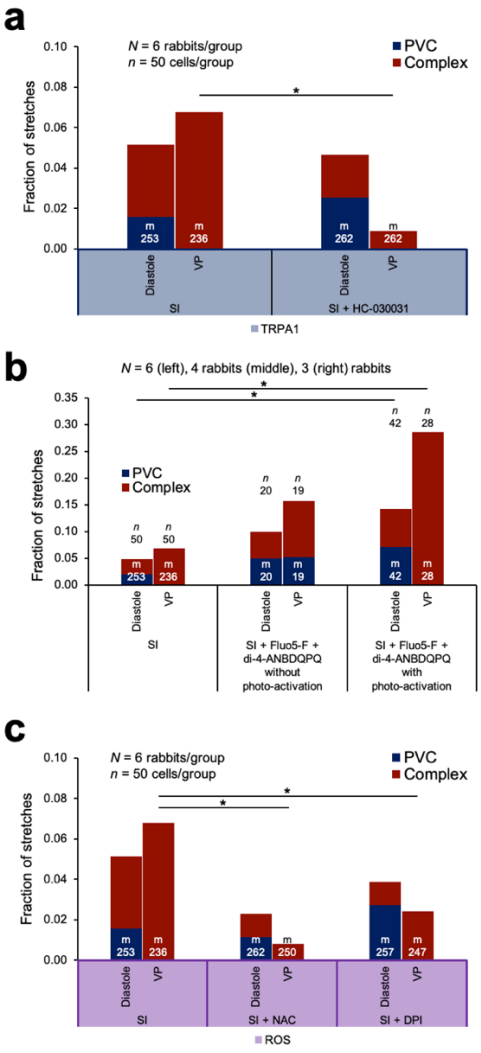

Figure 4.5 | Role of intracellular Ca^{2+} in ischaemic mechano-arrhythmogenicity. a, Incidence of premature excitation (PVC, blue) and complex arrhythmias (red) with transient stretch of ventricular myocytes during diastole or the vulnerable period (VP) in cells exposed to 5 min of simulated ischaemia (SI) pre-incubated with the Ca^{2+} chelator, BAPTA (middle; 1 μM for 20 min), or with the RyR stabiliser, dantrolene (right; DNT, 1 μM for 5 min). Differences in arrhythmic incidence assessed using chi-square contingency tables and Fisher's exact test. *p<0.05 between groups, #p<0.05 compared to NT. **b,** Percent change in diastolic Ca^{2+} load from control after 5 min exposure to SI, SI + NAC (N-acetyl-L-cysteine, 10 mM for 20 min pre-incubation), or SI + HC-030031 (10 μM for 30 min pre-incubation). Differences assessed using unpaired Student's t-test between groups. Error bars represent SEM. N = rabbits, n = cells, m = stretches.

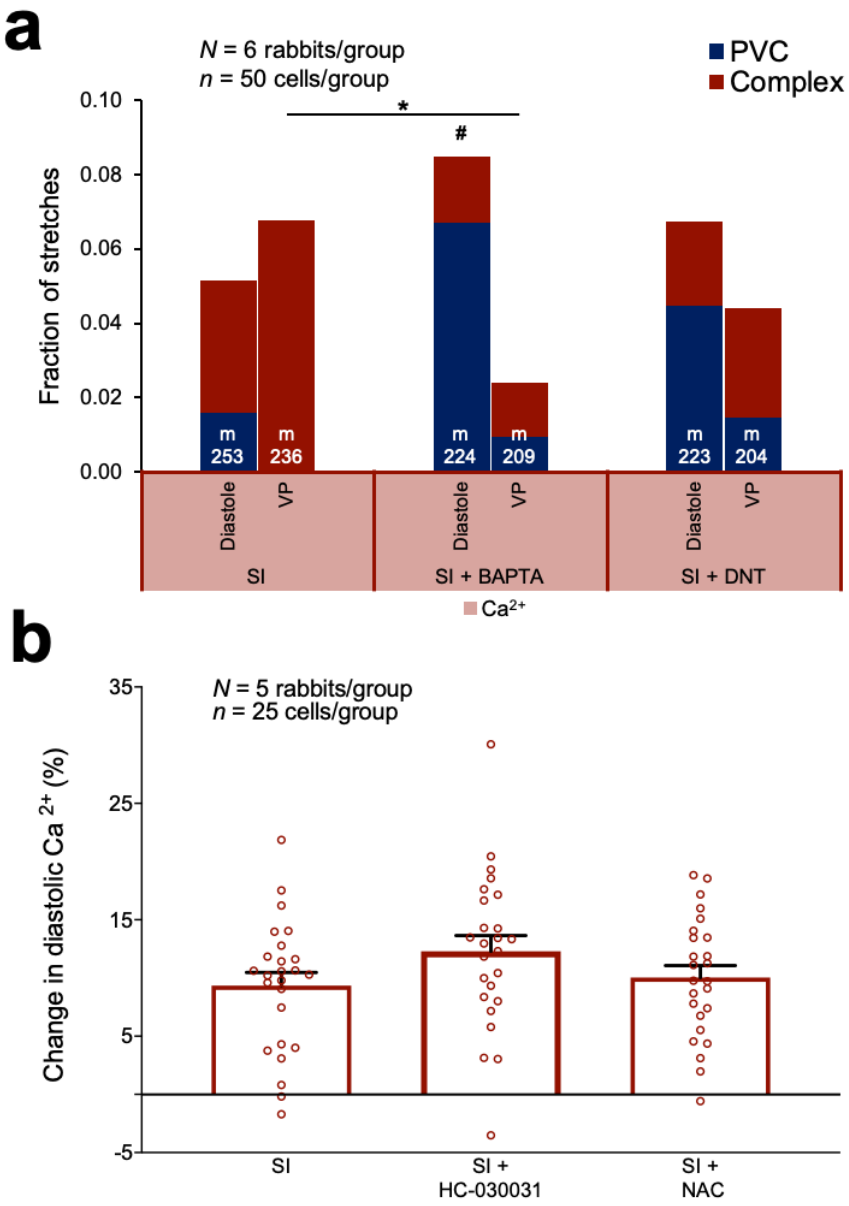

CHAPTER 5: INCREASED MICROTUBULE DETYROSINATION IN VENTRICULAR MYOCYTES ENHANCES MECHANO-ARRHYTHMOGENICITY BY REDUCING THE STRETCH-THRESHOLD FOR ARRHYTHMOGENESIS

The contents of this chapter represent ongoing work, which is currently being translated to the whole heart by another PhD student in the lab (Ms. Jessi Bak). In consultation with Dr. Alex Quinn, I was directly involved in the conception and design of the study and the development and establishment of the applied methodology. I performed all experiments, acquired and analysed all data, and wrote this chapter with suggestions from Dr. Quinn. Supplemental figures for this project are found in Appendix 4.

5.1. Abstract

Rationale: In hypertension, there is an increased risk of sudden cardiac death associated with acute haemodynamic fluctuations in the presence of ventricular remodelling. Increased MTN density (*via* polymerisation) or stability (*via* post-translational modifications, *e.g.*, detyrosination or acetylation) may enhance mechano-sensitivity, and reduce the stretch threshold for mechanically-induced arrhythmias ('mechano-arrhythmogenicity'). **Objective:** Determine the role of MTN alterations in mechano-arrhythmogenicity. **Methods**: Rabbit LV myocytes, exposed to paclitaxel to hyperpolymerise and stabilise the MTN, were rapidly stretched at increasing magnitudes (+7-16% change in sarcomere length over ~112ms) in diastole with carbon fibres. Drugs were used in paclitaxel-treated cells to reduce MTN density (colchicine) or detyrosination (parthenolide), and in control cells to increase acetylation (tubacin). Cellular stiffness was measured from stepwise generated force-length curves. **Results:** Paclitaxel reduced the stretch-threshold for arrhythmogenesis (≥12±1 *vs* ≥22±2% increase in sarcomere length), resulting in more arrhythmias than in control (14 *vs* 4% of stretches had an arrhythmia; $p<0.005$). Arrhythmia incidence with paclitaxel was reduced by colchicine (4%; $p<0.005$) or parthenolide (6%; $p<0.05$), while tubacin had no effect. Paclitaxel or tubacin increased stiffness compared to control (45±6 or 43±5 *vs* 29±3 nN/µm; $p<0.05$), which, with paclitaxel, was not prevented by colchicine or parthenolide. Paclitaxel increased stretch priming of microtubules (increase in cellular stiffness with repeated stretch) compared to control (44±8 *vs* 10±3 nN/µm; $p<0.0001$), which was prevented by colchicine (14±3) or parthenolide (14±6; $p<0.005$). **Conclusion:** Increased MTN detyrosination, rather than acetylation or cell stiffness, enhances mechano-arrhythmogenicity in ventricular myocytes.

5.2. Introduction

In heathy ventricular myocardium, the likelihood that diastolic tissue stretch triggers premature excitation ('mechano-arrhythmogenicity') is dependent on the degree of distension.[80,96,98,212,231,257] As a result, a stretch threshold for mechano-arrhythmogenicity exists, which we will refer to as the 'mechano-arrhythmogenic threshold'. Both global (*via* acute fluctuations in intraventricular volume)[80,96] and regional (*via* localised deformation)[26,61,157,231,266] transient, supra-threshold mechanical stimuli have been shown to elicit excitation. In pathological states, such as acute ischaemia (discussed in Chapters 3 and 4)[34] or chronic hypertension,[233,263,272,276] stretch-induced excitation in the presence of a disease-related arrhythmic substrate may result in its conversion into a complex, sustained arrhythmic event.

In patients with structural heart disease, acute fluctuations in ventricular haemodynamics (*i.e.,* blood pressure or volume) are more likely to initiate premature excitation. [263,272,276] In fact, arrhythmia incidence in these patients is affected by circadian oscillations[195] or daily variations in blood pressure,[240] as well as through pharmacological modulation.[259] This increase in mechano-arrhythmogenicity with acute mechanical loading suggests a reduction of the mechano-arrhythmogenic threshold. While in the whole heart, a reduced mechano-arrhythmogenic threshold may involve a contribution of increased tissue stiffness related to fibrosis and remodelling of non-myocytes,[229,284] at the cellular level, this may instead reflect modulation of components of cellular mechano-sensitivity, such as mechano-electric effectors (*e.g.*, MSC),[129,216] including TRP channels,[73,113,204,305] or mechano-electric transducers (*e.g.*, the MTN).[36,37,39,250]

The MTN is a latticed structure comprised of repeating units of *a* and ß-tubulin heterodimers existing in a state of dynamic equilibrium, as they continuously cycle through periods of assembly (polymerisation) and decay (catastrophe),[244] facilitating their role in intracellular trafficking of organelles (*e.g.*, mitochondria)[92] and ion channels.[265,268] Alterations in the MTN may therefore influence MSC activity, and consequentially their effective contribution to mechano-arrhythmogenicity.[34] This influence may be direct, through alterations in MTN-mediated ion channel trafficking and stretch-activation (*e.g.*, TRPA1, as demonstrated in Chapter 3),[34,88,216,265] or indirect, through mechano-transduction-mediated modulation of mechano-electric mediators[5,332] (*e.g.*, Ca^{2+} sparks and X-ROS, discussed in Chapters 2-4).[34,46,132] The degree to which mechano-transduction by microtubules affects these changes is modulated by the relative density (*via* their lateral reinforcement and changes in cellular stiffness)[24,36,37] and stability (*via* post-translational modifications, *e.g.,* detyrosination and acetylation) of the MTN.[15,218,250]

Detyrosination (a process through which a tyrosine residue is reversibly cleaved from the C-terminus of *a*-tubulin) is a microtubule post-translational modification that confers MTN stability by resisting catastrophe of existing microtubules,[123] as well as facilitating linkages with intermediate proteins (*e.g.*, desmin).[36,39,247] Interactions with proteins, such as desmin, cause a shift from low resistance sliding of microtubules during contraction to high-energy buckling, thus conferring viscoelastic resistance and increasing their ability to bear compressive load and transmit mechanical signals.[243] As a result, acute modulation of the level of detyrosination has been demonstrated to scale with mechanically-induced ROS production and changes in Ca^{2+} handling.[132]

Acetylation is another microtubule post-translational modification, characterised by the intraluminal addition of an acetyl group to *a*-tubulin, that confers resistance to repetitive compressive forces (*e.g.,* during cardiac contraction), thereby supressing mechanical fatigue of aged microtubules.[123,218] In fact, localised tubulin hyper-acetylation has been shown to correspond with regional stress in areas of high microtubule tortuosity.[321] Further, similar to with increased detyrosination, hyper-acetylation has been found to increase mechano-transduction, resulting in enhanced X-ROS production.[46]

In failing ventricular myocardium, the MTN remodels in an aetiology-dependent manner.[48,134] During chronic pressure overload, an increased density and stability of the MTN,[205,250,274] with a corresponding reduction in contractile function[39,49] and sensitisation of mechano-sensitive X-ROS production and Ca^{2+} release has been shown, a finding that was mitigated by reducing microtubule density or detyrosination.[132] Therefore, hypertensive alterations in the MTN may result in a stiff lattice structure with an associated increase in mechano-transduction, thus reducing the mechano-arrhythmogenic threshold and contributing to the substrate for complex arrhythmias.

The goal of this study was to assess the contribution of acute alterations in MTN density (*via* polymerisation) and stability (*via* detyrosination or acetylation) to changes in the mechano-arrhythmogenic threshold. Rabbit left ventricular myocytes were stretched in diastole at increasing magnitudes of piezo-electric translator displacement using a carbon fibre-based system, combined with video-based sarcomere analysis, generation of force-length curves, and pharmacological manipulation of MTN density and stability. It was hypothesised that acutely hyper-polymerising and stabilising the MTN would increase the propensity for stretch-induced arrhythmias, due to a decrease of the mechano-

arrhythmogenic threshold, and that reducing polymerisation or detyrosination would mitigate this effect.

5.3. Methods

5.3.1. Ethics Statement

All experiments followed the ethical guidelines of the Canadian Council on Animal Care. Protocols were approved by the Dalhousie University Committee for Laboratory Animals. Information has been described in accordance with the Minimum Information about a Cardiac Electrophysiology Experiment (MICEE) reporting standard.[225]

5.3.2. Enzymatic Isolation of Ventricular Myocytes

Left ventricular myocytes were enzymatically isolated from juvenile rabbits (female, NZW) using methodology previously described by our group.[34] Details are available in the Methods section of Chapters 3 and 4.

5.3.3. Carbon Fibre-Based Cell Stretch

Cells were subjected to: (i) rapid unidirectional axial stretch using a carbon fibre-based system with one compliant translating fibre (trimmed to 1.2 mm), and one stiff stationary fibre (trimmed to 0.6 mm) for assessment of mechano-arrhythmogenicity, or (ii) bidirectional stretch using two compliant translating fibres for generation of force length curves (described below). Carbon fibre stiffness was calibrated in advance using a force

transducer (406A, Aurora Scientific) and fibre position was controlled by a piezo amplifier/servo controller (E-665.CR, Physik Instrumente) driven by a voltage signal generated from a DAQ device (USB-6361; National Instruments) and dictated by custom LabVIEW routines (National Instruments). Development, calibration, and experimental positioning of the carbon fibres is described extensively in the Methods section of Chapters 2, 3, and 4. [33,34,116]

5.3.4. Mechano-Arrhythmogenicity Protocol

Following appropriate incubation with the relevant pharmacological agent(s) (described below), a single drop of cell-containing solution was added to an imaging chamber (RC-27NE2, Warner Instruments) containing 1 mL of NT maintained at 35°C by a temperature controller (TC-344C, Warner Instruments) and mounted on an inverted fluorescence microscope (IX-73, Olympus) with a 40× objective (UPLFLN40X, Olympus) for 5 min before initiation of cellular stretch.

The mechano-arrhythmogenicity protocol was modified from work presented in Chapters 3 and 4.[34] Transient (112-173 ms) stretch was applied using the left compliant carbon fibre to electrically paced (1 Hz) cells exclusively during mid-diastole (600 ms delay post-stimulation) at increasing magnitudes of piezo-electric translator displacement (20, 30, and 40 μm, corresponding with an average sarcomere length change of 9±1, 16±1, and 22±2% in control, and 7±1, 12±1, and 16±1% in paclitaxel-treated cells respectively). A total of six stretches were applied: two stretches with a 10 s pause in-between at each piezo-electric translator magnitude (20, 30, and 40 μm), and a 30 s pause between

increasing piezo-electric translator displacement. A schematic outlining the stretch protocol is presented in Figure 5.1a.

5.3.5. Assessment of Sarcomere Dynamics and Parameters of Cell Stretch

Sarcomere analysis was performed on signals obtained through video-based monitoring of sarcomere length and tracking of carbon fibre tip and piezo-electric translator position at 240 Hz (Myocyte Contractility Recording System, IonOptix). Within a given cell, parameters of sarcomere contractile (maximal rate and percent of sarcomere shortening) and relaxation dynamics (maximal rate of sarcomere relaxation and diastolic sarcomere length) were averaged over five successive cellular contractions immediately prior to the first stretch at each stretch magnitude (20, 30, and 40 μm), and following the final stretch in the protocol. Parameters of the applied stretch (diastolic sarcomere length, stretched sarcomere length, percent sarcomere stretch, and applied stretch force) were measured and compared between successive stretches at each magnitude, and at every consecutive increase in piezo-electric translator displacement thereafter, in both control and paclitaxel-treated cells.

5.3.6. Assessment of Mechano-Arrhythmogenicity

Arrhythmia incidence was determined from sarcomere length plots and classified into the following responses with stretch: normal paced rhythm (NPR, no change in rhythmicity), premature contractions (PVC, 1 or 2 unstimulated contractions), or complex activity (including spontaneously resolving arrhythmias or sustained arrhythmic activity that was

rescued by application of an additional stretch). Exclusion criteria were as follows: any stretch that resulted in carbon fibre slippage or cellular damage, or any complex arrhythmia that could not be resolved by a maximum of 2 stretches. A representative sarcomere trace for each classification (NPR, PVC, and complex) is shown in Fig 5.1.

5.3.7. Assessment of Cellular Mechanics

Parameters of cellular mechanics (diastolic stiffness and elastance) were measured from stepwise generated force-length curves using a pair of calibrated compliant carbon fibres. Electrically paced cells (1 Hz) were stretched in increments of 1 μm (up to a maximum of 10 μm) and held for 10 s at each length. To avoid potentially confounding effects of the slow force response on cellular contractile parameters,[141] piezo-electric translator position was returned to baseline for 10 s between each successive increase in piezo-electric translator displacement. This protocol was repeated in duplicate, with 15 s between each protocol, to assess the effect of repeated stretch on contractile parameters (Supplemental Fig. 5.6). The resulting diastolic (passive, minimal force) and systolic (active, maximal force) force-length data (force = carbon fibre stiffness x carbon fibre bending; length = fibre separation) were fitted by a linear regression using custom MATLAB routines (R2018a, MathWorks) to generate force-length curves. The slopes (m) of the end-systolic (ESFLR) and end-diastolic force-length relationship (EDFLR) represent cellular elastance and stiffness, respectively (Supplemental Fig. 5.7). Elastance and stiffness measurements derived from the first (m1) and second (m2) stepwise stretch protocol, as well as the change in values between the successive protocols ($\Delta_{EDFLR(m)}$, $\Delta_{ESFLR(m)}$) were compared between treatments.

5.3.8. Pharmacological Agents

All pharmacological agents were dissolved in dimethyl sulfoxide (DMSO) and applied to cells in NT either alone, or in combination with paclitaxel, as appropriate. Agents included: paclitaxel (10 μM, 90 min pre-incubation; Abcam), colchicine (10 μM, 90 min pre-incubation; Abcam), parthenolide (10 μM, 90 min pre-incubation; Abcam), and tubacin (10 μM, 120 min pre-incubation; Sigma).

5.3.9. Statistical Analysis

All statistics were performed using GraphPad Prism 9. Differences in the incidence of mechano-arrhythmogenicity were assessed using chi-square contingency tables and Fisher's exact test. Differences between group means were assessed by: (i) two-tailed, paired or unpaired Student's t-test (for normally distributed data) or Wilcoxon matched-pairs test or Mann-Whitney test (for data that was not normally distributed), or (ii) paired one-way ANOVA with the Geisser-Greenhouse correction (for normally distributed data) or the Friedman test (for data without normal distribution), where appropriate. In all cases, $p<0.05$ was considered significant. The relevant test and number of replicates is indicated in each figure caption. N = rabbits, n = cells, m = stretches.

5.3.10. Acknowledgements.

Carbon fibres were a gift from Jean-Yves LeGuennec and generously supplied by P. Kohl. We thank S. Fernando, G. Iribe, H. Kai, and K. Kaihara for technical assistance with the carbon fibre method.

5.3.11. Sources of Funding.

This work was made possible by support from the Dalhousie Medical Research Foundation (Hoegg Graduate Studentship to B.A.C and Capital Equipment Grant to T.A.Q.), the Canadian Institutes of Health Research (MOP 342562 to T.A.Q.), the Natural Sciences and Engineering Research Council of Canada (RGPIN-2016-04879 to T.A.Q.), the Heart and Stroke Foundation of Canada (National New Investigator Award to T.A.Q.), and the Canadian Foundation for Innovation (32962 to T.A.Q.).

5.4. Results

5.4.1. Transient Stretch of Ventricular Myocytes Results in Arrhythmic Behaviour

Rapid stretch of electrically paced (1 Hz) rabbit ventricular myocytes was performed in mid-diastole (600 ms post-stimulation delay, as determined from fluorescence imaging in Chapters 3 and 4) using a carbon fibre-based system (Fig. 5.1a) at increasing magnitudes (20, 30, 40 μm) of piezo-electric translator displacement (Fig. 5.1b). Stretch resulted in premature contractions (PVC, 1 or 2 unstimulated contractions: Fig. 5.1c) and complex activity, including spontaneously resolving sustained arrhythmias, or sustained arrhythmias rescued by application of an additional stretch (Fig. 5.1d).

To ensure that stretch did not result in cellular damage, sarcomere dynamics were assessed at baseline, and following each magnitude of piezo-electric translator displacement in both control and paclitaxel-treated cells. There was no effect of any magnitude of piezo-electric translator displacement on parameters of sarcomere contraction (maximal rate or percent of sarcomere shortening) or relaxation (maximal rate

of sarcomere relaxation or diastolic sarcomere length) within either treatment, suggesting cellular damage did not occur with stretch (Supplemental Fig. 5.1).

The magnitude of the cellular response to stretch may by modulated by an intrinsic variation in the mechanical state of enzymatically isolated cell populations. To assess this, characteristics of stretch were measured at each increase in piezo-electric translator displacement in both NT and paclitaxel-treated cells. While there was indeed cellular variability in stretch parameters at baseline, within a given NT or paclitaxel-treated cell, each increase in programmed piezo-electric translator displacement (20, 30, 40 μm) corresponded with an increase in the percent sarcomere stretch (NT: 9±1, 16±1, 22±2%; paclitaxel: 7±1, 12±1, and 16±2%; $p<0.0001$), stretched sarcomere length (NT: 1.94±0.02, 2.06±0.02, 2.17±0.03 μm; paclitaxel: 1.93±0.02, 2.01±0.03, and 2.09±0.03 μm; $p<0.0001$), and applied force (NT: 0.58±0.01, 0.77±0.01, 0.93±0.01 μN; paclitaxel: 0.56±0.01, 0.77±0.01, and 0.92±0.01 μN; $p<0.0001$), indicating that the effective stretch experienced by cells scaled with the programmed displacement. Importantly, diastolic sarcomere length remained constant after each magnitude of stretch in both treatments, indicating that carbon fibre slippage or cell buckling did not occur with stretch (Supplemental Fig. 5.2).

5.4.2. Paclitaxel Reduces the Mechano-Arrhythmogenic Threshold

Elicitation of stretch-induced arrhythmias was dependent on the magnitude of piezo-electric translator displacement. Within control cells, arrhythmia incidence was greater with 40 μm than 30 μm piezo-electric translator displacement (8% *vs* 0%; $p<0.05$). Contrarily, for paclitaxel-treated cells, the incidence of arrhythmias was greater at 30 μm

displacement than at 20 μm (9% *vs* 1%; $p<0.05$), but there was no difference between 30 μm and 40 μm (although there was a prominent trend), suggesting a reduction in the mechano-arrhythmogenic threshold with paclitaxel treatment. Furthermore, compared to NT, there was a greater arrhythmia incidence with paclitaxel at both 30 μm (9% *vs* 0%; $p<0.05$) and 40 μm (20% *vs* 8%; $p<0.05$) piezo-electric translator displacement, but not at 20 μm, suggesting the cells were generally more prone to stretch-induced arrhythmias. Together, this data suggests that paclitaxel reduced the mechano-arrhythmogenic threshold (Fig. 5.2). Interestingly, the increased mechano-arrhythmogenicity in paclitaxel-treated cells aligned with a decreased change in sarcomere length with stretch compared to NT cells (12±1 *vs* 16±1% and 16±2% *vs* 22±2% for 30 μm 40 μm piezo-electric translator movement, respectively; $p<0.05$), suggesting that paclitaxel may have increased cellular stiffness, and indicating that paclitaxel-treated cells were being stretched less, yet still displayed greater levels of mechano-arrhythmogenicity (Supplemental Fig. 5.2).

To account for the potential arrhythmogenic influence of repeated stretch, the incidence of arrhythmias initiated by the first and second stretch at each relevant level of piezo-electric translator displacement (*i.e.,* above the mechano-arrhythmogenic threshold; 30 and 40 μm) were compared. There was no difference in arrhythmia occurrence between the two stretches in NT (30 μm: 0% *vs* 0%, 40 μm: 8% *vs* 8%) or with paclitaxel (30 μm: 8% *vs* 11%, 40 μm: 21% *vs* 16%; data not shown). In paclitaxel-treated cells, this aligned with a consistent percent sarcomere change with each stretch at both 30 and 40 μm displacement (which additionally remained consistently lower than NT in all four stretches). In NT, there was similarly no change in the percent sarcomere change between stretches at 40 μm (the magnitude at which there was increased arrhythmia incidence in

these cells). However, while there was a slight increase with the second stretch at 30 μm in NT (16±1% *vs* 17±1%; $p<0.05$), neither stretch resulted in arrhythmias (Supplemental Fig. 5.3).

As there was no change in arrhythmia incidence between the two stretches within a magnitude of piezo-electric translator displacement, or in the overall arrhythmia incidence between 30 and 40 μm in paclitaxel-treated cells (where arrhythmia incidence was increased compared to control), both stretches at each magnitude were pooled for further analysis. While consideration of 20 μm stretches was excluded, they were still performed in subsequent experiments to account for potential confounding effects of additional stretches.

5.4.3. Detyrosination Contributes to Arrhythmogenesis Through Effects on the Mechano-Arrhythmogenic Threshold

Paclitaxel-treated cells had an increased incidence of arrhythmias with stretch compared to control (14 *vs* 4%; $p<0.005$). This increase in mechano-arrhythmogenicity with paclitaxel was prevented by disrupting microtubule polymerisation with the addition of colchicine (4%; $p<0.005$), or by destabilising microtubules through reduced detyrosination with parthenolide (6%; $p<0.05$). In contrast, treating control cells exclusively with tubacin to increase acetylation did not increase arrhythmia incidence compared to NT (4%; Fig. 5.3a). Importantly, neither colchicine nor parthenolide alone increased mechano-arrhythmogenicity in control cells (3 and 4% *vs* 4%, respectively; Fig. 5.3b).

To further elucidate the anti-arrhythmic mechanisms of colchicine and parthenolide, their influence on the mechano-arrhythmogenic threshold was assessed. Both colchicine and parthenolide prevented the reduction in the mechano-arrhythmogenic threshold that occurred with paclitaxel alone. With either treatment, there was no difference in arrhythmia incidence between 20 and 30 μm (colchicine: 0 *vs* 2%; parthenolide: 1 *vs* 6%), or between 30 and 40 μm (colchicine: 2 *vs* 5%; parthenolide: 6 *vs* 6%) piezo-electric translator displacement. Correspondingly, arrhythmia incidence was not greater than control at either 30 or 40 μm displacement for colchicine (30 μm: 2 *vs* 0%; 40 μm: 5 *vs* 8%) or parthenolide (30 μm: 6 *vs* 0%; 40 μm: 6 *vs* 8%). In control cells, increased acetylation with tubacin, or either colchicine or parthenolide alone also had no effect on the mechano-arrhythmogenic threshold (Supplemental Fig. 5.4).

Since the stretch magnitude-dependent increase in mechano-arrhythmogenicity aligned with a lower degree of sarcomere stretch in paclitaxel-treated cells (Supplemental Fig. 5.2), we sought to assess whether the abolished mechano-arrhythmogenic threshold with the addition of colchicine or parthenolide had a corresponding effect on the mechanical response to stretch. Interestingly, despite reducing arrhythmia incidence, sarcomere stretch was still reduced at 30 and 40 μm piezo-electric translator displacement with parthenolide compared to control (30 μm: 13±1% *vs* 16±1%; 40 μm: 17±1% *vs* 22±2%; $p<0.05$) and at 40 μm with colchicine (18±1% *vs* 22±2%; $p<0.01$, although it was not reduced at 30 μm; Supplemental Fig. 5.5).

5.4.4. Changes in Cell Stiffness Do Not Account for Increased Mechano-arrhythmogenicity

To assess whether paclitaxel altered cell stiffness, and if that effect could account for the reduced sarcomere stretch and increased mechano-arrhythmogenicity seen in paclitaxel-treated cells, cellular mechanics were assessed through the generation of two sequential force-length curves (Supplemental Fig. 5.6). Stiffness, measured as the slope (m) of the end-diastolic force length relationship (EDFLR) was compared between treatments. As mechano-transduction and the generation of mechano-electric mediators (*e.g.,* X-ROS, Ca^{2+} release) can be enhanced with repetitive stretch,[223] which may further increase cellular stiffness, the change in stiffness and elastance between the two sequential stretch protocols (m2 - m1 = $\Delta_{EDFLR(m)}$ or $\Delta_{ESFLR(m)}$) was additionally measured (Supplemental Fig. 5.7).

Stiffness was first measured in cells exposed to either 5 min or 2 hrs of NT, to assess whether there was an effect of incubation time (as is necessary with pharmacological agents). There was no difference in stiffness or $\Delta_{EDFLR(m)}$ between the two groups (Supplemental Fig. 5.8). Accordingly, cells were grouped together for further analysis.

When stiffness was measured in control or paclitaxel-treated cells, there was an increase in cell stiffness between the first and second protocol (NT: 29±3*vs* 39±4 nN/µm, $p<0.0001$; paclitaxel: 45±6 *vs* 89±10 nN/µm, $p<0.0001$) and paclitaxel-treated cells were stiffer than control for both (m1: 45±6 *vs* 29±3 nN/µm, $p<0.05$; m2: 89±10 *vs* 39±4 nN/µm, $p<0.0001$; Fig. 5.4a). The increase in stiffness during the first protocol (m1) with paclitaxel was not prevented by simultaneous treatment with either colchicine or parthenolide, and these cells remained stiffer than in control during both protocols (m1 and m2) when co-treated with either colchicine (m1: 42±3 *vs* 29±3 nN/µm, $p<0.05$; m2: 56±3 *vs* 39±4

nN/μm, $p<0.005$) or parthenolide (m1: 59±6 *vs* 29±3 nN/μm, $p<0.0001$; m2: 73±6 *vs* 39±4 nN/μm, $p<0.0001$). Increased acetylation alone with tubacin also increased stiffness compared to control (m1: 43±5 *vs* 29±3 nN/μm, $p<0.05$; m2: 68±7 *vs* 39±4 nN/μm, $p<0.0005$; Fig.5.4b).

Elastance, measured as the slope (m) of the end-systolic force length relationship (ESFLR) was also assessed. Like stiffness, elastance was increased between the first and second protocol (m1 *vs* m2), both in control and with paclitaxel (NT: 55±5 *vs* 72±7 nN/μm, $p<0.01$; paclitaxel: 65±5 *vs* 124±11 nN/μm, $p<0.0001$). However, compared to control, paclitaxel-treated cells had an increased elastance only after the second protocol (124±11 *vs* 72±7 nN/μm, $p<0.0001$). The increased elastance during the second protocol with paclitaxel was prevented by co-treatment with either colchicine (86±8 *vs* 124±11 nN/μm, $p<0.01$) or parthenolide (92±6 *vs* 124±11 nN/μm, $p<0.05$), although elastance with parthenolide remained higher than in control (92±6 *vs* 72±7 nN/μm, $p<0.05$). Increased acetylation with tubacin also increased elastance after the second protocol compared to control (95±8 *vs* 72±7 nN/μm, $p<0.05$), although it remained less than with paclitaxel (95±8 *vs* 124±11 nN/μm, $p<0.05$; Supplemental Fig. 5.9).

As neither colchicine nor parthenolide prevented the increase in stiffness during the first protocol with paclitaxel, we assessed the effects of these drugs alone. Surprisingly, cells incubated with either colchicine (m1: 42±3 *vs* 29±3 nN/μm, $p<0.005$; m2: 58±4 *vs* 39±4 nN/μm, $p<0.001$) or parthenolide (m1: 57±5 *vs* 29±3 nN/μm, $p<0.0001$; m2: 73±6 *vs* 39±4 nN/μm, $p<0.0001$) were stiffer than control in both protocols. Elastance, however,

was only greater than control with parthenolide, and exclusively in the first protocol (78±7 *vs* 55±5 nN/µm, $p<0.01$; Supplemental Fig. 5.10).

The increase in stiffness with colchicine or parthenolide alone may explain the maintained level of stiffness measured in paclitaxel-treated cells co-loaded with colchicine or parthenolide. This aligns with the maintained reduction in sarcomere stretch in paclitaxel-treated cells incubated with either colchicine or parthenolide compared to control. However, as both colchicine and parthenolide did decrease mechano-arrhythmogenicity in paclitaxel-treated cells, but did not increase incidence in control cells, this suggests that it is not cell stiffness that is responsible for the increase in mechano-arrhythmogenicity with paclitaxel. Rather, the increased mechano-arrhythmogenicity may relate to enhanced mechano-transduction *via* microtubules. Moreover, as an increase in stiffness was seen between the two sequential protocols, this may reflect a priming of the cell for subsequent mechanical stimulation.

5.4.5. Microtubule Stabilisation by Detyrosination Primes Microtubules for Repeated Stretch

The change in stiffness between the first and second protocol ($\Delta_{EDFLR(m)}$), which represents the response of the cell to repetitive stretch (*i.e.*, priming), was greater with paclitaxel treatment than in control (44±8 *vs* 10±3 nN/µm, $p<0.0001$; Fig. 5.4c). This increase in $\Delta_{EDFLR(m)}$ with paclitaxel was prevented by simultaneous treatment with either colchicine (14±3 *vs* 44±8 nN/µm; $p<0.0005$) or parthenolide (14±6 *vs* 44±8 nN/µm; $p<0.005$). While increased acetylation with tubacin alone also increased $\Delta_{EDFLR(m)}$ compared to control

(25±5 *vs* 10±3 nN/μm; $p<0.005$), it was still less than in paclitaxel-treated cells (25±5 *vs* 44±8 nN/μm; $p<0.05$; Fig. 5.4d).

Similarly, the change in elastance between protocols ($\Delta_{ESFLR(m)}$) was greater in paclitaxel-treated cells than in control (59±12 *vs* 17±6 nN/μm, $p<0.0005$), and was prevented by co-treatment with either colchicine (25±6 *vs* 59±12 nN/μm, $p<0.05$) or parthenolide (22±6 *vs* 59±12 nN/μm, $p<0.05$). Increased acetylation alone with tubacin, however, did not increase the $\Delta_{ESFLR(m)}$ compared to control (Supplemental Fig. 5.9).

The increased $\Delta_{EDFLR(m)}$ in paclitaxel-treated cells, and the reduction in $\Delta_{EDFLR(m)}$ with simultaneous colchicine or parthenolide treatment, aligned with effects of the pharmacological agents on both arrhythmia incidence (Fig. 5.3) and the presence of the mechano-arrhythmogenic threshold (Supplemental Fig. 5.4). Further, while tubacin increased $\Delta_{EDFLR(m)}$ compared to control, it remained less than with paclitaxel, corresponding with fewer arrhythmias. This may therefore suggest that sufficient priming of the mechano-transducers, facilitated by microtubule post-translational modifications (*i.e.*, detyrosination, as evidenced from the ability of parthenolide to mitigate these effects), may increase mechano-sensitivity, and contribute to the decrease in the mechano-arrhythmogenic threshold and associated increase in mechano-arrhythmogenicity seen with paclitaxel treatment.

5.5. Discussion

In this study, we sought to determine the impact of acute pharmacological alterations of cellular MTN density (*via* polymerisation) and stability (*via* microtubule post-translational modifications, *i.e.*, detyrosination and acetylation) on mechano-arrhythmogenicity in rabbit ventricular myocytes subjected to controlled stretch. We showed that increased MTN density and post-translational modifications reduced the mechano-arrhythmogenic threshold (Fig. 5.2) and primed microtubules for subsequent mechanical stimulation (Fig. 5.4), and that the enhanced arrhythmogenesis was driven primarily by detyrosination, rather than acetylation or cell stiffness (Fig. 5.3, 4).

5.5.1. Effect of the MTN Density and Stability on the Mechano-Arrhythmogenic Threshold

During diastole, there is a mechano-arrhythmogenic threshold over which a mechanical stimulus may elicit premature excitation.[80,96,98,212,231,257] This process is driven by intrinsic cardiac mechano-sensitivity involving mechano-electric effectors (*e.g.*, MSC),[73,129,204,216,305] mechano-electric transducers (*e.g.*, the MTN),[36,37,39,205,250,323] and mechano-electric mediators (*e.g.,* X-ROS and mechano-sensitive Ca^{2+} release),[116,221] that allows the heart to acutely sense and respond to mechanical stimulation. However, chronic changes in the mechanical environment (as, for instance, occurs with hypertension) may induce remodelling of mechano-sensitive components, including stiffening and stabilisation of the MTN to compensate for the increased mechanical load.[37,39,250,274] This MTN remodelling may lead to enhanced mechano-sensation through MTN-mediated MSC

modulation[5,88,216,265,332] (as we demonstrated with TRPA1 activity in Chapter 3),[34] and through MTN-mediated intracellular signalling.[116,221] The resultant increase in mechano-sensitivity could then lower the mechano-arrhythmogenic threshold, such that acute fluctuations in haemodynamic load associated with physiological fluctuations in blood pressure become emergent supra-threshold triggers for mechano-arrhythmogenicity.[195]

In the present study, pharmacological agents were used to acutely model hypertensive effects on the MTN, including paclitaxel (through increased polymerisation and detyrosination)[132,252,319] and tubacin (through increased acetylation),[269] to isolate their relative contribution to mechano-arrhythmogenicity in hypertension. We showed that in addition to increasing overall arrhythmia incidence (Fig. 5.3), an observation also found in the whole heart,[212] paclitaxel reduced the mechano-arrhythmogenic threshold such that smaller changes in sarcomere length with stretch induced arrhythmias (Fig. 5.2). Simultaneously destabilising microtubule polymerisation in these cells with colchicine or reducing microtubule detyrosination with parthenolide prevented the reduction in the mechanical threshold (Supplemental Fig. 5.4a), with an associated decrease in overall arrhythmia incidence (Fig. 5.3). Moreover, increasing acetylation alone with tubacin did not reduce the mechano-arrhythmogenic threshold (Supplemental Fig. 5.4a), nor did it increase arrhythmia incidence (Fig. 5.3).

Overall, these results support the idea that hypertensive remodelling of the MTN contributes to a reduction in the mechano-arrhythmogenic threshold. Importantly, while disrupting overall microtubule density with colchicine (and thus, the number of microtubules available for post-translational modification) had anti-arrhythmic effects, the observation that suppression of microtubule detyrosination with parthenolide alone

decreased mechano-arrhythmogenicity suggests that pathologic increases in detyrosination may be sufficient to increase mechano-arrhythmogenicity in hypertension.

5.5.2. Effects of Changes in MTN-Mediated Cell Stiffness on Mechano-Arrhythmogenicity

The present study has supported a role of MTN remodelling in reducing the mechano-arrhythmogenic threshold (Fig. 5.2) and increasing mechano-arrhythmogenicity. While these effects could be prevented by simultaneous treatment of paclitaxel-treated cells with colchicine or parthenolide (Fig. 5.3), the mechanistic action of these anti-arrhythmic agents warrants further investigation. One potential mechanism is through MTN-mediated changes in cell stiffness, which has been demonstrated to correspond with increased mechano-arrhythmogenicity in the whole heart (following treatment with paclitaxel),[212] and increased mechanically-induced arrhythmogenic Ca^{2+} waves in isolated myocytes (an effect that was mitigated by decreasing microtubule density or detyrosination).[132] Therefore, MTN-mediated cell stiffening could underly the observed increase in mechano-sensitivity and contribute to the reduction in the mechano-arrhythmogenic threshold.

Our results demonstrated that paclitaxel did indeed increase cellular stiffness compared to control (Fig. 5.4). Correspondingly, there was a reduction in the effective change in sarcomere length with programmed stretch in paclitaxel-treated cells compared to control, exclusively at the magnitudes of piezo-electric translator displacement above the mechano-arrhythmogenic threshold (30, 40 μm; Supplemental Fig. 5.2). This further corroborates the notion of an increase in mechano-sensitivity with paclitaxel treatment, as not only did these cells become more arrhythmogenic at a lower programmed piezo-electric

translator displacement, but the associated sarcomere stretch needed for arrhythmia induction was lower. This would suggest that if the paclitaxel-treated cells were instead programmed to stretch to the same change in sarcomere length as that experienced by the control cells, then the arrhythmia incidence would have been even higher. Importantly, this effect may alternatively be explained by alterations in the cellular viscoelasticity rather than stiffness, as increased MTN polymerisation and detyrosination have been shown to increase viscoelasticity.[250] However, viscoelasticity was not measured in this thesis, and thus its potential role warrants further investigation.

We subsequently showed that the increased stiffness (Fig. 5.4) and the reduction in sarcomere stretch (Supplemental Fig. 5.2) with paclitaxel was not prevented by co-treatment with either colchicine or parthenolide (Fig. 5.4 and Supplemental Fig. 5.5), despite them preventing the change in the mechano-arrhythmogenic threshold (Supplemental Fig. 5.4) and their anti-arrhythmic effects (Fig. 5.3). Tubacin also increased stiffness compared to control (Fig. 5.4), but this too was not associated with a reduction of the mechano-arrhythmogenic threshold (Supplemental Fig. 5.4) or an increased arrhythmia incidence (Fig. 5.3). Furthermore, we showed that both colchicine and parthenolide alone increased cellular stiffness (Supplemental Fig. 5.10), a surprising effect with conflicting results in the literature,[36,44,45,205,285] but one that may explain why they did not prevent the increase in stiffness when co-loaded with paclitaxel (Fig. 5.4). Importantly, however, neither colchicine nor parthenolide alone increased mechano-arrhythmogenicity (Fig. 5.3) or reduced the mechano-arrhythmogenic threshold (Supplemental Fig. 5.4), despite increasing stiffness.

Overall, the discrepancy between the effects of the various pharmacological agents on cell stiffness, the mechano-arrhythmogenic threshold, and arrhythmia incidence suggests that stiffness of the remodelled MTN does not determine mechano-arrhythmogenicity. Instead, increased mechano-arrhythmogenicity appears to relate to changes in mechano-transduction mediated by microtubule polymerisation and post-translational modifications, in particular, detyrosination.

5.5.3. The Potential Role of MTN Priming in Mechano-Arrhythmogenicity

Post-translational modifications that stabilise the MTN (*e.g.*, detyrosination and acetylation) increase the number of mature, mechanically-resilient,[218,321] and tightly anchored microtubules able to bear compressive load and transduce mechanical signals to elicit intracellular responses.[24,243,247] In fact, increased detyrosination[132] or acetylation[46] alone, without a change in MTN density, can increase X-ROS production with an associated increase in Ca^{2+} release through RyR, an effect that scales with the level of detyrosination.[132]

As oxidative stress has been shown to increase microtubule acetylation,[87] increased MTN-mediated ROS production caused by stretch,[221] and enhanced by microtubule stabilisation,[46,132] may create a positive feedback loop that drives further increases in MTN acetylation. This concept is supported by the finding that both X-ROS[223] and acetylation[321] are increased with cyclic stretch. If this is the case, then through this feedback, a mechanical stimulus could effectively prime the MTN for subsequent mechanical stimuli, which would manifest as an increase in mechano-sensitivity and a reduction of the mechano-arrhythmogenic threshold.

In the present work, we measured the change in stiffness between the first and second generated force-length curve ($\Delta_{EDFLR(m)}$), representing the response of the cell to repetitive stretch, and therefore acting as a surrogate for MTN priming. We showed that $\Delta_{EDFLR(m)}$ was increased in paclitaxel-treated cells compared to control (Fig. 5.4), an effect that was prevented by simultaneous treatment of these cells with colchicine or parthenolide. This aligned with the decrease they caused in arrhythmia incidence (Fig. 5.3) and their prevention of the decrease in mechano-arrhythmogenic threshold (Supplemental Fig. 5.4). We also showed that tubacin alone increased $\Delta_{EDFLR(m)}$ compared to control, although to a lesser extent than with paclitaxel treatment (Fig. 5.4), but unlike paclitaxel, tubacin had no effect on mechano-arrhythmogenicity (Fig. 5.3) or the mechano-arrhythmogenic threshold (Supplemental Fig. 5.4).

The effect of microtubule priming on mechano-arrhythmogenicity warrants further investigation. While our results suggest that increased detyrosination rather than acetylation alone has a greater priming effect on the MTN (as evidenced by the mitigation of this result with parthenolide), it should be considered that in a clinical hypertensive setting, or those characterised by elevated oxidative stress (*e.g.*, ischaemia), the priming effect of these two post-translational modifications (as well those not discussed in this thesis)[123,250] could be summative.

5.6. Conclusion

Acute alterations in MTN density and stability simulating hypertensive remodelling were associated with a decrease of the mechano-arrhythmogenic threshold, with a consequential

increase in mechano-arrhythmogenicity. These changes appear to be specifically related to an increase in detyrosination-mediated mechano-transduction, rather than changes in cell stiffness or acetylation. Since a pathologic increase in MTN-mediated mechano-transduction, such as during ischaemia[33] (discussed in Chapter 2) or hypertension,[132] can modulate MSC activity (*e.g.*, TRPA1),[5,332] which can act as both a trigger for premature excitation and contribute to a substrate for complex arrhythmias (discussed in Chapters 3 and 4),[34] the MTN may be an promising target for novel anti-arrhythmic therapies, and an important factor to consider for ventricular mechano-arrhythmogenicity.

5.7. Figures

Figure 5.1 | Mechano-arrhythmogenicity protocol for the diastolic stretch of single ventricular myocytes and classification of associated arrhythmias. a, Schematic of the stretch protocol applied on single myocytes during diastole at increasing magnitudes of PZT displacement (20, 30, 40 µm) **b**, Sarcomere trace of a cell (paced at 1Hz, orange dots) loaded with paclitaxel (10 µM) and stretched in diastole at increasing magnitudes of PZT displacement (green arrows) that maintained normal paced rhythm (NPR). **c**, Stretch-induced premature excitation (PVC, blue segment) in a paclitaxel-treated cell when stretched at 30 µm. NPR was maintained for stretch at 20 µm PZT displacement. **d,** Stretch-induced complex arrhythmia (red segment) with paclitaxel at 30 µm PZT displacement that was terminated by a rescue stretch. NPR with stretch at 20 µm PZT.

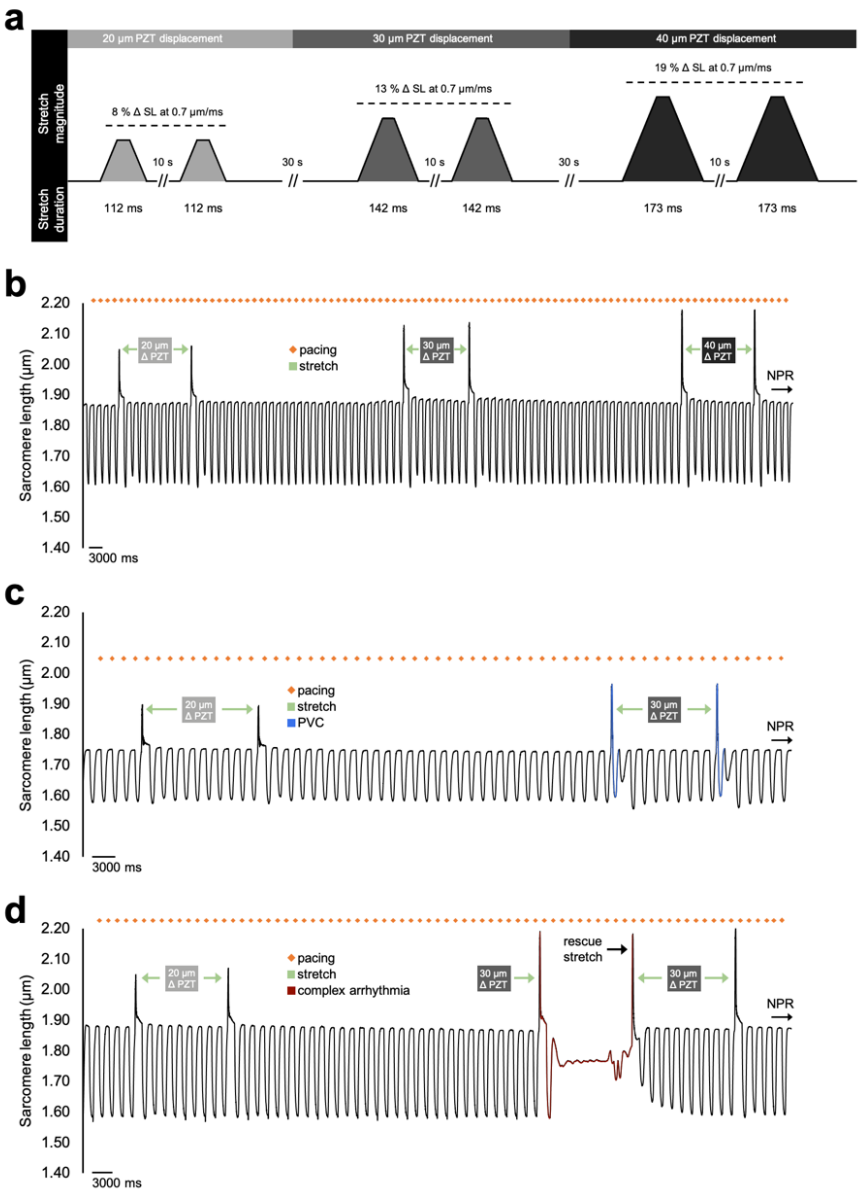

Figure 5.2 | Effect of paclitaxel on the mechano-arrhythmogenic threshold. a, Incidence of premature excitation (PVC, blue) and complex arrhythmias (red) with transient stretch in diastole at increasing levels of PZT movement (20, 30, and 40 µm) in rabbit isolated ventricular myocytes exposed to normal Tyrode (NT) alone (left), or to paclitaxel (TAX, 10 µM for 90 min) in NT (right). The mechano-arrhythmogenic threshold (minimum stretch magnitude to elicit premature excitation) is shown in orange. Differences assessed using chi-square contingency tables and Fisher's exact test: line = $p<0.05$ within a treatment, *$p<0.05$ compared to control. N = rabbits, n = cells, m = stretches.

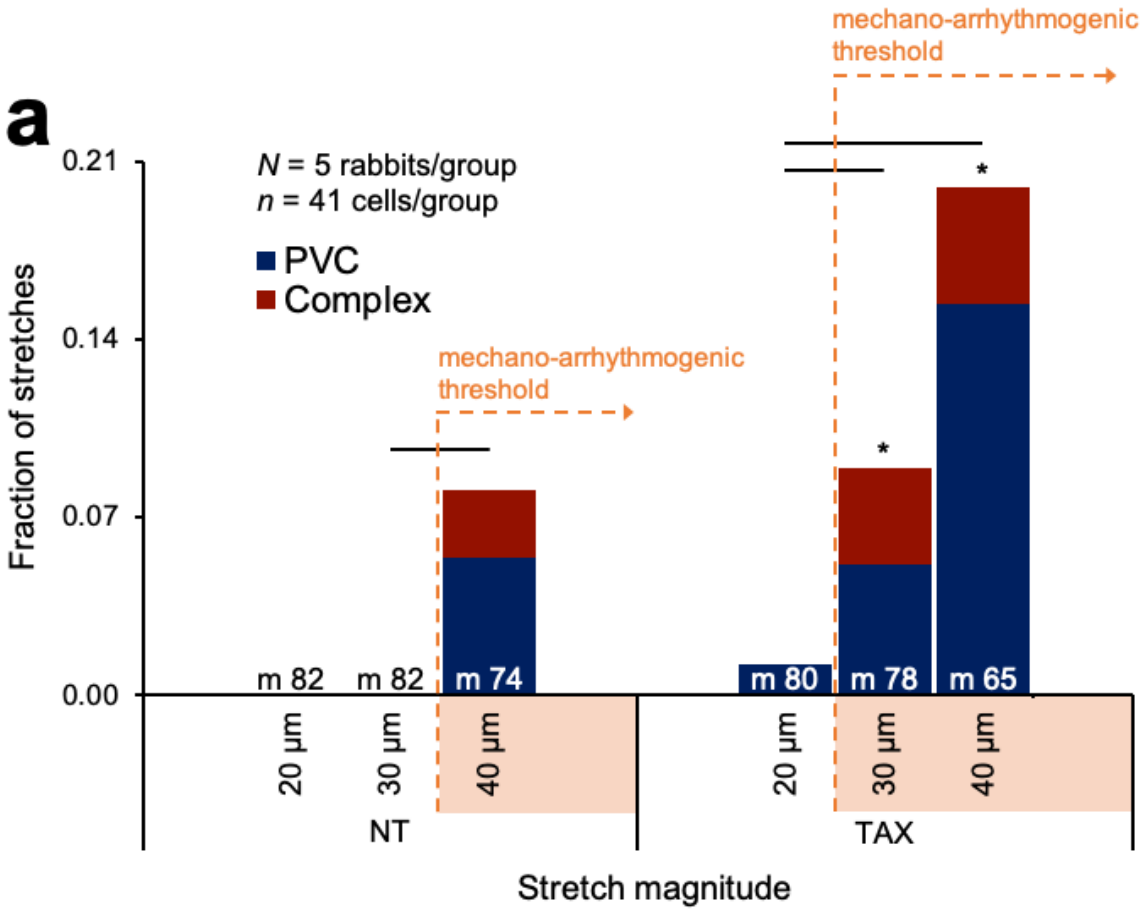

Figure 5.3 | Effect of microtubule polymerisation and post-translational modifications on mechano-arrhythmogenicity. a, Incidence of premature excitation (PVC, blue) and complex arrhythmias (red) with transient stretch of rabbit ventricular myocytes during diastole in cells exposed to: (i) normal Tyrode (NT); (ii) paclitaxel (TAX, 10 µM for 90 min) alone; (iii) a combination of paclitaxel and either colchicine (COL, 10 µM for 90 min) or parthenolide (PTL, 10 µM for 90 min); or to (iv) tubacin alone (TUB, 10 µM for 2 hours). **b,** Incidence of arrhythmias in cells either in NT alone, or with the addition of COL or PTL. Differences in arrhythmia incidence assessed using chi-square contingency tables and Fisher's exact test. Line = $p<0.05$ between groups. N = rabbits, n = cells, m = stretches.

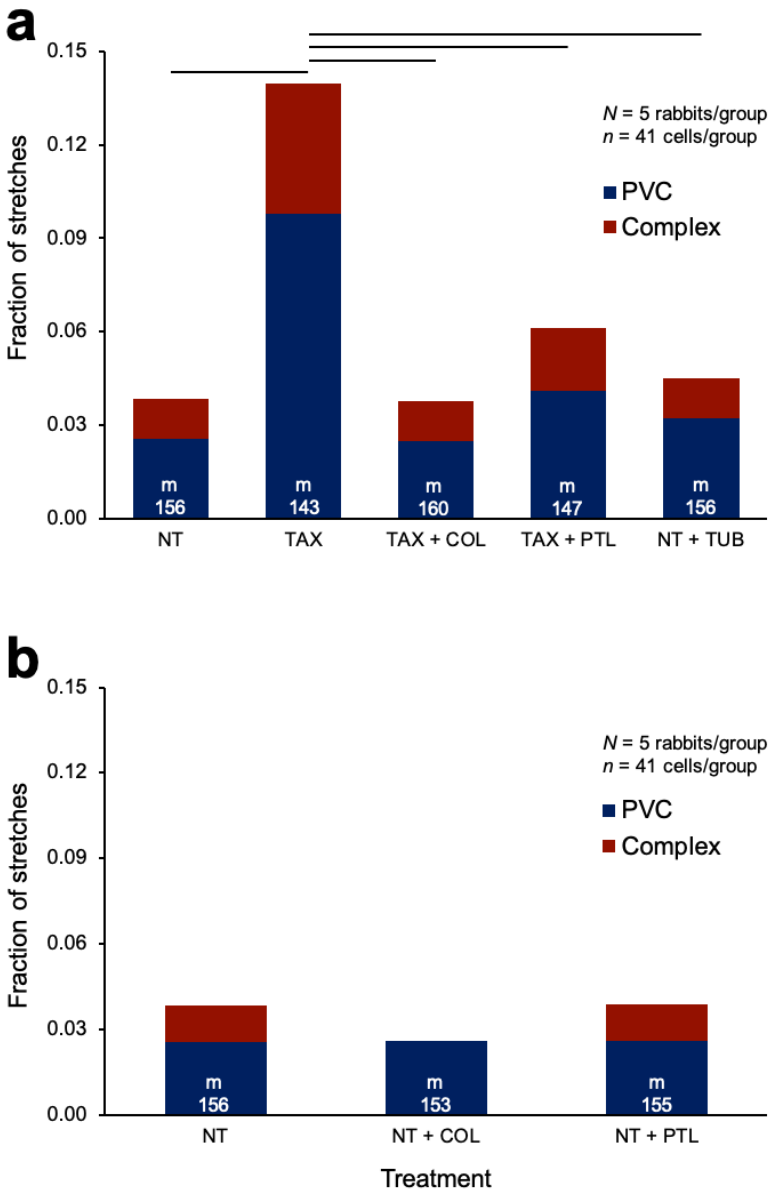

Figure 5.4 | Contribution of MTN polymerisation and post-translational modifications to cellular stiffness and microtubule priming. a, Stiffness (measured as the slope of the end-diastolic force-length relationship, EDFLR) of rabbit ventricular myocytes in normal Tyrode (NT) alone, or incubated with paclitaxel (TAX, 10 μM for 90 min) in NT, measured from two sequentially generated force-length curves (m1 and m2). **b,** Stiffness of cells treated with paclitaxel alone or co-loaded with colchicine (COL, 10 μM for 90 min) or parthenolide (PTL, 10 μM for 90 min), or cells loaded with tubacin alone (TUB, 10 μM for 2 hrs). **c,** Difference in the stiffness between the first and second generated force-length curve ($\Delta_{EDFLR(m)}$), measured as a metric of microtubule priming, in control and TAX cells, or **d,** in TAX cells co-loaded with COL or PTL and in cells loaded with TUB alone. Differences within groups assessed by paired Student's t-test (for normally distributed data) or Wilcoxon matched-pairs signed rank test (for non-normally distributed data). Differences compared to control or compared to TAX assessed by unpaired Student's t-test (for normally distributed data), or Mann-Whitney test (for non-normally distributed data). *p<0.05 compared to NT, **p<0.05 within a group, #p<0.05 compared to TAX. N = rabbits, n = cells.

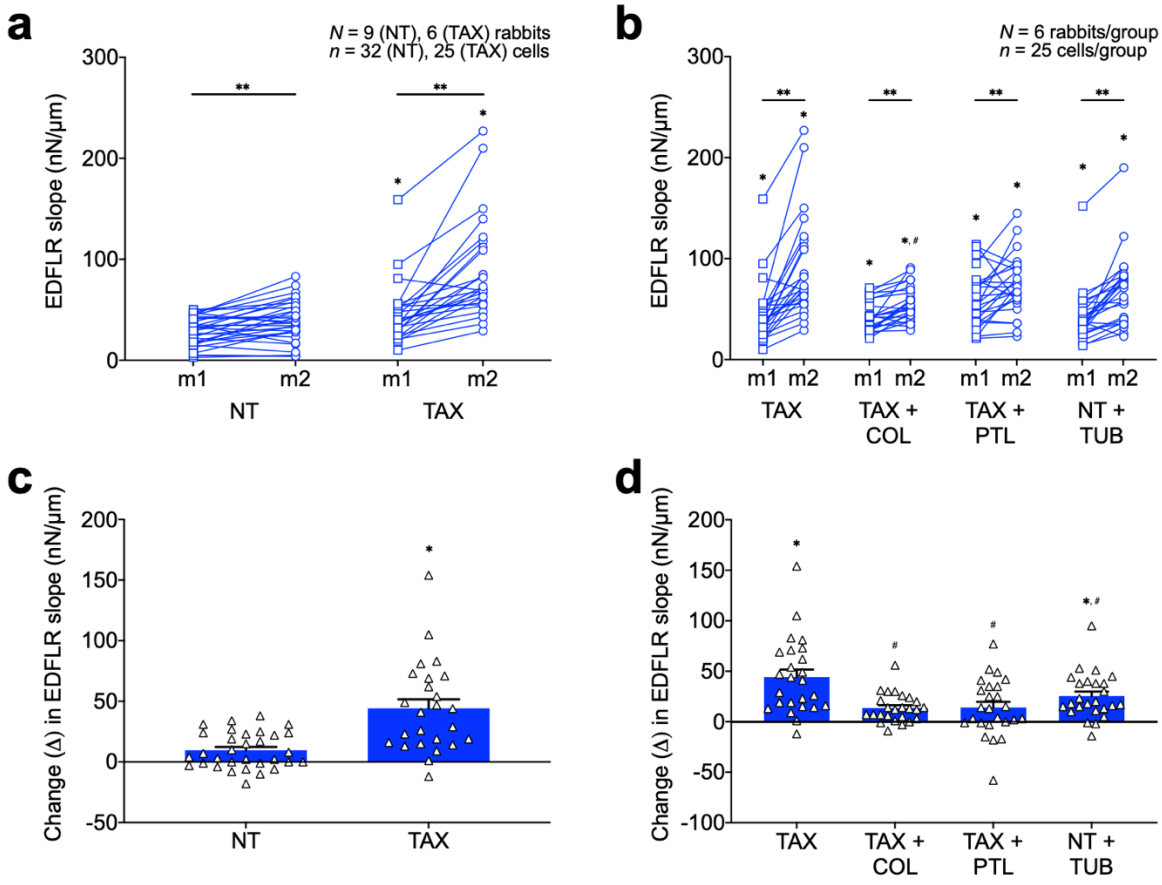

CHAPTER 6: DISCUSSION

The heart is an electrically-controlled mechanical pump with intricate feedback mechanisms designed to facilitate its response to acute changes in its mechanical environment (*i.e.*, mechano-electric coupling), such as postural- or circadian-related haemodynamic fluctuations, in order to meet systemic circulatory demand.[232] This ability relies on components of cardiac mechano-sensitivity at the cellular and subcellular level, including mechano-electric effectors (*e.g.*, MSC),[216] mechano-electric transducers (*e.g.*, microtubules),[36] and mechano-electric mediators[41,121,224] (*e.g.*, intracellular ROS and Ca^{2+}),[116,221] which allow the heart to respond to mechanical stimuli through electrophysiological changes.

The ability for a mechanical stimulus to elicit an electrical response is dependent on both its timing (*i.e.*, during systole or diastole) and magnitude.[232] Therefore, disease states characterised by alterations in APD dynamics (*e.g.*, ischaemia), which consequently alter the relative systolic and diastolic period,[13,34] or changes in the components underlying cardiac mechano-sensitivity (*e.g.*, hypertension),[36,250] which can modulate the stretch-magnitude threshold,[233,263,272,276] may be more prone to mechanically-induced excitation. These arrhythmogenic triggers, when in the presence of a disease-mediated pro-arrhythmic substrate, can convert into more complex arrhythmias.[34,272] Accordingly, this work sought to identify specific cellular and subcellular mechanisms of mechano-arrhythmogenicity in models of two pathophysiological states: acute ischemia and chronic hypertension.

6.1. Mechano-Electric Mediators in Mechano-Arrhythmogenicity

Under physiological conditions, the mechano-sensitive increase in X-ROS production,[221] and the associated increase in Ca^{2+} release through RyR (Ca^{2+} sparks),[116] has been suggested to tune excitation-contraction coupling to meet physiological demand.[169,224] However, pathological alterations in RyR activity,[14,176,220,249] or in the local (*e.g.*, regional ischemia)[84,161,219,246,283] or global (*e.g.*, hypertension)[149,174] mechanical state of the heart, may lead to the augmentation of these processes,[33] and consequentially, contribute to mechano-arrhythmogenicity.

In Chapter 2, we found that simulated ischemia does indeed augment both the baseline and stretch-induced increase in ROS production and Ca^{2+} spark rate, suggesting an enhanced mechano-sensitivity of these subcellular processes during ischaemia.[33] Other groups have demonstrated in a murine model of Duchenne's muscular dystrophy (characterised by enhanced MTN detyrosination,[132] also evident in hypertrophy)[15,250] that there is an increased rate of X-ROS production and Ca^{2+} spark rate. It appears that this enhanced mechano-electric transduction relates to MTN remodeling, as it scaled with suppression of detyrosination.[132] In failing cardiomyocytes, reducing detyrosination improved contractile function, suggesting a MTN-mediated augmentation of mechano-electro transduction in these cells[37,39] (although, NOX2 has been found to be upregulated during pressure overload, which may additionally contribute to this phenomenon).[151]

In both ischaemia and hypertension, the effects of increased mechano-electric mediators on arrhythmogenesis may be multifaceted. Firstly, through NCX-mediated depolarisation[137,155] or through secondary agonism of mechano-electric effectors[5,332] (*e.g.*, TRPA1, discussed below),[34] they may contribute to triggering of premature excitation

(especially in regional ischemia characterised by areas of localised stretch).[192] Secondly, they may contribute to the substrate for complex events through intracellular Ca^{2+} accumulation.[179] Finally, as these processes have been shown to be dependent on the integrity of the MTN (as they were abolished by MTN disruption,[116,221] and reduced by de-stabilising pathologically sensitised MTN),[132] and as oxidative stress has been demonstrated to increase acetylation of the MTN[87] (a process that, in addition to X-ROS and Ca^{2+} spark rate, is graded by cyclic stretch),[223,321] which subsequently increases mechano-transduction,[46] there may be an emergent positive-feedback loop wherein these disease-related modulations in mechano-electric mediators may both contribute to, and result from, alterations that manifest at the level of the mechano-transducers.

6.2. Mechano-Electric Transducers in Mechano-Arrhythmogenicity

One of the primary functions of the MTN is the transduction of mechanical signals to facilitate a cellular response.[244] The transmission of a mechanical stimulus is dependent on the mechano-sensitivity of the MTN, which can be enhanced by increasing density (*via* polymerisation) or stability (*via* post-translational modifications, such as detyrosination or acetylation).[36] Pathologic remodelling of the MTN, as occurs in hypertension, is characterised by microtubule densification and stabilisation.[15,36,37,39,250,274] Combined with the associated increase in latticed anchoring of microtubules, through interactions between post-translationally modified microtubules and intermediate proteins (*e.g.,* detyrosinated microtubule-desmin junctions),[243,247] this remodelling would create a dense rigid scaffold in which a single microtubule would experience lateral viscous load. In this setting,

microtubules would have a higher incident force,[24] and thus confer increased viscous resistance and load bearing capabilities, resulting in augmented mechano-transduction.[24,243,244,323]

In Chapter 5, we found that acutely increasing microtubule polymerisation and stability with paclitaxel resulted in an overall increase in arrhythmia incidence, with an associated reduction of the mechano-arrhythmogenic threshold, such that lower magnitude stretches elicited premature excitation. We further demonstrated that this effect could be prevented by simultaneously disrupting polymerisation (with colchicine) or detyrosination (with parthenolide) of microtubules in paclitaxel-treated cells, but that this effect did not occur with increased acetylation alone. This result did not appear to relate to cell stiffness, as colchicine and parthenolide did not reduce the increased stiffness seen with paclitaxel treatment, despite their anti-arrhythmic action. Rather, this effect may relate to the feedback mechanism described above: positive-feedback of microtubule post-translational modification-mediated mechano-transduction (increasing X-ROS) on microtubule stability (*i.e.,* microtubule priming). These microtubules would then be expected to have increased mechano-sensitivity that would manifest as a lower mechano-arrhythmogenic threshold and an increased arrhythmia incidence. In this study, we measured the difference in stiffness between two consecutively generated force-length curves as a surrogate for microtubule priming. We demonstrated that priming was increased in paclitaxel-treated cells, and that this response could be prevented with either colchicine or parthenolide, which aligned with the anti-arrhythmic effect of these agents. Conversely, while increased acetylation alone also increased microtubule priming, it remained less than with paclitaxel and was not associated with an increase in arrhythmogenicity.

While in paclitaxel-treated cells, it appears that detyrosination suppression is sufficient to prevent an increase in mechano-sensitivity, it should be considered that in a clinical setting, the effects of multiple post-translational modifications on MTN mechano-sensitivity may become summative. Specifically, during hypertension (or other conditions characterised by oxidative stress where this potential positive-feedback mechanism could be engaged), it may be that primarily detyrosination-mediated mechano-transduction increases oxidative stress (*via* X-ROS),[132] which reciprocally increases acetylation[87] that stabilises the MTN against cyclic compression,[218] resulting in a graded increase in acetylation and X-ROS production,[223,321] and consequentially, a progressive priming of the MTN (a schematic of this concept is shown in Fig. 6.1). Additionally (or alternatively), in disease states characterised by increased levels of desmin and detyrosination (*e.g.,* hypertension),[243] enhanced detyrosination-mediated microtubule stability results in more aged microtubules. Increased microtubule lifetime itself promotes acetylation, which facilitates microtubule longevity,[218] and consequentially, the likelihood for additional post-translational modifications to further stabilise the MTN.[247] Either of these concepts could contribute to the observed microtubule priming, and would progressively increase mechano-transduction and thus the production of mechano-electric mediators (*i.e.,* X-ROS, Ca^{2+} release).

In addition to the potential mechanistic role of the MTN involving mechano-electric mediator production, alterations in the MTN may act through modulation of mechano-electric effector activity (*i.e.*, MSC). This could involve changes in the effective stretch experienced by the MSC (either by modulating the dampening effect of the MTN or the transmission of mechanical stimuli),[216] or conversely, it may relate to MTN-mediated

alterations in mechano-electric mediators that secondarily modulate MSC channel sensitivity[5,34,332] (*i.e.*, secondary agonism). Alternatively, it could be a combination of the two, such that (i) an increase in MTN-mediated mechano-transduction augments the stretch experienced by the MSC[88,216,265] and increases mechano-electric mediator production,[46,132] and (ii) MTN-mediated secondary agonism sensitises the MSC.[5,34,332] This effect would then lower the mechano-arrhythmogenic threshold (while simultaneously contributing to an arrhythmogenic substrate, discussed in Chapter 3), such that a smaller stretch could elicit premature excitation (as shown in Chapter 5). These mechanisms could also potentially explain the results shown in Chapter 3 that described an increased mechano-arrhythmogenicity with paclitaxel that was prevented by block of TRPA1 channels.

6.3. Mechano-Electric Effectors in Mechano-Arrhythmogenicity

In addition to stretch, MSC gating can be modulated by cytoskeletal components (*e.g.,* the MTN), voltage, and endogenous agonists (*e.g.,* mechano-electric mediators).[216] Moreover, these modulators can have a summative effect on MSC activity, such that agonism of baseline MSC function may sensitise channels to activation by mechanical forces,[25] or cause a shift in their voltage dependence.[183,184,185] Therefore, pathologic alterations in the cytoskeleton or endogenous agonists may modulate MSC mechano-sensitivity, and thus their resultant contribution to mechano-arrhythmogenicity.

This work explored the contribution of a specific MSC (TRPA1) to ventricular mechano-arrhythmogenicity based on its (i) inherent mechano-sensitivity,[193] (ii) preferential Ca^{2+} permeability,[21] (iii) activation by mechano-electric mediators (*i.e.*, Ca^{2+}

and ROS),[5,332] and (iv) based on the known increase of its activity during ischaemia[47] and hypertension.[301] Initially, we demonstrated that TRPA1 activation can indeed act as an arrhythmogenic trigger (presumably through a mechano-sensitive depolarising influx of Ca^{2+}), and, when constitutively active in pathologies with enhanced agonist factors (*e.g.*, intracellular Ca^{2+} or ROS), contribute to a substrate for complex arrhythmic behaviour (Chapter 3).[34] We therefore sought to test its involvement in models of two specific pathologic states: acute ischemia (Chapter 4, discussed below) and chronic hypertension (Chapters 3 and 5, discussed in the previous section).

During simulated ischemia (Chapter 4), we demonstrated that TRPA1 contributed to the enhanced mechano-arrhythmogenicity through a Ca^{2+} and ROS-mediated mechanism. We found that in this setting, arrhythmia incidence was dependent on stretch-timing, as stretch applied exclusively during the VP in late repolarisation resulted in increased arrhythmic activity (an effect that was mitigated by reducing the size of the ischaemic VP). We went on to show that the diastolic Ca^{2+} loading observed with simulated ischaemia, while necessary, was not sufficient for the generation of these arrhythmias, as it required stretch-induced TRPA1 activation to act as an arrhythmogenic trigger.

The contribution of TRPA1 to the observed temporal-dependence of mechano-arrhythmogenicity during simulated ischaemia may relate to a persistent endogenous agonism of the channel (*via* Ca^{2+} and ROS),[5,332] an effect that may be further enhanced by the increased mechano-electric mediator production during ischaemia (demonstrated in Chapter 2).[33] This effect may modulate TRPA1 mechano-sensitivity by simultaneously shifting its voltage dependence into the physiological range and inhibiting its Ca^{2+}-mediated antagonism.[183,184,185] The effect of increased mechano-electric mediator agonism

on the voltage dependence of TRPA1 could also explain why mechano-arrhythmogenicity was temporally dependent in full ischaemia (Chapter 4), but not with activation of K_{ATP} channels with pinacidil (a model we used to isolate the specific role of the VP; Chapter 3). It warrants noting that TRPA1 activity could additionally be modulated by other MSC not discussed in this study.

In summary, we have demonstrated that TRPA1 channels, through their ability to contribute to both arrhythmogenic triggering and substrate mechanisms, can modulate the temporal- (as evidenced by the ischaemia studies, Chapters 2-4) and magnitude-dependence (as evidenced by the hypertension studies, Chapters 3 and 5) of ventricular mechano-arrhythmogenicity.[34] Due to the intricate integration of the elements of cardiac mechano-sensitivity described in this thesis, TRPA1 is an enticing anti-arrhythmic target in diseases characterised by alterations of mechano-electric mediators, mechano-electric transducers, or mechano-electric effectors.

6.4. Limitations

Firstly, while the results relating to the ischemia-induced potentiation of X-ROS production and Ca^{2+} spark frequency greatly supplement the subsequent studies laid out in this thesis, it should be noted that these experiments were carried out in mice whereas the other projects were performed in rabbits. This was a result of species-specific differences in sarcoplasmic reticulum (SR) Ca^{2+} loading at rest (which facilitates Ca^{2+} spark production), wherein rabbits exhibit a "rest-decay" phenomenon, governed by the competitively lower SERCA uptake than RyR and NCX extrusion. Conversely, mice load

their SR at rest due to relatively higher SERCA activity. Since imaging of Ca^{2+} sparks must be done in quiescent cells to mitigate motion artefacts, the kinetics of murine SR loading make them the superior model for Ca^{2+} spark studies.[115] Additional limitations associated with this study (*i.e.*, temperature, ischaemic model) are discussed in Chapter 2.

Secondly, during the mechano-arrhythmogenicity protocol, stretch was applied exclusively at increasing magnitudes of piezo-electric translator displacement (20, 30, then 40 μm), rather than a randomised order of stretch magnitude. However, regarding the ischaemia studies (Chapters 3 and 4), this may not be as relevant a limitation, as (i) magnitude was not found to be significant, and (ii) stretches of all magnitudes were grouped together, rather than assessed separately. Further, in the protocol where we performed the mechano-arrhythmogenicity test in cells loaded with fluorescence probes, stretch was applied solely at the largest magnitude (40 μm) and the incidence was the same as the largest stretch in cells in which the lower magnitude stretches were perfomed first (20, 30, then 40 μm). In the paclitaxel study, however (Chapter 5), it would have been beneficial to change the order of stretches, as stretch magnitude was shown to be an important factor. That said, stretch parameters, sarcomere dynamics, and arrhythmia incidence were compared between stretches at each magnitude, as well as between magnitudes thereafter to ensure no changes had occurred to cellular contractile function that could have confounded the resultant mechano-arrhythmogenesis.

It is important to note that while confounding influences of sex differences were controlled by exclusively testing female rabbits, that there may be significant sex-dependent effects on the relative contributions of the mechanisms laid out in this thesis, and so caution should be taken in extrapolating results to male subjects.

Finally, while cellular and subcellular studies are beneficial for identifying targets and understanding their mechanistic action, it warrants noting that when translated to a whole heart, additional tissue-level factors such as gap junctions, fibrosis, and non-myocytes may modulate the relative contribution of the mechanisms identified in this thesis. However, to answer the highly specific questions of these studies, single cell investigations were necessary, as they simultaneously allow the physiological environment to be precisely modulated, transient stretch timed around the VP to be applied, and pharmacological interventions to be used to probe underlying mechanisms.

6.5. Future Directions

This thesis has demonstrated the potential role of TRPA1 as an anti-arrhythmic target in diseases characterised by altered APD dynamics (*i.e.,* acute ischaemia) or mechanics (*i.e.,* acute regional ischaemia and hypertension) that affect components underlying ventricular mechano-sensitivity, and consequentially, the temporal- and magnitude-dependence of ventricular mechano-arrhythmogenicity. Future studies to assess contributions of other mechano-sensitive channels would be beneficial.

We have also revealed a critical role for microtubules in mechano-arrhythmogenicity. In relation to this, it would be interesting to further probe the importance and mechanisms of microtubule priming and test whether additional mechanical stimuli (beyond the two protocols performed in this study), cause greater increases in stiffness, or whether this phenomenon plateaus (or diminishes) with

subsequent mechanical stimulation. Further, testing whether mechano-arrhythmogenicity is indeed increased in primed cells is needed.

While we have gained insights into how acute manipulations of the MTN can increase mechano-arrhythmogenicity, it would be interesting to see whether the identified mechanisms (*i.e.*, decreased mechano-arrhythmogenic threshold, microtubule priming) occur in failing myocytes that have been chronically remodelled. Importantly, unlike in our study using paclitaxel, colchicine and parthenolide have been demonstrated to reduce stiffness and improve contractile function in failing myocytes,[37,39] which may reflect differences between paclitaxel and disease-related MTN alterations. Further to this, as MTN remodelling in heart failure is aetiology-dependent, testing how divergences in the MTN remodeling influences the relative contribution of the mechanisms identified in this thesis would be beneficial. In particular, while pressure overload is characterised by densification and increased detyrosination of the MTN, volume overload results in a reduction in detyrosination-desmin interactions,[92] and therefore the contribution of the MTN (and its effects on MSC, ROS, and Ca^{2+}) may be attenuated.

6.6. Summary

This project has identified specific targets contributing to ventricular mechano-arrhythmogenicity in models of acute ischaemia and hypertension, across the elements of cardiac mechano-sensitivity: mechano-electric mediators, mechano-electric transducers, and mechano-electric effectors. The intricate interaction between these components results in mechanistic targets that contribute to both the trigger and substrate for arrhythmogenesis.

Understanding the precise integration of these components will facilitate the development of a mechanistic map that provides a framework for understanding how alterations in the cellular and subcellular microarchitecture manifest at the level of ventricular mechano-arrhythmogenicity.

6.7. Figures

Figure 6.1 | Mechanisms of MTN-mediated mechano-arrhythmogenicity in ventricular myocytes. Schematic representation of the proposed mechanisms of MTN-mediated mechano-sensitivity and reduction of the mechano-arrhythmogenic threshold

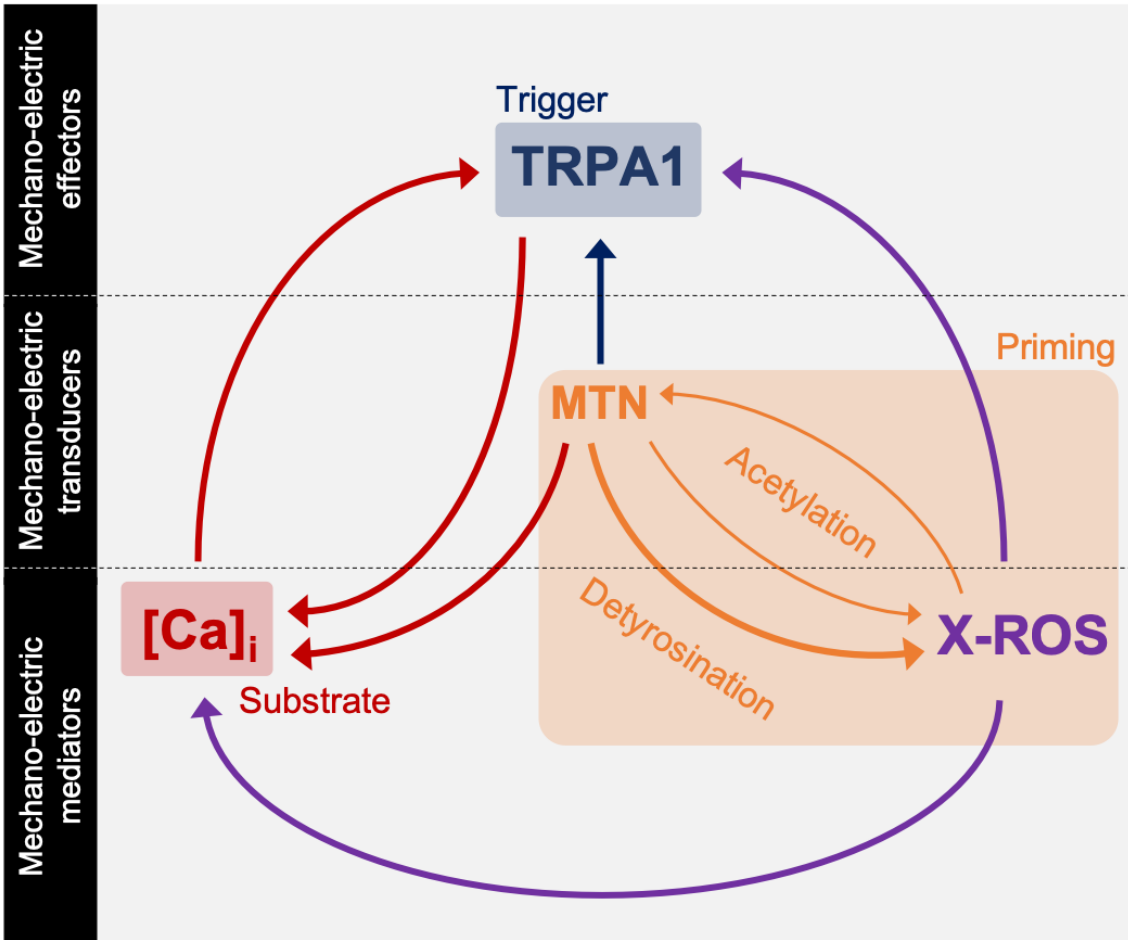

REFERENCES

1. Ai X, Curran JW, Shannon TR, Bers DM, Pogwizd SM. Ca^{2+};/Calmodulin–dependent protein kinase modulates cardiac ryanodine receptor phosphorylation and sarcoplasmic reticulum Ca^{2+}; leak in heart failure. *Circ Res*. 2005;97:1314–1322.
2. Allen DG, Kentish JC. Calcium concentration in the myoplasm of skinned ferret ventricular muscle following changes in muscle length. *J Physiol*. 1988;407**:**489-503.
3. Alsheikh-Ali AA, Akelman C, Madias C, Link MS. Endocardial mapping of ventricular fibrillation in commotio cordis. *Heart Rhythm*. 2008;5:1355-1356.
4. Ambrosi P, Habib G, Kreitmann B, Faugère G, Métras D. Valsalva manoeuvre for supraventricular tachycardia in transplanted heart recipient. *Lancet*.1995;346:713.
5. Andersson DA, Gentry C, Moss S, Bevan S. Transient receptor potential A1 is a sensory receptor for multiple products of oxidative stress. *J Neurosci*. 2008;28:2485-2494.
6. Andrei SR, Ghosh M, Sinharoy P, Dey S, Bratz IN, Damron DS. TRPA1 Ion Channel Stimulation Enhances Cardiomyocyte Contractile Function via a CaMKII-dependent Pathway. *Channels Austin Tex*. 2017;0.
7. Barrabés JA, Figueras J, Candell-Riera J, Agullo L, Inserte J, Garcia-Dorado D. Distension of the ischaemic region predicts increased ventricular fibrillation inducibility following coronary occlusion in swine. *Rev Esp Cardiol (Engl Ed)*. 2013;66:171-176.
8. Barrabés JA, Garcia-Dorado D, González MA, Ruiz-Meana M, Solares J, Puigfel Y, et al. Regional expansion during myocardial ischaemia predicts ventricular fibrillation and coronary reocclusion. *Am J Physiology Heart Circ Physiol*. 1998;274:H1767-H1775.
9. Barrabés JA, Garcia-Dorado D, Padilla F, Agulló L, Trobo L, Carballo J, et al. Ventricular fibrillation during acute coronary occlusion is related to the dilation of the ischaemic region. *Basic Res Cardiol*. 2002;97:445-451.
10. Barrabés JA, Inserte J, Agulló L, Rodríguez-Sinovas A, Alburquerque-Béjar JJ, Garcia-Dorado D. Effects of the selective stretch-activated channel blocker GsMtx4 on stretch-induced changes in refractoriness in isolated rat hearts and on ventricular

premature beats and arrhythmias after coronary occlusion in swine. *PLoS One*. 2015;10:e0125753.

11. Barrabes JA, Inserte J, Rodriguez-Sinovas A, Ruiz-Meana M, Garcia-Dorado D. Early regional wall distension is strongly associated with vulnerability to ventricular fibrillation but not arrhythmia triggers following coronary occlusion in vivo. *Prog Biophys Mol Biol*. 2017;130(Pt B):387-393.
12. Baumeister P, Quinn TA. Altered calcium handling and ventricular arrhythmias in acute ischaemia. *Clin Medicine Insights Cardiol*. 2016;10s1:CMC.S39706.
13. Baumeister PA, Lawen T, Rafferty SA, Taeb B, Uzelac I, Fenton FH, et al. Mechanically-induced ventricular arrhythmias during acute regional ischaemia. *J Mol Cell Cardiol*. 2018;124:87–88.
14. Belevych AE, Terentyev D, Viatchenko-Karpinski S, Terentyeva R, Sridhar A, NishijimaY, et al. Redox modification of ryanodine receptors underlies calcium alternans in a canine model of sudden cardiac death. *Cardiovasc Res*. 2009;84:387-95.
15. Belmadani S, Poüs C, Ventura-Clapier R, Fishmeister R, Mery PF. Post-translational modifications of cardiac tubulin during chronic heart failure in the rat. *Mol Cell Biochem*. 2002;237:39-46.
16. Belus A, White E. Streptomycin and intracellular calcium modulate the response of single guinea-pig ventricular myocytes to axial stretch. *J Physiol*. 2003;546: 501-509.
17. Benditt DG, Kriett JM, Tobler HG, Gornick CC, Detloff BL, Anderson RW. Electrophysiological effects of transient aortic occlusion in intact canine heart. *Am J Physiol Heart Circ Physiol*. 1985;249:H1017–H1023.
18. Bers DM. Cardiac excitation–contraction coupling. *Nature*. 2002;415:198-205.
19. Betsuyaku T. [A study of microtubules in hypertrophied cardiomyocytes]. *Hokkaido J Medical Sci*. 1994;69:13–23.
20. Billman GE, McIlroy B, Johnson JD. Elevated cardiac myocardial calcium and its role in sudden cardiac death. *FASEB J*. 1991;5:2586-2592.
21. Bobkov YV, Corey EA, Ache BW. The pore properties of human nociceptor channel TRPA1 evaluated in single channel recordings. *Biochim Biophys Acta*. 2010;1808:1120-1128.

22. Bode F, Franz MR, Wilke I, Bonnemeier H, Schunkert H, Wiegand UKH. Ventricular fibrillation induced by stretch pulse: implications for sudden death due to commotio cordis. *J Cardiovasc Electr*. 2006;17:1011-1017.
23. Bõhm A, Pintér A, Préda I. Ventricular tachycardia induced by a pacemaker lead. *Acta Cardiol*. 2002;57: 23-24.
24. Brangwynne CP, MacKintosh FC, Kumar S, Geisse NA, Talbot J, Mahadevan L, Parker KK, Ingber DE, Weitz DA. Microtubules can bear enhanced compressive loads in living cells because of lateral reinforcement. *J Cell Biol*. 2006;173:733-741.
25. Brierley SM, Castro J, Harrington AM, Hughes PA, Page AJ, Rychkov GY, et al. TRPA1 contributes to specific mechanically activated currents and sensory neuron mechanical hypersensitivity. *J Physiology*. 2011;589:3575-3593.
26. Brooks CM, Gilbert JL, Suckling EE. Excitable cycle of the heart as determined by mechanical stimuli. *Proc Soc Exp Biol Med*. 1964;117:634-637.
27. Burton FL, Cobbe SM. Effect of sustained stretch on dispersion of ventricular fibrillation intervals in normal rabbit hearts. *Cardiovasc Res*. 1998;39:351-359.
28. Calaghan SC, White E. The role of calcium in the response of cardiac muscle to stretch. *Prog Biophysics Mol Biology*. 1999;71:59-90.
29. Calaghan SC, Belus A, White E. Do stretch-induced changes in intracellular calcium modify the electrical activity of cardiac muscle? *Prog Biophys Mol Biol*. 2003;82:81–95.
30. Califf RM, Burks JM, Behar VS, Margolis JR, Wagner GS. Relationships among ventricular arrhythmias, coronary artery disease, and angiographic and electrocardiographic indicators of myocardial fibrosis. *Circulation*. 1978;57:725-732.
31. Calkins H, Levine JH, Kass DA. Electrophysiological effect of varied rate and extent of acute in vivo left ventricular load increase. *Cardiovasc Res*. 1991;25:637- 644.
32. Calkins H, Maughan WL, Weisman HF, Sugiura S, Sagawa K, Levine JH. Effect of acute volume load on refractoriness and arrhythmia development in isolated, chronically infarcted canine hearts. *Circulation*. 1989;79:687-697.
33. Cameron BA, Kai H, Kaihara K, Iribe G, Quinn TA. Ischaemia enhances the acute stretch-induced increase in calcium spark rate in ventricular myocytes. *Front Physiol*. 2020;11:289.

34. Cameron BA, Stoyek MR, Bak JJ, Quinn TA. TRPA1 channels are a source of calcium-driven cardiac mechano-arrhythmogenicity. *bioRxiv*. 2020;2020.10.01.321638.
35. Cannell, M.B. Pulling on the heart strings: a new mechanism within Starling's law of the heart? *Circ Res*. 2009;104:715-716.
36. Caporizzo MA, Chen CY, Prosser BL. Cardiac microtubules in health and heart disease. *Exp Biol Med*. 2019;244:1255-1272.
37. Caporizzo MA, Chen CY, Bedi K, Margulies KB, Prosser BL. Microtubules increase diastolic stiffness in failing human cardiomyocytes and myocardium. *Circulation*. 2020;141:902-915.
38. Carmeliet, E. Cardiac ionic currents and acute ischaemia: from channels to arrhythmias. *Physiol Rev*. 1999;9:917-1017.
39. Chen CY, Caporizzo MA, Bedi K, Vite A, Bogush AI, Robinson P, Heffler JG, Salomon AK, Kelly NA, Babu A, et al. Suppression of detyrosinated microtubules improves cardiomyocyte function in human heart failure. *Nature Med*. 2018;24:1225-1233.
40. Chen RL, Penny DJ, Greve G, Lab MJ. Stretch-induced regional mechanoelectric dispersion and arrhythmia in the right ventricle of anesthetized lambs. *Am J Physiol-heart C*. 2004;286:H1008–H1014.
41. Chen-Izu Y, Izu LT. Mechano-chemo-transduction in cardiac myocytes. *J Physiol*. 2017;595:3949-3958.
42. Cheng G, Takahashi M, Shunmugavel A, Wallenborn JG, DePaoli-Roach AA, Gergs U, Neumann J, Kuppuswamy D, Menick DR, Cooper G. Basis for MAP4 dephosphorylation-related microtubule network densification in pressure overload cardiac hypertrophy. *J Biol Chem*. 2010;285:38125-38140.
43. Cheng H, Lederer WJ. Calcium sparks. *Physiol Rev*. 2008;88:1491-1545.
44. Cicogna AC, Brooks WW, Hayes JA, Robinson KG, Sen S, Conrad CH, et al. Effect of chronic colchicine administration on the myocardium of the aging spontaneously hypertensive rat. Mol Cell Biochem. 1997;166:45–54.
45. Cicogna AC, Robinson KG, Conrad CH, Singh K, Squire R, Okoshi MP, et al. Direct Effects of Colchicine on Myocardial Function. *Hypertension*. 1999;33:60-65.

46. Coleman AK, Joca HC, Shi G, Lederer WJ, Ward CW. Tubulin acetylation increases cytoskeletal stiffness to regulate mechanotransduction in striated muscle. *Biorxiv*. 2020;144931.
47. Conklin DJ, Guo Y, Nystoriak MA, Jagatheesan G, Obal D, Kilfoil PJ, et al. TRPA1 channel contributes to myocardial ischaemia-reperfusion injury. *Am J Physiol-Heart C*. 2019;316:H889-H899.
48. Cooper G. Cardiocyte cytoskeleton in hypertrophied myocardium. *Heart Fail Rev*. 2000;5:187-201.
49. Cooper G. Cytoskeletal networks and the regulation of cardiac contractility: microtubules, hypertrophy, and cardiac dysfunction. *Am J Physiol-Heart C*. 2006;291:H1003-H1014.
50. Cordeiro JM, Howlett SE, Ferrier GR. Simulated ischaemia and reperfusion in isolated guinea pig ventricular myocytes. *Cardiovasc Res*. 1994*;*28:1794-1802.
51. Corey DP, García-Añoveros J, Holt JR, Kwan KY, Lin SY, Vollrath MA, Amalfitano A, Cheung EL-M, Derfler BH, Duggan A, et al. TRPA1 is a candidate for the mechanosensitive transduction channel of vertebrate hair cells. *Nature*. 2004;432:723-730.
52. Coronel R, Fiolet JW, Wilms-Schopman FJ, Schaapherder AF, Johnson TA, Gettes LS, Janse MJ. Distribution of extracellular potassium and its relation to electrophysiologic changes during acute myocardial ischaemia in the isolated perfused porcine heart. *Circulation*. 1988;77:1125-1138.
53. Coronel R, Wilms-Schopman FJ, deGroot JR. Origin of ischaemia-induced phase 1b ventricular arrhythmias in pig hearts. *J Am Coll Cardiol*. 2002;39:166-176.
54. Coronel R, Wilms-Schopman FJG, Opthof T, Janse MJ. Dispersion of repolarization and arrhythmogenesis. *Heart Rhythm*. 2009;6:537-543.
55. Coronel R, Wilms-Schopman FJ, Opthof T, Capelle FJ van, Janse MJ. Injury current and gradients of diastolic stimulation threshold, TQ potential, and extracellular potassium concentration during acute regional ischaemia in the isolated perfused pig heart. *Circ Res*. 1991;68:1241-1249.

56. Coste B, Mathur J, Schmidt M, Earley TJ, Ranade S, Petrus MJ, Dubin AE, Patapoutian A. Piezo1 and Piezo2 are essential components of distinct mechanically activated cation channels. *Science*. 2010;330:55-60.
57. Coulshed DS, Cowan JC. Contraction-excitation feedback in an ejecting whole heart model– dependence of action potential duration on left ventricular diastolic and systolic pressures. *Cardiovasc Res*. 1991;25: 343-352.
58. Coulshed DS, Cowan JC, Drinkhill MJ, Hainsworth R. The effects of ventricular enddiastolic and systolic pressures on action potential and duration in anaesthetized dogs. *J Physiol*. 1992;457:75-91.
59. Coulshed DS, Hainsworth R, Cowan JC. The influence of myocardial systolic shortening on action potential duration following changes in left ventricular end-diastolic pressure. *J Cardiovasc Electrophysiol*. 1994;5:919 -932.
60. Craelius W. Stretch-activation of rat cardiac myocytes. *Exp Physiol*. 1993;78:411-423.
61. Damen J. Ventricular arrhythmias during insertion and removal of pulmonary artery catheters. *Chest*. 1985;88:190-193.
62. Dean JW, Lab MJ. Effect of changes in load on monophasic action potential and segment length of pig heart in situ. *Cardiovasc Res*. 1989;23:887- 896.
63. Dean JW, Lab MJ. Regional changes in ventricular excitability during load manipulation of the in situ pig heart. *J Physiol*. 1990;429: 387-400.
64. Dhein S, Englert C, Riethdorf S, Kostelka M, Dohmen PM, Mohr FW. Arrhythmogenic effects by local left ventricular stretch: effects of flecainide and streptomycin. *Naunyn Schmiedebergs Arch Pharmacol*. 2014;387: 763-775.
65. di Diego JM, Antzelevitch C. Ischaemic ventricular arrhythmias: experimental models and their clinical relevance. *Heart Rhythm*. 2011;8:1963-1968.
66. Dick DJ, Lab MJ. Mechanical modulation of stretch-induced premature ventricular beats: induction of a mechanoelectric adaptation period. *Cardiovasc Res*. 1998;38:181-191.
67. Donoso P, Finkelstein JP, Montecinos L, Said M, Sanchez G, Vittone L, et al. Stimulation of NOX2 in isolated hearts reversibly sensitizes RyR2 channels to activation by cytoplasmic calcium. *J Mol Cell Cardiol*. 2014;68:38-46.

68. Dunn FG, Pringle SD. Left ventricular hypertrophy and myocardial ischaemia in systemic hypertension. *Am J Cardiol*. 1987;60:19-22.
69. Eckardt L, Kirchhof P, Mönnig G, Breithardt G, Borggrefe M, Haverkamp W. Modification of stretch-induced shortening of repolarization by streptomycin in the isolated rabbit heart. *J Cardiovasc Pharm*. 2000;36:711-721.
70. Eisner DA, Nichols CG, O'Neill SC, Smith GL, Valdeolmillos M. The effects of metabolic inhibition on intracellular calcium and pH in isolated rat ventricular cells. *J Physiology*. 1989;411:393-418.
71. Elliott CG, Zimmerman GA, Clemmer TP. Complications of pulmonary artery catheterization in the care of critically ill patients. A prospective study. *Chest*. 1979;76: 647- 652.
72. Erickson JR, Joiner MA, Guan X, Kutschke W, Yang J, Oddis CV, Bartlett RK, Lowe JS, O'Donnell SE, Aykin-Burns N, et al. A Dynamic Pathway for Calcium-Independent Activation of CaMKII by Methionine Oxidation. *Cell*. 2008;133:462–474.
73. Falcón D, Galeano-Otero I, Calderón-Sánchez E, Toro RD, Martín-Bórnez M, Rosado JA, Hmadcha A, Smani T. TRP Channels: current perspectives in the adverse cardiac remodeling. *Front Physiol*. 2019;10:159.
74. Fassett JT, Xu X, Hu X, Zhu G, French J, Chen Y, Bache RJ. Adenosine regulation of microtubule dynamics in cardiac hypertrophy. *Am J Physiology Hear Circ Physiol*. 2009;297:H523-32.
75. Ferrari R, Ceconi C, Curello S, Guarnieri C, Caldarera CM, Albertini A, et al. Oxygen-mediated myocardial damage during ischaemia and reperfusion: role of the cellular defences against oxygen toxicity. *J Mol Cell Cardiol*. 1985;17:937-945.
76. Ferrier GR, Smith RH, Howlett SE. Calcium sparks in mouse ventricular myocytes at physiological temperature. *Am J Physiol Heart Circ Physiol*. 2003;285:H1495-1505.
77. Fiaccadori E, Gonzi G, Zambrelli P, Tortorella G. Cardiac arrhythmias during central venous catheter procedures in acute renal failure: a prospective study. *J Am Soc Nephrol*. 1996;7:1079 -1084.

78. Flaherty JT, Weisfeldt ML, Bulkley BH, Gardner TJ, Gott VL, Jacobus WE. Mechanisms of ischaemic myocardial cell damage assessed by phosphorus-31 nuclear magnetic resonance. *Circulation*. 1982;65:561-570.
79. Franz MR, Burkhoff D, Yue DT, Sagawa K. Mechanically induced action potential changes and arrhythmia in isolated and in situ canine hearts. *Cardiovasc Res*. 1989;23:213-223.
80. Franz MR, Cima R, Wang D, Profitt D, Kurz R. Electrophysiological effects of myocardial stretch and mechanical determinants of stretch-activated arrhythmias. *Circulation*. 1992;86: 968-978.
81. Frohlich ED, Susic D. Pressure overload. *Heart Fail Clin*. 2012;8:21-32.
82. Fu Y, Zhang GQ, Hao XM, Wu CH, Chai Z, Wang SQ. Temperature dependence and thermodynamic properties of Ca^{2+} sparks in rat cardiomyocytes. *Biophys J*. 2005;89:2533-2541.
83. Fujita A, Kurachi Y. Molecular aspects of ATP-sensitive K^+ channels in the cardiovascular system and K^+ channel openers. *Pharmacol. Ther.* 2000;85,39-53.
84. Gallagher KP, Gerren RA, Choy M, Stirling MC, Dysko RC. Subendocardial segment length shortening at lateral margins of ischaemic myocardium in dogs. *Am J Physiol-heart C*. 1987;253:H826-H837.
85. Gannier F, White E, Lacampagne A, Garnier D, Le Guennec JYL. Streptomycin reverses a large stretch induced increase in $[Ca^{2+}]_i$ in isolated guinea pig ventricular myocytes. *Cardiovasc Res*. 1994;28:1193-1198.
86. Garny A, Kohl P. Mechanical induction of arrhythmias during ventricular repolarization: modeling cellular mechanisms and their interaction in two dimensions. *Ann N Y Acad Sci*. 2004;1015:133-143.
87. Goldblum RR, McClellan M, Hou C, Thompson BR, White K, Vang HX, Cohen H, Metzger JM, Gardner MK. Oxidative stress pathogenically remodels the cardiac myocyte cytoskeleton via structural alterations to the microtubule lattice. *bioRxiv*. 2020;2020.06.30.174532.
88. Goswami C, Hucho T. Submembraneous microtubule cytoskeleton: biochemical and functional interplay of TRP channels with the cytoskeleton. *FEBS J*. 2008;275:4684-99.

89. Greve G, Lab MJ, Chen R, Barron D, White PA, Redington AN, Penny DJ. Right ventricular distension alters monophasic action potential duration during pulmonary arterial occlusion in anaesthetised lambs: evidence for arrhythmogenic right ventricular mechanoelectrical feedback. *Exp Physiol*. 2001;86: 651-657.
90. Grimes KM, Prasad V, McNamara JW. Supporting the heart: functions of the cardiomyocyte's non-sarcomeric cytoskeleton. *J Mol Cell Cardiol*. 2019;131:187-196.
91. Groot JR de, Coronel R. Acute ischaemia-induced gap junctional uncoupling and arrhythmogenesis. *Cardiovasc Res*. 2004;62:323-334.
92. Guichard JL, Rogowski M, Agnetti G, Fu L, Powell P, Wei C, Collawn J, Dell'Italia LJ. Desmin loss and mitochondrial damage precede left ventricular systolic failure in volume overload heart failure. *Am J Physiol Heart Circ Physiol*. 2017;313:H32-H45.
93. Haemers P, Sutherland G, Cikes M, Jakus N, Holemans P, Sipido KR, Willems R, Claus P. Further insights into blood pressure induced premature beats: transient depolarizations are associated with fast myocardial deformation upon pressure decline. *Heart Rhythm*. 2015;12:2305–2315.
94. Halperin BD, Adler SW, Mann DE, Reiter MJ. Mechanical correlates of contraction-excitation feedback during acute ventricular dilatation. *Cardiovasc Res*. 1993;27:1084-1087.
95. Haman L, Parizek P, Vojacek J. Precordial thump efficacy in termination of induced ventricular arrhythmias. *Resuscitation*. 2009;80:14-16.
96. Hansen DE, Craig CS, Hondeghem LM. Stretch-induced arrhythmias in the isolated canine ventricle. Evidence for the importance of mechanoelectrical feedback. *Circulation*. 1990;81:1094-1105.
97. Hansen DE, Borganelli M, Jr GPS, Taylor LK. Dose-dependent inhibition of stretch-induced arrhythmias by gadolinium in isolated canine ventricles. Evidence for a unique mode of antiarrhythmic action. *Circ Res*. 1991;69:820–831.
98. Hansen DE, Stacy GP, Taylor LK, Jobe RL, Wang Z, Denton PK, Alexander J. Calcium- and sodium-dependent modulation of stretch-induced arrhythmias in isolated canine ventricles. *Am J Physiol-heart C*. 1995;268:H1803–H1813.

99. Hartmann N, Pabel S, Herting J, Schatter F, Renner A, Gummert J, Schotola H, Danner BC, Maier LS, Frey N, et al. Antiarrhythmic effects of dantrolene in human diseased cardiomyocytes. *Heart Rhythm*. 2017;14:412-419.
100. Harris C. Aortic stenosis. *Ann Cardiothorac Surg*. 2015;4:99.
101. Healy SN, McCulloch AD. An ionic model of stretch-activated and stretch-modulated currents in rabbit ventricular myocytes. *Ep Europace*. 2005;7:S128-S134.
102. Hirata H, Tatsumi H, Hayakawa K, Sokabe M. Non-channel mechanosensors working at focal adhesion-stress fiber complex. *Pflügers Archiv - European J Physiology*. 2015;467:141-155.
103. Hirche H, Hoeher M, Risse JH. Inotropic changes in ischaemic and non-ischaemic myocardium and arrhythmias within the first 120 minutes of coronary occlusion in pigs. *Basic Res Cardiol*. 1987;82:301-310.
104. Hoebart C, Rojas-Galvan NS, Ciotu CI, Aykac I, Reissig LF, Weninger WJ, Kiss A, Podesser BK, Fischer MJM, Heber S. No functional TRPA1 in cardiomyocytes. *Acta Physiol*. 2021;e13659.
105. Hof T, Chaigne S, Récalde A, Sallé L, Brette F, Guinamard R. Transient receptor potential channels in cardiac health and disease. *Nat Rev Cardiol*. 2019;16:344-360.
106. Horner SM, Dick DJ, Murphy CF, Lab MJ. Cycle length dependence of the electrophysiological effects of increased load on the myocardium. *Circulation*. 1996;94: 1131-1136.
107. Huang H, Wei H, Liu P, Wang W, Sachs F, Niu W. A simple automated stimulator of mechanically induced arrhythmias in the isolated rat heart. *Exp Physiol*. 2009;94:1054-1061.
108. Huke S, Knollmann BC. Increased myofilament Ca^{2+}-sensitivity and arrhythmia susceptibility. *J Mol Cell Cardiol*. 2010;48:824–833.
109. Hwang E-S, Pak H-N. Mid-septal hypertrophy and apical ballooning; potential mechanism of ventricular tachycardia storm in patients with hypertrophic cardiomyopathy. *Yonsei Med J*. 2012;53:221-223.
110. Iberti TJ, Benjamin E, Gruppi L, Raskin JM. Ventricular arrhythmias during pulmonary artery catheterization in the intensive care unit. Prospective study. *Am J Med*. 1985;78: 451-454.

111. Inoue R, Jensen LJ, Shi J, Morita H, Nishida M, Honda A, Ito Y. Transient receptor potential channels in cardiovascular function and disease. *Circ Res*. 2006;99:119-131.
112. Inoue R, Jian Z, Kawarabayashi Y. Mechanosensitive TRP channels in cardiovascular pathophysiology. *Pharmacol Therapeut*. 2009;123:371-385.
113. Inoue R, Kurahara LH, Hiraishi K. TRP channels in cardiac and intestinal fibrosis. *Semin Cell Dev Biol*. 2019;94:40-9.
114. Iribe G, Helmes M, Kohl P. Force-length relations in isolated intact cardiomyocytes subjected to dynamic changes in mechanical load. *Am J Physiol Heart Circ Physiol*. 2007;292:H1487-1497.
115. Iribe G, Kohl P. Axial stretch enhances sarcoplasmic reticulum Ca^{2+} leak and cellular Ca^{2+} reuptake in guinea pig ventricular myocytes: experiments and models. *Prog Biophysics Mol Biology*. 2008;97:298-311.
116. Iribe G, Ward CW, Camelliti P, Bollensdorff C, Mason F, Burton RAB, et al. Axial stretch of rat single ventricular cardiomyocytes causes an acute and transient increase in Ca^{2+} spark rate. *Circ Res*. 2009;104:787-795.
117. Iribe G, Kaihara K, Ito H, Naruse K. Effect of azelnidipine and amlodipine on single cell mechanics in mouse cardiomyocytes. *Eur J Pharmacol*. 2013;715:142-146.
118. Iribe G, Kaneko T, Yamaguchi Y, Naruse K. Load dependency in force-length relations in isolated single cardiomyocytes. *Prog Biophys Mol Biol*. 2014;115:103-114.
119. Iribe G, Kaihara K, Yamaguchi Y, Nakaya, M, Inoue R, Naruse K. Mechano-sensitivity of mitochondrial function in mouse cardiac myocytes. *Prog Biophys Mol Biol*. 2017;130(Pt B):315-322.
120. Israeli-Rosenberg S, Chen C, Li R, Deussen DN, Niesman IR, Okada H, Pately HH, Roth DM, Ross RS. Caveolin modulates integrin function and mechanical activation in the cardiomyocyte. *FASEB J*. 2015;29:374-384.
121. Izu LT, Kohl P, Boyden PA, Miura M, Banyasz T, Chiamvimonvat N, Trayanova N, Bers DM, Chen-Izu Y. Mechano-electric and mechano-chemo-transduction in cardiomyocytes. *J Physiology*. 2020;598:1285-1305.

122. Jakob D, Klesen A, Allegrini B, Darkow E, Aria D, Emig R, Chica AS, Rog-Zielinska EA, Guth T, Beyersdorf F, et al. Piezo1 and BKCa channels in human atrial fibroblasts: interplay and remodelling in atrial fibrillation. *bioRxiv*. 2021;2021.01.21.427388.
123. Janke C, Bulinski JC. Post-translational regulation of the microtubule cytoskeleton: mechanisms and functions. *Nat Rev Mol Cell Bio*. 2011;12:773-786.
124. Janse MJ, Wit AL. Electrophysiological mechanisms of ventricular arrhythmias resulting from myocardial ischaemia and infarction. *Physiol Rev*. 1989;69:1049-1169.
125. Jie X, Gurev V, Trayanova N. Mechanisms of mechanically induced spontaneous arrhythmias in acute regional ischaemia. *Circ Res*. 2010;106:185-192.
126. Joca HC, Coleman AK, Ward CW, Williams GSB. Quantitative tests reveal that microtubules tune the healthy heart but underlie arrhythmias in pathology. *J Physiol*. 2020;598:1327-1338.
127. Jordt SE, Bautista DM, Chuang H, McKemy DD, Zygmunt PM, Högestätt ED, Meng ID, Julius D. Mustard oils and cannabinoids excite sensory nerve fibres through the TRP channel ANKTM1. *Nature*. 2004;427:260-265.
128. Kahan T, Bergfeldt L. Left ventricular hypertrophy in hypertension: its arrhythmogenic potential. *Heart*. 2005;91:250-6.
129. Kamkin A, Kiseleva I, Isenberg G. Stretch-activated currents in ventricular myocytes: amplitude and arrhythmogenic effects increase with hypertrophy. *Cardiovasc Res*. 2000;48:409-20.
130. Kaneko Y, Szallasi A. Transient receptor potential (TRP) channels: a clinical perspective. *Brit J Pharmacol*. 2014;171:2474-507.
131. Kelly D, Mackenzie L, Hunter P, Smaill B, Saint D. Gene expression of stretch-activated channels and mechanoelectric feedback in the heart. *Clin Exp Pharmacol P*. 2006;33:642-648.
132. Kerr JP, Robison P, Shi G, Bogush AI, Kempema AM, Hexum JK, et al. Detyrosinated microtubules modulate mechanotransduction in heart and skeletal muscle. *Nat Commun*. 2015;6:8526.

133. Kerstein PC, Camino D del, Moran MM, Stucky CL. Pharmacological Blockade of TRPA1 Inhibits Mechanical Firing in Nociceptors. *Mol Pain*. 2009;5:1744-8069-5-19.
134. Keurs HEDJ ter. Microtubules in cardiac hypertrophy. *Circ Res*. 1998;82:828-831.
135. Keurs HEDJ ter, Wakayama Y, Miura M, Shinozaki T, Stuyvers BD, Boyden PA, et al. Arrhythmogenic Ca^{2+} release from cardiac myofilaments. *Prog Biophys Mol Biol*. 2006;90:151-171.
136. Keurs HEDJ, Wakayama Y, Sugai Y, Price G, Kagaya Y, Boyden PA, et al. Role of sarcomere mechanics and Ca^{2+} overload in Ca^{2+} waves and arrhythmias in rat cardiac muscle. *Ann N Y Acad Sci*. 2006;1080:248-267.
137. Keurs HEDJ ter, Boyden PA. Calcium and Arrhythmogenesis. *Physiol Rev*. 2007;87:457-506.
138. Keurs HEDJ ter, Shi dnozaki T, Zhang YM, Zhang ML, Wakayama Y, Sugai Y, Kagaya Y, Miura M, Boyden PA, Stuyvers BDM, Landesberg A. Sarcomere mechanics in uniform and non-uniform cardiac muscle: a link between pump function and arrhythmias. *Prog Biophysics Mol Biology*. 2008;97:312-331.
139. Khokhlova A, Iribe G, Yamaguchi Y, Naruse K, Solovyova O. Effects of simulated ischaemia on the transmural differences in the frank-starling relationship in isolated mouse ventricular cardiomyocytes. *Prog Biophys Mol Biol*. 2017;130:323-332.
140. Kim DY, White E, Saint DA. Increased mechanically-induced ectopy in the hypertrophied heart. *Prog Biophys Mol Biol*. 2012;110:331-339.
141. Kockskämper J, Lewinski D von, Khafaga M, Elgner A, Grimm M, Eschenhagen T, et al. The slow force response to stretch in atrial and ventricular myocardium from human heart: Functional relevance and subcellular mechanisms. *Prog Biophys Mol Biol*. 2008;97:250-267.
142. Kohl P, Bollensdorff C, Garny A. Effects of mechanosensitive ion channels on ventricular electrophysiology: experimental and theoretical models. *Exp Physiol*. 2006;91:307-321.
143. Kohl P, Hunter P, Noble D. Stretch-induced changes in heart rate and rhythm: clinical observations, experiments and mathematical models. *Prog Biophys Mol Biol*. 1999;71:91-138.

144. Kohl P, Nesbitt AD, Cooper PJ, Lei M. Sudden cardiac death by Commotio cordis: role of mechano-electric feedback. *Cardiovasc Res*. 2001;50:280-289.
145. Kohl P, Ravens U. Cardiac mechano-electric feedback: past, present, and prospect. *Prog Biophys Mol Biol*. 2003;82:3-9.
146. Kohl P, Sachs F, Franz MR (editors). Cardiac mechano-electric coupling and arrhythmias (2 ed.). *Oxford University Press*. 2011.
147. Köhler AC, Sag CM, Maier LS. Reactive oxygen species and excitation–contraction coupling in the context of cardiac pathology. *J Mol Cell Cardiol.* 2014;73:92-102.
148. Koide M, Hamawaki M, Narishige T, Sato H, Nemoto S, DeFreyte G, Zile MR, Cooper G, Carabello BA. Microtubule depolymerization normalizes in vivo myocardial contractile function in dogs with pressure-overload left ventricular hypertrophy. *Circulation*. 2000;102:1045-1052.
149. Konstam MA, Kramer DG, Patel AR, Maron MS, Udelson JE. Left ventricular remodeling in heart failure. *JACC-Cardiovasc Imag*. 2011;4:98-108.
150. Kreitzer G, Liao G, Gundersen GG. Detyrosination of tubulin regulates the interaction of intermediate filaments with microtubules in vivo via a kinesin-dependent mechanism. *Mol Biol Cell*. 1999;10:1105-1118.
151. Kuroda J, Sadoshima J. NADPH oxidase and cardiac failure. *J Cardiovasc Transl. Res*. 2010;3:314-320.
152. Kusminsky RE. Complications of central venous catheterization. *J Am Coll Surg*. 2007;204:681-696.
153. Lab MJ. Transient depolarisation and action potential alterations following mechanical changes in isolated myocardium. *Cardiovasc Res*. 1980;14:624-637.
154. Lab MJ. Contribution of mechano-electric coupling to ventricular arrhythmias during reduced perfusion. *Int J Microcirc Clin Exp*. 1989;8:433-442.
155. Landstrom AP, Dobrev D, Wehrens XHT. Calcium signaling and cardiac arrhythmias. *Circ Res*. 2017;120:1969-1993.
156. Lang D, Holzem K, Kang C, Xiao M, Hwang HJ, Ewald GA, et al. Arrhythmogenic remodeling of β_2 versus β_2 adrenergic signaling in the human failing heart. *Circ Arr Electrophysiol*. 2015;8:409-419.

157. Lee JC, Epstein LM, Huffer LL, Stevenson WG, Koplan BA, Tedrow UB. ICD lead proarrhythmia cured by lead extraction. *Heart Rhythm*. 2009;6:613-618.
158. Lee TY, Sung CS, Chu YC, Liou JT, Lui PW. Incidence and risk factors of guidewire-induced arrhythmia during internal jugular venous catheterization: comparison of marked and plain J-wires. *J Clin Anesth*. 1996;8:348-351.
159. Lee YC, Sutton FJ. Valsalva termination of ventricular tachycardia. *Circulation*. 1982;65:1287-1288.
160. Lerman BB, Burkhoff D, Yue DT, Franz MR, Sagawa K. Mechanoelectrical feedback: independent role of preload and contractility in modulation of canine ventricular excitability. *J Clin Invest*. 1985;76:1843-1850.
161. Leuven SLV, Waldman LK, McCulloch AD, Covell JW. Gradients of epicardial strain across the perfusion boundary during acute myocardial ischaemia. *Am J Physiol-heart C*. 1994;267:H2348–H2362.
162. Levine JH, Guarnieri T, Kadish AH, White RI, Calkins H, Kan JS. Changes in myocardial repolarization in patients undergoing balloon valvuloplasty for congenital pulmonary stenosis: evidence for contraction-excitation feedback in humans. *Circulation*. 1988;77:70-77.
163. Lewis YE, Moskovitz A, Mutlak M, Heineke J, Caspi LH, Kehat I. Localization of transcripts, translation, and degradation for spatiotemporal sarcomere maintenance. *J Mol Cell Cardiol*. 2018;116:16-28.
164. Li R, Liu R, Yan F, Zhuang X, Shi H, Gao X. Inhibition of TRPA1 promotes cardiac repair in mice after myocardial infarction. *J. Cardiovasc. Pharmacol.* 2020;75,240-9.
165. Li W, Kohl P, Trayanova N. Induction of ventricular arrhythmias following mechanical impact: a simulation study in 3D. *J Mol Histol*. 2004;35:679-686.
166. Li W, Kohl P, Trayanova N. Myocardial ischaemia lowers precordial thump efficacy: an inquiry into mechanisms using three-dimensional simulations. *Heart Rhythm*. 2006;3:179-186.
167. Liao G, Gundersen GG. Kinesin is a candidate for cross-bridging microtubules and intermediate filaments. *J Biol Chem*. 1998;273:9797-9803.
168. Limbu S, Hoang-Trong TM, Prosser BL, Lederer WJ, Jafri MS. Modeling local X-ROS and calcium signaling in the heart. *Biophys J*. 2015;109:2037-2050.

169. Limbu S, Prosser BL, Lederer WJ, Ward CW, Jafri MS. X-ROS signaling depends on length-dependent calcium buffering by troponin. *Cells*. 2021;10:1189.
170. Lindsay AC, Wong T, Segal O, Peters NS. An unusual twist: ventricular tachycardia induced by a loop in a right ventricular pacing wire. *QJM*. 2006;99:347–348.
171. Link MS, Maron BJ, VanderBrink BA, Takeuchi M, Pandian NG, Wang PJ, Estes NAM. Impact directly over the cardiac silhouette is necessary to produce ventricular fibrillation in an experimental model of commotio cordis. *J Am Coll Cardiol*. 2001;37:649-654.
172. Link MS, Maron BJ, Wang PJ, VanderBrink BA, Zhu W, Estes NA III. Upper and lower limits of vulnerability to sudden arrhythmic death with chest-wall impact (commotio cordis). *J Am Coll Cardiol*. 2003;41: 99-104.
173. Link MS, Wang PJ, Pandian NG, Bharati S, Udelson JE, Lee M-Y, Vecchiotti MA, VanderBrink BA, Mirra G, Maron BJ, et al. An experimental model of sudden death due to low-energy chest-wall impact (commotio cordis). *New Engl J Med*. 1998;338:1805-1811.
174. Lorell BH, Carabello BA. Left ventricular hypertrophy pathogenesis, detection, and prognosis. *Circulation*. 2000;102:470-479.
175. Ma L, Deng Y, Zhang B, Bai Y, Cao J, Li S, Liu J. Pinacidil, a Katp channel opener, identified as a novel agonist for TRPA1. *Chinese Sci Bull*. 2012;57:1810-1817.
176. Maier LS, Bers DM. Role of Ca^{2+}/calmodulin-dependent protein kinase (CaMK) in excitation-contraction coupling in the heart. *Cardiovasc Res*. 2007;73:631-640.
177. Maron BJ, Doerer JJ, Haas TS, Tierney DM, Mueller FO. Sudden deaths in young competitive athletes. *Circulation*. 2009;119:1085-1092.
178. Maron BJ, Estes NAM. Commotio cordis. *New Engl J Med*. 2010;362:917-927.
179. Mattiazzi A, Argenziano M, Aguilar-Sanchez Y, Mazzocchi G, Escobar AL. Ca^{2+} Sparks and Ca^{2+} waves are the subcellular events underlying Ca^{2+} overload during ischaemia and reperfusion in perfused intact hearts. *J Mol Cell Cardiol*. 2015;79:69-78.
180. Mattiazzi A, Bassani RA, Escobar AL, Palomeque J, Valverde CA, Vila Petroff M, et al. Chasing cardiac physiology and pathology down the CaMKII cascade. *Am J Physiol Heart Circ Physiol*. 2015;308:H1177-1191.

181. McLenachan JM, Henderson E, Morris KI, Dargie HJ. Ventricular arrhythmias in patients with hypertensive left ventricular hypertrophy. *N Engl J Med*. 1987;317:787-92.
182. McNamara CR, Mandel-Brehm J, Bautista DM, Siemens J, Deranian KL, Zhao M, Hayward NJ, Chong JA, Julius D, Moran MM, Fanger CM. TRPA1 mediates formalin-induced pain. *Proc National Acad Sci*. 2007;104:13525-13530.
183. Meents JE, Ciotu CI, Fischer MJM. TRPA1: a molecular view. *J Neurophysiol*. 2019;121:427-443.
184. Meents JE, Fischer MJM, McNaughton PA. Agonist-induced sensitisation of the irritant receptor ion channel TRPA1. *J Physiology*. 2016;594:6643-6660.
185. Meents JE, Fischer MJM, McNaughton PA. Sensitization of TRPA1 by Protein Kinase A. *PLoS One*. 2017;12:e0170097.
186. Michailova A, Lorentz W, McCulloch A. Modeling transmural heterogeneity of KATP current in rabbit ventricular myocytes. *Am J Physiol Cell Ph*. 2007;293:C542-C557.
187. Michel J, Johnson AD, Bridges WC, Lehmann JH, Gray F, Field L, Green DM. Arrhythmias during intracardiac catheterization. *Circulation*. 1950;2:240-244.
188. Miura M, Wakayama Y, Endoh H, Nakano M, Sugai Y, Hirose M, et al. Spatial non-uniformity of excitation-contraction coupling can enhance arrhythmogenic-delayed afterdepolarizations in rat cardiac muscle. *Cardiovasc Res*. 2008;80:55-61.
189. Miura M, Nishio T, Hattori T, Murai N, Stuyvers BD, Shindoh C, et al. Effect of nonuniform muscle contraction on sustainability and frequency of triggered arrhythmias in rat cardiac muscle. *Circulation.* 2010;121**,** 2711-2717.
190. Miura M, Murai N, Hattori T, Nagano T, Stuyvers BD, Shindoh C. Role of reactive oxygen species and Ca^{2+} dissociation from the myofilaments in determination of Ca^{2+} wave propagation in rat cardiac muscle. *J Mol Cell Cardiol*. 2013;56:97-105.
191. Miura M, Taguchi Y, Nagano T, Sasaki M, Handoh T, Shindoh C. Effect of myofilament Ca^{2+} sensitivity on Ca^{2+} wave propagation in rat ventricular muscle. *J Mol Cell Cardiol*. 2015;84:162-169.

192. Miura M, Taguchi Y, Handoh T, Hasegawa T, Takahashi Y, Morita N, et al. Regional increase in ROS within stretched region exacerbates arrhythmias in rat trabeculae with nonuniform contraction. *Pflugers Arch*. 2018;470:1349-1357.
193. Moparthi L, Zygmunt PM. Human TRPA1 is an inherently mechanosensitive bilayer-gated ion channel. *Cell Calcium*. 2020;91:102255.
194. Moran MM. TRP Channels as Potential Drug Targets. *Annu Rev Pharmacol*. 2018;58:309-330.
195. Muller JE, Tofler GH, Stone PH. Circadian variation and triggers of onset of acute cardiovascular disease. *Circulation*. 1989;79:733-s43.
196. Murata M, Akao M, O'Rourke B, Marbán E. Mitochondrial ATP-sensitive potassium channels attenuate matrix Ca^{2+} overload during simulated ischaemia and reperfusion. *Circ Res*. 2001;89:891-898.
197. Murphy SR, Wang L, Wang Z, Domondon P, Lang D, Habecker BA, et al. β-Adrenergic inhibition prevents action potential and calcium handling changes during regional myocardial ischaemia. *Front Physiol*. 2017;8:630.
198. Myerburg RJ, Interian A Jr, Mitrani RM, Kessler KM, Castellanos A. Frequency of sudden cardiac death and profiles of risk. *Am J Cardiol*. 1997;80:10F-19F.
199. Nazir SA, Dick DJ, Lab MJ. Mechanoelectric feedback and arrhythmia in the atrium of the isolated, Langendorf-perfused guinea pig hearts and its modulation by streptomycin. *J Physiol*. 1995;483:24-25P.
200. Nazir SA, Lab MJ. Mechanoelectric feedback in the atrium of the isolated guinea-pig heart. *Cardiovasc Res*. 1996;32:112-119.
201. Nesbitt AD, Cooper PJ, Kohl P. Rediscovering commotio cordis. *Lancet*. 2001;357:1195-1197.
202. Nikolaev YA, Cox CD, Ridone P, Rohde PR, Cordero-Morales JF, Vásquez V, Laver DR, Martinac B. Mammalian TRP ion channels are insensitive to membrane stretch. *J Cell Sci*. 2019;132:jcs238360.
203. Nilius B, Appendino G, Owsianik G. The transient receptor potential channel TRPA1: from gene to pathophysiology. *Pflügers Arch European J Physiol*. 2012;464:425–58.

204. Nishida M, Kurose H. Roles of TRP channels in the development of cardiac hypertrophy. *Naunyn Schmiedebergs Arch Pharmacol*. 2008;378:395-406.
205. Nishimura S, Nagai S, Katoh M, Yamashita H, Saeki Y, Okada J, et al. Microtubules modulate the stiffness of cardiomyocytes against shear stress. *Circ Res*. 2006;98:81-87.
206. O'Brien JD, Ferguson JH, Howlett SE. Effects of ischaemia and reperfusion on isolated ventricular myocytes from young adult and aged Fischer 344 rat hearts. *Am J Physiol Heart Circ Physiol*. 2008;294:H2174-2183.
207. Oguri G, Nakajima T, Kikuchi H, Obi S, Nakamura F, Komuro I. Allyl isothiocyanate (AITC) activates nonselective cation currents in human cardiac fibroblasts: possible involvement of TRPA1. *Heliyon*. 2021;7:e05816.
208. Oh SJ, Lee JM, Kim HB, Lee J, Han S, Bae JY, Hong GS, Koh W, Kwon J, Hwang ES, et al. Ultrasonic Neuromodulation via Astrocytic TRPA1. *Curr Biol*. 2019;29:3386-3401.e8.
209. Ohba T, Watanabe H, Murakami M, Takahashi Y, Iino K, Kuromitsu S, Mori Y, Ono K, Iijima T, Ito H. Upregulation of TRPC1 in the development of cardiac hypertrophy. *J Mol Cell Cardiol*. 2007;42:498-507.
210. Owens LM, Fralix TA, Murphy E, Cascio WE, Gettes LS. Correlation of ischaemia-induced extracellular and intracellular ion changes to cell-to-cell electrical uncoupling in isolated blood-perfused rabbit hearts. *Circulation*. 1996;94:10-13.
211. Parker KK, Lavelle JA, Taylor LK, Wang Z, Hansen DE. Stretch-induced ventricular arrhythmias during acute ischaemia and reperfusion. *J Appl Physiol*. 2004;97:377-383.
212. Parker KK, Taylor LK, Atkinson JB, Hansen DE, Wikswo JP, Atkinson B. The effects of tubulin-binding agents on stretch-induced ventricular arrhythmias. *Eur J Pharmacol*. 2001;417:131-140.
213. Pennington JE, Taylor J, Lown B. Chest thump for reverting ventricular tachycardia. *New Engl J Med*. 1970;283:1192-1195.
214. Perticone F, Ceravolo R, Maio R, Cosco C, Giancotti F, Mattioli PL. [Mechano-electric feedback and ventricular arrhythmias in heart failure. The possible role of

permanent cardiac stimulation in preventing ventricular tachycardia]. *Cardiologia*. 1993;38:247-52.

215. Peyronnet R, Bollensdorff C, Capel RA, Rog-Zielinska EA, Woods CE, Charo DN, et al. Load-dependent effects of apelin on murine cardiomyocytes. *Prog Biophys Mol Biol*. 2017;130:333-343.

216. Peyronnet R, Nerbonne JM, Kohl P. Cardiac mechano-gated ion channels and arrhythmias. *Circ Res*. 2016;118:311-329.

217. Poluektov YM, Petrushanko IY, Undrovina NA, Lakunina VA, Khapchaev AY, Kapelko VI, et al. Glutathione-related substances maintain cardiomyocyte contractile function in hypoxic conditions. *Sci Rep*. 2019;9:4872.

218. Portran D, Schaedel L, Xu Z, Théry M, Nachury MV. Tubulin acetylation protects long-lived microtubules against mechanical ageing. *Nat Cell Biol*. 2017;19:391-398.

219. Prinzen FW, Arts T, Hoeks APG, Reneman RS. Discrepancies between myocardial blood flow and fiber shortening in the ischaemic border zone as assessed with video mapping of epicardial deformation. *Pflügers Archiv*. 1989;415:220-229.

220. Prosser BL, Ward CW, Lederer WJ. Subcellular Ca^{2+} signaling in the heart: the role of ryanodine receptor sensitivity. *J Gen Physiol*. 2010;136:135-142.

221. Prosser BL, Ward CW, Lederer WJ. X-ROS Signaling: rapid mechano-chemo transduction in heart. *Science*. 2011;333:1440-1445.

222. Prosser BL, Khairallah RJ, Ziman AP, Ward CW, Lederer WJ. X-ROS signaling in the heart and skeletal muscle: stretch-dependent local ROS regulates $[Ca^{2+}]_i$. *J Mol Cell Cardiol*. 2013;58:172-181.

223. Prosser BL, Ward CW, Lederer WJ. X-ROS signalling is enhanced and graded by cyclic cardiomyocyte stretch. *Cardiovasc Res*. 2013;98:307-314.

224. Prosser BL, Ward CW. Mechano-chemo transduction tunes the heartstrings. *Sci Signal*. 2014;7:pe7–pe7.

225. Quinn TA, Granite S, Allessie MA, Antzelevitch C, Bollensdorff C, Bub G, et al. Minimum information about a cardiac electrophysiology experiment (MICEE): standardised reporting for model reproducibility, interoperability, and data sharing. *Prog Biophys Mol Biol*. 2011;107:4-10.

226. Quinn TA. The importance of non-uniformities in mechano-electric coupling for ventricular arrhythmias. *J Interv Card Electr*. 2014;39:25-35.
227. Quinn TA, Kohl P, Ravens U. Cardiac mechano-electric coupling research: fifty years of progress and scientific innovation. *Prog Biophys Mol Biol*. 2014;115:71-75.
228. Quinn TA. Cardiac mechano-electric coupling: a role in regulating normal function of the heart? *Cardiovasc Res*. 2015;108:1-3.
229. Quinn TA, Camelliti P, Rog-Zielinska EA, et al. Electrotonic coupling of excitable and nonexcitable cells in the heart revealed by optogenetics. *Proc Natl Acad Sci USA*. 2016;113:14852-7.
230. Quinn TA, Kohl P. Rabbit models of cardiac mechano-electric and mechano-mechanical coupling. *Prog Biophys Mol Biol*. 2016;121:110-122.
231. Quinn TA, Jin H, Lee P, Kohl P. Mechanically induced ectopy via stretch-activated cation-nonselective channels is caused by local tissue deformation and results in ventricular fibrillation if triggered on the repolarization wave edge (commotio cordis). *Circ Arrhythm Electrophysiol*. 2017;10:e004777.
232. Quinn TA, Kohl P. Cardiac mechano-electric coupling: acute effects of mechanical stimulation on heart rate and rhythm. *Physiol Rev*. 2021;101:37-92.
233. Quintanilla JG, Moreno J, Archondo T, Usandizaga E, Molina-Morúa R, Rodríguez-Bobada C, González P, García-Torrent MJ, Filgueiras-Rama D, Pérez-Castellano N, et al. Increased intraventricular pressures are as harmful as the electrophysiological substrate of heart failure in favoring sustained reentry in the swine heart. *Heart Rhythm*. 2015;12:2172-2183.
234. Raedschelders K, Ansley DM, Chen DDY. The cellular and molecular origin of reactive oxygen species generation during myocardial ischaemia and reperfusion. *Pharmacol Ther*. 2012;133:230-255.
235. Rapsomaniki E, Timmis A, George J, Pujades-Rodriguez M, Shah AD, Denaxas S, White IR, Caulfield MJ, Deanfield JE, Smeeth L, et al. Blood pressure and incidence of twelve cardiovascular diseases: lifetime risks, healthy life-years lost, and age-specific associations in 1.25 million people. *Lancet*. 2014;383:1899-911.
236. Ravens U. Mechano-electric feedback and arrhythmias. *Prog Biophys Mol Biol*. 2003;82:255-266.

237. Reiter MJ, Synhorst DP, Mann DE. Electrophysiological effects of acute ventricular dilatation in the isolated rabbit heart. *Circ Res*. 1988;62:554-562.
238. Reiter MJ, Zetelaki Z, Kirchhof CJ, Boersma L, Allessie MA. Interaction of acute ventricular dilatation and d-sotalol during sustained reentrant ventricular tachycardia around a fixed obstacle. *Circulation*. 1994;89:423-431.
239. Reiter MJ, Landers M, Zetelaki Z, Kirchhof CJ, Allessie MA. Electrophysiological effects of acute dilatation in the isolated rabbit heart: cycle length-dependent effects on ventricular refractoriness and conduction velocity. *Circulation*. 1997;96:4050-4056.
240. Reiter MJ, Stromberg KD, Whitman TA, Adamson PB, Benditt DG, Gold MR. Influence of intracardiac pressure on spontaneous ventricular arrhythmias in patients with systolic heart failure: insights from the REDUCEhf trial. *Circ Arrhythm Electrophysiol*. 2013;6:272-278.
241. Rice JJ, Winslow RL, Dekanski J, McVeigh E. Model studies of the role of mechano-sensitive currents in the generation of cardiac arrhythmias. *J Theor Biol*. 1998;190:295-312.
242. Riemer TL, Tung L. Stretch-induced excitation and action potential changes of single cardiac cells. *Prog Biophys Mol Biol*. 2003;82:97-110.
243. Robison P, Caporizzo MA, Ahmadzadeh H, Bogush AI, Chen CY, Margulies KB, et al. Detyrosinated microtubules buckle and bear load in contracting cardiomyocytes. *Science*. 2016;352:aaf0659.
244. Robison P, Prosser BL. Microtubule mechanics in the working myocyte. *J Physiol*. 2017;595:3931-3937.
245. Rubart M, Zipes DP. Mechanisms of sudden cardiac death. *J Clin Invest*. 2005;115:2305-2315.
246. Sakai K, Watanabe K, Millard RW. Defining the mechanical border zone: a study in the pig heart. *Am J Physiol Heart C*. 1985;249:H88-H94.
247. Salomon AK, Okami N, Heffler J, Lee J-J, Robison P, Bogush AI, Prosser BL. Desmin intermediate filaments and tubulin detyrosination stabilize growing microtubules in the cardiomyocyte. *bioRxiv*. 2021;2021.05.26.445641.

248. Sánchez G, Pedrozo Z, Domenech RJ, Hidalgo C, Donoso P. Tachycardia increases NADPH oxidase activity and RyR2 S-glutathionylation in ventricular muscle. *J Mol Cell Cardiol*. 2005;39:982-991.
249. Sato D, Bartos DC, Ginsburg KS, Bers DM. Depolarization of cardiac membrane potential synchronizes calcium sparks and waves in tissue. *Biophys J.* 2014;107:1313-1317.
250. Sato H, Nagai T, Kuppuswamy D, Narishige T, Koide M, Menick DR, et al. Microtubule stabilization in pressure overload cardiac hypertrophy. *J Cell Biol*. 1997;139:963-973.
251. Scarborough EA, Uchida K, Vogel M, Erlitzki N, Iyer M, Phyo SA, Bogush A, Kehat I, Prosser BL. Microtubules orchestrate local translation to enable cardiac growth. *Nat Commun*. 2021;12:1547.
252. Schiff PB, Fant J, Horwitz SB. Promotion of microtubule assembly in vitro by taxol. *Nature*. 1979;277:665-667.
253. Scholz D, Baicu CF, Tuxworth WJ, Xu L, Kasiganesan H, Menick DR, Cooper G. Microtubule-dependent distribution of mRNA in adult cardiocytes. *Am J Physiol Heart C*. 2008;294:H1135-H1144.
254. Schönleitner P, Schotten U, Antoons G. Mechanosensitivity of microdomain calcium signalling in the heart. *Prog Biophys Mol Biol*. 2017;130:288-301.
255. Scopacasa BS, Teixeira VPA, Franchini KG. Colchicine attenuates left ventricular hypertrophy but preserves cardiac function of aortic-constricted rats. *J Appl Physiol*. 2003;94:1627-1633.
256. Sénatore S., Reddy, V. R., Sémériva, M., Perrin, L. & Lalevée, N. Response to mechanical stress is mediated by the TRPA channel painless in the *Drosophila* heart. *PLoS Genet.*2010;6,e1001088.
257. Seo K, Inagaki M, Nishimura S, Hidaka I, Sugimachi M, Hisada T, Sugiura S. Structural heterogeneity in the ventricular wall plays a significant role in the initiation of stretch-induced arrhythmias in perfused rabbit right ventricular tissues and whole heart preparations. *Circ Res*. 2010;106:176-184.
258. Shenasa M, Shenasa H. Hypertension, left ventricular hypertrophy, and sudden cardiac death. *Int J Cardiol*. 2017;237:60-3.

259. Sideris DA, Kontoyannis DA, Michalis L, et al. Acute changes in blood pressure as a cause of cardiac arrhythmias. *Eur Heart J*. 1987;8:45-52.
260. Sideris DA, Chrysos DN, Maliaras GK, Michalis LK, Moulopoulos SD. Effect of acute hypertension on the cardiac rhythm. Experimental observations. *J Electrocardiol*. 1988;21:183-191.
261. Sideris DA, Toumanidis ST, Kostis EB, Diakos A, Moulopoulos SD. Arrhythmogenic effect of high blood pressure: some observations on its mechanism. *Cardiovasc Res*. 1989;23:983-992.
262. Sideris DA, Toumanidis ST, Kostis EB, Spyropoulos G, Moulopoulos SD. Effect of adrenergic blockade on pressure-related ventricular arrhythmias. *Acta Cardiol*. 1991;46:215-225.
263. Sideris DA. High blood pressure and ventricular arrhythmias. *Eur Heart J*. 1993;14:1548-1553.
264. Siogas K, Pappas S, Graekas G, Goudevenos J, Liapi G, Sideris DA. Segmental wall motion abnormalities alter vulnerability to ventricular ectopic beats associated with acute increases in aortic pressure in patients with underlying coronary artery disease. *Heart*. 1998;79:268-273.
265. Smani T, Dionisio N, López JJ, Berna-Erro A, Rosado JA. Cytoskeletal and scaffolding proteins as structural and functional determinants of TRP channels. *Biochimica Et Biophysica Acta Bba-Biomembr*. 2014;1838:658-664.
266. Sprung CL, Pozen RG, Rozanski JJ, Pinero JR, Eisler BR, Castellanos A. Advanced ventricular arrhythmias during bedside pulmonary artery catheterization. *Am J Medicine*. 1982;72:203-208.
267. Stacy GP, Jobe RL, Taylor LK, Hansen DE. Stretch-induced depolarizations as a trigger of arrhythmias in isolated canine left ventricles. *Am J Physiol Heart C*. 1992;263:H613-H621.
268. Steele DF, Fedida D. Cytoskeletal roles in cardiac ion channel expression. *Biochimica Et Biophysica Acta Bba-Biomembr*. 2014;1838:665-673.
269. Stones R, Benoist D, Peckham M, White E. Microtubule proliferation in right ventricular myocytes of rats with monocrotaline-induced pulmonary hypertension. *J Mol Cell Cardiol*. 2013;56:91-96.

270. Stuart RK, Shikora SA, Akerman P, Lowell JA, Baxter JK, Apovian C, Champagne C, Jennings A, Keane-Ellison M, Bistrian BR. Incidence of arrhythmia with central venous catheter insertion and exchange. *JPEN J Parenter Enteral Nutr.* 1990;14:152-155.

271. Sung D, Mills RW, Schettler J, Narayan SM, Omens JH, McCulloch AD. Ventricular filling slows epicardial conduction and increases action potential duration in an optical mapping study of the isolated rabbit heart. *J Cardiovasc Electrophysiol*. 2003;14:739-749.

272. Sutherland GR. Sudden cardiac death: the pro-arrhythmic interaction of an acute loading with an underlying substrate. *Eur Heart J*. 2017;38:2986-2994.

273. Tagawa H, Rozich JD, Tsutsui H, Narishige T, Kuppuswamy D, Sato H, McDermott PJ, Koide M, Cooper G. Basis for increased microtubules in pressure-hypertrophied cardiocytes. *Circulation*. 1996;93:1230-1243.

274. Tagawa H, Wang N, Narishige T, Ingber DE, Zile MR, Cooper G. Cytoskeletal mechanics in pressure-overload cardiac hypertrophy. *Circ Res*. 1997;80:281-289.

275. Tagawa H, Koide M, Sato H, Zile MR, Carabello BA, IV GC. Cytoskeletal role in the transition from compensated to decompensated hypertrophy during adult canine left ventricular pressure overloading. *Circ Res*. 1998;82:751-761.

276. Taggart P, Sutton PM. Cardiac mechano-electric feedback in man: clinical relevance. *Prog Biophys Mol Biol*. 1999;71:139-54.

277. Takahashi M, Shiraishi H, Ishibashi Y, Blade KL, McDermott PJ, Menick DR, Kuppuswamy D, Cooper G. Phenotypic consequences of β 1 -tubulin expression and MAP4 decoration of microtubules in adult cardiocytes. *Am J Physiol Heart C*. 2003;285:H2072-H2083.

278. Takahashi M, Yokoshiki H, Mitsuyama H, Watanabe M, Temma T, Kamada R, Hagiwara H, Takahashi Y, Anzai T. SK channel blockade prevents hypoxia-induced ventricular arrhythmias through inhibition of Ca^{2+}/voltage uncoupling in hypertrophied hearts. *Am. J. Physiol Heart Circ Physiol.* 2021;320,H1456-69.

279. Tan JHC, Liu W, Saint DA. Differential expression of the mechanosensitive potassium channel TREK-1 in epicardial and endocardial myocytes in rat ventricle. *Exp Physiol*. 2004;89:237-242.

280. Tang L, Joung B, Ogawa M, Chen P-S, Lin S-F. Intracellular calcium dynamics, shortened action potential duration, and late-phase 3 early afterdepolarization in Langendorff-perfused rabbit ventricles. *J Cardiovasc Electr*. 2012;23:1364-1371.
281. Tang Q, Ma J, Zhang P, Wan W, Kong L, Wu L. Persistent sodium current and Na^+/H^+ exchange contributes to the augmentation of the reverse Na^+/Ca^{2+} exchange during hypoxia or acute ischaemia in ventricular myocytes. *Pflügers Arch*. 2021;463:513-522.
282. Tereshchenko LG, Soliman EZ, Davis BR, Oparil S. Risk stratification of sudden cardiac death in hypertension. *J Electrocardiol*. 2017;50:798-801.
283. Theroux P, Franklin D, Ross J, Kemper WS. Regional myocardial function during acute coronary artery occlusion and its modification by pharmacologic agents in the dog. *Circ Res*. 1974;35:896-908.
284. Thompson SA, Copeland CR, Reich DH, et al. Mechanical coupling between myofibroblasts and cardiomyocytes slows electric conduction in fibrotic cell monolayers. *Circulation*. 2011;123:2083-93.
285. Tombe PP de. Altered contractile function in heart failure. *Cardiovasc Res*. 1998;37:367-380.
286. Tsikitis M, Galata Z, Mavroidis M, Psarras S, Capetanaki Y. Intermediate filaments in cardiomyopathy. *Biophysical Rev*. 2018;10:1007-1031.
287. Tsutsui H, Ishibashi Y, Takahashi M, Namba T, Tagawa H, Imanaka-Yoshida K, Takeshita A. Chronic colchicine administration attenuates cardiac hypertrophy in spontaneously hypertensive rats. *J Mol Cell Cardiol*. 1999;31:1203-1213.
288. Tsutsui H, Ishihara K, Cooper G. Cytoskeletal role in the contractile dysfunction of hypertrophied myocardium. *Science*. 1993;260:682-687.
289. Vermeulen JT, Tan HL, Rademaker H, Schumacher CA, Loh P, Opthof T, et al. Electrophysiologic and extracellular ionic changes during acute ischaemia in failing and normal rabbit myocardium. *J Mol Cell Cardiol*. 1996;28:123–131.
290. Veteto AB, Peana D, Lambert MD, McDonald KS, Domeier TL. Transient receptor potential vanilloid-4 contributes to stretch-induced hypercontractility and time-dependent dysfunction in the aged heart. *Cardiovasc Res*. 2019;116:1887-1896.

291. Vilceanu D, Stucky CL. TRPA1 Mediates Mechanical Currents in the Plasma Membrane of Mouse Sensory Neurons. *PLoS One*. 2010;5:e12177.
292. Volkers L, Mechioukhi Y, Coste B. Piezo channels: from structure to function. *Pflügers Archiv-European J Physiology*. 2015;467:95-99.
293. Wagoner DR, Lamorgese M. ischaemia potentiates the mechanosensitive modulation of atrial atp-sensitive potassium channels. *Ann Ny Acad Sci*. 1994;723:392-395.
294. Wagoner DR. Mechanosensitive gating of atrial ATP-sensitive potassium channels. *Circ Res*. 1993;72:973-983.
295. Wakayama Y, Miura M, Stuyvers BD, Boyden PA, ter Keurs HE. Spatial nonuniformity of excitation-contraction coupling causes arrhythmogenic Ca^{2+} waves in rat cardiac muscle. *Circ Res*. 2005;96:1266-1273.
296. Wang K, Terrar D, Gavaghan DJ, Mu-U-Min R, Kohl P, Bollensdorff C. Living cardiac tissue slices: an organotypic pseudo two-dimensional model for cardiac biophysics research. *Prog Biophys Mol Biol*. 2014;115:314-327.
297. Wang X, Li F, Campbell SE, Gerdes AM. Chronic pressure overload cardiac hypertrophy and failure in guinea pigs: ii. cytoskeletal remodeling. *J Mol Cell Cardiol*. 1999;31:319-331.
298. Wang XX, Cheng LX, Chen JZ, Zhou LL, Zhu JH, Guo XG, Shang YP. [Dependence of ventricular wall stress-induced refractoriness changes on pacing cycle lengths and its mechanism]. *Sheng Li Xue Bao*. 2003;55:336-338.
299. Wang YY, Chang RB, Waters HN, McKemy DD, Liman ER. The nociceptor ion channel TRPA1 is potentiated and inactivated by permeating calcium ions. *J Biological Chem*. 2008;283:32691-32703.
300. Wang Z, Taylor LK, Denney WD, et al. Initiation of ventricular extrasystoles by myocardial stretch in chronically dilated and failing canine left ventricle. *Circulation*. 1994;90:2022-31.
301. Wang Z, Xu Y, Wang M, Ye J, Liu J, Jiang H, et al. TRPA1 inhibition ameliorates pressure overload-induced cardiac hypertrophy and fibrosis in mice. *EBioMedicine*. 2018;36:54-62.

302. Wang Z, Ye D, Ye J, Wang M, Liu J, Jiang H, et al. The TRPA1 channel in the cardiovascular system: promising features and challenges. *Front Pharmacol*. 2019;10:1253.
303. Ward CW, Prosser BL, Lederer WJ. Mechanical stretch-induced activation of ROS/RNS signaling in striated muscle. *Antioxid Redox Signal*. 2014;20:929-936.
304. Ward ML, Williams IA, Chu Y, Cooper PJ, Ju YK, Allen DG. Stretch-activated channels in the heart: contributions to length-dependence and to cardiomyopathy. *Prog Biophys Mol Biol*. 2008;97:232-249.
305. Watanabe H, Murakami M, Ohba T, Takahashi Y, Ito H. TRP channel and cardiovascular disease. *Pharmacol Therapeut*. 2008;118:337-351.
306. Watanabe H, Murakami M, Ohba T, Ono K, Ito H. The Pathological Role of Transient Receptor Potential Channels in Heart Disease. *Circ J*. 2009;73:419-427.
307. Watkins SC, Samuel JL, Marotte F, Bertier-Savalle B, Rappaport L. Microtubules and desmin filaments during onset of heart hypertrophy in rat: a double immunoelectron microscope study. *Circ Res*. 1987;60:327-336.
308. Waxman MB, Wald RW, Finley JP, Bonet JF, Downar E, Sharma AD. Valsalva termination of ventricular tachycardia. *Circulation*. 1980;62:843-851.
309. Webster DR. Microtubules in cardiac toxicity and disease. *Cardiovasc Toxicol*. 2002;2:75-89.
310. Wei H, Zhang ZF, Huang HX, Niu WZ. [Arrhythmia triggered by stretching rabbit left ventricles and the block effect of streptomysin]. *Chin J Appl Physiology*. 2008;24:286-289.
311. Wei JY, Greene HL, Weisfeldt ML. Cough-facilitated conversion of ventricular tachycardia. *Am J Cardiol*. 1980;45:174-176.
312. Weiss J, Shine KI. Extracellular K^+ accumulation during myocardial ischaemia in isolated rabbit heart. *Am J Physiol Heart C*. 1982;242:H619-H628.
313. Werdich AA, Brzezinski A, Jeyaraj D, Khaled Sabeh M, Ficker E, Wan X, McDermott BM Jr, Macrae CA, Rosenbaum DS. The zebrafish as a novel animal model to study the molecular mechanisms of mechano-electrical feedback in the heart. *Prog Biophys Mol Biol*. 2012;110:154-165.

314. Whelton PK, Carey RM, Aronow WS, Casey DE, Collins KJ, Himmelfarb CD, DePalma SM, Gidding S, Jamerson KA, Jones DW, et al. 2017 ACC/AHA/AAPA/ABC/ACPM/AGS/APhA/ASH/ASPC/NMA/PCNA guideline for the prevention, detection, evaluation, and management of high blood pressure in adults: a report of the American College of Cardiology/American Heart Association Task Force on Clinical Practice Guidelines. *Hypertension*. 2018;71:e13-e115.
315. White E. Mechanosensitive channels: therapeutic targets in the myocardium? *Curr Pharm Des*. 2006;12,3645-63.
316. White E, Guennec JL, Nigretto J, Gannier F, Argibay J, Garnier D. The effects of increasing cell length on auxotonic contractions; membrane potential and intracellular calcium transients in single guinea-pig ventricular myocytes. *Exp Physiol*. 1993;78:65-78.
317. Wilde AA, Escande D, Schumacher CA, Thuringer D, Mestre M, Fiolet JW, et al. Potassium accumulation in the globally ischaemic mammalian heart. A role for the ATP-sensitive potassium channel. *Circ Res*. 1990;67:835-843.
318. Wu TJ, Lin S-F, Hsieh Y-C, Lin T-C, Lin J-C, Ting C-T. Pretreatment of BAPTA-AM suppresses the genesis of repetitive endocardial focal discharges and pacing-induced ventricular arrhythmia during global ischaemia. *J Cardiovasc Electrophysiol*. 2011;22:1154-1162.
319. Xiao H, Verdier-Pinard P, Fernandez-Fuentes N, Burd B, Angeletti R, Fiser A, et al. Insights into the mechanism of microtubule stabilization by Taxol. *Proc National Acad Sci*. 2006;103:10166-10173.
320. Xing D, Martins JB. Triggered activity due to delayed afterdepolarizations in sites of focal origin of ischaemic ventricular tachycardia. *Am J Physiol Heart Circ Physiol*. 2004;287:H2078-H2084.
321. Xu Z, Schaedel L, Portran D, Aguilar A, Gaillard J, Marinkovich MP, et al. Microtubules acquire resistance from mechanical breakage through intralumenal acetylation. *Science*. 2017;356:328-332.
322. Yamamoto S, Shimizu S. Significance of TRP channels in oxidative stress. *Eur J Pharmacol*. 2016;793:109-111.

323. Yamamoto S, Tsutsui H, Takahashi M, Ishibashi Y, Tagawa H, Imanaka-Yoshida K, et al. Role of microtubules in the viscoelastic properties of isolated cardiac muscle. *J Mol Cell Cardiol*. 1998;30:1841-1853.
324. Yiu KH, Tse HF. Hypertension and cardiac arrhythmias: a review of the epidemiology, pathophysiology and clinical implications. *J Hum Hypertens*. 2008;22:380-388.
325. Zabel M, Koller BS, Sachs F, Franz MR. Stretch-induced voltage changes in the isolated beating heart: importance of the timing of stretch and implications for stretch-activated ion channels. *Cardiovasc Res*. 1996;32:120-130.
326. Zabel M, Portnoy S, Franz MR. Effect of sustained load on dispersion of ventricular repolarization and conduction time in the isolated intact rabbit heart. *J Cardiovasc Electrophysiol*. 1996;7:9-16.
327. Zhang H, Gomez AM, Wang X, Yan Y, Zheng M, Cheng H. ROS regulation of microdomain Ca^{2+} signalling at the dyads. *Cardiovasc Res*. 2013;98:248-258.
328. Zheng Q, Jockusch S, Zhou Z, Blanchard SC. The contribution of reactive oxygen species to the photobleaching of organic fluorophores. *Photochem Photobiol*. 2014;90:448-454.
329. Zile MR, Koide M, Sato H, Ishiguro Y, Conrad CH, Buckley JM, Morgan JP, Cooper G. Role of microtubules in the contractile dysfunction of hypertrophied myocardium. *J Am Coll Cardiol*. 1999;33:250-260.
330. Zile MR, Richardson K, Cowles MK, Buckley JM, Koide M, Cowles BA, et al. Constitutive properties of adult mammalian cardiac muscle cells. *Circulation*. 1998;98:567-579.
331. Zipes DP, Wellens HJ. Sudden cardiac death. *Circulation*. 1998;98:2334-2351.
332. Zurborg S, Yurgionas B, Jira JA, Caspani O, Heppenstall PA. Direct activation of the ion channel TRPA1 by Ca^{2+}. *Nat Neurosci*. 2007;10:277-279.

APPENDIX 1: COPYRIGHT AGREEEMENT STATEMENTS

The manuscript comprising Chapter 2 entitled: “Ischaemia enhances the acute stretch-induced increase in calcium spark rate in ventricular myocytes” (Cameron BA, Kaihara K, Kai H, Iribe G, Quinn TA. Ischaemia enhances the acute stretch-induced increase in calcium spark rate in ventricular myocytes. *Front Physiol*. 2020; 11:289) is an open-access article distributed under the terms of the Creative Commons Attribution Licence (CC BY), which states: “the use, distribution, or reproduction in other forums is permitted, provided the original author(s) and the copyright owner(s) are credited and that the original publication in this journal is cited, in accordance with accepted academic practice.” As the first author of the manuscript, I own the copyright permission for use of the article in this dissertation.

Figure 1.1: This image was used with permission from a previous publication (Quinn TA, Kohl P. Cardiac Mechano-Electric Coupling: Acute Effects of Mechanical Stimulation on Heart Rate and Rhythm. *Physiol Rev*. 2021;101:37–92.). Use of this image is permitted under the Creative Commons Attribution CC BY 4.0 @ the American Physiological Society, as long as the following conditions are met: you must give appropriate credit, provide a link to the license, and indicate if any changes were made.” The author has been credited and a link is provided. No alterations were made to the Figure. https://creativecommons.org/licenses/by/4.0/deed.en_US

WOLTERS KLUWER HEALTH, INC. LICENSE
TERMS AND CONDITIONS

Apr 30, 2021

This Agreement between Miss. Breanne Cameron ("You") and Wolters Kluwer Health, Inc. ("Wolters Kluwer Health, Inc.") consists of your license details and the terms and conditions provided by Wolters Kluwer Health, Inc. and Copyright Clearance Center.

License Number	5058880295029
License date	Apr 30, 2021
Licensed Content Publisher	Wolters Kluwer Health, Inc.
Licensed Content Publication	Circulation Research
Licensed Content Title	Cardiac Mechano-Gated Ion Channels and Arrhythmias

Print This Page

Figure 1.2: This Figure was previously published and is used with permission from the Wolters Kluwer Health Inc. 1. Peyronnet R, Nerbonne JM, Kohl P. Cardiac Mechano-Gated Ion Channels and Arrhythmias. *Circ Res*. 2016;118:311–329.

APPENDIX 2: CHAPTER 3 SUPPLEMENTAL FIGURES

Supplemental Figure 3.1 | Mechanical characteristics of cell stretch. a, Percent sarcomere stretch, **b,** stretched sarcomere length, and **c,** maximal applied stress during rapid, transient diastolic stretch of rabbit isolated ventricular myocytes exposed to normal Tyrode (NT, grey) or pinacidil (PIN, white) with increasing levels of piezo-electric translator (PZT) displacement (20, 30, and 40 μm). Differences assessed by one-way ANOVA, with Tukey *post-hoc* tests for **a** and **b**, and by Kruskal-Wallis test for **c**. **p*< 0.05 within groups. *N* = rabbits, *n* = cells.

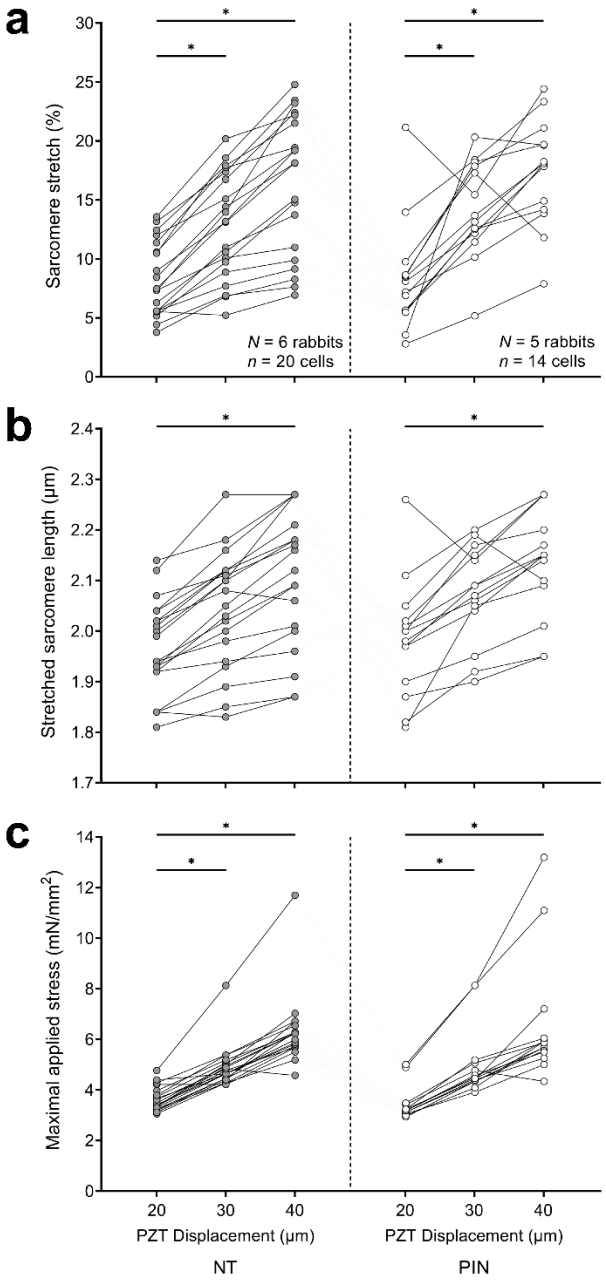

Supplemental Figure 3.2 | Effect of pharmacological interventions on mechano-arrhythmogenicity in control conditions. a, Incidence of premature contractions (blue) and other arrhythmic activity (shades of red) with rapid, transient stretch of rabbit isolated ventricular myocytes during diastole or the vulnerable period (VP) exposed to: normal Tyrode (NT); NT + streptomycin (STP); NT + HC-030031; NT + BAPTA; or NT + dantrolene (DNT). Ca^{2+}, calcium; MSC, mechano-sensitive channels. Differences assessed using chi-square contingency tables and Fisher's exact test. *$p < 0.05$. N = rabbits, n = cells, m = stretches.

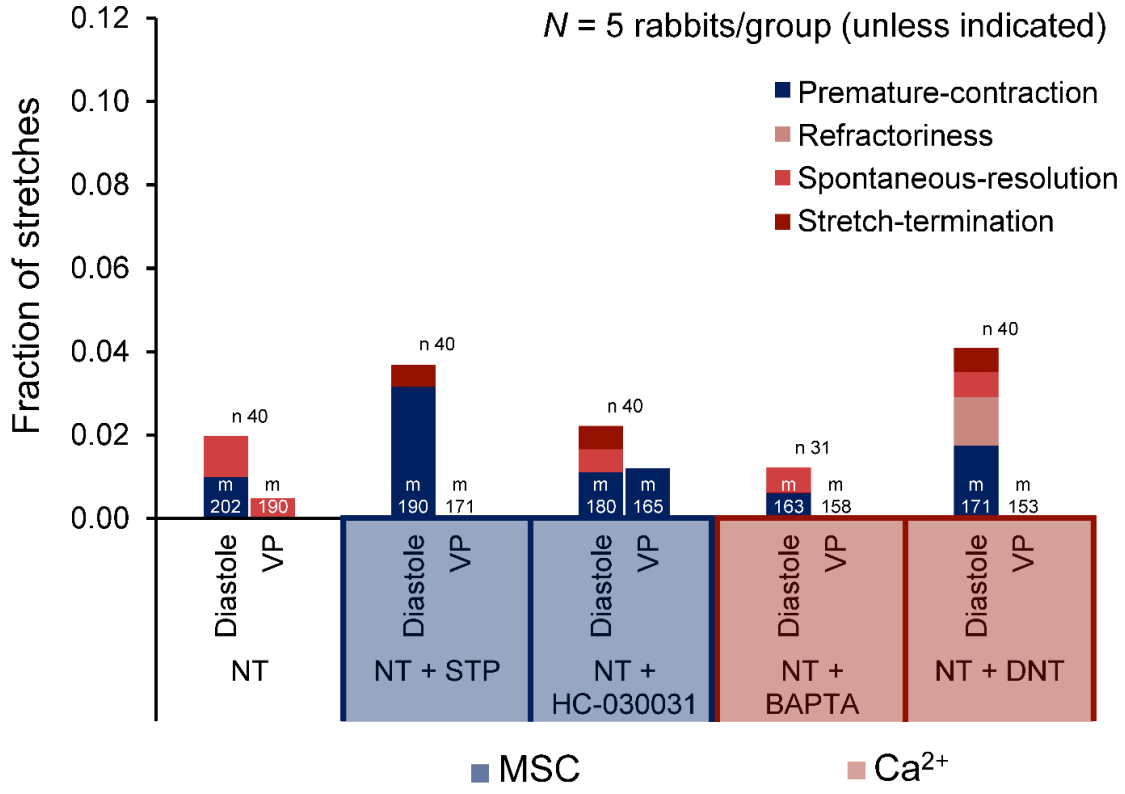

Supplemental Figure 3.3 | Effect of stretch magnitude on the incidence of mechano-arrhythmogenicity. a, Incidence of premature contractions (blue) and other arrhythmic activity (shades of red) with rapid, transient stretch during diastole (left) and the vulnerable period (VP, right) with increasing levels of piezo-electric translator (PZT) displacement (20, 30, and 40 μm) in rabbit isolated ventricular myocytes exposed to normal Tyrode (NT) and **b,** pinacidil (PIN). Differences assessed using chi-square contingency tables and Fisher's exact test. *$p < 0.05$. N = rabbits, n = cells, m = stretches.

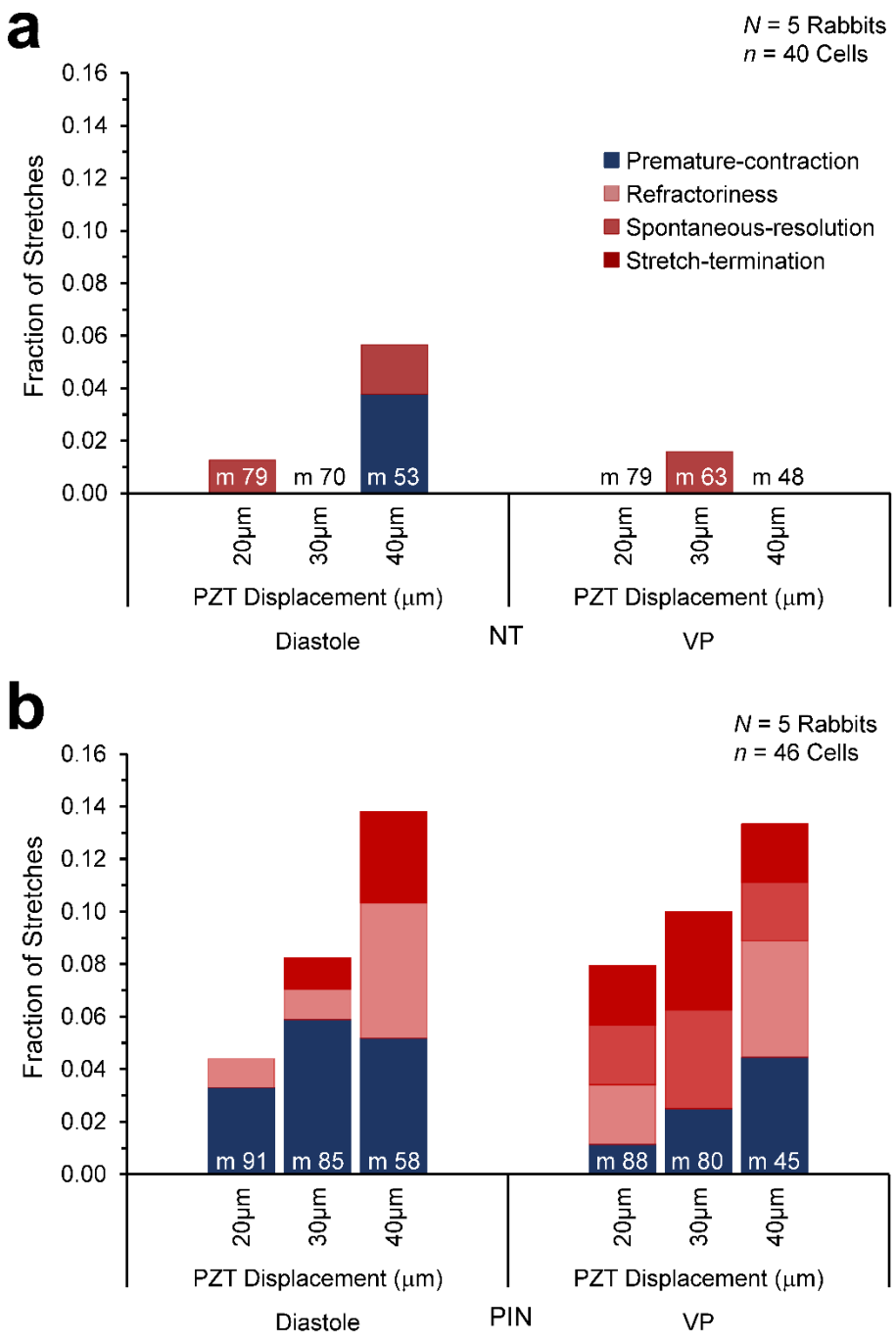

Supplemental Figure 3.4 | Effect of stretch on contractile function. a, Diastolic sarcomere length and **b,** maximal rate and **c,** percent of sarcomere shortening during contraction of rabbit isolated ventricular myocytes exposed to normal Tyrode (NT, grey) or pinacidil (PIN, white) before (pre-stretch) and after three successive diastolic stretches generated with an increasing level of piezo-electric translator (PZT) displacement (20, 30, and 40 μm). Differences assessed by one-way ANOVA, with Tukey *post-hoc* tests. *p<0.05. N = rabbits, n = cells.

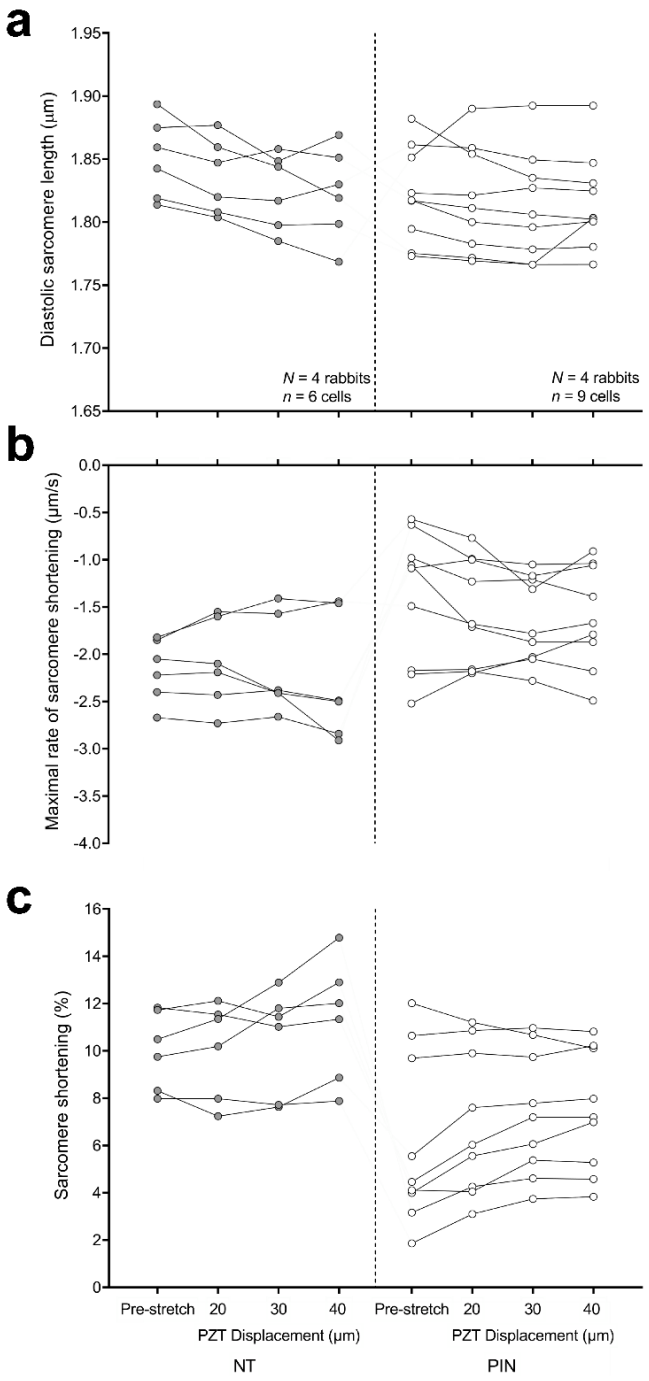

Supplemental Figure 3.5 | Contractile function after sustained arrhythmic activity. a, Diastolic sarcomere length and **b,** maximal rate and **c,** percentage of sarcomere shortening during contraction of rabbit isolated ventricular myocytes exposed to pinacidil before (green) and after termination of stretch-induced sustained arrhythmic activity (red). Differences assessed using two-tailed, paired Student's t-test. *p< 0.05. N = rabbits, n = cells.

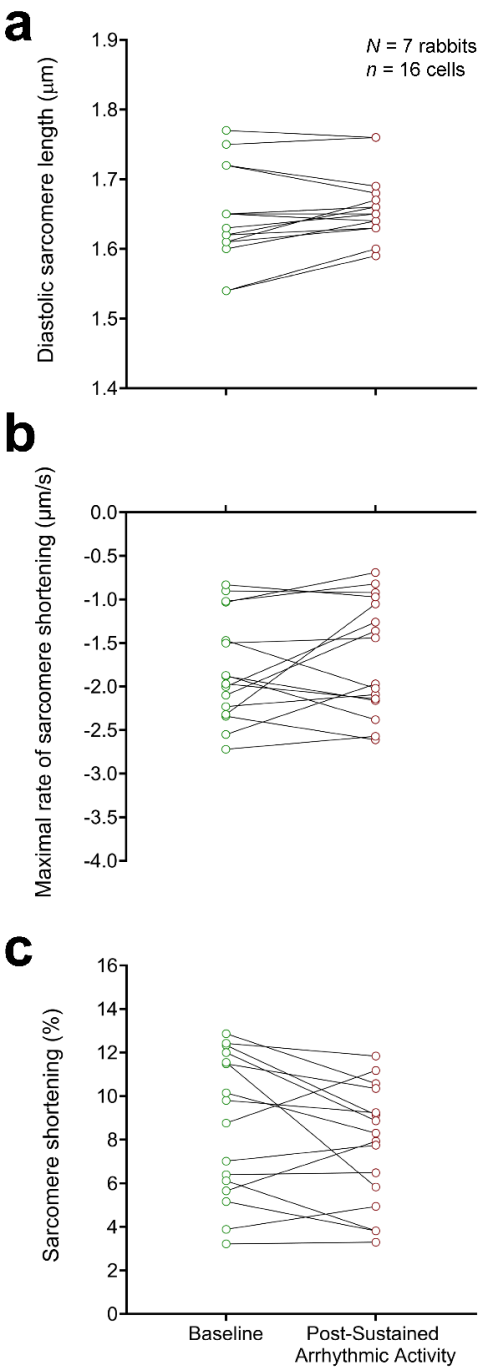

Supplemental Figure 3.6 | Expression of TRPA1 channels in rabbit left ventricular myocytes. a, Western blot of TRPA1 and myosin heavy chain (MF20) protein expression in rabbit left ventricular free wall tissue. **b**, Representative recording of channel activation in response to AITC exposure in a cell-attached patch at +40 mV. **Inset**, Detail of channel activation with visible single channel events. **c**, Quantification of AITC-induced current, and current in time-matched controls. Differences assessed with the non-parametric Mann-Whitney test. *$p < 0.05$.

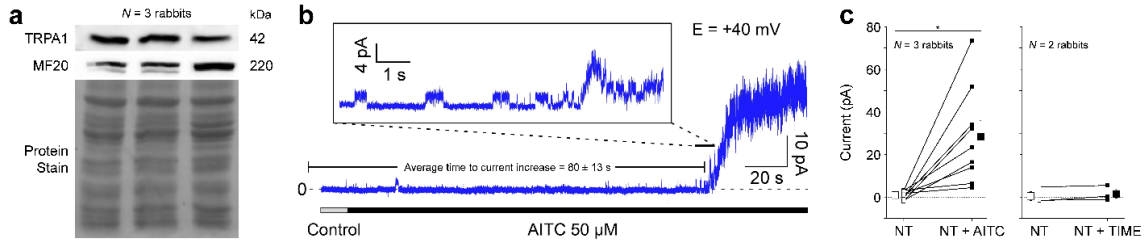

Supplemental Figure 3.7 | Effect of pharmacological interventions on contractile function in control conditions. a, Diastolic sarcomere length and **b**, maximal rate and **c**, percent sarcomere shortening during contraction of rabbit isolated ventricular myocytes exposed to: normal Tyrode (NT); NT + streptomycin (STP); NT + HC-030031; NT + BAPTA; or NT + dantrolene (DNT). Differences assessed by one-way ANOVA, with Tukey *post-hoc* tests for **a** and **b,** and by Kruskal-Wallis test for **c**. **p*< 0.05. Error bars represent standard error of the mean. *N* = rabbits, *n* = cells, *m* = stretches.

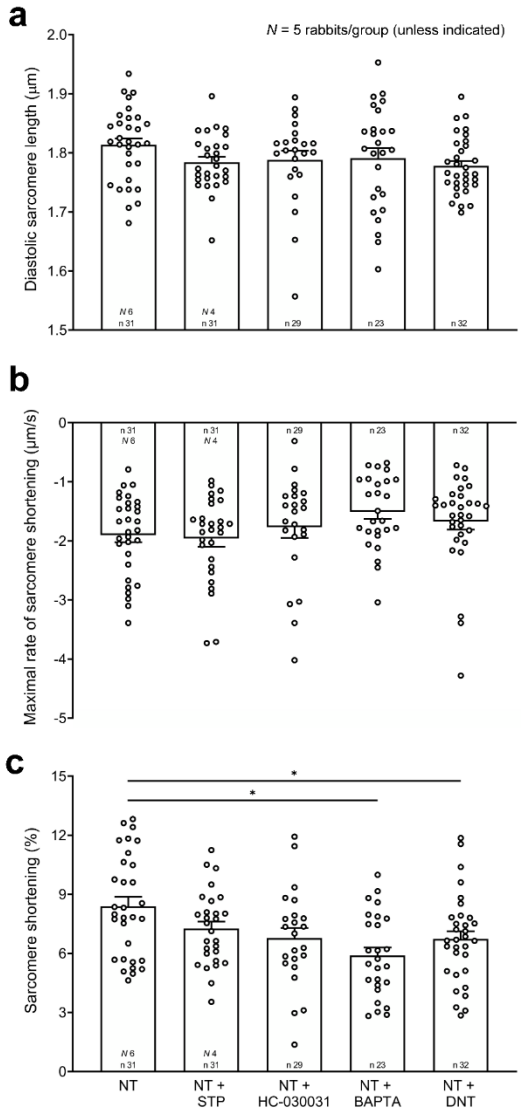

Supplemental Figure 3.8 | Effect of paclitaxel on microtubule density. Confocal immunofluorescence images of stained microtubules in **a,** control and **b,** after 90 min of paclitaxel exposure. **c,** Microtubule assessed as the microtubule positive fraction of the total cell area.

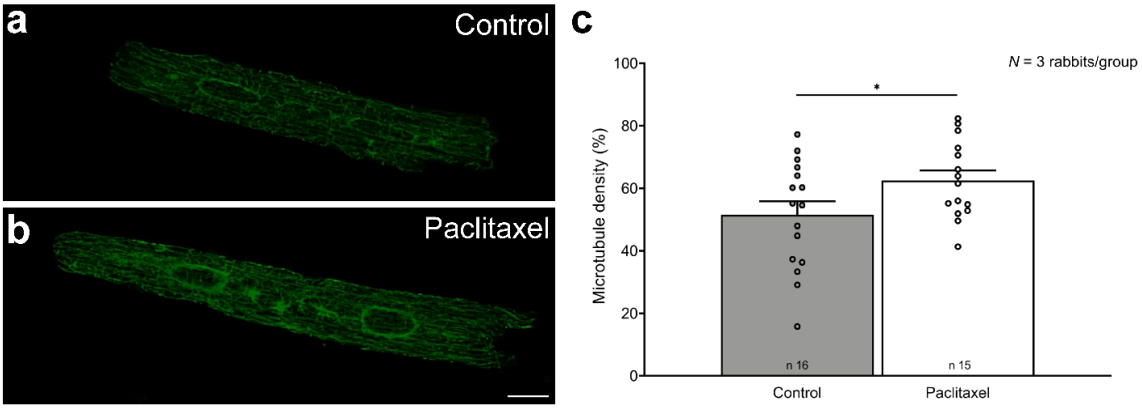

Supplemental Figure 3.9 | Effect of pinacidil on cellular mechanics. a, Stiffness (represented by the slope of the end-diastolic stress-length relationship, EDSLR) and **b** elastance (represented by the slope of the end-systolic stress-length relationship, ESSLR) of rabbit isolated ventricular myocytes exposed to normal Tyrode (NT, grey) or pinacidil (PIN, white). Differences assessed using two-tailed, unpaired Student's t-test. *p< 0.05. Error bars represent standard error of the mean. N = rabbits, n = cells.

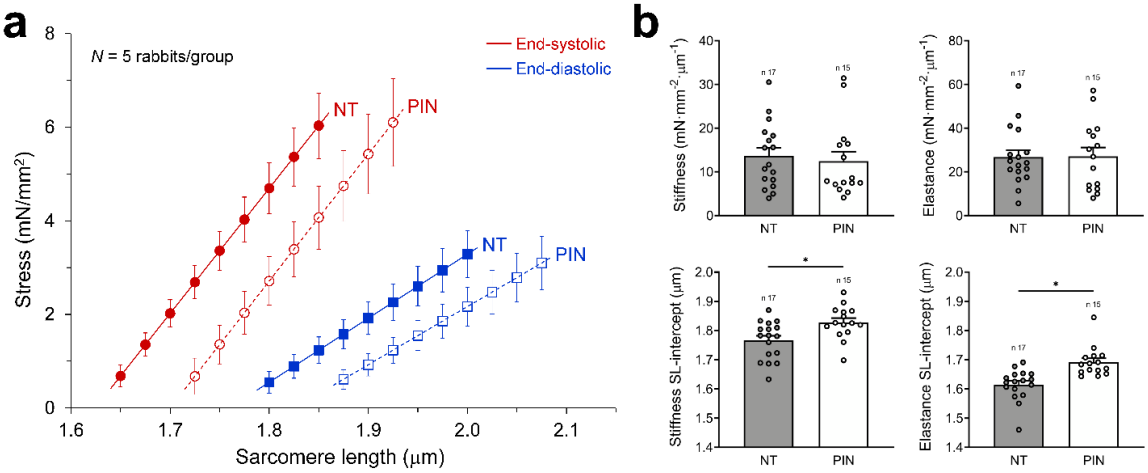

Supplemental Figure 3.10 | Mechanical characteristics of cell stretch with differing electrophysiological outcomes. a, Maximal applied stress, **b,** percent sarcomere stretch, and **c,** maximal sarcomere length for two consecutive rapid, transient diastolic stretches of PIN-treated rabbit isolated ventricular myocytes, for which one caused an arrhythmia (ARR, red) and the other did not (NSR, green). Differences assessed using the Wilcoxon matched-pairs test. *p< 0.05. N = rabbits, n = cells.

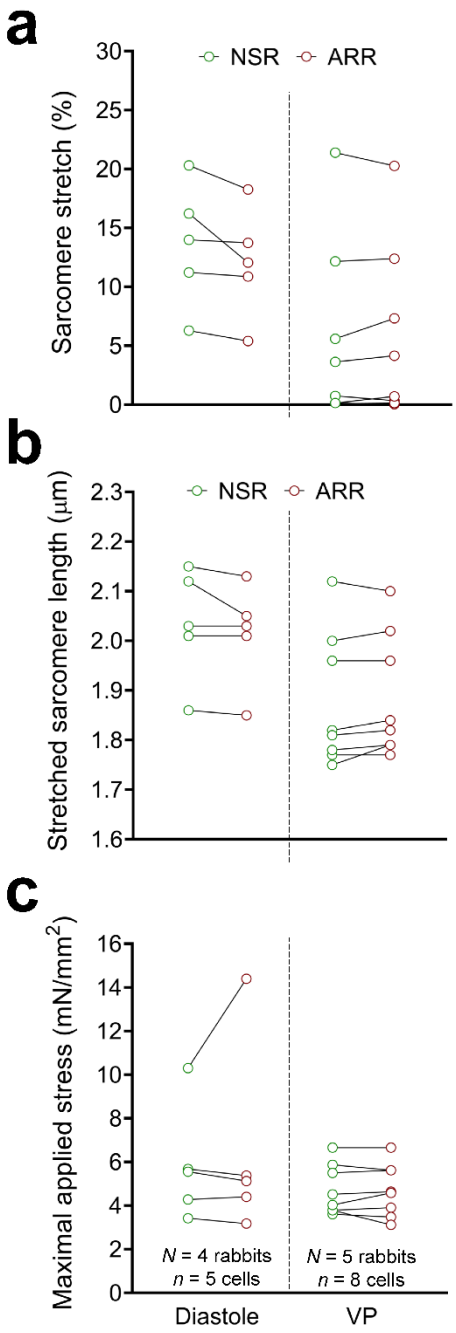

APPENDIX 3: CHAPTER 4 SUPPLEMENTAL FIGURES

Supplemental Figure 4.1 | Effect of normal Tyrode, or simulated ischaemia alone or following pre-incubation with glibenclamide on cellular voltage-Ca^{2+} dynamics. a, Average APD (blue) and CaTD (red) at 20, 30, 50, and 80% repolarisation after 5 min in normal Tyrode (NT) measured using a fluorescence imaging technique with voltage (di-4-ANBDQPQ, 20 μM for 14 min) and Ca^{2+} (Fluo-5F-AM, 5 μM for 20 min) fluorescent indicators and a single camera-image splitter system. **b,** Average APD (blue) and CaTD (red) at 20, 30, 50, and 80 % repolarisation after 5 min in simulated ischaemia (SI). **c,** Average APD (blue) and CaTD (red) at 20, 30, 50, and 80 % repolarisation after 5 min in SI following pre-incubation with glibenclamide (20 μM for 15 min, SI + GLIB). Differences assessed by one-way ANOVA, with Tukey *post-hoc* tests. **p*<0.05 between groups, #*p*<0.05 compared to NT group, ***p*<0.05 compared to SI group. Error bars represent standard error of the mean. *N* = rabbits, *n* = cells.

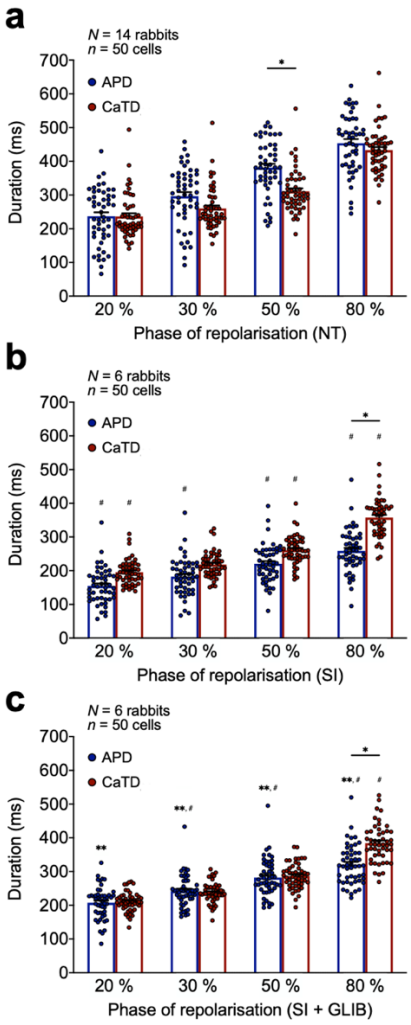

Supplemental Figure 4.2 | Effect of complex arrhythmias on contractile function. a, Diastolic sarcomere length **b,** percentage sarcomere shortening, and **c,** maximal rate of sarcomere shortening before and after resolution of a complex arrhythmia in ventricular myocytes exposed to 5 min of simulated ischaemia. Differences assessed by paired Student's t-test. *N* = rabbits, *n* = cells.

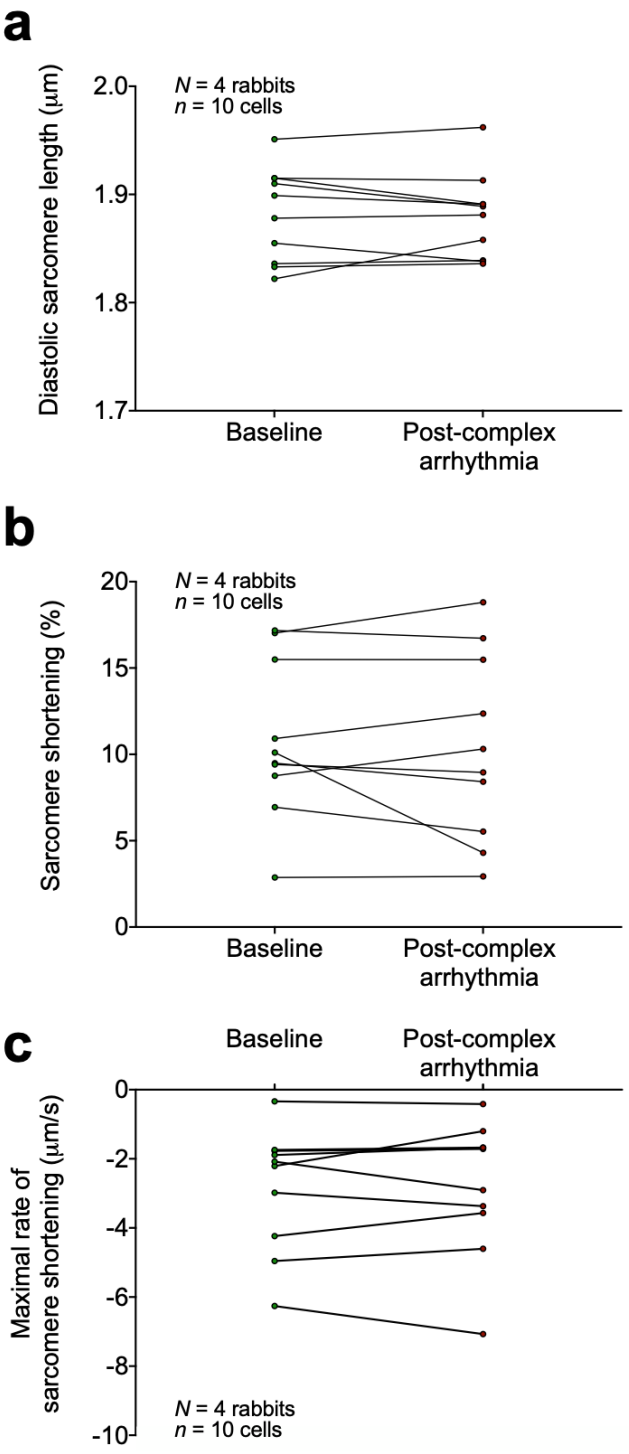

Supplemental Figure 4.3 | Mechanical parameters of cell stretch in ischaemic cells. a, Percentage sarcomere stretch, **b,** maximal stretched sarcomere length **c,** maximal applied force during-, and **d,** diastolic sarcomere length following rapid, transient stretch of rabbit isolated ventricular myocytes exposed to 5 min of simulated ischaemia with increasing levels of piezo-electric translator movement (20, 30, and 40 µm). Differences assessed by one-way ANOVA with Tukey *post-hoc* tests. **p*< 0.05 within groups. *N* = rabbits, *n* = cells.

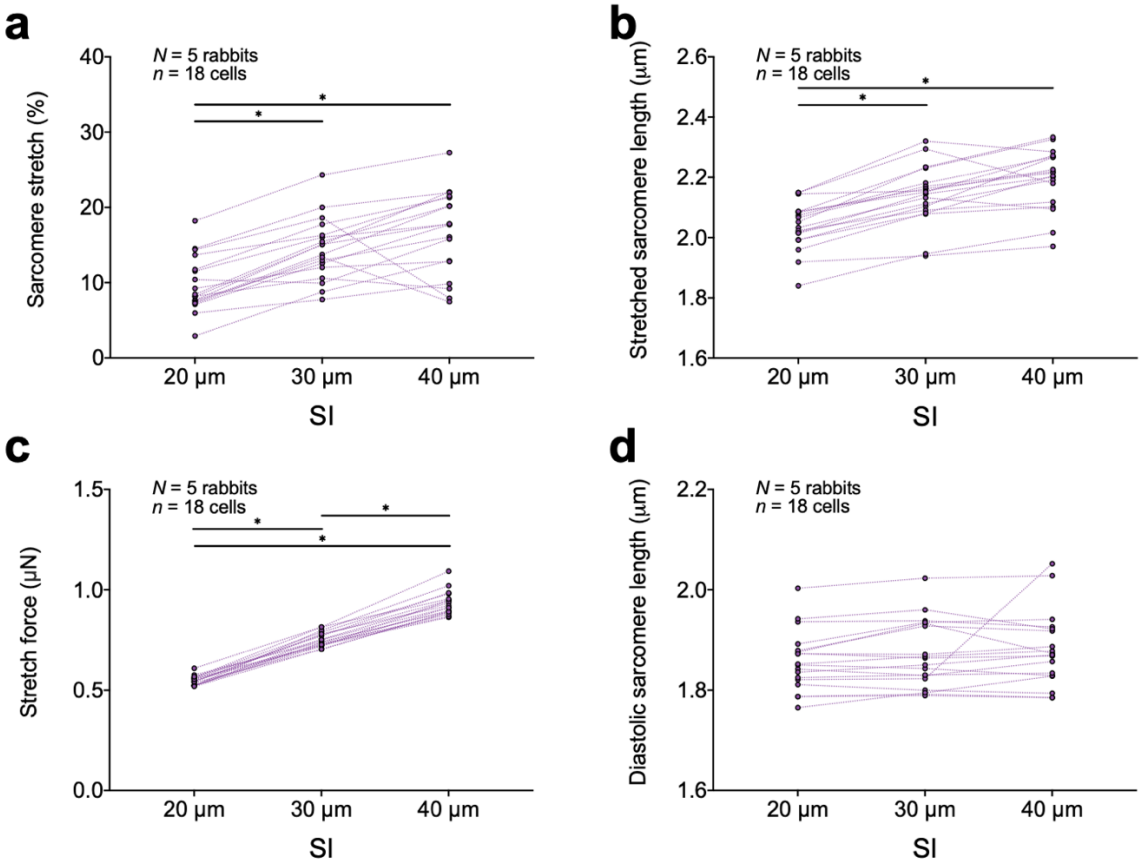

Supplemental Figure 4.4 | Effect of stretch magnitude on the incidence of mechano-arrhythmogenicity. a, Incidence of premature ventricular contractions (PVC, blue) and complex arrhythmias (red) with rapid, transient stretch during diastole (left) and the vulnerable period (VP, right) with increasing levels of piezo-electric translator movement (20, 30, and 40 µm) in rabbit isolated ventricular myocytes exposed to 5 min of normal Tyrode (NT). **b,** Incidence of arrhythmias in cells exposed to 5 min of simulated ischaemia. Differences assessed using chi-square contingency tables and Fisher's exact test. *N* = rabbits, *n* = cells, *m* = stretches.

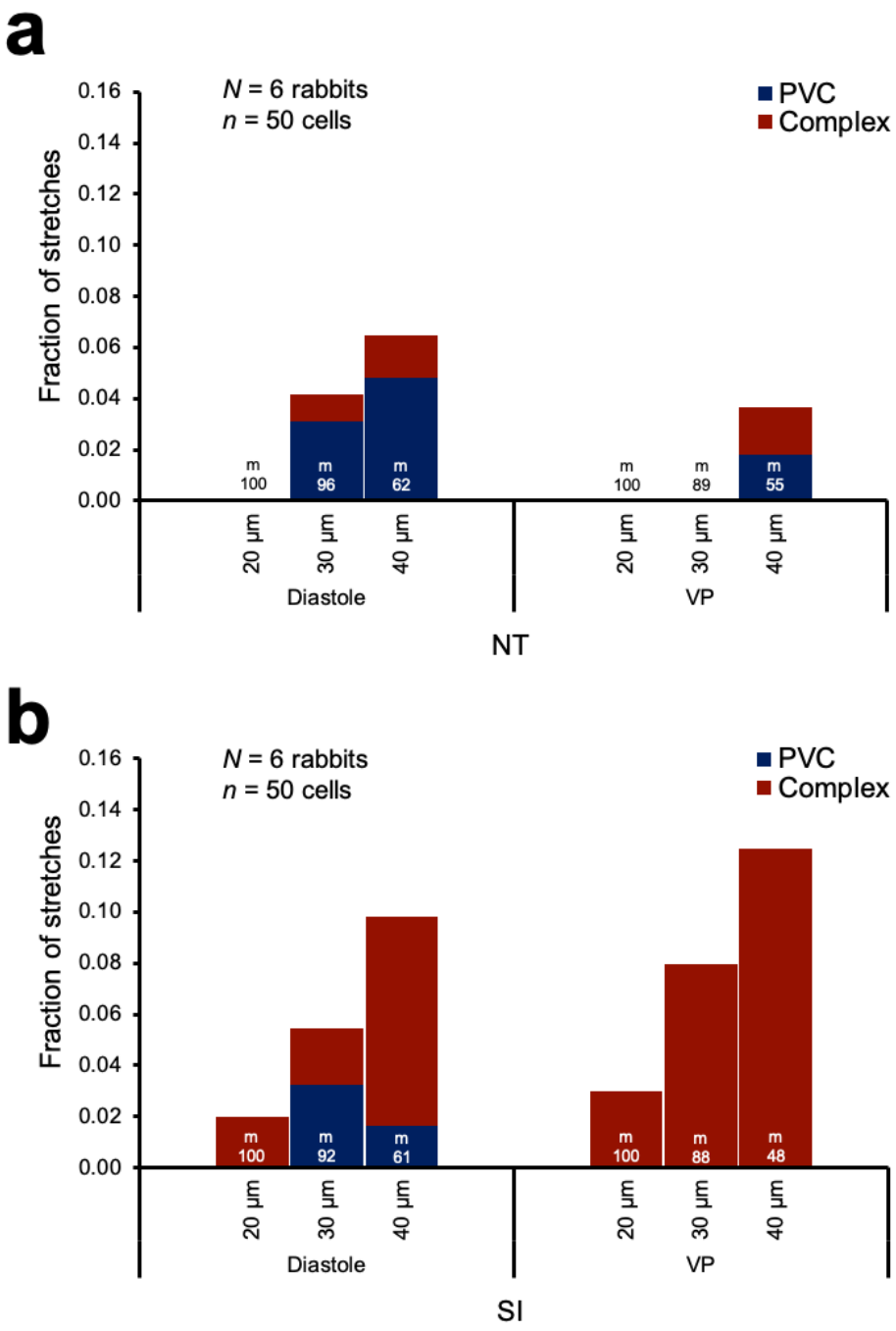

Supplemental Figure 4.5 | Role of stretch and/or release during the VP in ischaemic mechano-arrhythmogenicity. a, Fraction of the stretch pulse segment (only stretch, only release, or both stretch and release) that occurred within (IN) or outside (OUT) the VP in ischaemic cells, revealed by fluorescence imaging (di-4-ANBDQPQ, 20 μM for 14 min; and Fluo-5F-AM, 5 μM for 20 min) combined with timed stretch. **b**, Of the stretch pulse segments revealed to be within the VP, the fractions that were (i) stretch only, (ii) release only, or (iii) both stretch and release. Associated arrhythmias shown in red. **c**, Fraction of resultant arrhythmias during the VP associated with (i) stretch only, (ii) release only, or (iii) stretch and release. *m* = stretches, *c* = complex arrhythmias.

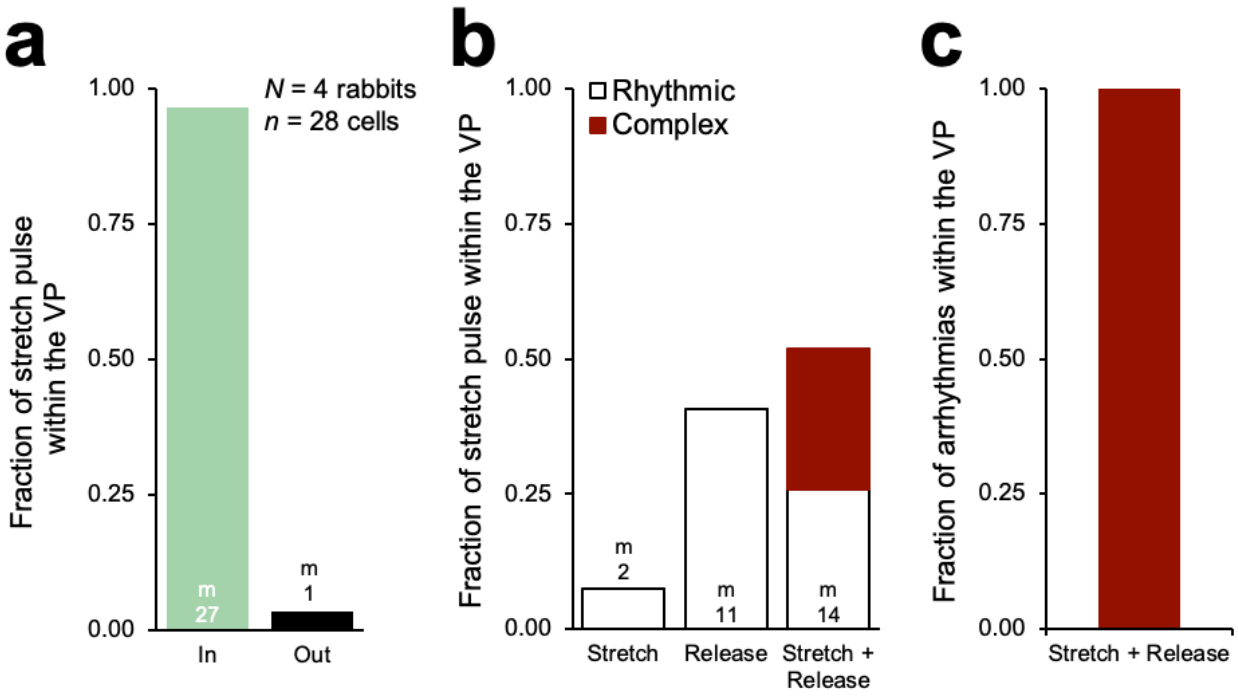

APPENDIX 4: CHAPTER 5 SUPPLEMENTAL FIGURES

Supplemental Figure 5.1 | Effect of stretch magnitude on sarcomere dynamics in control and paclitaxel-treated cells. a, Diastolic sarcomere length, **b,** percent sarcomere shortening **c,** maximal rate of sarcomere shortening, and **d,** maximum rate of sarcomere relaxation following increasing magnitudes of transient stretch (20, 30, 40 μm piezo-electric translator displacement) for rabbit isolated ventricular myocytes exposed to normal Tyrode (NT) alone, or incubated with paclitaxel (TAX, 10 μM for 90 min) in NT. Differences within a treatment (NT or TAX) assessed by paired one-way ANOVA with the Geisser-Greenhouse correction (for normally distributed data), or the Friedman test (for non-normally distributed data). *N* = rabbits, *n* = cells.

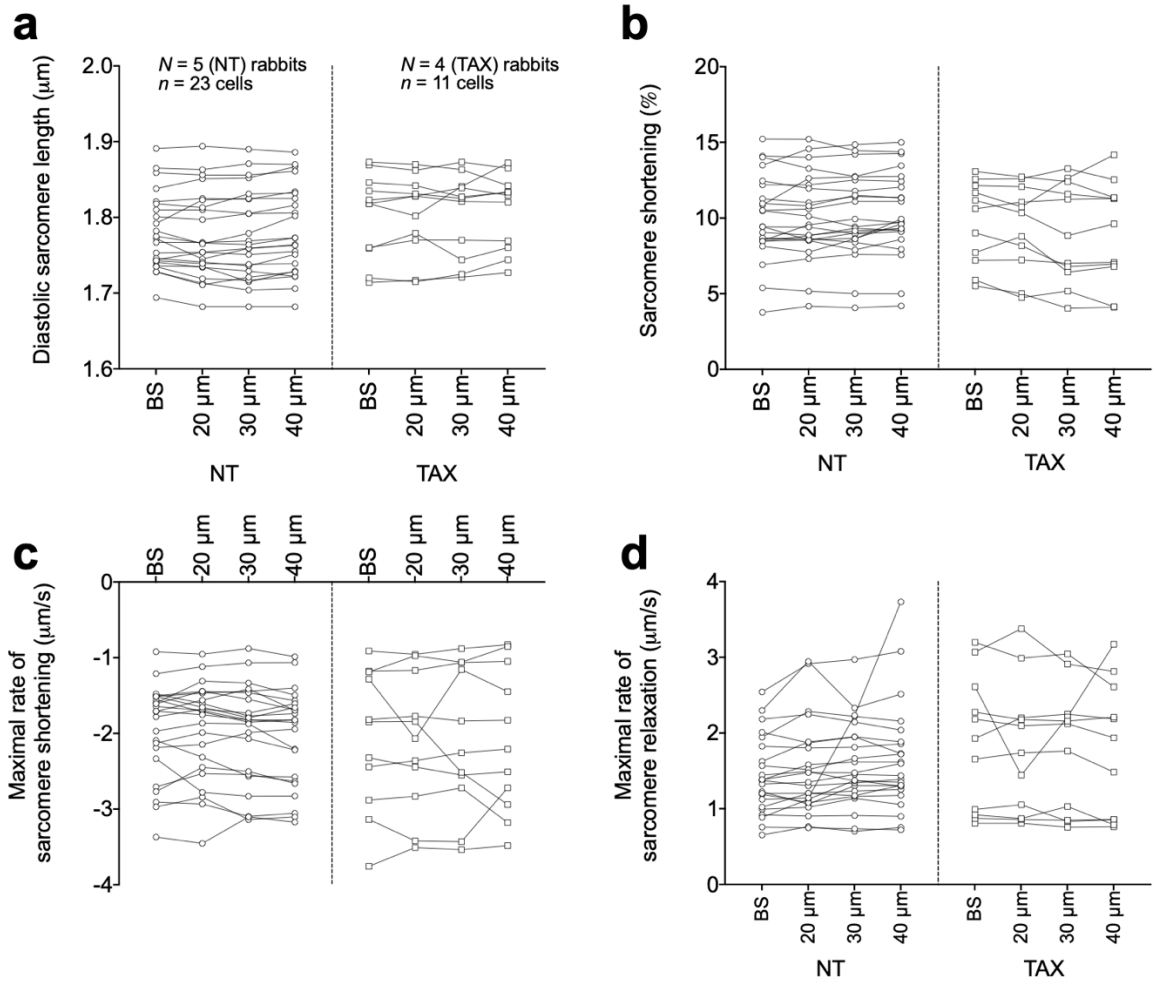

Supplemental Figure 5.2 | Mechanical parameters of stretch in control or paclitaxel-treated cells. a, Sarcomere stretch, **b,** stretched sarcomere length **c,** stretch force during-, and **d,** diastolic sarcomere length following rapid, transient stretch of rabbit isolated ventricular myocytes exposed normal Tyrode (NT) alone, or incubated with paclitaxel (TAX, 10 μM for 90 min) in NT, with increasing levels of piezo-electric translator movement (20, 30, and 40 μm). Differences within a treatment (NT or TAX) assessed by paired one-way ANOVA with the Geisser-Greenhouse correction. Differences between groups assessed by the unpaired Student's t-test (for normally distributed data), or Mann-Whitney test (for non-normally distributed data). *N* = rabbits, *n* = cells. **p*< 0.05 compared to NT, ***p*< 0.05 within treatment. *N* = rabbits, *n* = cells.

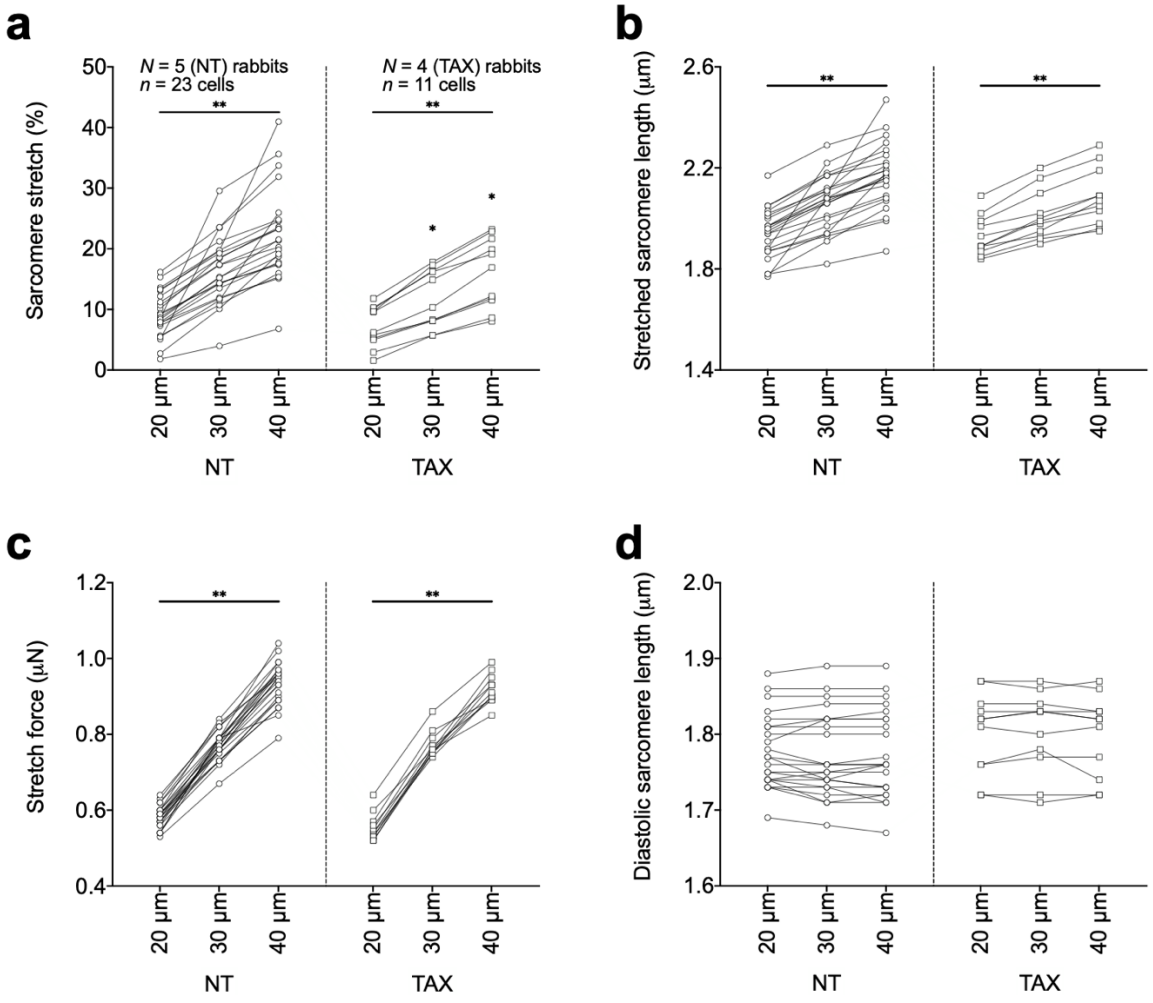

Supplemental Figure 5.3 | Effect of two consecutive stretches on the mechanical parameters of stretch. Percent sarcomere stretch in **a,** control (NT) and **b,** paclitaxel-treated (TAX, 10 μM for 90 min) cells with two consecutive stretches (10 s apart) at increasing levels of piezo-electric translator movement (20, 30, and 40 μm). Differences within groups assessed by the paired Student's t-test, differences between groups assessed with the unpaired Student's t-test. *$p< 0.05$ compared to NT, **$p< 0.05$ within group. N = rabbits, n = cells.

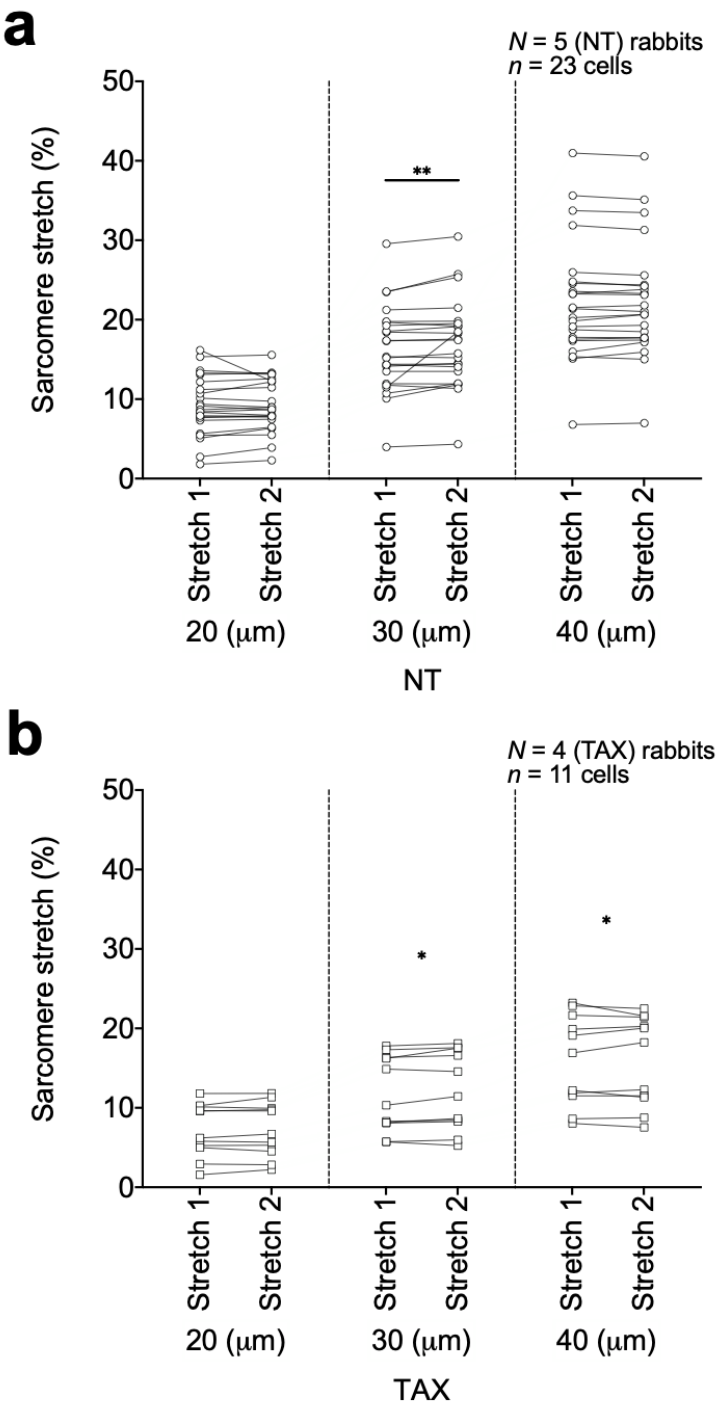

Supplemental Figure 5.4 | Effect of microtubule polymerisation and post-translational modifications on the mechano-arrhythmogenic threshold. Incidence of premature excitation (PVC, blue) and complex arrhythmias (red) with transient stretch in diastole at increasing levels of piezo-electric translator movement (20, 30, and 40 μm) in rabbit isolated ventricular myocytes exposed to paclitaxel alone (TAX, 10 μM for 90 min) or co-loaded with colchicine (COL, 10 μM for 90 min) or parthenolide (PTL, 10 μM for 90 min), or with tubacin alone (TUB, 10 μM for 2 hours). The mechano-arrhythmogenic threshold (minimum stretch magnitude to elicit premature excitation) is shown in orange. Differences assessed using chi-square contingency tables and Fisher's exact test: line = $p<0.05$ within a treatment, *$p<0.05$ compared to control. N = rabbits, n = cells, m = stretches.

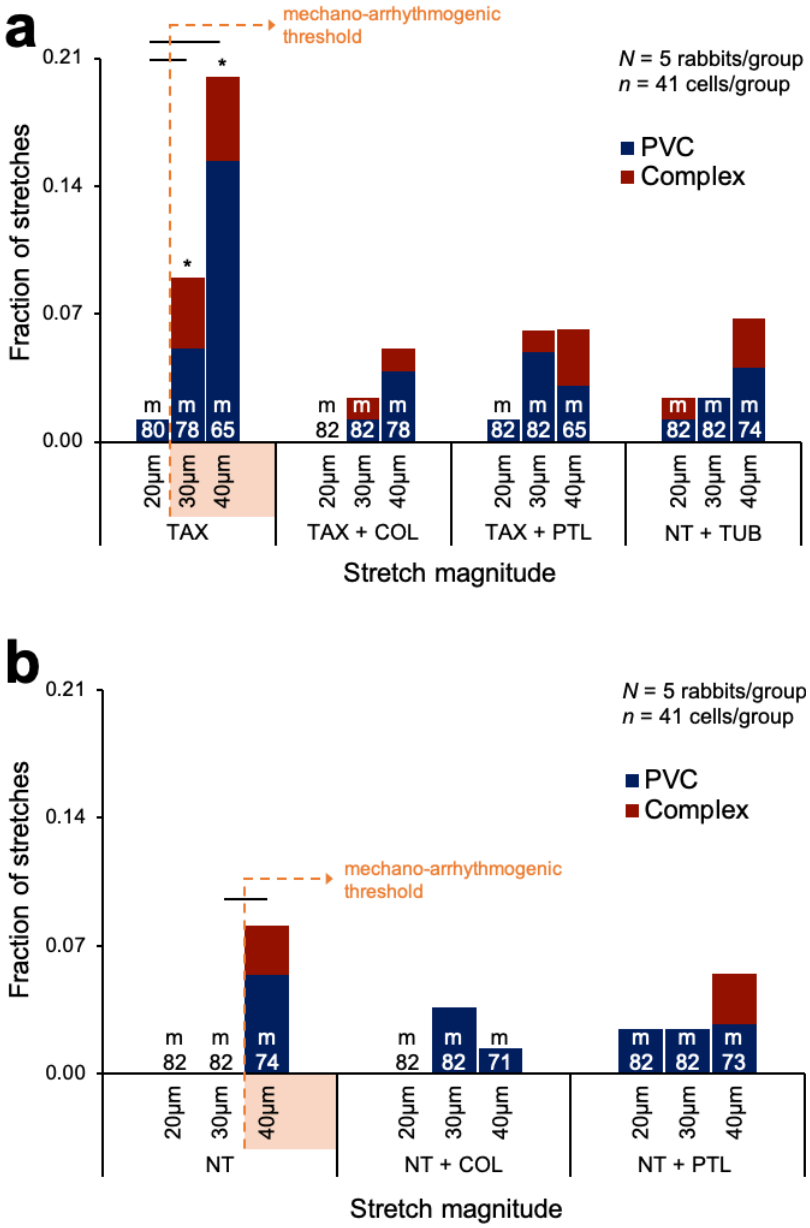

Supplemental Figure 5.5 | Effect of colchicine and parthenolide on the reduced sarcomere stretch with paclitaxel. a, Percent sarcomere stretch following transient stretch at increasing levels of piezo-electric translator movement (20, 30, and 40 μm) of rabbit isolated ventricular myocytes exposed to normal Tyrode (NT) alone, or to paclitaxel (TAX, 10 μM) co-loaded with colchicine (COL, 10 μM for 90 min) or parthenolide (PTL, 10 μM for 90 min). Differences within group assessed by paired one-way ANOVA with the Geisser-Greenhouse correction. Differences between groups assessed by the unpaired Student's t-test. *p<0.05 compared to control, **p< 0.05 within group. N = rabbits, n = cells.

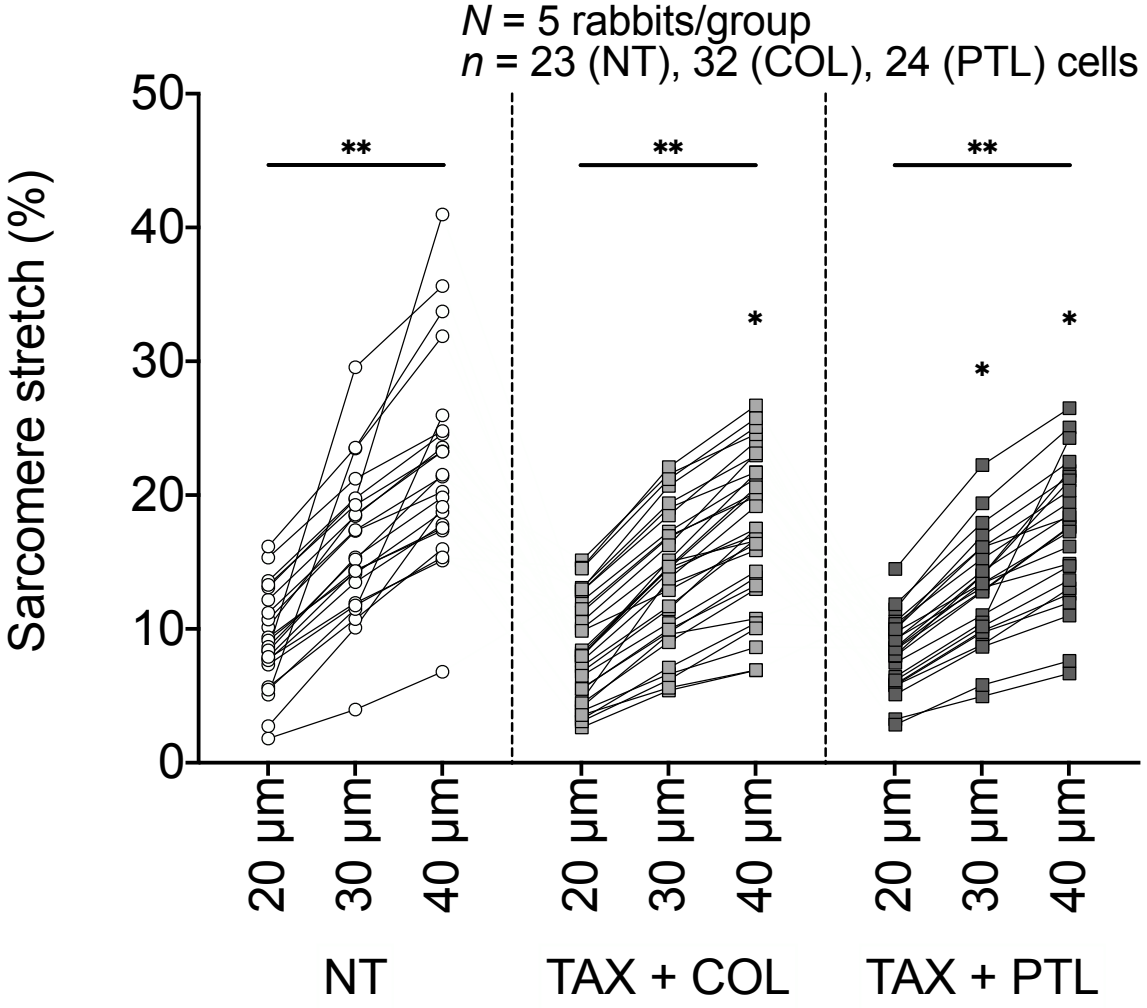

Supplemental Figure 5.6 | Carbon fibre position tracking and force measurement in a single ventricular myocyte. a, Measured force of the left and right compliant carbon fibres over time for a single ventricular myocyte undergoing a stepwise increase in stretch (up to 10 μm) over two sequential (15 s pause in between) protocols (top and bottom). The black lines represent contractions. **b,** Average measured carbon fibre position (left) during systole (red) and diastole (blue), and the average measured systolic (red, maximal) and diastolic (blue, minimal) force after the first (top) and second (bottom) protocol.

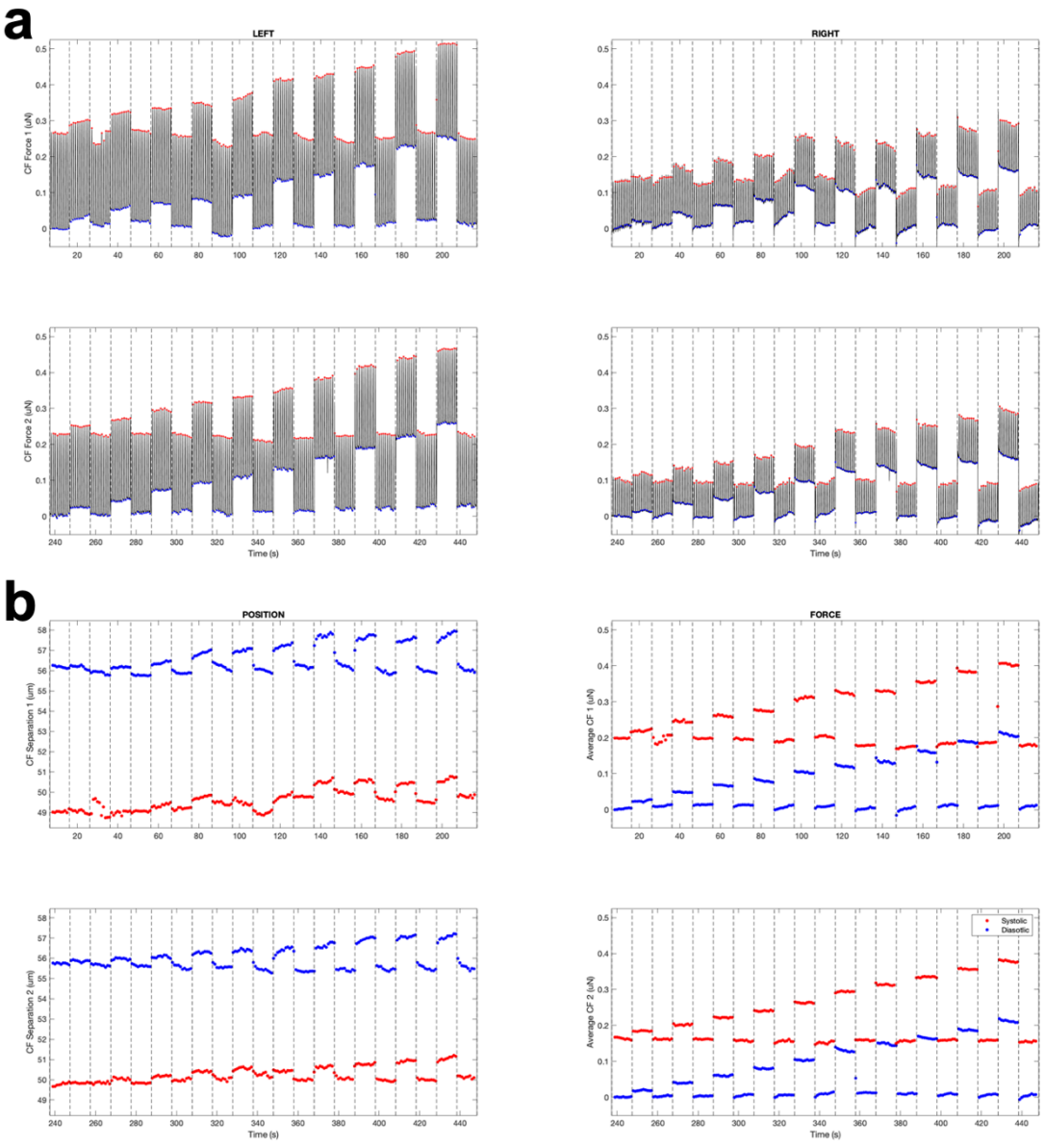

Supplemental Figure 5.7 | Cellular force-length curves generated for measurement of stiffness and elastance. Force-length relationship for **a,** a paclitaxel-treated cell (TAX, 10 μM for 90 min), and **b,** a control (NT) cell from two consecutive (15 s pause in-between) stepwise generated stretch protocols (up to 10 μm length) showing the end-systolic (red) and end-diastolic (blue) force-length relationships, representing cellular elastance and stiffness respectively. m1 = slope of the first generated curve (circles), m2 = slope of the second generated curve (diamonds), $\Delta_{EDFLR(m)}$ = difference between the first and second protocol, measured as a metric for microtubule priming.

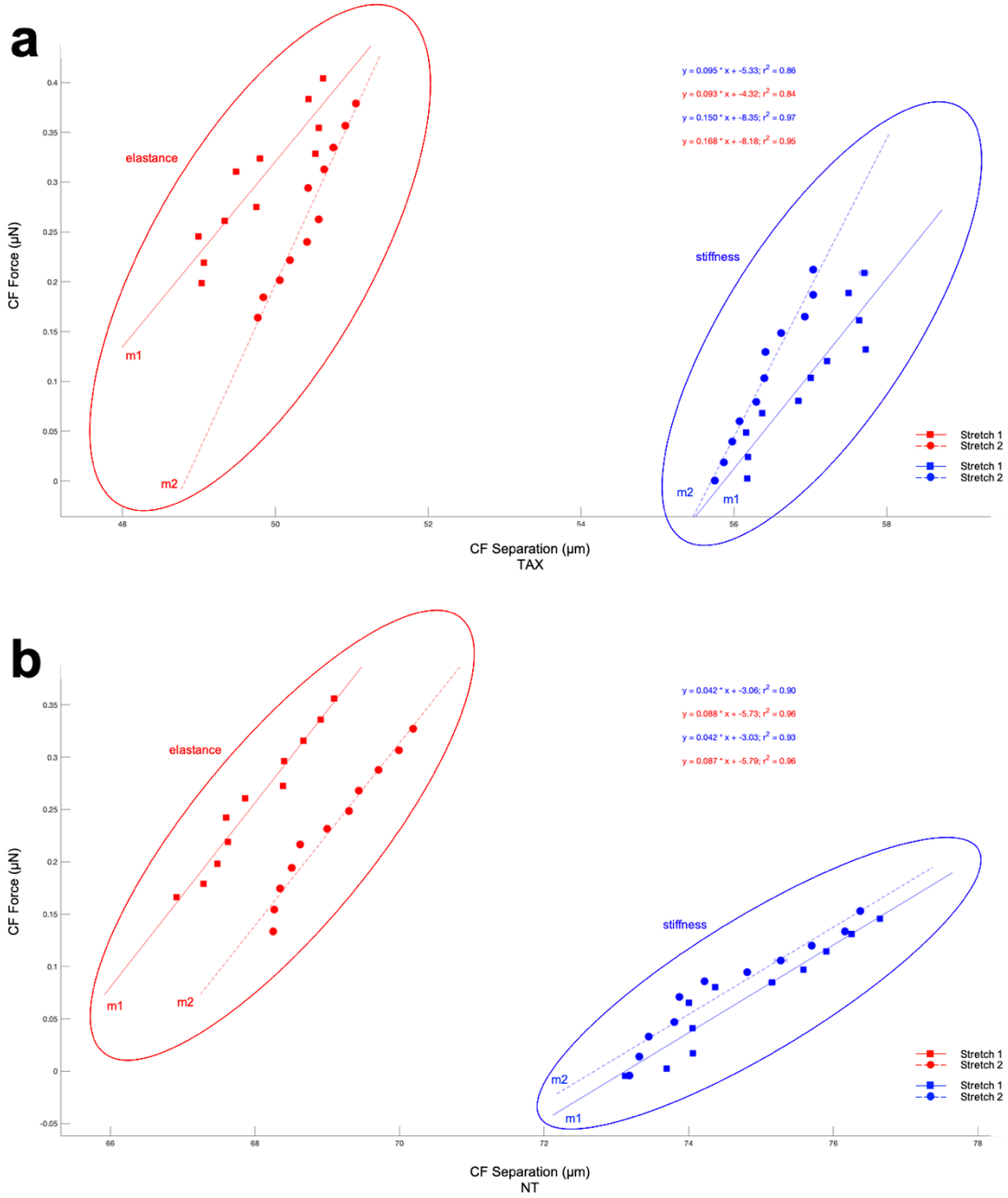

Supplemental Figure 5.8 | Effect of NT exposure duration on cellular mechanics. a, Stiffness (measured as the slope of the end-diastolic force-length relationship, EDFLR) of rabbit ventricular myocytes in normal Tyrode (NT) for 5 min (left), or 2 hrs (right), measured from the first (m1) and second (m2) sequentially generated force-length curve. **b,** Elastance (measured from slope of the end-systolic force length relationship, ESFLR) in cells in NT for 5 min (left) or 2 hrs (right). **c,** Difference in the stiffness ($\Delta_{EDFLR(m)}$), or **d,** elastance ($\Delta_{ESFLR(m)}$) between the first and second protocol from myocytes in NT for 5 min or 2 hrs. Differences assessed by the unpaired Student's t-test (for normally distributed data), or Mann-Whitney test (for non-normally distributed data). *p< 0.05 between groups. N = rabbits, n = cells

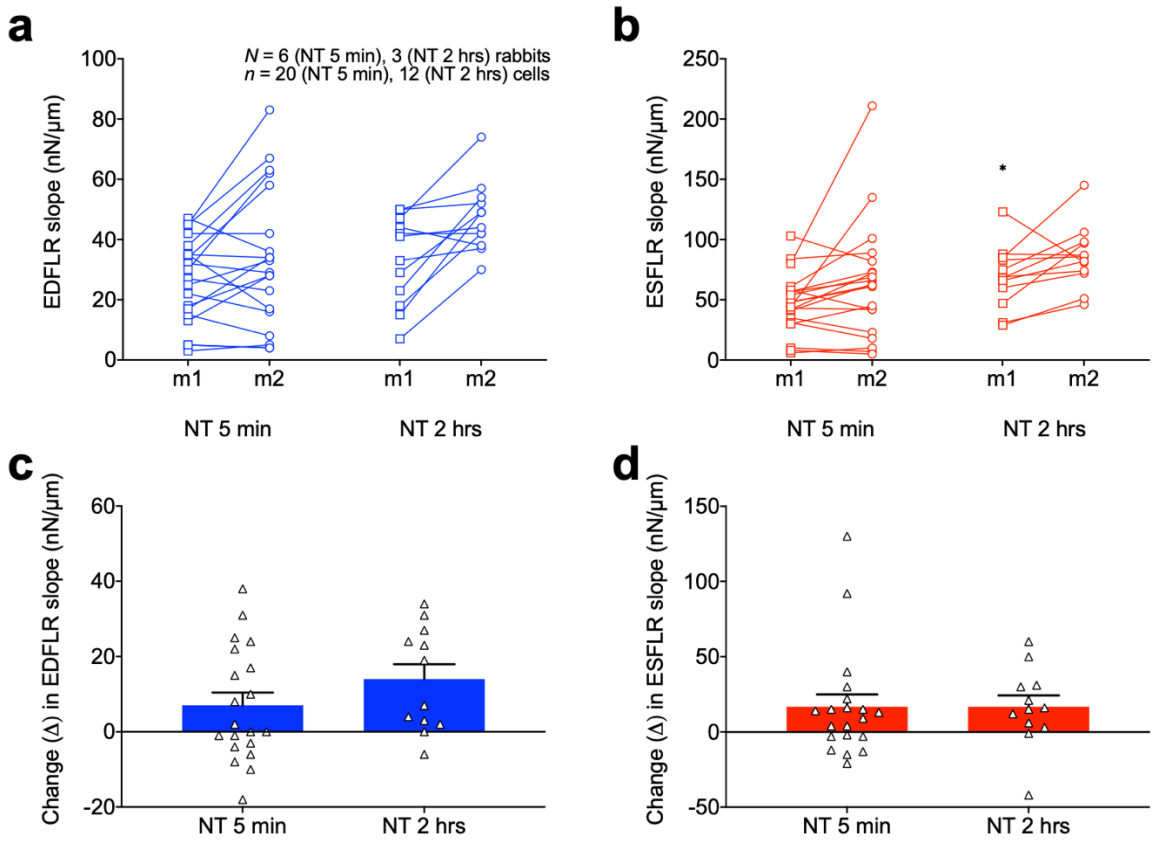

Figure 5.9 | Contribution of MTN polymerisation and post-translational modifications to cellular elastance. a, Elastance (measured as the slope of the end-systolic, force-length relationship, ESFLR) of rabbit ventricular myocytes in normal Tyrode (NT) alone, or incubated with paclitaxel (TAX, 10 μM for 90 min) in NT, measured from the first (m1) and second (m2) sequentially generated force-length curve. **b,** Elastance after the first and second protocol from cells in TAX alone, or co-incubated with colchicine (COL, 10 μM for 90 min) or parthenolide (PTL, 10 μM for 90 min), or cells loaded with tubacin alone (TUB, 10 μM for 2 hrs). **c,** Difference in the elastance between the first and second protocols ($\Delta_{ESFLR(m)}$) in control or TAX cells, or **d,** in TAX cells co-loaded with either COL or PTL, or control cells loaded with TUB alone. Differences within groups assessed by paired Student's t test (for normally distributed data) or Wilcoxon matched-pairs signed rank test (for non-normally distributed data). Differences compared to control or TAX assessed by unpaired Student's t-test (for normally distributed data), or Mann-Whitney test (for non-normally distributed data). *p<0.05 compared to NT, **p<0.05 within a group, #p<0.05 compared to TAX. N = rabbits, n = cells.

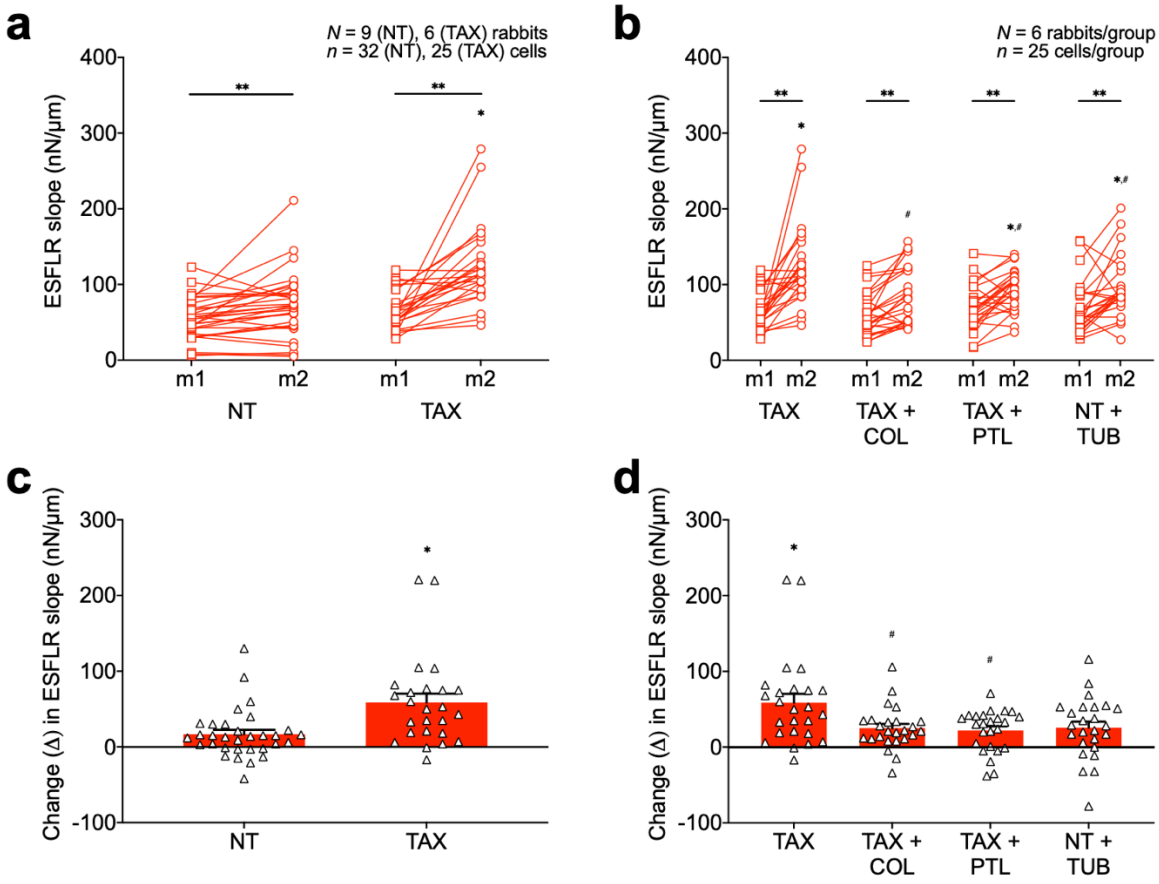

Figure 5.10 | Effect of pharmacological agents on cellular mechanics in control cells. **a,** Stiffness (measured as the slope of the end-diastolic force-length relationship, EDFLR) or **b,** elastance (measured as the slope of the end-systolic force-length relationship, ESFLR) of rabbit ventricular myocytes in normal Tyrode (NT) alone, or with colchicine (COL, 10 μM for 90 min) or parthenolide (PTL, 10 μM for 90 min) in NT, measured from the first (m1) and second (m2) sequentially generated force-length curve. **c,** Differences in the stiffness or, **d,** differences in the elastance between the first and second protocol ($\Delta_{EDFLR(m)}$ or $\Delta_{ESFLR(m)}$). Differences within groups assessed by paired Student's t test (for normally distributed data) or Wilcoxon matched-pairs signed rank test (for non-normally distributed data). Differences compared to control assessed by unpaired Student's t-test (for normally distributed data), or Mann-Whitney test (for non-normally distributed data). *p<0.05 compared to NT, **p<0.05 within a group. N = rabbits, n = cells.